TECHNICAL REPORT NO. 4-763

SHOCK-ABSORBING MATERIALS

Report 2

CELLULAR CONCRETE AS A BACKPACKING MATERIAL

by

C. C. Hoff

June 1971

Sponsored by Defense Atomic Support Agency

Conducted by U. S. Army Engineer Waterways Experiment Station, Vicksburg, Mississippi

Unclassified
Security Classification

DOCUMENT CONTROL DATA - R & D

(Security classification of title, body of abstract and indexing annotation must be entered when the overall report is classified)

1. ORIGINATING ACTIVITY (Corporate author) U. S. Army Engineer Waterways Experiment Station Vicksburg, Mississippi	2a. REPORT SECURITY CLASSIFICATION Unclassified 2b. GROUP

3. REPORT TITLE

SHOCK-ABSORBING MATERIALS; Report 2, CELLULAR CONCRETE AS A BACKPACKING MATERIAL

4. DESCRIPTIVE NOTES (Type of report and inclusive dates)
Report 2 of a series

5. AUTHOR(S) (First name, middle initial, last name)

George C. Hoff

6. REPORT DATE	7a. TOTAL NO. OF PAGES	7b. NO. OF REFS
June 1971	184	21

8a. CONTRACT OR GRANT NO.	9a. ORIGINATOR'S REPORT NUMBER(S)
b. PROJECT NO. c. Nuclear Weapons Effects Research Subtask SC 210 d.	Technical Report No. 6-763, Report 2 9b. OTHER REPORT NO(S) (Any other numbers that may be assigned this report)

10. DISTRIBUTION STATEMENT

Approved for public release; distribution unlimited.

11. SUPPLEMENTARY NOTES	12. SPONSORING MILITARY ACTIVITY
	Defense Atomic Support Agency Washington, D. C.

13. ABSTRACT

The use of low-density cellular concrete, having an oven-dry unit weight of 50 pcf or less, as a backpacking material for deeply buried protective structures was studied. Cellular concrete was found to be suitable for this type of application. A number of physical properties of cellular concrete were determined to provide input to design codes. Constrained compressive crushing stress levels from 20 to 1,000 psi for slow rates of loading were observed. Rapid-loading tests and equation of state measurements were also made to determine the rate sensitivity of the concrete. Compressional wave velocities from 2,000 to 6,000 ft/sec were also measured. Modulus of elasticity values from 20,000 to 220,000 psi were measured for concretes in the as-cast condition with respect to moisture. Flexural strength to compressive strength ratios from 0.16 to 0.33 were observed. Early age stiffening characteristics of cellular concrete were also studied. Some design procedures based on the data analysis are suggested. Some possible areas of difficulty during prototype use of cellular concrete as a backpacking, such as lift heights, cold joints, temperature problems, and water-saturation problems, are also explored. Lift heights should not exceed those that cause an increase in density over the desired density by more than a stipulated amount in the lower portion of the lift. The effects of joint roughness and curing on the joint performance are minimal. Temperatures over about 120 F tend to cause collapse of the structure of unhardened low-density cellular concrete. In a free-water environment, saturation of the cellular concrete is inevitable unless steps are taken to prevent the water from reaching the concrete. Suggestions for doing this are offered.

DD FORM 1 NOV 68 1473 REPLACES DD FORM 1473, 1 JAN 64, WHICH IS OBSOLETE FOR ARMY USE.

Unclassified
Security Classification

14. KEY WORDS	LINK A		LINK B		LINK C	
	ROLE	WT	ROLE	WT	ROLE	WT
Backpacking						
Cellular concretes						
Shock absorption						

TECHNICAL REPORT NO. 6-763

SHOCK-ABSORBING MATERIALS

Report 2

CELLULAR CONCRETE AS A BACKPACKING MATERIAL

by

G. C. Hoff

June 1971

Sponsored by Defense Atomic Support Agency
Nuclear Weapons Effects Research SC 210

Conducted by U. S. Army Engineer Waterways Experiment Station, Vicksburg, Mississippi

ARMY-MRC VICKSBURG, MISS.

BLANK PAGE

THE CONTENTS OF THIS REPORT ARE NOT TO BE USED FOR ADVERTISING, PUBLICATION, OR PROMOTIONAL PURPOSES. CITATION OF TRADE NAMES DOES NOT CONSTITUTE AN OFFICIAL ENDORSEMENT OR APPROVAL OF THE USE OF SUCH COMMERCIAL PRODUCTS.

ABSTRACT

The use of low-density cellular concrete, having an oven-dry unit weight of 50 pcf or less, as a backpacking material for deeply buried protective structures was studied. Cellular concrete was found to be suitable for this type of application. A number of physical properties of cellular concrete were determined to provide input to design codes. Constrained compressive crushing stress levels from 20 to 1,000 psi for slow rates of loading were observed. Rapid-loading tests and equation of state measurements were also made to determine the rate sensitivity of the concrete. Compressional wave velocities from 2,000 to 6,000 ft/sec were also measured. Modulus of elasticity values from 20,000 to 220,000 psi were measured for concretes in the as-cast condition with respect to moisture. Flexural strength to compressive strength ratios from 0.16 to 0.33 were observed. Early age stiffening characteristics of cellular concrete were also studied. Some design procedures based on the data analysis are suggested.

Some possible areas of difficulty during prototype use of cellular concrete as a backpacking, such as lift heights, cold joints, temperature problems, and water-saturation problems, are also explored. Lift heights should not exceed those that cause an increase in density over the desired density by more than a stipulated amount in the lower portion of the lift. The effects of joint roughness and curing on the joint performance are minimal. Temperatures over about 120 F tend to cause collapse of the structure of unhardened low-density cellular concrete. In a free-water environment, saturation of the cellular concrete is inevitable unless steps are taken to prevent the water from reaching the concrete. Suggestions for doing this are offered.

PREFACE

This study was conducted in the Concrete Division of the U. S. Army Engineer Waterways Experiment Station (WES) under the sponsorship of the Defense Atomic Support Agency (DASA) as part of Nuclear Weapons Effects Research (NWER) Subtask SC 210, "Response of Buried Structures to Ground Shock." The work was accomplished under the general supervision of Mr. T. B. Kennedy, former Chief of the Concrete Division, Mr. Bryant Mather, present Chief of the Concrete Division, and Mr. J. M. Polatty, Chief of the Engineering Mechanics Branch. Other staff members actively participating in the investigation were Messrs. J. L. Hawley, Donato Brescia, and G. C. Hoff. Mr. B. R. Sullivan, Chief of the Engineering Physics Section, prepared Appendix C. Mr. Hoff was project leader and prepared this report.

Directors of the WES during the investigation and the preparation and publication of this report were COL Alex G. Sutton, Jr., CE, COL John R. Oswalt, Jr., CE, COL Levi A. Brown, CE, and COL Ernest D. Peixotto, CE. Technical Directors were Messrs. J. B. Tiffany and F. R. Brown.

CONTENTS

TABLES

FIGURES

NOTATION

The principal symbols used in this report are listed below. Special-purpose subscripts and symbols are not listed but are explained in the text.

a,b = equation coefficients
B = beam width
C = cement content, or elastic wave velocity
d = density
D = beam depth
E = modulus of elasticity
f'_c = yield strength
k = water-cement ratio
L = length
n = porosity
p = pressure
P = load
r = radius
R = modulus of rupture
S = strength
T = time
u = particle velocity
U = energy, or shock wave velocity
V = compressional wave velocity; also, volume (with appropriate subscripts)
W = weight
X,Y = rectilinear coordinates
ϵ = strain or deformation
γ = unit weight
ρ = specific gravity
σ = stress

CONVERSION FACTORS, BRITISH TO METRIC UNITS OF MEASUREMENT

British units of measurement used in this report can be converted to metric units as follows.

Multiply	By	To Obtain
inches	2.54	centimeters
feet	0.3048	meters
cubic feet	0.02832	cubic meters
cubic yard	0.764555	cubic meters
pounds	453.5924	grams
pounds per square inch	0.070307	kilograms per square centimeter
pounds per cubic foot	16.02	kilograms per cubic meter
Fahrenheit degrees	5/9	Celsius or Kelvin degrees[a]
foot-pounds	0.138255	meter-kilograms
feet per second	0.3048	meters per second

[a] To obtain Celsius (C) temperature readings from Fahrenheit (F) readings, use the following formula: $C = (5/9)(F - 32)$. To obtain Kelvin (K) readings, use: $K = (5/9)(F - 32) + 273.15$.

CHAPTER 1

INTRODUCTION

1.1 DESIGN AND CONSTRUCTION CONSIDERATIONS

The use of low-density[1] cellular concrete as a backpacking for deeply buried structures requires an understanding of the properties and characteristics of these concretes when they are placed as large volume sections in underground environments. The protective structure designer requires numbers that represent the physical properties of the in-place concrete; and because of the special use of cellular concrete in this situation, these numbers are generally not available in the literature. The construction engineer is faced with the problem of using a material as backpacking that normally is used for roof and floor fills (Reference 1). Some of the construction problems associated with making this transition are unique.

The first area of concern is the in-place physical properties of the cellular concrete. The effective use of a backpacking requires that its compressive strength and deformation capabilities be known (Reference 2). A number of external factors will influence the resistance to loading offered by a cellular concrete of predetermined design. The first of these will be the degree of constrainment of the concrete when loaded. This constraint is a result of the deeply buried configuration (Appendix A). The values used to describe the strength of the backpacking should reflect this constrainment. Unfortunately, the actual amount of constrainment and manner of loading of the concrete are variables that may never be exactly known and, therefore, must be approximated.

Cellular concrete is a load- and strain-rate sensitive material (Reference 3). The time rate and history of loading of the backpacking are variables that will depend on a number of external factors over which a designer may have no control; yet these factors can influence the

---

[1] Low-density means the concrete has an oven-dried density of less than 50 pcf. (A table of factors for converting British units of measurement to metric units is presented on page 12.)

resistance offered by the backpacking when it is loaded. The backpacking may also be subjected to repeated shock loadings, the frequency and intensity of which may not be known.

Other physical properties such as flexural strength, compressional wave velocity, modulus of elasticity, and Poisson's ratio are also essential for design purposes. These properties and the compressive strength of the cellular concrete should be obtained in such a manner that the condition of the concrete when evaluated approaches that of the in-place concrete. An important consideration in this respect is the moisture condition of the concrete when tested. The in-place concrete will remain at essentially the same moisture content as when cast, because it will be sealed on the outer periphery by competent rock and on the ends and inner periphery by the liner it is protecting. The characterizing parameters for each type of test should represent concrete in the as-cast moisture condition.

The cellular concrete, having been designed properly, must then be fabricated and put in place in such a manner that the finished product actually represents the designed concrete. Some of the construction problems associated with the actual use of cellular concrete as backpacking have been examined (Reference 4), but some others require additional study. Assuming the concrete can be satisfactorily made and brought to the point of placement, the depth or lift height to which the concrete can be placed at one time must be known.

In a deep lift, the very high air content of the cellular concrete allows the lower regions of the lift to compress or consolidate in the unhardened state due to the increasing superincumbent loads resulting from the unhardened concrete in the upper region. As will be mentioned later, the consolidation problem may be further compounded by increasing temperatures of and moisture migration in the concrete. In consolidating, the density of the concrete is increased. As the cellular concrete strength is a function of the density (Reference 3), the strength will also increase. When a particular backpacking design strength is to be uniform throughout the concrete mass, this increase, and hence strength gradient, is not desirable. It is also not desirable from an economy standpoint because it

will take more cement to fill a given volume than was initially planned. Once a satisfactory lift height is determined, where a controlled amount of density change occurs for a given cellular concrete design, construction schedules can be established.

By having to place the cellular concrete in lifts for large sections, the problem of joint preparation arises. Because of the planned mode of resistance of the buried structure to loading, it is desirable that large sections of the backpacking do not slide across joints and thus produce a more serious loading condition than anticipated. Properly designed cold joints should enable the cellular concrete backpacking to act as a single mass.

Associated with both the lift height and cold joint problems is the problem of heat both in and around the cellular concrete. Because of the high air content of the concrete and, hence, its insulating characteristics, and the possibility of the confining rock medium behaving as an infinite heat sink, large amounts of the heat caused by the hydration of the cement will remain in the concrete for long periods of time. Unhardened cellular concrete placed in hot environments will experience a reduction of the surface tension of the air bubbles in the void system and a subsequent expansion of the heated air in the bubble. This causes the bubbles to burst with resulting consolidation of the concrete. This hot environment can exist in the upper regions of large placements where the bottom of the placement has begun to stiffen and is developing very hot temperatures. It can also exist at the interface between a lift of older hot concrete and a lift of new unhardened concrete, or it can exist in the hot air environment provided by heat loss from hydrating adjacent sections of concrete. Again, this is not desirable from the standpoints of both design and economy. Appropriate steps must be taken to reduce, eliminate, or work around these temperature problems.

Once the cellular concrete is in place it probably will not be seriously affected by any external factors other than loading (Reference 3), with the exception of water. For the strengths and densities of cellular concrete being considered for backpacking in this study, cellular concrete should be considered as being susceptible to water infiltration even at

very low water pressures (Reference 3). The presence of additional water in the concrete reduces the amount of void space and greatly affects the performance of the concrete. To adequately design against the infiltration of water into the cellular concrete, an understanding of the saturation characteristics of this concrete is essential.

The problems described above will vary in complexity and severity for each set of field conditions. Obtaining solutions to these problems for all possible situations would be a formidable task. The studies described herein were done, for the most part, in preparation for an actual field job involving buried structures backpacked with cellular concrete (References 4 and 5). In most cases, the studies were not designed to provide in-depth answers to the specific problem area studied, but were meant instead to produce qualitative results that would provide guidance to the individuals undertaking the actual work.

1.2 OBJECTIVE

The objective of the study was to investigate low-density cellular concrete for use as a backpacking material for deeply buried structures. Specifically, the investigation was to determine some physical properties of the concrete that were indicative of its desired in-place performance and to examine some problems associated with placing large mass sections of cellular concrete in underground environment.

1.3 SCOPE

1.3.1 Physical Properties. A constrained compression test was developed (Appendix A) and used to evaluate numerous mixture designs of cellular concrete for both slow and rapid rates of loading. A limited number of test specimens were evaluated for multiple-shot loading capabilities.

Other physical properties such as flexural strength, compressional wave velocity, modulus of elasticity, and Poisson's ratio were also determined for a number of different mixture proportions. All physical properties were determined while the concrete was in a moisture condition approximating that of the as-cast condition. Some measurements of the response of concrete to high-pressure shock loading were also attempted (Appendix C).

1.3.2 Construction Problem Areas. Selected mixtures were studied for hydration temperature development, techniques for reducing this temperature, and the effects of this temperature on additional placements of fresh concrete. The effect of lift height on density of the concrete and the preparation of cold joints related to lift construction were also studied.

The effect of free water on in-place cellular concrete was studied and an examination of some surface sealers for moisture exclusion was conducted.

CHAPTER 2

MATERIALS AND FABRICATION, AND PLACING EQUIPMENT AND PROCEDURES

2.1 MATERIALS

2.1.1 Portland Cement. Type III cement was used for all the concrete in the program with the exception of some Type I cement that was used in portions of the temperature studies. The portland cements representing both the Type I (RC-554) and Type III (RC-560) met the requirements for Types I and III, respectively, and had the following chemical and physical characteristics:

Chemical Analysis			Physical Properties		
Constituents	Percent			Type I RC-554	Type III RC-560
	Type I RC-554	Type III RC-560			
SiO_2	20.7	21.1	Normal consistency, pct	25.0	27.2
Al_2O_3	4.8	4.8	Setting time, Gillmore, hours:minutes		
Fe_2O_3	4.1	4.0	Initial	3:45	3:20
CaO	64.7	64.6	Final	5:30	6:50
MgO	1.8	1.8	Autoclave expansion, pct	0.01	0.01
SO_3	2.3	2.4	Air content of mortar, pct	8.3	7.2
Ignition loss	1.4	1.4	Compressive strength of mortar, psi		
Total	0.99	100.1	1 day	--	2,390
Insoluble residue	0.10	0.01	3 days	2,850	3,810
Na_2O	0.18	0.13	7 days	3,765	5,165
K_2O	0.26	0.23	28 days	5,145	--
Total alkalies as Na_2O	0.35	0.28			
C_3A	6	6			
C_3S	60	58			

(Continued)

Chemical Analysis			Physical Properties		
Constituents	Percent			Type I RC-554	Type III RC-560
	Type I RC-554	Type III RC-560			
C_2S	14	17	Surface area, air permeability fineness (Blaine), cm^2/g	3,845	4,790
C_4AF	--	12	Specific gravity	3.14	3.13
			Heat of hydration, cal/g		
			7 days	77.7	80.8
			28 days	89.7	91.4

2.1.2 Foaming Agent. A foaming agent, AD-186, was used to provide the stable air-bubble system necessary for the fabrication of cellular concrete. A spectroscopic analysis of the foaming agent indicated the presence of decomposition products of proteins reacted with aliphatic fatty acids or salts of fatty acids. The manufacturer refers to his product as a hydrolyzed stabilized protein foaming agent.

For use, a premixed solution of a predetermined concentration of foaming agent and water was prepared. The solution was then placed in a pressure container and subjected to a controlled air pressure. The air pressure forced the solution through a discharge line into a blending nozzle that agitated the solution and combined it with compressed air. The resulting product that issued from the blending nozzle was a stable, preformed foam having the consistency of shaving cream obtained from aerosol cans. This preformed foam provides the stable air-bubble system in the cellular concrete.

2.2 MIXTURE PROCEDURES AND PROPORTIONS

All the cellular concrete was batched in a 5.5-ft^3 horizontal-drum mortar mixer. The rubber-edged blades of the mixer were modified to obtain

better mixing action by adding heavy-duty 1-inch screening between the struts of each individual blade. The batching sequence was water followed by cement, which was mixed until a well-blended slurry was obtained. The preformed foam was then added and blended into the slurry until a uniform consistency of cellular concrete was obtained.

The following procedure was used to design all of the neat cellular concretes used during the program.

The total size of a batch of neat cellular concrete can be expressed in terms of the volumes of all the constituents in the batch:

$$V_b = V_s + V_f \tag{2.1}$$

where

V_b = volume of batch, ft^3

V_s = volume of neat slurry, ft^3

V_f = volume of preformed foam, ft^3

The volume of slurry is composed of cement, water, and entrained air:

$$V_s = V_c + V_{sw} + V_{sa} \tag{2.2}$$

where

V_c = volume of cement, ft^3

V_{sw} = volume of slurry water, ft^3

V_{sa} = volume of entrained slurry air, ft^3

The preformed foam volume is composed of the volume of foam air and the volume of premixed solution:

$$V_f = V_{fa} + V_{fw} \tag{2.3}$$

where

V_{fa} = volume of foam air, ft^3

V_{fw} = volume of foam water, ft^3

Substituting in Equation 2.1:

$$V_b = V_c + V_{sw} + V_{sa} + V_{fa} + V_{fw} \tag{2.4}$$

The proportioning of the cellular concrete begins with the selection of the desired freshly mixed density and water-cement ratio for the concrete. The water-cement ratio by weight of the ingredients of the concrete can be expressed as

$$k = \frac{W_{tw}}{W_c} \tag{2.5}$$

where

k = water-cement ratio of the slurry, dimensionless

W_{tw} = weight of total water in concrete, pounds

W_c = weight of cement in concrete, pounds

The weight of the total water is composed of the weight of the slurry water plus the foam water:

$$W_{tw} = W_{sw} + W_{fw} \tag{2.6}$$

where

W_{sw} = weight of slurry water, pounds

W_{fw} = weight of foam water, pounds

The amount of air needed to form the cellular structure of the concrete is determined by the density of concrete desired once the water-cement and properties of the cement are known. The density is expressed as:

$$d_c = \frac{W_b}{V_b} \tag{2.7}$$

where

d_c = freshly mixed concrete density, pcf

W_b = total weight of mixture ingredients, pounds

V_b = total batch volume, ft^3

The total batch weight is:

$$\begin{aligned} W_b &= W_c + W_{tw} \\ &= W_c + W_{sw} + W_{fw} \end{aligned} \tag{2.8}$$

From Equations 2.5, 2.7, and 2.8, the batch volume can be written as:

$$V_b = \frac{W_c + W_{tw}}{d_c}$$

$$= \frac{W_c + kw_c}{d_c}$$

$$V_b = \frac{W_c}{d_c}(k + 1) \tag{2.9}$$

or

$$W_c = \frac{V_b d_c}{k + 1} \tag{2.10}$$

The concrete volume requirement and/or batching equipment capacity will then determine the amount of cement in the batch. Having determined the amount of cement, the total amount of water needed can be found from Equation 2.5. The volumes of cement and water can then be found as:

$$V_c = \frac{W_c}{\rho_c \gamma_w} \tag{2.11}$$

and

$$V_{tw} = \frac{W_{tw}}{\gamma_w} \tag{2.12}$$

where

ρ_c = specific gravity of the cement, dimensionless

γ_w = unit weight of water, pcf

The volume of air in the slurry V_{sa} is usually small with respect to the air volume provided by the foam. For simplicity in design, the required batch air, V_a, can be written as:

$$V_a = V_{sa} + V_{fa} \approx V_{fa} \tag{2.13}$$

and assumed to be provided entirely by the foam. From Equation 2.4, then

$$V_a = V_b - V_c - V_{tw} \tag{2.14}$$

where V_b, V_c, and V_{tw} have already been determined.

The foam-producing generator nozzle operates at a constant discharge rate and produces a foam of constant density. Assuming all of the solids of the foam to be water, the foam density, d_f, is expressed as:

$$d_f = \frac{W_{fw}}{V_f} \tag{2.15}$$

From Equations 2.3 and 2.15

$$V_{fa} \approx V_a = V_f - V_{fw}$$

$$= V_f - \frac{d_f V_f}{\gamma_w}$$

$$V_a = V_f \frac{1 - d_f}{\gamma_w} \tag{2.16}$$

and

$$V_f = \frac{\gamma_w}{\gamma_w - d_f} V_a \tag{2.17}$$

From Equation 2.17, the exact amount of foam to be put in the batch is determined.

The amount of slurry water that must be initially added to the cement can be found from Equations 2.6 and 2.15, where:

$$W_{fw} = d_f V_f \tag{2.18}$$

and

$$W_{sw} = W_{tw} - W_{fw} \tag{2.19}$$

The water-cement ratio in the slurry before the foam is added is then:

$$k_1 = \frac{W_{sw}}{W_c}$$

where k_1 = water-cement ratio of ingredients initially added to mixer, dimensionless

As an example, assume that a 4.0-ft^3 batch of 32-pcf concrete with a final water-cement ratio of 0.86 is needed. The specific gravity of the cement is 3.15; the foam density is 2.3 pcf; and the unit weight of water is 62.3 pcf from Equations 2.5, 2.10, 2.11, and 2.12.

$$W_c = \frac{V_b d_c}{k + 1} = \frac{(4.0)(32)}{1.86} = 68.8 \text{ pounds}$$

$$W_{tw} = kW_c = 0.86(68.8) = 59.2 \text{ pounds}$$

$$V_c = \frac{W_c}{\rho_c \gamma_w} = \frac{68.8}{(3.15)62.3} = 0.350 \text{ ft}^3$$

$$V_{tw} = \frac{W_{tw}}{\gamma_w} = \frac{59.2}{62.3} = 0.950 \text{ ft}^3$$

The volume of air and foam required can then be found from Equations 2.14 and 2.17.

$$V_a = V_b - V_c - V_{tw} = (4.0 - 0.350 - 0.950)\ ft^3$$

$$V_a = 2.700\ ft^3$$

$$V_f = \frac{\gamma_w}{\gamma_w - d_f} V_a = \frac{62.3}{62.3 - 2.3} 2.700\ ft^3$$

$$V_f = 2.925\ ft^3$$

The foam and slurry waters can then be found from Equations 2.18 and 2.19.

$$W_{fw} = d_f V_f = 2.3(2.925) \text{ pounds}$$

$$= 6.7 \text{ pounds}$$

$$W_{sw} = W_{tw} - W_{fw} = 59.2 - 6.7$$

$$= 52.5 \text{ pounds}$$

Hence, if 68.8 pounds of cement and 52.5 pounds of water are blended in the mixer to form a slurry and the 2.925 ft^3 of foam is added, the desired concrete with respect to density and water-cement ratio should be obtained. Small adjustments may have to be made to compensate for air content changes during mixing.

For comparison purposes throughout the studies reported herein, it was attempted to use five specific water-cement ratios by weight, i.e. 0.66, 0.76; 0.86, 0.96, and 1.06, and four specific freshly mixed densities of 23, 32, 39, and 43 pcf at each water-cement ratio. Exceptions were not uncommon and are noted where they occurred. The number of batches providing test specimens for the slow-loading tests were 13, 31, 31, 21, and 36 for the 0.66, 0.76, 0.86, 0.96, and 1.06 water-cement ratios, respectively. The number of batches providing specimens for the rapid-loading test were 16, 22, 16, and 30 for the 0.76, 0.86, 0.96, and 1.06 water-cement ratios, respectively.

2.3 SPECIMEN PREPARATION AND CURING

Except where stated otherwise, all specimens were cured in their casting molds for 24 hours and upon removal from these molds were immediately placed and sealed in polyethylene plastic bags and stored at 73 F until tested.

The test specimens for all of the constrained compression tests were cast as 6- by 12-inch cylinders. Forty-eight hours before being tested, each specimen was removed from its bag and the top and bottom 3 inches were sawed off. The remaining 6- by 6-inch cylinder was then resealed in its plastic bag until tested. At testing time, the time lapse from removal of the specimen from the bag to the start of test was only a few minutes. When a 6- by 12-inch cylinder was used for a specific type of test, the unformed end of the cylinder was trimmed with a saw to eliminate surface irregularities.

Each 6- by 12-inch cylinder used for the Poisson's ratio and modulus of elasticity determinations was instrumented with two A-9-6 electrical strain gages placed vertically and diametrically opposite and two similar gages placed circumferentially and diametrically opposite. The gages were bonded to the specimens by means of a very low modulus, flexible epoxy binder (CRD-EP-1). The binder also was used to cover the gage for waterproofing purposes. To avoid moisture loss from the specimens during gage mounting, a special polyethylene tent was built and the mounting was done within the tent at a relative humidity of 98 percent. The surface of the specimen was not dried in any way before, during, or after the gages were mounted. The gages were mounted after 24 days of continuous bag curing.

2.4 PLACING EQUIPMENT AND PROCEDURES

The placing of the cellular concrete in all molds and formwork with the exception of the lift height study was done by pouring the very fluid concrete from the mixer into a bucket and from the bucket into the desired container. No vibration or consolidation of the concrete was attempted. The concrete for the columns cast during the lift height study was pumped from the mixer to the point of placing using an open-throat positive displacement pump and continuous plastic hose.

2.5 SURFACE SEALERS

The following materials were used as surface sealers in the moisture studies.

WES Designation	Description
CRD CM-9	Styrene-butadiene product
CRD CM-10	Two-component epoxy thinned with a volatile solvent
CRD CM-11	Paraffin-resin mixture
CRD CM-12	Liquid latex
CRD CM-8	Vinyl-based liquid-type solvent
CRD CM-13	Asphalt
CRD CM-14	Latex wall paint
RC-560	Neat Type III cement slurry
--	Hydraulic cement slurry

CHAPTER 3

TEST EQUIPMENT AND PROCEDURES

3.1 CONSTRAINED COMPRESSION TESTS

The details of the design of the constrained compression test are contained in Appendix A.

A split-wall confining pipe was used to provide lateral constraint to the concrete tested in compression. The steel pipe (Figure A.3) had a 6-inch-inside diameter with 1/4-inch-thick walls and accommodated a 6-inch-high specimen. The 1/4-inch wall thickness resulted in negligible lateral strains for the largest vertical loads experienced during the program. After placing the specimen in the pipe, both closure bolts were torqued to a final closure of 5 ft-lb. Loads were applied through a 4-inch-diameter loading piston centered on the 6-inch-diameter specimen. The constraining pipe, loading piston, closure torque, and specimen size (6- by 6-inch cylinder) were the same for both the slow- and rapid-loading tests.

3.1.1 Slow-Loading Tests. Load was applied to the specimens using a 30,000-pound Universal testing machine operating at a constant rate of loading piston movement of 0.18 in/min (3 percent deformation per minute). Deformations were measured by a linear slide-wire potentiometer affixed to the base platform and the moving loading head of the testing machine. Loads were converted to applied stress by dividing the magnitude of the applied load by the area of the 4-inch-diameter loading piston. The resulting stress-deformation data from each test were recorded in a graphical form (Figure 3.1) using an X-Y recorder. Figure 3.2 shows the slow-loading test arrangement.

3.1.2 Rapid-Loading Tests. Rapid-loading tests were conducted using the Impact Air Hammer Apparatus (IAHA). A cross section of the IAHA is shown in Figure 3.3. Load was applied to the specimen through the 4-inch-diameter piston on the end of the driving shaft. The driving shaft had a maximum travel distance of 4 inches.

Before beginning a test, a small amount of gas pressure is placed in the trigger actuator chamber to lock the triggering mechanism in place on the driving shaft. The specimen is then placed and centered under the

loading piston. The upper surface of the specimen is brought in full contact with the bottom surface of the loading piston by means of an adjustable turnscrew on the bottom of the base bearing plate of the apparatus. The desired amount of gas pressure is then placed in the accumulator tank, and the specimen is ready for testing. By electrically releasing the gas pressure through an orifice in the actuator chamber, the triggering mechanism rotates and releases the driving shaft that, due to the accumulator tank pressure, drives the loading piston into the specimen.

Compressed nitrogen gas was used as the load gas for all tests. The amount of gas pressure required for each individual test depended on the energy absorbing capacity of the sample being evaluated. Experience with the IAHA and the cellular concrete allowed the IAHA operators to vary the gas pressure from test to test, depending on the material being evaluated, such that the total time of test for a full 4 inches of deformation of each sample never varied from 15 $\pm$ 3 msec. Rise times to the start of the crushing plateau varied between 2 and 4 msec.

Loads were measured by a recording load cell placed between the driving shaft and the loading piston. Deformations were measured using a linear slide-wire potentiometer fastened to the IAHA frame and the driving shaft. The output from both the load cell and the slide-wire potentiometer was recorded on a dual-trace oscilloscope photograph record such as that shown in Figure 3.4. The electrical impulse that released the gas in the trigger actuator chamber also operated the shutter on the oscilloscope camera, thus opening the shutter at the instant the test began. Both traces on the photograph record are on a common time basis. The upper trace indicates total deformation in inches at any point in time; the lower trace indicates the load on the sample at any point in time. By combining the load and deformation on a common time basis and converting the load to stress over the area of the loading piston and deformation to percent of total sample height, a stress-deformation record such as shown in Figure 3.1 was obtained.

3.1.3 Multiple-Shot Loading Tests. The multiple-shot loading tests were conducted exactly like the rapid-loading tests (Section 3.1.2) with the exception that only enough pressure was used in the accumulator tank

to partially deform the specimen on the first loading. After the first loading shot, the driving shaft and piston were reset for firing, the loading surface of the specimen was brought in contact with the piston face by means of the baseplate turnscrew, the accumulator tank was recharged, and the air hammer was fired again. This behavior would duplicate a rock fragment driven into the backpacking by an initial shock wave and then driven in even farther by a second shock wave.

Two oscilloscope records were obtained for each test, one for each of the two shots. The records were combined so that the point where the first record ended was the point where the second record began. Deformation for both shots, expressed in percent, was referenced to the initial height of the specimen before the testing began.

3.2 FLEXURAL STRENGTH TESTS

Flexural strength tests were made to determine the modulus of rupture of the cellular concrete at various densities and water-cement ratios and also to evaluate the effects of cold joints in the concrete for a selected mixture. In both cases, the equipment and testing were in accordance with CRD-C 16-66, "Flexural Strength of Concrete (Using Simple Beam with Third-Point Loading)."

3.2.1 Modulus of Rupture Determinations. Six-inch-square by 20-inch-long beams were evaluated. The distance between each support and its closest loading point and between both loading points was 6 inches. All beams were placed in plastic bags immediately after removal from the casting forms and were bag-cured at 73 F until tested at 28 days age. Each beam remained in the bag until testing time when it was removed, immediately placed in the load apparatus, and tested.

3.2.2 Horizontal Joint Tests. Cellular concrete with a freshly placed density of 32.7 pcf at a water-cement ratio of 0.86 by weight was used to fabricate sixteen 2-foot cubes. Each cube was placed in two lifts. The first lift was placed to a depth of 1 foot and allowed to harden. Before placing the second lift, the top surface of the first lift was prepared four different ways. Eight cubes had the top surface exposed to air for 3 days before the next lift was placed. Four of these eight had the

surface scribed in a waffle pattern to provide some roughness for the next lift to bond to. The remaining four air-dried cubes were left in the as-cast condition. The last cubes were treated in the same manner as the first eight with the exception that the exposed surface was sealed in plastic to prevent drying. The seal was removed at the time the fresh concrete was placed.

The scribing was done using a simple apparatus resembling an ordinary leaf and grass rake. Eight 5/32-inch-diameter by 3/4-inch-long prongs tapered to a point were used as shown in Figure 3.5a. The scribing was done at right angles to the cube mold, with the first indentation occurring at a distance of 3/4 inch from the mold. The resulting pattern is shown in Figure 3.5b. The depth of scribing was approximately 1/2 inch. All loose material resulting from scribing was removed with a vacuum cleaner.

The second lift was placed to the top of the mold. The top surfaces of the first eight blocks were again exposed to air drying while the surfaces of the second eight were sealed in plastic. After the second lift had cured 28 days, the forms were removed and the blocks sampled. The sampling originally was to involve drilling some 6-inch-diameter cores from each block and also to saw some 6- by 6- by 24-inch beams from each cube. The sampling arrangement is shown in Figure 3.6. Half of the beams shown in the top view were to have been drilled cores. The drilling operation was extremely difficult; and because of the weak, brittle nature of the concrete, very few intact cores were obtained. None of the cores were tested because no useful comparison data could be obtained from the small number of cores available. Only 11 of the 16 blocks were cored.

A no-joint control beam was obtained from each lift. The other beams from each block included the joint at their center. Immediately after sawing, each beam was placed in a plastic bag and stored until the concrete in the second lift was 60 days old, at which time each beam was tested in third-point flexure. This method placed the cold joint in the region of maximum moment and presented a severe loading situation for the joint. The plane of failure was noted for each beam along with the maximum failure load.

A 4-inch cube was sawed from each half of each broken flexure beam and oven-dried to a constant weight. The densities of the cubes were then determined in order to establish if density variations between the two lifts of concrete were influencing the failures of the beams. Compressive strengths of each cube were also determined in accordance with ASTM C513.

3.3 ULTRASONIC PULSE VELOCITY TESTS

Ultrasonic pulse velocity equipment and tests were in accordance with CRD-C 51-68, "Tentative Method of Test for Pulse Velocity Through Concrete." All samples were 6-inch-diameter by 12-inch-(normal) high cylinders that were continuously bag-cured with interruptions in curing occurring only for the few minutes required to obtain a pulse velocity reading at a given age. Velocities were determined for all pulse velocity samples at ages of 3, 7, 14, 28, and 60 days and also at 90 and 180 days for concrete samples made with water-cement ratios of 0.86 and 0.96.

3.4 RATE-OF-HARDENING TESTS

Rate of hardening of the cellular concrete was determined in accordance with CRD-C 68-69, "Time of Setting of Concrete Mixtures by Penetration Resistance," with the exceptions that none of the specimens were consolidated by mechanical means and that the minimum spacing between penetration points was 2 inches. Specimens of concrete made at water-cement ratios of 0.76, 0.86, 0.96, and 1.06 with nominal densities of 23, 32, 39, and 43 pcf at each water-cement ratio were evaluated at varying time intervals to 90 hours total elapsed time after batching.

3.5 MODULUS OF ELASTICITY AND POISSON'S RATIO TESTS

The modulus of elasticity and Poisson's ratio were determined in accordance with CRD-C 19-66, "Static Young's Modulus of Elasticity and Poisson's Ratio in Compression of Cylindrical Concrete Specimens."

The test specimens were 6- by 12-inch cylinders with sawed ends so capping was not necessary. All specimens were bag-cured from the time of removal from the mold until tested. The curing of each specimen was interrupted for a few hours at 24 days of age for the instrumenting of the

specimen with electrical-resistance strain gages. Care was taken during instrumentation to prevent moisture loss from the specimens. Two 6-inch gages were mounted diametrically opposed in a vertical direction with two similar gages mounted circumferentially opposed at the midpoint of the specimen. After the gage installation, each specimen was returned to its curing bag where it remained until testing at 28 days age. With the exception of the ends of each cylinder that were in contact with the testing machine, the curing bag remained around the specimen during test to prevent surface drying of the cylinder. When tested, each cylinder had a moisture content approximating that of the as-cast condition. Data were obtained in the form of stress-strain records for both sets of gages by using an X-Y recorder.

3.6 TEMPERATURE STUDIES

3.6.1 Adiabatic Temperature Rise. The adiabatic temperature rise of cellular concrete made with Type III cement (RC-560) with a water-cement ratio of 0.86 and a freshly mixed density of 43.9 pcf was determined in accordance with CRD-C 38-66, "Method of Test for Temperature Rise in Concrete," with the exception that the concrete was not vibrated when placed.

3.6.2 Mixture Water Temperature Study. Because of the expense involved in conducting the quantitative adiabatic tests, a simpler but quantitatively less accurate test was used to obtain qualitative heat development results that would reflect the general effects of varying the mixing water temperature.

Eight thick-walled polystyrene picnic coolers were used as both the container and insulator for the concrete. Each cooler was filled with one batch of concrete. Each batch of concrete was a different combination of the cement type and mixing water temperature variables. Using thermometers, two concurrent temperature measurements were made in each cooler at points near the center of the concrete mass. The measurements were made at various time intervals through 15 hours total elapsed time.

3.6.3 Lift Heat Effects. This test was designed to produce qualitative results relating to the effects of the heat generated in a hardened lift of concrete on the temperatures developed in fresh cellular concrete

placed on the surface of the hardened concrete.

Two 2-foot cubes of concrete were cast, each cube being composed of two 1-foot lifts. Three thermocouples were placed in each lift. In each cube, the first thermocouple was placed 1-1/2 inches below the top surface of the lift and at the center of the horizontal area of the lift. The second and third thermocouples were placed directly below the first but at depths of 6 and 10-1/2 inches below the lift surface, respectively. The concrete placed in each lift was not vibrated. After placing the concrete in the first lift, the thermocouples in that lift were monitored to determine the heat development in the lift. After initial stiffening of the first lift had occurred, the second lift was placed and its thermocouples were monitored along with the first lift thermocouple nearest the joint between the two lifts. The heat development as indicated by these thermocouples was measured until it appeared to reach peak values and began to decline.

3.6.4 Ambient Air Temperature Effects. Three 6- by 12-inch cylinders were made from each of four different densities of cellular concrete. Immediately after casting, one cylinder from each density was placed in air temperatures of 80, 100, and 120 F and allowed to harden. After 24 hours curing, one-half of the cylinder mold was removed and the amount of damage to each cylinder noted.

3.7 LIFT HEIGHT STUDY

Two columns of cellular concrete were placed and sampled to determine the variation in density of the concrete with increasing lift height. The first column was cast in a 6-inch-inside-diameter by 30-foot-long plastic pipe (Figure 3.7). The pipe was plugged on the lower end and placed in a 9-inch-inside-diameter cased hole in the ground. Concrete with a unit weight of 32.4 pcf and a water-cement ratio of 0.86 was pumped into the pipe through a 50-foot-long, 2-inch-inside-diameter plastic hose. Pumping was done with an open-throat, positive displacement pump. The end of the discharge hose was kept at a distance of approximately 1 foot from the freshly placed concrete surface with the hose being continually withdrawn from the pipe during placing.

The concrete was allowed to harden and cure for 3 days at which time the annulus between the hole casing and the pipe was gradually filled with water. The water caused the pipe to be displaced and float out of the casing. As the pipe moved out of the casing, sections of the pipe approximately 12 inches long were cut off and immediately measured and weighed. Twenty-nine sections were obtained. At a later date, the concrete in each section was removed and the weight of the plastic pipe determined. By subtracting this weight from the original weight measurement that included the pipe, the density of the concrete in each section was calculated.

The second column was cast in a 48-inch-diameter by 16-foot-long corrugated culvert pipe (Figure 3.8). The cellular concrete mixture had a unit weight of 31.8 pcf. The pumping equipment and procedures were the same as for the 30-foot column. After hardening and curing for 3 days, 3-foot sections of the corrugated pipe were removed from top to bottom of the pipe and 1-foot-thick slices were cut from the exposed concrete by means of a chain saw. Each slice was immediately quartered with an 8-inch cube being cut from the center of each quarter by a diamond saw. The weight and measurements of each cube were determined immediately after cutting. Cutting was done without the use of water or oil so as not to change the density of the concrete through the addition of some fluid which might have been absorbed. The average density of the four cubes from each slice was reported as the as-cast density of the concrete at that point. The cubes were then oven-dried, and the oven-dry density of the concrete was obtained so as to get an indication of moisture variations in the column.

3.8 MOISTURE STUDIES

3.8.1 Saturation Study. Five 6- by 12-inch cylinders were used to determine the amount of available voids in a selected design of concrete that could be filled with free water. The 28-day bag-cured and oven-dried densities of the concrete were 51 and 33 pcf, respectively.

Each cylinder, in the bag-cured condition, was placed in a pressure pycnometer (Figure 3.9). The pycnometer was filled with measured amounts of water until it contained a specified volume of material (specimen plus water). The water completely covered the specimen. Pressure was then

applied gradually to the surface of the water, thus forcing the water into the specimen. Additional measured amounts of water were continually added to the pycnometer to maintain a constant filled volume as the water in the pycnometer was forced into one specimen. When a pressure of 1,200 psi was reached, no additional water could be added to the system, thus indicating saturation of the specimen. The amount of voids available for filling by water was determined from the volume of water forced into the specimen plus the volume of water initially in the specimen (bag-cured weight minus oven-dry weight divided by 62.3). During the buildup to 1,200-psi water pressure, the amounts of water forced into the specimen at pressures of 50, 150, 300, and 600 psi were also noted.

3.8.2 Flow and Erosion Tests. A low-head, unlimited reservoir permeability unit (Figure 3.10) was used to determine the water flow characteristics and erosion possibilities of the cellular concrete. The unit, as used, tested six 6- by 6-inch test cylinders simultaneously at pressure heads that were determined by the head losses through the system.

Each specimen was bag-cured 28 days before being placed in a specimen container (Figure 3.11). The specimen container was constructed from a standard 6- by 12-inch concrete cylinder mold that was held between two 8- by 8- by 1/4-inch-thick steel plates by means of four bolts. Rubber gaskets were used as seals between the container and end plates. A 1-inch nipple was welded in the center of the top plate for connection to the water reservoir. A deflection flange was placed directly under the nipple opening to prevent surface erosion of the specimen by water coming into the container. The bottom plate had a 1-inch-diameter hole in its center to allow water passing through the concrete to discharge from the container.

Immediately after removal from the curing bag, the peripheral area of the cylinder was given an initial coating of vinyl-based sealer and the specimen was replaced in the curing bag. Approximately 4 hours later, a second coat of sealer was applied over the first; and before it could harden, the specimen was placed in the bottom half of the split-walled specimen container that was then tightly closed about the specimen to prevent leakage. Molding clay was used to seal the top edge of the specimen.

The water reservoir consisted of an elevated barrel of a constant

volume. The barrel was continually filled with water, with an overflow outlet at the top of the barrel providing a constant water level in the barrel. Outlets at the bottom of the barrel provided the source of water for the test specimens.

The bottom of each specimen container was immersed in water contained in a metal trough (Figure 3.11). An overflow was provided in the trough to maintain the water level in the trough at a constant level. The overflow was constructed so it would allow the collection of overflow water.

After the specimen was in place in the container and the hoses from the reservoir to the container were connected, water was allowed to flow through the system with any air in the system being bled off through a bleeder tube. The head on each specimen was determined from piezometer tubes. After 15 minutes of flow time, the initial flow determination was made by collecting the overflow water in a known volume container and measuring the time it took to collect it. The water sample was also used to determine total solids of the water passing through the specimen. Additional measurements of the same type were made over the duration of the test. The total elapsed flow time did not exceed 80 hours for any test.

3.8.3 Surface Sealer Tests. A falling head permeameter was used to determine the effectiveness of various types of surface sealers. By placing a known head of water on a sealed concrete surface and then measuring the loss of head with time as the water passes through the sealed surface, an indication of the sealers' effectiveness can be obtained.

The permeameter was constructed by placing a 6-inch-inside-diameter by 6-foot-long Plexiglas pipe on the sealed surface of an 18-inch cellular concrete cube (Figure 3.12). The concrete had a freshly mixed density of 31 pcf and water-cement ratio of 1.06 by weight. Ten cubes were cast and cured 7 days in the wooden forms in which they were cast. The exposed top surface of the concrete was covered with a polyethylene sheet during curing to prevent drying. On the seventh day, the polyethylene sheet was removed and surface irregularities of the concrete were scraped off. The coating was then applied over the entire surface and allowed to dry for 3 days.

The coating thickness varied from material to material because of the widely different consistencies of the various material sealers.

Manufacturers' guidelines for coating application were followed when provided. In all cases only one coat was applied. The average thickness of the paraffin and cement slurry coatings was approximately 1/16 inch.

After the coating had dried for 3 days, the bottom of the wooden form was removed and the cube with the side forms still on was placed on wooden supports in a large tank as shown in Figure 3.12. The tank was filled with water to the level of the top surface of the concrete, with an outlet provided in the tank to maintain that level. The vertical Plexiglas pipe was centered on the block and sealed around the outer edge with modeling clay to prevent water leakage. The pipe was then filled to its top with water and the test observations were immediately begun. The filling of the pipe took approximately 2 minutes. Care was taken not to erode or damage the sealed surface during filling.

Water-level determinations were made visually using a tape measure affixed to the pipe. The total elapsed time at which any given water level was observed was measured with a stopwatch and referenced to the time at which the pipe was completely filled.

The same procedure was used for all nine sealers. The control block (no sealer) was evaluated at 10 days age using the same procedures.

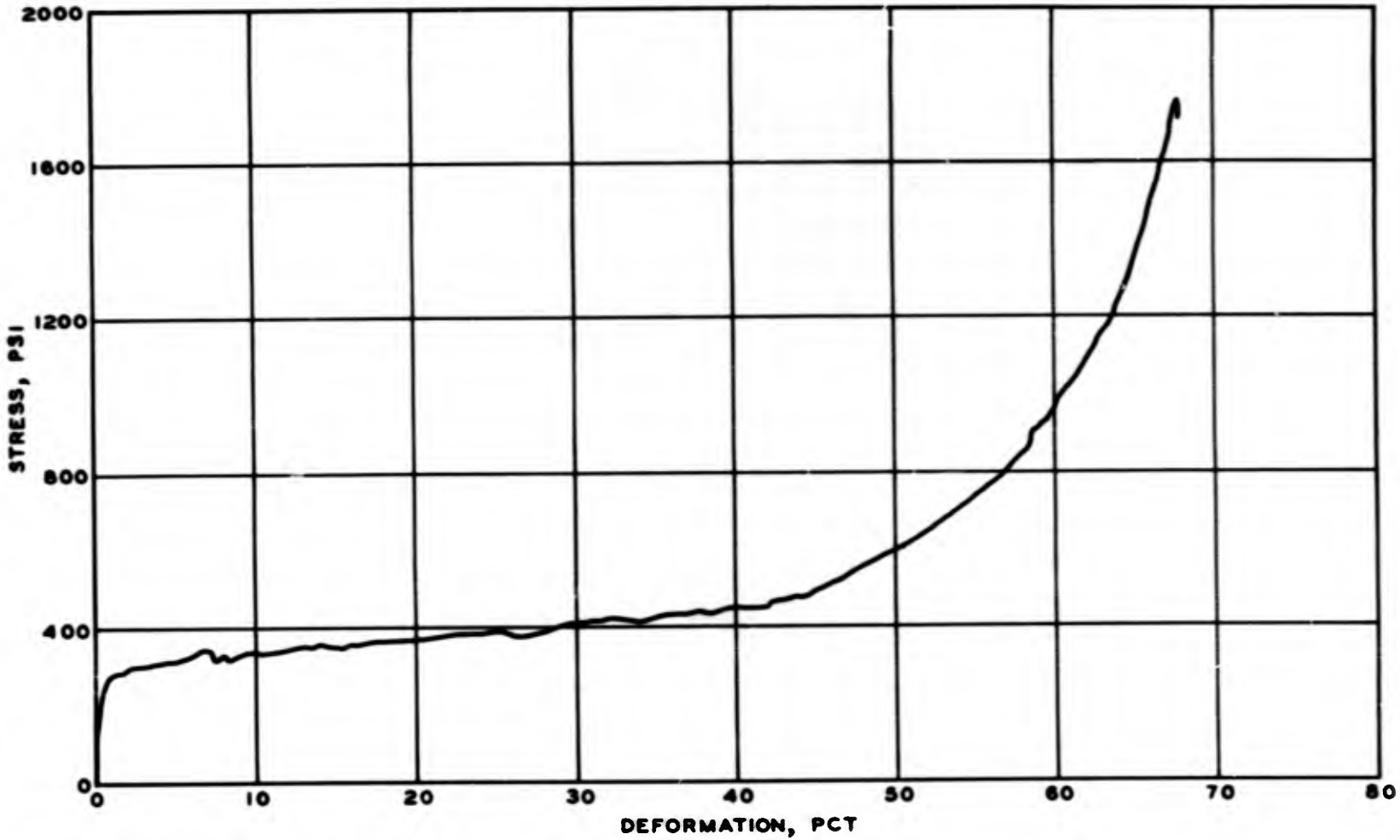

Figure 3.1 Typical test record for a slow-loading test.

Figure 3.2 Slow-loading constrained compression test configuration.

A

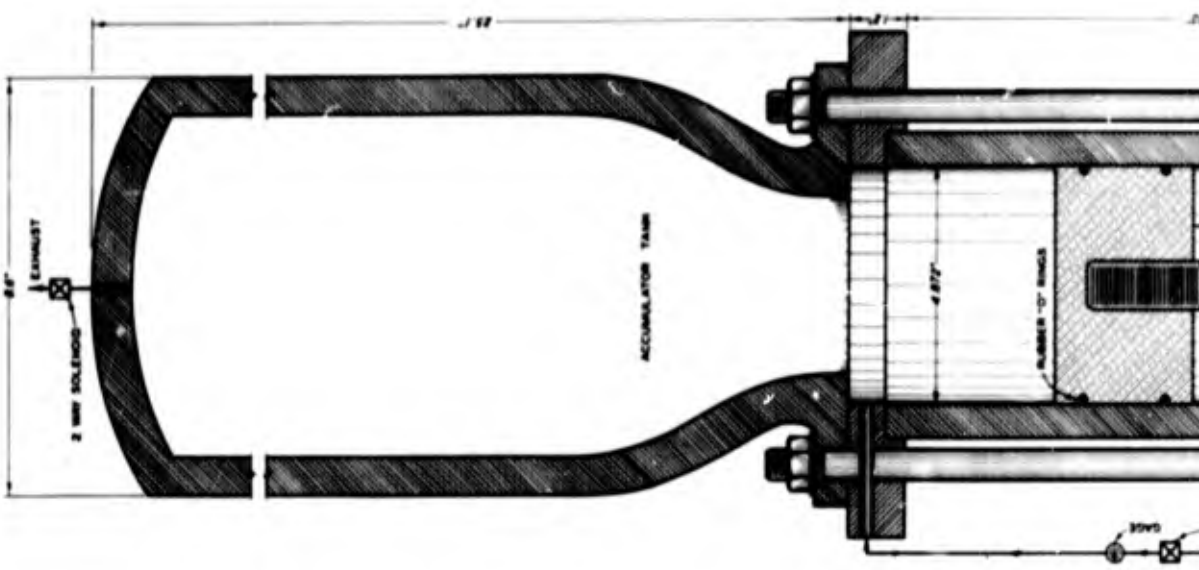

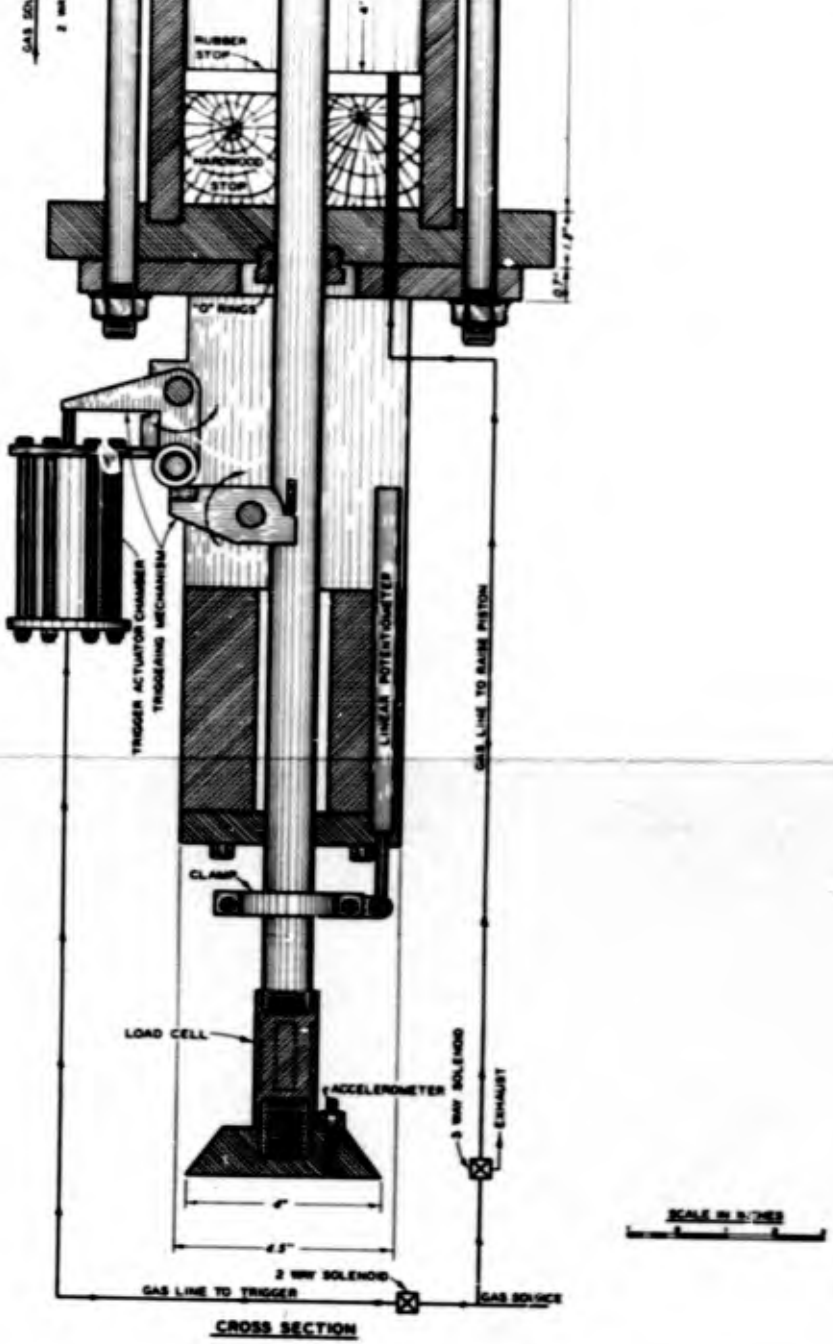

Figure 3.3 Impact air hammer apparatus (IAHA).

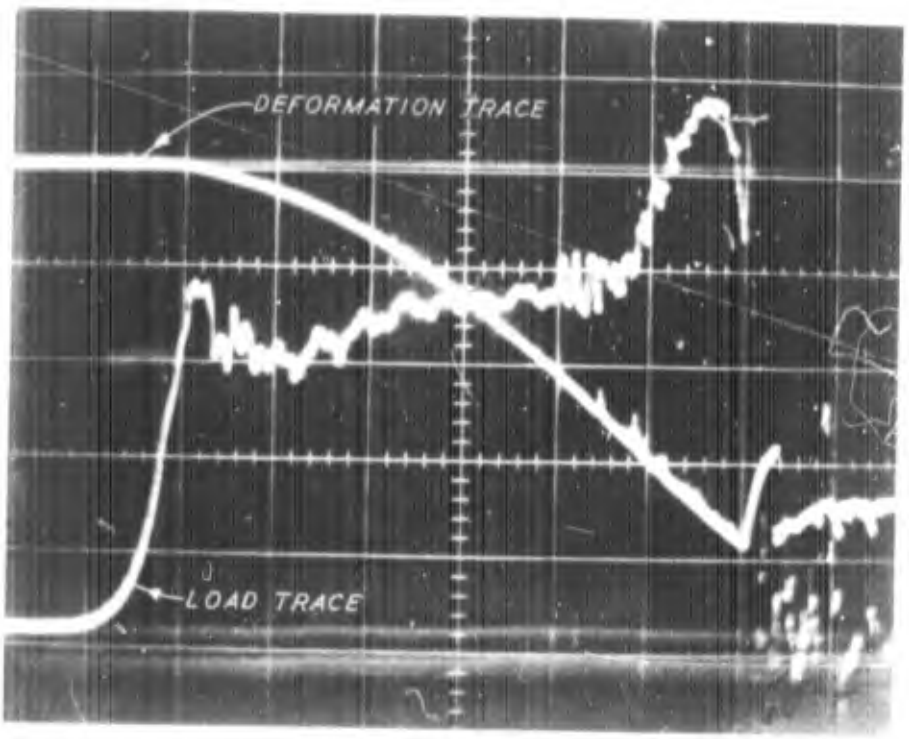

Figure 3.4 Typical test record for a rapid-loading test.

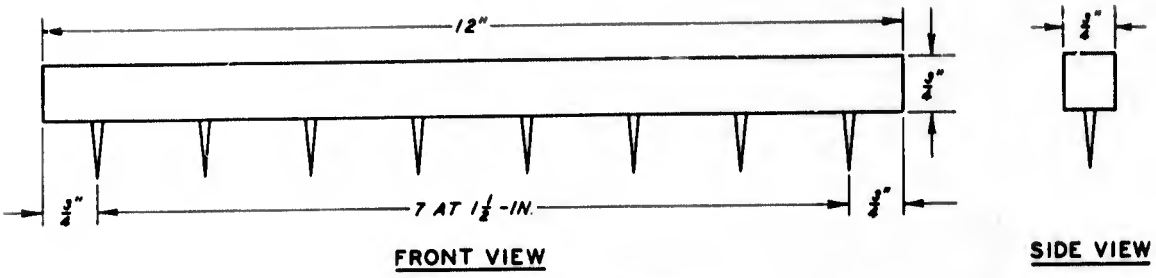

a. JOINT SCRIBER

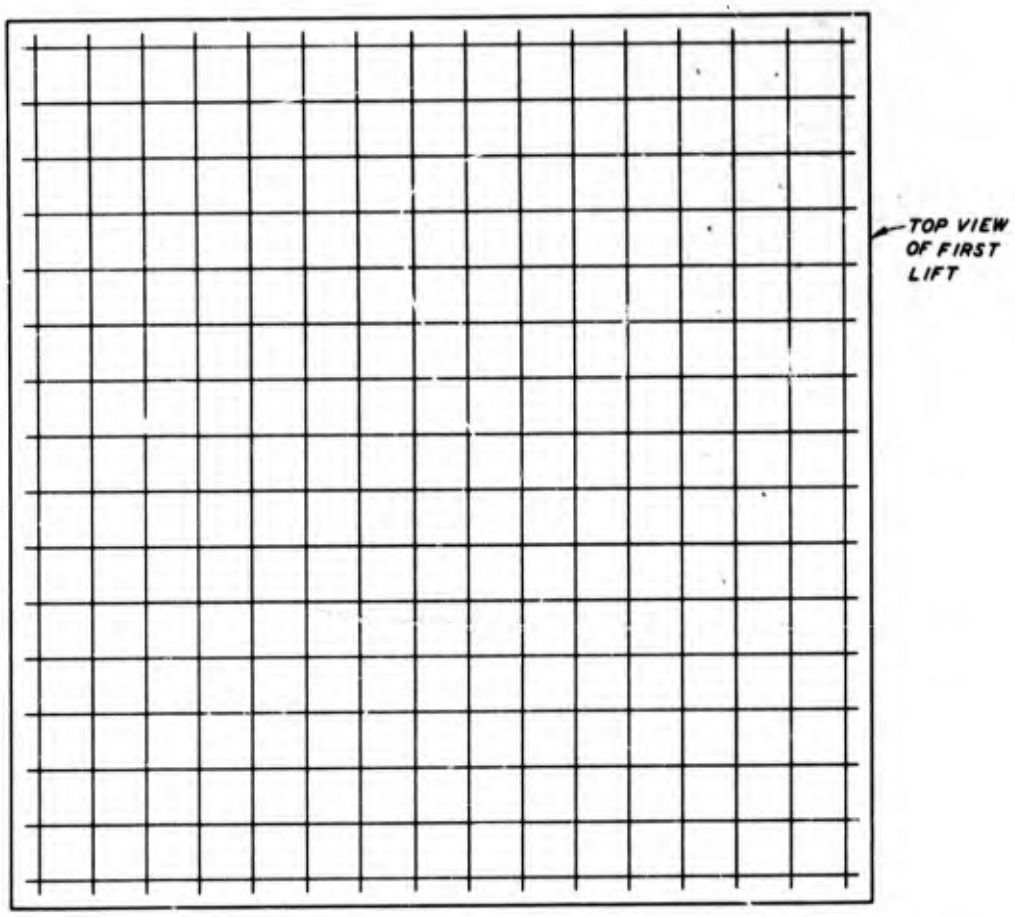

b. JOINT SCRIBE PATTERN

Figure 3.5 Joint scriber and scribe pattern.

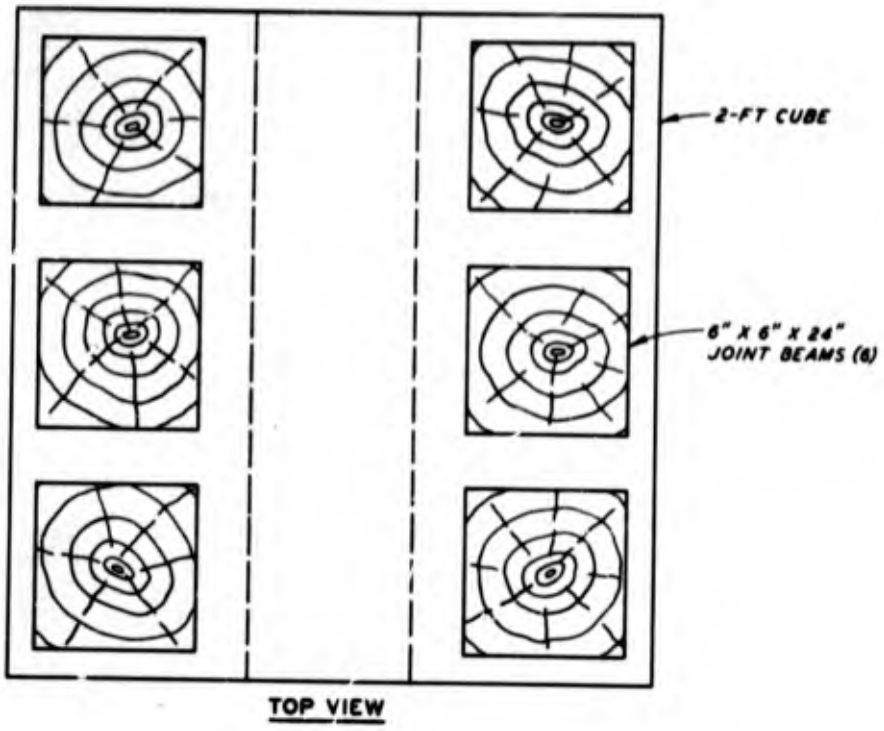

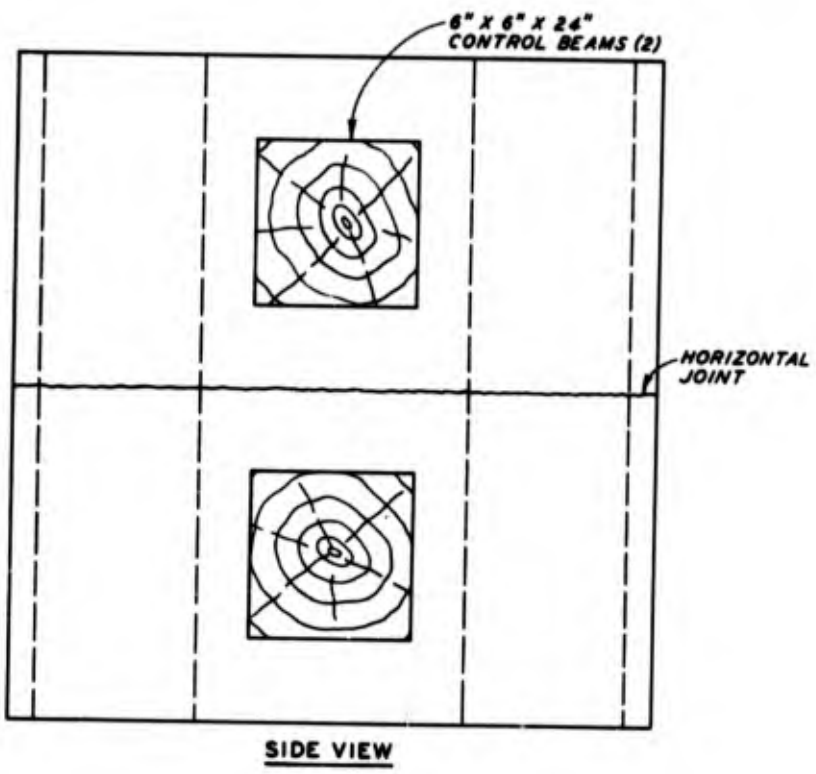

Figure 3.6 Horizontal joint study sampling schedule.

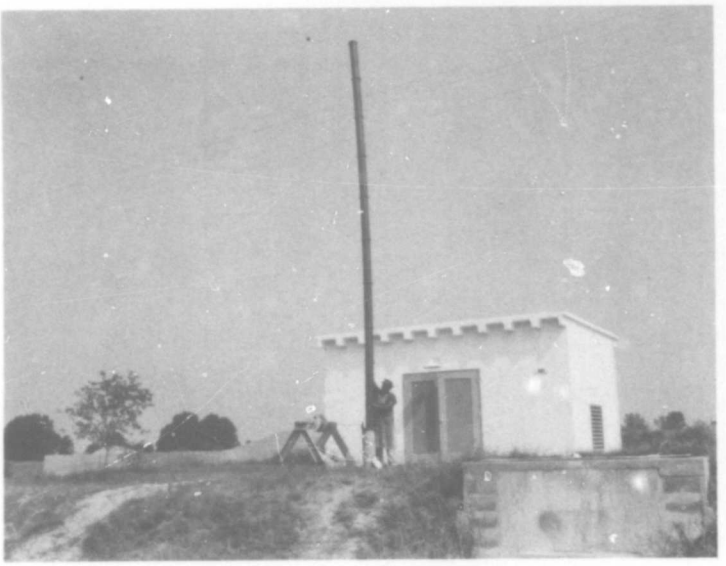

Figure 3.7 Lift height study, 30-foot column.

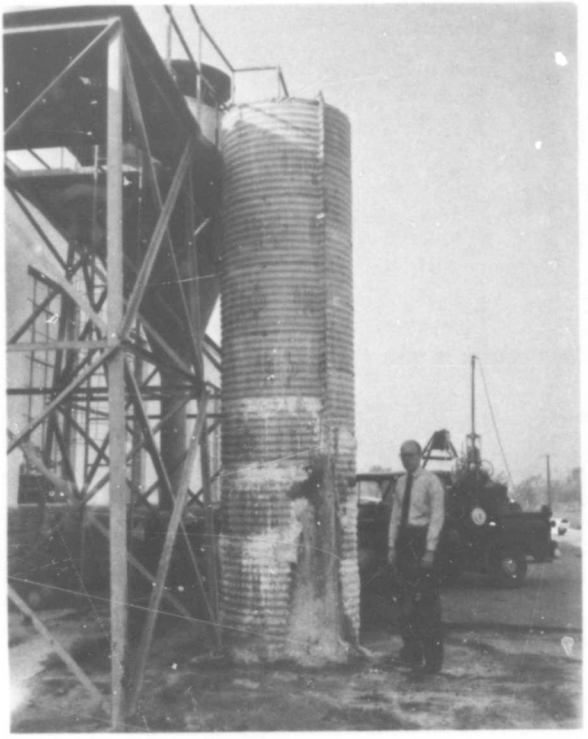

Figure 3.8 Lift height study, 16-foot column.

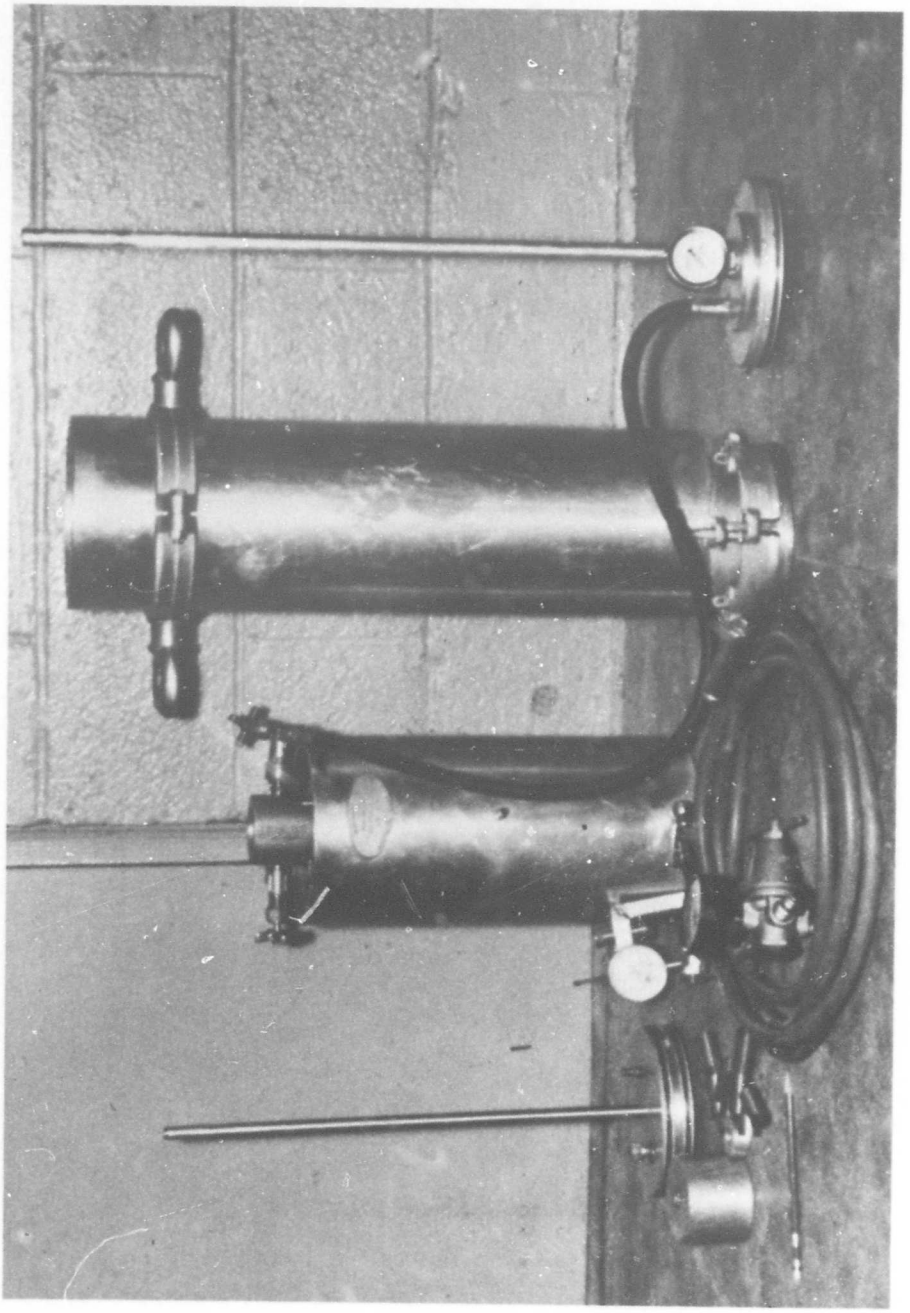

Figure 3.9 Pressure pycnometer.

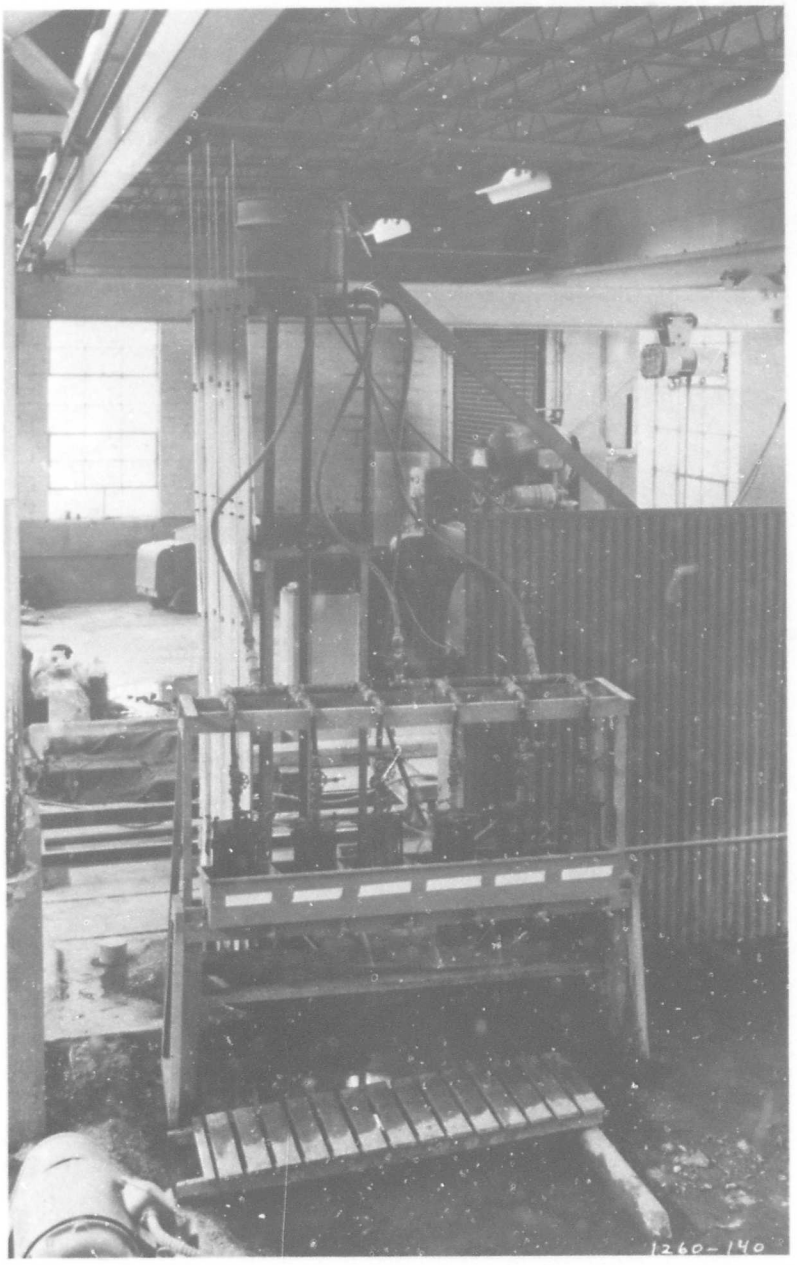

Figure 3.10 Low-head, unlimited reservoir permeability test equipment.

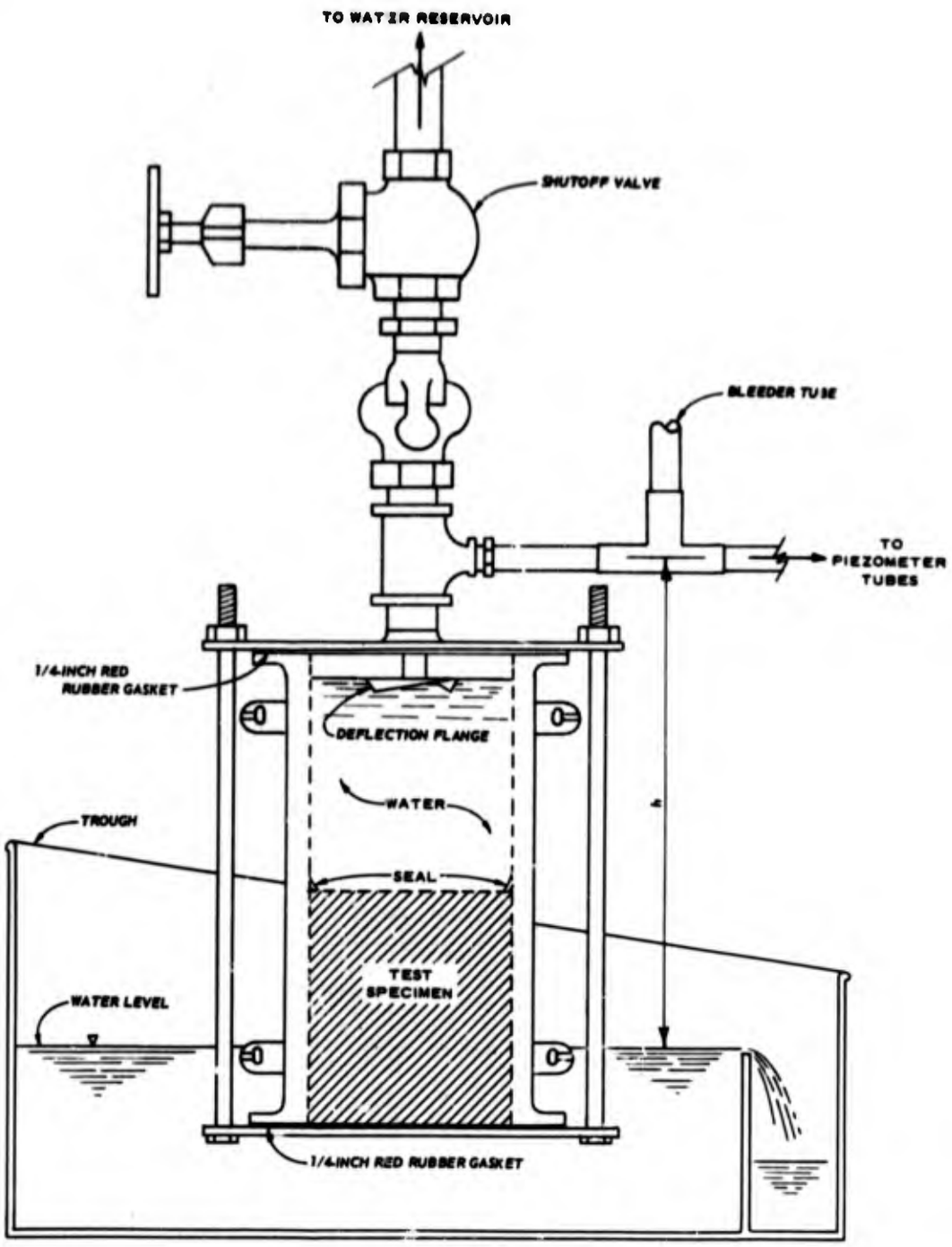

Figure 3.11 Specimen container.

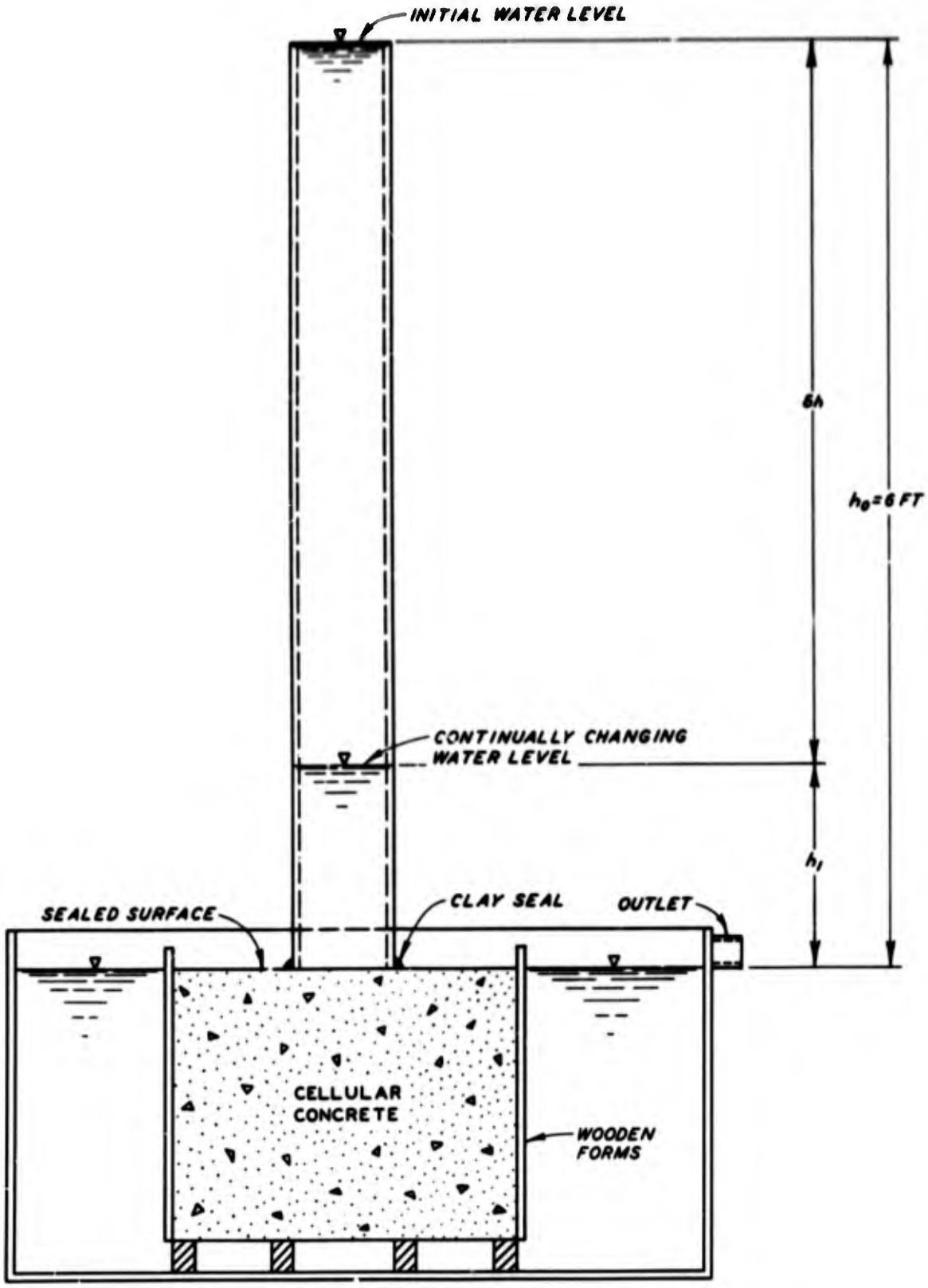

Figure 3.12 Sealer study falling head permeameter.

CHAPTER 4

TEST DATA AND ANALYSIS PLAN

4.1 CONSTRAINED STRENGTH DETERMINATIONS

All measured loads were converted to stress in pounds per square inch of area of contact of the loading piston. The stress to yield strain is predominantly a compressional stress and from yield strain to 40 percent deformation is a combination of compressive and shear stresses. The deformation of each sample was expressed as the amount of deformation per unit length of sample times 100 to equal percent deformation. Typical stress-deformation curves for the cellular concrete are shown in Figure 5.1.

In order to describe the stress-deformation characteristics of each sample tested in constrained compression, three values of stress are determined. These values in pounds per square inch are: (a) yield stress σ_y, (b) average stress to 40 percent deformation $\bar{\sigma}_{0.40}$, and (c) stress at 40 percent deformation $\sigma_{0.40}$. The percent of deformation at which the average stress $\bar{\sigma}_{0.40}$ occurs is midway between yield strain and 40 percent deformation. Yield strain can be assumed to be approximately 2 percent when not specifically given.

The values of yield strain ϵ_y, yield stress σ_y, and stress at 40 percent deformation $\sigma_{0.40}$ are obtained directly from the output records from each test. The average compressive stress between yield strain and 40 percent deformation for curves such as those shown in Figure 5.1 can be calculated by first determining the amount of plastic energy (nonrecoverable) U_p absorbed per unit volume of material. The general case for determining the absorbed plastic energy is:

$$U_p = \int_{\epsilon_y}^{\epsilon_{0.40}} \cdot \, d_\epsilon \qquad (4.1)$$

where U_p is equal to the area under the stress-deformation curve between the yield strain ϵ_y and 40 percent deformation $\epsilon_{0.40}$. The average stress $\bar{\sigma}_{0.40}$ to 40 percent deformation can then be expressed as:

$$\bar{\sigma}_{0.40} = \frac{U_p}{\epsilon_{0.40} - \epsilon_y} \tag{4.2}$$

Various techniques can be used to determine U_p . The stress-deformation records obtained from the constrained loading tests of this program were integrated by mechanical means.

4.2 MODULUS OF RUPTURE DETERMINATIONS

The flexural strength of concrete as determined from the third-point loading of simple beams (Test Method CRD-C 16) is characterized by a parameter, R , called the modulus of rupture. When the fracture occurred within the middle third of the span length as it did for all the flexural strength test beams and horizontal joint beams in the study, the modulus of rupture was calculated as

$$R = \frac{PL}{BD^2} \tag{4.3}$$

where

R = modulus of rupture, psi

P = maximum applied load, pounds

L = span length, inches

B = average width of beam specimen, inches

D = average depth of beam specimen, inches

4.3 ULTRASONIC PULSE VELOCITY DETERMINATIONS

The compressional wave velocity of concrete as determined from the ultrasonic pulse velocity test (Test Method CRD-C 51) is characterized by a parameter, V , called the pulse velocity. It is determined simply as

$$V = \frac{L}{T} \tag{4.4}$$

where

V = pulse velocity, ft/sec

L = path length, feet

T = effective time it takes the pulse to pass through the specimen, seconds

4.4 MODULUS OF ELASTICITY AND POISSON'S RATIO DETERMINATIONS

The electrical resistance strain gages provided output for both vertical and circumferential strains. X-Y recorders were used to put the output in the form of stress-strain curves. By using each test record separately and the secant technique at 40 percent of the yield strength of the concrete as shown on the record being used, the modulus of elasticity, E , was determined. Poisson's ratio was determined at the same point.

4.5 REGRESSION ANALYSIS

Where a sufficient range of freshly mixed densities and characterization parameters associated with these densities existed for a particular cellular concrete water-cement ratio, a relation between the density and the test parameter was developed. This was done for the characterization values representing stress, modulus of rupture, ultrasonic pulse velocity, and secant modulus of elasticity. Inspection and analysis of the data indicated that the line-of-best-fit as determined by least-squares techniques for the relations developed could be expressed in most cases in the form of a curvilinear regression of the equation

$$Y = aX^b \tag{4.5}$$

where

Y = characterization value (σ, R, V, or E)

X = freshly mixed density, pcf

a,b = equation coefficients

The graphical presentations of these relations include statistical

tolerance limits for the data. These limits were established from the standard error of the estimate, $S_{est,y}$, where:

$$S_{est,y} = \sum_{i=1}^{n} \frac{(y_i - y)^2}{n - 2} \tag{4.6}$$

and

y_i = observed dependent variable

y = predicted dependent variable

n = number of observations

An expression of $\pm 2\, S_{est,y}$ established statistical tolerance limits that enclosed the range within which approximately 95 percent of all future observations can be expected to fall.

4.6 DATA DISPERSION

When a number of observations were made of particular test measurements involving specified test variables, the measure of dispersion used for those observations was the standard deviation of a single observation. It was calculated as

$$s(x) = \sqrt{\frac{\Sigma x^2 - \bar{x}\,\Sigma x}{n - 1}} \tag{4.7}$$

where

$s(x)$ = standard deviation of a single observation

x = observed dependent variable

CHAPTER 5

TEST RESULTS

5.1 CONSTRAINED COMPRESSION TEST RESULTS

5.1.1 Slow-Loading Test Results. Each test produced a stress-deformation record similar to those shown in Figure 5.1. The curves in Figure 5.1 are typical of those obtained over the range of densities at each water-cement ratio. Using the stress characterization values, a relation between density and stress for each water-cement ratio was obtained. These relations are summarized in Table 5.1 and are shown graphically in Figures B.1 through B.15. Summaries of the curvilinear regressions for each characterization stress are shown in Figure 5.2.

5.1.2 Rapid-Loading Test Results. The stress-deformation curves were obtained by combining, on a common time basis, the two traces from each oscilloscope photograph. In each case, the resulting stress-deformation curve had the same general shape as the curve obtained from the slow-loading test of a companion specimen (see Figure 5.1). The characterizing stress values were different, however, and were used to develop the stress-density relations shown in Figures B.16 to B.27. These relations are summarized in Table 5.1 and in Figure 5.3.

5.1.3 Multiple-Shot Loading Test Results. Four cylinders each at densities of 21 and 45 pcf, and five cylinders each at densities of 29.5 and 40 pcf were evaluated. All the concrete had a water-cement ratio of 0.86. The stress-deformation curves were derived from oscilloscope records and were combined for each density so as to obtain an average stress-deformation curve for that density. The average curves for all four densities are shown in Figure 5.4.

5.2 FLEXURAL STRENGTH TEST RESULTS

5.2.1 Modulus of Rupture Test Results. A total of 180 flexure beams were tested. Concretes with water-cement ratios of 0.76, 0.86, 0.96, and 1.06 were evaluated with the number of beams for each water-cement ratio being 51, 44, 51, and 34, respectively. The beams for each water-cement ratio represented 11 batches of concrete with the exception of the

1.06 water-cement ratio where only 8 batches were made.

The results of the modulus of rupture determinations were related to the freshly mixed density and are shown in Figures B.28 to B.31. A summary of the regression analyses for this data is shown in Figure 5.5 and Table 5.2.

5.2.2 Horizontal Joint Test Results. A summary of the horizontal joint test results is shown in Table 5.3. In the few instances where data omissions occur, the samples from those blocks were not suitable for testing. One entire block (for the moist-cured, unprepared surface variables) did not have any satisfactory samples.

None of the joint beams experienced a failure across the joint. Only one of the fifty beams tested did not fail in the concrete from the lower lift.

5.3 ULTRASONIC PULSE VELOCITY TEST RESULTS

A total of 172, 6- by 12-inch cylinders were tested. Concretes with water-cement ratios of 0.66, 0.76, 0.86, and 0.96 were evaluated with the number of cylinders for each water-cement ratio being 36, 36, 48, and 52, respectively. The cylinders for each water-cement ratio represented 12 batches of concrete. In most instances, the ultrasonic pulse velocity was determined for each cylinder at ages of the concrete of 3, 7, 14, 28, and 60 days. The 0.86 and 0.96 water-cement ratio concrete cylinders were also evaluated at 90 and 180 days age.

Ultrasonic pulse velocity versus freshly mixed density relations were developed for each water-cement ratio and concrete age and are summarized in Figures 5.6 and 5.7. The line-of-best-fit in each case can be represented by the relation $X = aX^b$. A summary of the regression coefficients and related statistical information is given in Table 5.4. The effect of water-cement ratio on the pulse velocity for the range of densities evaluated at 28 days age is shown in Figure 5.8.

5.4 RATE-OF-HARDENING TEST RESULTS

One sample each from concretes with water-cement ratios of 0.76, 0.86, 0.96, and 1.06 and nominal densities of 23, 32, 39, and 43 pcf at each

water-cement ratio was evaluated. The resulting penetration resistance versus elapsed time curves (from the time the water in the mixture first came in contact with the cement) for each sample are shown in Figures 5.9 and 5.10. The median value of the freshly mixed density for the four batches representing each nominal density is also indicated along with the variation in density that occurred.

5.5 MODULUS OF ELASTICITY AND POISSON'S RATIO TEST RESULTS

Modulus of elasticity and Poisson's ratio determinations were made for concrete with nominal densities of 23, 32, 39, and 43 pcf each at water-cement ratios of 0.66, 0.76, 0.86, and 0.96. One batch of concrete at each density and water-cement ratio provided the specimens for those variables. A summary of the data is shown in Table 5.5. The modulus was determined using the secant technique at 40 percent of the yield strength of the concrete cylinder being tested. Poisson's ratio was determined at the same point.

Relations between the freshly mixed density at 28 days age and the secant modulus at the same age are shown for each water-cement ratio in Figures B.32 to B.35 and are summarized in Figure 5.11 and Table 5.6. The line-of-best-fit for the limited amount of data available was in the form $Y = aX^b$ in each case.

5.6 TEMPERATURE STUDY RESULTS

5.6.1 Adiabatic Temperature-Rise Results. Three batches of concrete were used to fill the adiabatic container. The concrete had an average freshly mixed density of 43.9 pcf and a cement content of 6.78 bags/cu yd. The temperatures of the mixture ingredients and resulting concrete at time of placement are shown in Table 5.7.

The adiabatic temperature development curve for the concrete is shown in Figure 5.12. Testing was terminated at 213 F because of the possibility of equipment damage due to the increasing water vapor pressure in the concrete.

5.6.2 Mixture Water-Temperature Results. The initial temperatures of the mixture ingredients and the temperature of the concrete when placed are

shown in Table 5.7. The temperature development curves for concretes made with mixing water temperatures of 40, 60, 80, and 100 F for both Type I (RC-554) and Type III (RC-560) cement are shown in Figure 5.13.

5.6.3 Lift Heat Effects Results. The concrete, made with both Type I (RC-554) and Type III (RC-560) cement, had a water-cement ratio of 0.86 with average (for both lifts) freshly mixed densities of 36.8 and 35.2 pcf, respectively, and cement contents of 4.75 and 4.95 bags/cu yd, respectively. The heat development curves for both lifts of both mixtures are shown in Figure 5.14 in the form of a temperature increase from the initial placing temperature versus elapsed time from initial placing of each lift. Peak temperatures of 170 and 182 F occurred in the bottom of the second lifts for the Type I and Type III mixtures, respectively.

5.6.4 Ambient Air Temperature Effects. The concrete was made at nominal densities of 23, 32, 39, and 43 pcf, all with a water-cement ratio of 0.86 by weight. The measure of damage due to the increased curing temperature was by visual inspection and resulted in only qualitative comparisons. These comparisons can be made from the photographs in Figures 5.15 and 5.16.

5.7 LIFT HEIGHT RESULTS

Figure 5.17 shows the hardened densities for both lift heights as functions of the depth of concrete in the lift. In the as-cast condition, the density appeared to vary approximately 7 pcf in a 16-foot lift and approximately 20 pcf in a 30-foot lift. The first 16 feet of the 30-foot lift showed a density change of approximately 12 pcf. The amount of evaporable water in the 16-foot lift appeared to be a fairly uniform amount over the entire lift height, varying from approximately 11 pcf near the top of the lift to 13 pcf at the bottom.

5.8 MOISTURE STUDY RESULTS

5.8.1 Saturation Results. The saturation data for the five cylinders evaluated were averaged and are presented in Figure 5.18 as the relation between available void space filled and water pressure. No measurable amounts of water, as dictated by the degree of sophistication of the

pycnometer, could be forced into the specimens after a water pressure of 1,200 psi was reached.

5.8.2 Flow and Erosion Test Results. Two specimens each of concrete with water-cement ratios of 0.76, 0.86, and 0.96 and nominal freshly mixed densities of 23, 32, and 43 pcf, respectively, were tested. All specimens were bag-cured 28 days before testing.

The waterhead was determined at any given time by the varying losses in the system. The densities of 23, 32, and 43 pcf had average heads of 5.10, 6.09, and 6.61 feet, respectively, over the test time period and range of water-cement ratios used.

The results of the flow portion of the tests are shown in Figures 5.19 and 5.20 for the 23- and 32-pcf concrete, respectively. The total flow time was approximately 50 hours for the 23-pcf concrete and 80 hours for the 32-pcf concrete. No flow was observed for the 43-pcf concrete.

The results of the erosion portion of the test are shown in Figures 5.21 and 5.22 for the 23- and 32-pcf concrete, respectively. The average total solids in the tap water prior to its passing through each specimen was 333 ppm. This determination and the other total solids measurements were made by evaporating the water samples at 194 F and drying the residue at 210 F.

5.8.3 Surface Sealer Test Results. The results of the sealer study are shown in Figure 5.23 in the form of a waterhead-time relation. The sealers showing little reduction in head with time can be considered as being more effective than those that show a rapid head loss with time. The reference numbers in Figure 5.23 correspond to the following sealer types: (1) no sealer, (2) styrene-butadiene product, (3) two-component epoxy thinned with a volatile solvent, (4) paraffin-resin mixture, (5) liquid latex, (6) vinyl based liquid-type solvent, (7) asphalt, (8) latex wall paint, (9) neat Type III cement slurry, and (10) hydraulic cement slurry.

TABLE 5.1 SUMMARY OF CONSTRAINED STRESS VERSUS FRESHLY MIXED DENSITY, CORRELATION REGRESSION COEFFICIENTS, $\sigma = a(d)^b \pm S_{est,y}$

Water-Cement Ratio	Freshly Mixed Density Range	No. of Samples	Yield Stress, σ_y				Average Stress to 40% Deformation, $\bar{\sigma}_{0.40}$				Stress at 40% Deformation, $\sigma_{0.40}$			
			a	b	$S_{est,y}$	Correlation Coefficient	a	b	$S_{est,y}$	Correlation Coefficient	a	b	$S_{est,y}$	Correlation Coefficient
	pcf													
Slow-Loading Tests:														
0.66	20 to 47	143	23.25×10^{-5}	3.875	50.2	0.952	10.82×10^{-5}	4.141	53.7	0.964	49.33×10^{-6}	4.407	69.6	0.964
0.76	22 to 43	98	32.76×10^{-5}	3.713	39.3	0.963	22.16×10^{-5}	3.873	37.0	0.978	11.81×10^{-5}	4.086	45.8	0.974
0.86	23 to 46	109	22.32×10^{-4}	3.095	25.5	0.944	14.06×10^{-4}	3.268	18.0	0.972	48.55×10^{-5}	3.605	28.9	0.970
0.96	18 to 44	64	30.79×10^{-4}	2.960	20.5	0.949	38.12×10^{-4}	2.927	18.3	0.980	22.99×10^{-4}	3.110	27.9	0.969
1.06	23 to 45	111	13.75×10^{-4}	2.625	21.0	0.943	64.61×10^{-4}	2.756	19.6	0.975	23.18×10^{-4}	3.080	28.3	0.961
Rapid-Loading Tests:														
0.76	23 to 43	47	17.99×10^{-4}	3.391	48.0	0.975	13.41×10^{-4}	3.478	47.6	0.981	37.97×10^{-5}	3.851	59.4	0.980
0.86	23 to 46	68	20.56×10^{-3}	2.643	52.4	0.963	15.62×10^{-3}	2.715	55.1	0.964	53.46×10^{-4}	3.039	63.8	0.973
0.96	18 to 43	46	28.73×10^{-3}	2.550	24.3	0.988	25.81×10^{-3}	2.558	18.8	0.994	14.73×10^{-3}	2.726	27.9	0.987
1.06	23 to 46	83	31.28×10^{-3}	2.467	42.3	0.935	24.71×10^{-3}	2.528	33.0	0.965	16.65×10^{-3}	2.657	52.9	0.951

TABLE 5.2 SUMMARY OF MODULUS OF RUPTURE VERSUS FRESHLY MIXED DENSITY, CORRELATION REGRESSION COEFFICIENTS, $R = a(d)^b \pm 2\, S_{est,y}$, psi

Water-Cement Ratio	Freshly Mixed Density Range	No. of Samples	Regression Coefficients		Standard Error of the Estimate $S_{est,y}$	Correlation Coefficient
			a	b		
	pcf					
0.76	23 to 42.8	51	2.740×10^{-3}	2.665	5.2	0.953
0.86	23 to 43	44	6.983×10^{-4}	2.970	4.0	0.971
0.96	22 to 43	51	6.569×10^{-4}	2.962	4.7	0.969
1.06	23 to 42	34	7.022×10^{-4}	2.930	2.9	0.979

TABLE 5.3 SUMMARY OF HORIZONTAL JOINT TEST RESULTS

Block No.	Surface Curing	Joint Surface	Lift Location	Cube Test Results					Beam Test Results					
				No. of Cubes	Oven-Dry Density		Cube Strength		Control Beams	Joint Beams			Failure Locations	
					Mean	s(x)	Mean	s(x)	Modulus of Rupture	No. of Beams	Modulus of Rupture	s(x)	Bottom Lift	Across Joint	Top Lift
					pcf	pcf	psi	psi	psi		psi	psi			
7	Air	Unprepared	Bottom	4	21.7	0.39	62.1	7.97	16.1	2	10.8	1.48	2	0	0
			Top	4	21.4	0.64	70.9	3.59	21.2						
8			Bottom	4	21.2	0.34	64.4	4.90	20.6	2	9.6	2.19	2	0	0
			Top	2	20.9	0.26	63.9	4.10	--						
9			Bottom	4	21.7	0.29	57.4	7.87	18.2	2	13.8	3.32	1	0	1
			Top	4	22.4	0.54	71.0	10.43	20.5						
14			Bottom	8	20.7	0.27	51.0	5.27	16.0	6	13.2	1.36	6	0	0
			Top	6	21.4	0.53	67.7	10.91	16.7						
2	Air	Prepared	Bottom	5	20.2	0.57	49.5	2.70	18.8	3	13.6	2.37	3	0	0
			Top	5	21.1	0.22	77.6	13.22	21.2						
4			Bottom	5	20.8	0.54	58.6	3.95	16.8	3	13.3	1.62	3	0	0
			Top	5	21.2	0.42	87.8	21.80	--						
5			Bottom	4	21.0	0.13	54.2	3.22	18.2	2	10.0	0.92	2	0	0
			Top	4	21.9	0.49	68.6	6.27	21.2						
8			Bottom	8	20.7	0.39	46.8	6.20	16.4	6	11.5	2.20	6	0	0
			Top	7	21.5	0.60	73.8	14.53	16.1						
11	Moist	Unprepared	Bottom	3	21.2	0.11	60.0	4.59	21.9	1	12.0	--	1	0	0
			Top	3	21.9	0.11	74.2	13.81	20.9						
17			Bottom	7	21.6	1.20	57.0	15.80	18.3	6	13.5	4.13	6	0	0
			Top	8	21.6	0.35	67.2	4.31	18.5						
19			Bottom	6	21.6	0.55	65.8	7.01	22.3	4	16.6	1.74	6	0	0
			Top	6	21.5	0.39	65.4	5.96	22.9						
1	Moist	Prepared	Bottom	5	20.5	0.20	50.4	4.93	17.0	3	12.8	0.46	3	0	0
			Top	5	21.0	0.17	92.6	6.38	19.4						
3			Bottom	4	21.2	0.37	55.0	6.44	18.5	2	15.3	3.54	2	0	0
			Top	4	21.1	0.33	70.4	4.87	18.5						
6			Bottom	5	21.5	0.27	58.6	3.50	17.4	2	20.0	6.01	2	0	0
			Top	5	22.9	0.62	79.8	12.55	20.6						
15			Bottom	8	21.3	0.37	51.5	3.75	15.7	6	13.1	1.07	6	0	0
			Top	8	21.6	0.70	65.3	6.93	18.9						

TABLE 5.4 SUMMARY OF ULTRASONIC PULSE VELOCITY VERSUS FRESHLY MIXED DENSITY, CORRELATION REGRESSION COEFFICIENTS, $V = ad^b \pm 2 S_{est,y}$

Age	w/c = 0.66					w/c = 0.76					w/c = 0.86					w/c = 0.96				
	No. of Observations	a	b	Standard Error of Estimate $S_{est,y}$	Correlation Coefficient	No. of Observations	a	b	Standard Error of Estimate $S_{est,y}$	Correlation Coefficient	No. of Observations	a	b	Standard Error of Estimate $S_{est,y}$	Correlation Coefficient	No. of Observations	a	b	Standard Error of Estimate $S_{est,y}$	Correlation Coefficient
days				ft/sec					ft/sec					ft/sec					ft/sec	
3	36	154.45	0.897	146	0.985	36	368.75	0.621	129	0.972	48	274.71	0.647	191	0.915	36	685.45	0.345	64	0.934
7	36	189.22	0.875	203	0.977	36	344.37	0.680	11	0.983	48	297.17	0.660	232	0.909	36	562.92	0.476	82	0.973
14	36	187.73	0.896	193	0.982	36	332.18	0.716	144	0.984	48	258.41	0.744	181	0.962	52	506.26	0.543	75	0.984
28	36	215.16	0.870	194	0.982	36	374.23	0.696	119	0.988	48	308.36	0.722	235	0.948	52	495.49	0.575	86	0.985
60	36	225.59	0.863	211	0.979	36	428.81	0.668	133	0.986	48	334.10	0.724	249	0.951	52	499.98	0.586	85	0.986
90	--	--	--	--	--	--	--	--	--	--	48	312.58	0.747	281	0.944	52	542.45	0.564	114	0.973
180	--	--	--	--	--	--	--	--	--	--	34	356.82	0.714	244	0.959	52	570.58	0.549	105	0.977

TABLE 5.5 SUMMARY OF MODULUS OF ELASTICITY AND POISSON'S RATIO DATA

Water-Cement Ratio	Freshly Mixed Density	No. of Tests	Yield Stress, σ_y		Yield Strain, ϵ_y		Poisson's Ratio[b]		Secant Modulus of Elasticity[b]	
			Mean	s(x)[a]	Mean	s(x)[a]	Mean	s(x)[a]	Mean	s(x)[a]
	pcf		psi	psi	in/in	in/in			psi	psi
0.66	22.8	4	19	1.0	1,322	88	0.198	0.023	17,370	2,320
	32.2	5	78	7.4	1,334	207	0.219	0.014	69,770	3,650
	38.4	5	213	25.4	1,826	282	0.205	0.025	140,930	20,490
	43.2	5	257	54.7	1,508	362	0.195	0.018	188,190	9,890
0.76	23.6	4	34	1.5	1,355	115	0.227	0.015	33,700	720
	31.8	5	74	9.1	1,428	256	0.250	0.013	63,930	1,000
	39.0	5	166	13.9	1,548	82	0.205	0.029	121,950	13,960
	43.8	3	213	25.8	1,460	227	0.193	0.009	167,680	5,070
0.86	23.6	5	22	0.7	1,060	42	0.252	0.039	26,850	860
	32.0	5	57	6.5	1,000	41	0.201	0.025	72,620	6,740
	39.4	5	106	18.1	1,182	246	0.227	0.023	110,030	5,640
	43.0	5	160	17.0	1,404	235	0.226	0.017	145,980	2,780
0.96	23.2	5	21	1.5	1,032	33	0.234	0.012	22,720	860
	31.6	5	29	2.9	544	43	0.192	0.041	59,850	8,770
	39.2	4	56	11.4	650	133	0.237	0.034	92,440	9,600
	43.0	5	55	2.7	562	23	0.214	0.016	105,370	2,000

[a] s(x) = standard deviation of a single observation.

[b] Calculated at 0.4 σ_y .

TABLE 5.6 SECANT MODULUS OF ELASTICITY VERSUS HARDENED DENSITY RELATION, $E_s = a(d)^b \pm 2\, S_{est,y}$

All concrete made with Foaming Agent M and evaluated at the as-cast moisture condition.

Water-Cement Ratio	No. of Specimens	Density Range	a	b	$S_{est,y}$	Correlation Coefficient
		pcf				
0.66	19	22.8 to 43.2	0.00023	3.637	14.15	0.993
0.76	17	23.6 to 43.8	0.00797	2.623	9.90	0.990
0.86	20	23.6 to 43.0	0.00449	2.765	6.70	0.992
0.96	19	23.2 to 43.0	0.00914	2.507	6.10	0.983

TABLE 5.7 SUMMARY OF TEMPERATURE-RISE STUDY BATCHING DATA

Cement	Round No.	Water-Cement Ratio	Freshly Mixed Density	Initial Temperature, °F			
				Water	Cement	Slurry	Concrete
			pcf				
Type I (RC-566)	1	0.86	35.6	40	65	50	58
	2	0.86	35.2	60	65	64	67
	3	0.86	35.0	80	65	82	80
	4	0.86	33.6	100	65	94	92
Type III (RC-567)	1	0.86	37.6	40	65	45	58
	2	0.86	36.8	60	65	65	69
	3	0.86	35.6	80	65	81	82
	4	0.86	36.4	100	65	95	92
Adiabatic Test:							
Type III (RC-567)	Avg of three batches	0.86	43.9	42	60	50	52

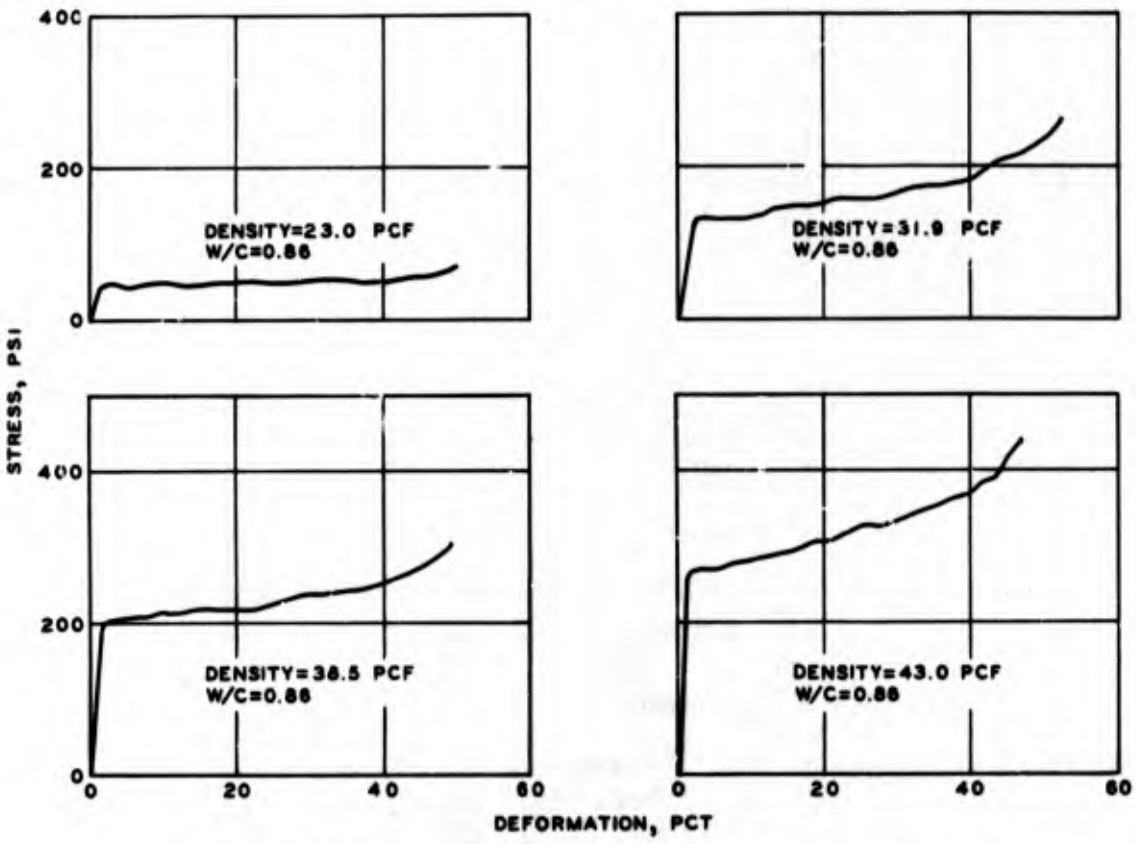

Figure 5.1 Typical stress-deformation curves.

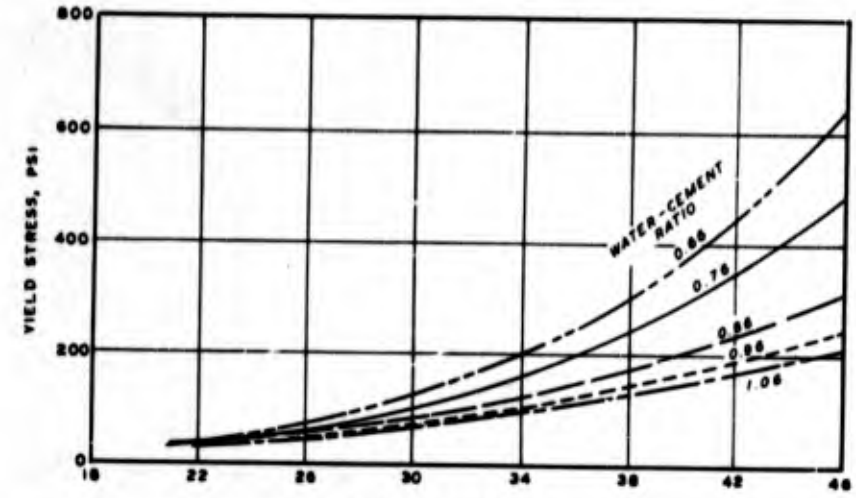

a. YIELD STRESS

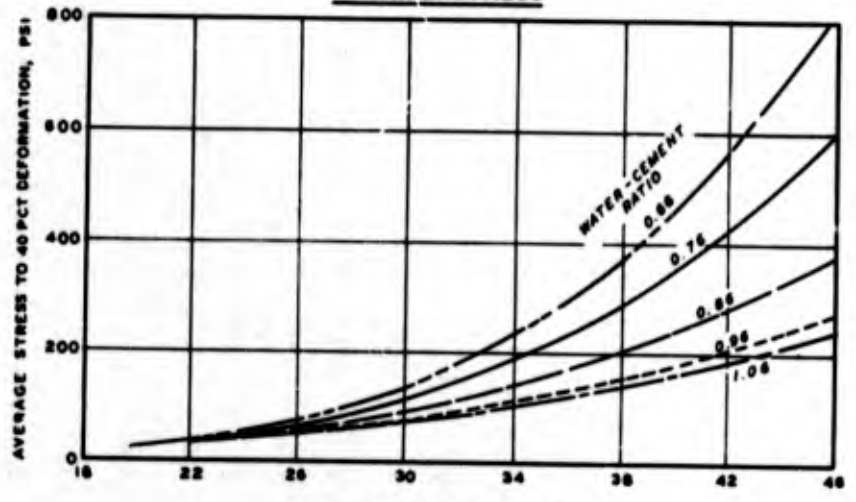

b. AVERAGE STRESS

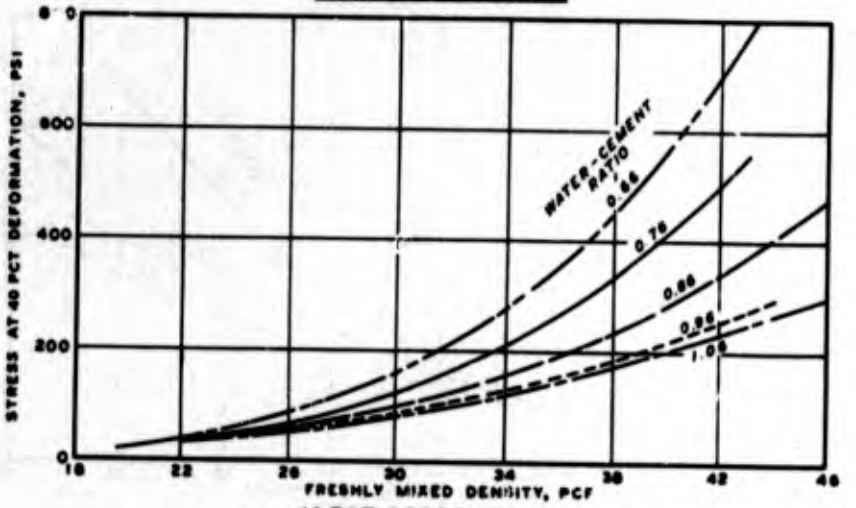

c. 40 PCT DEFORMATION

Figure 5.2 Summary of stress versus freshly mixed density relations, slow-loading tests, 28-day strength.

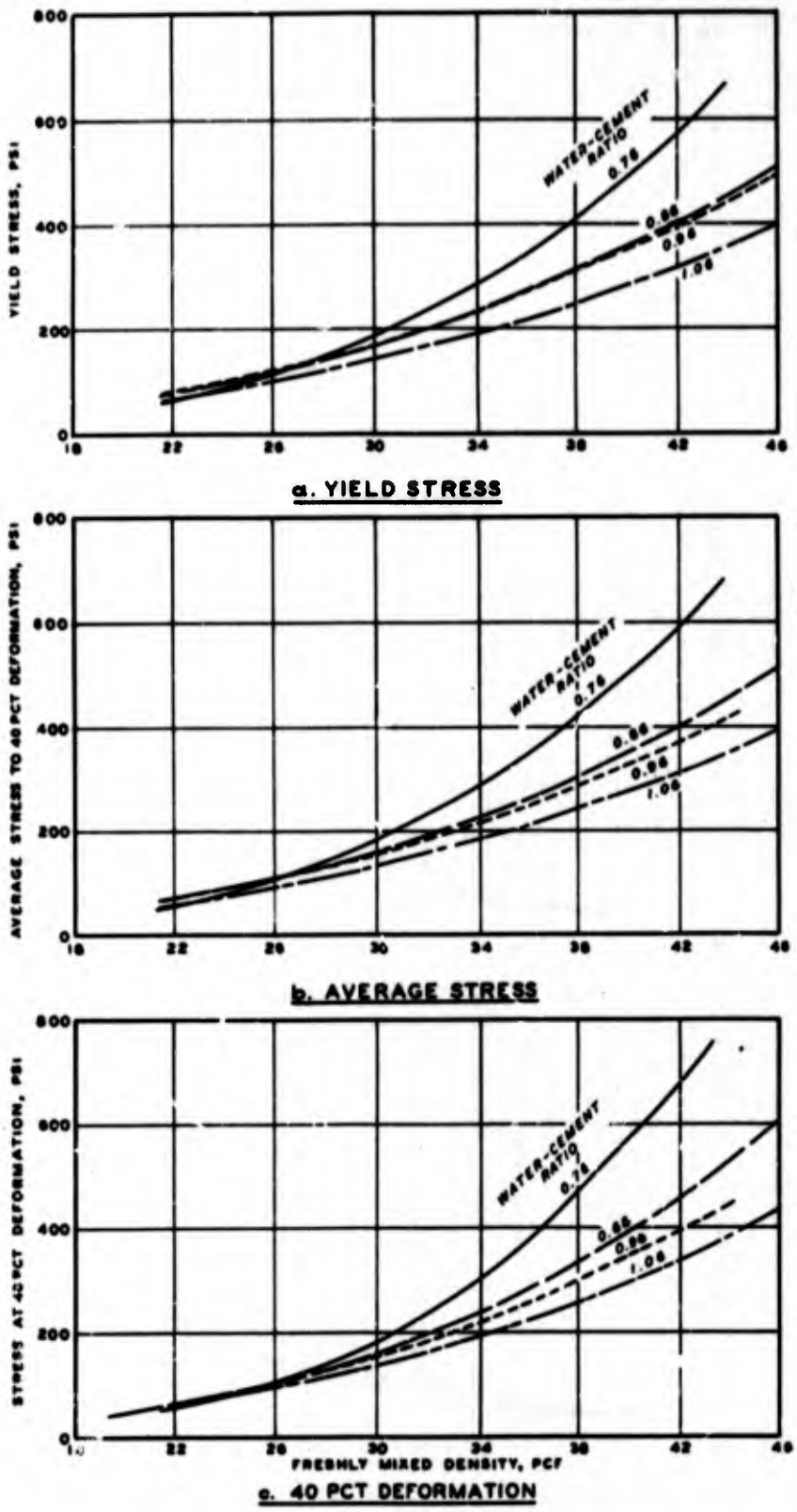

Figure 5.3 Summary of stress versus freshly mixed density relations for rapid-loading tests, 28-day strength.

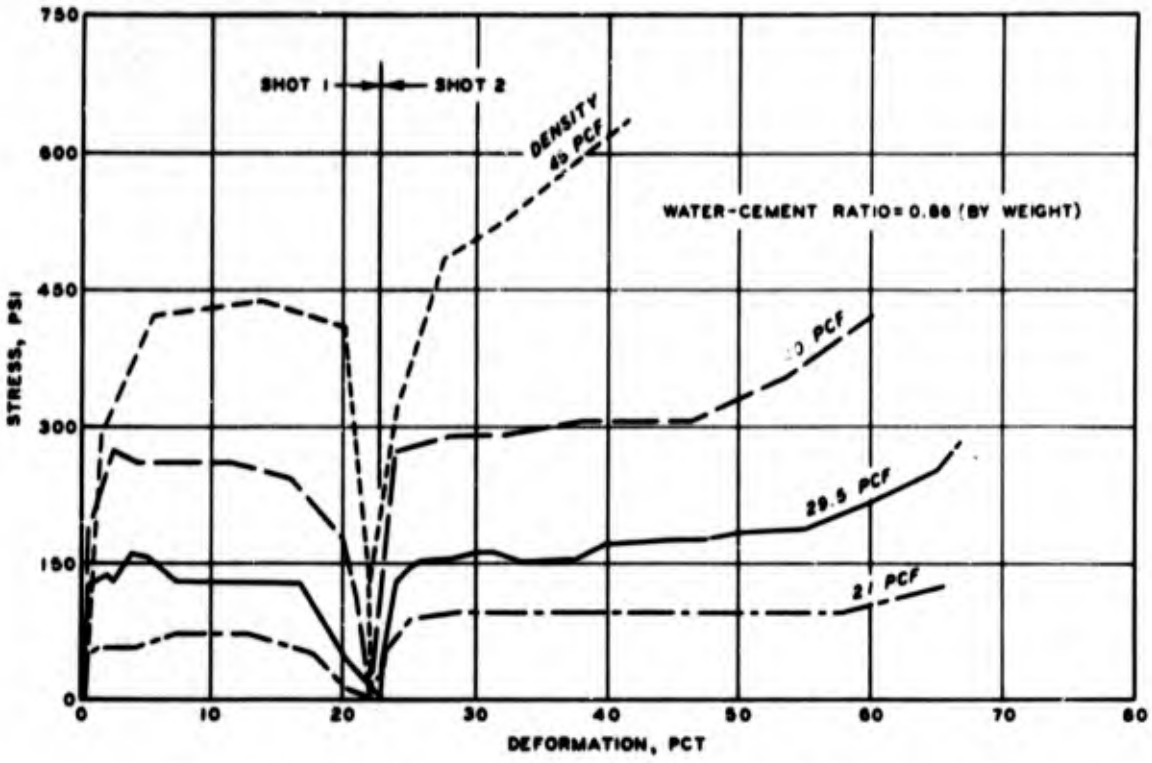

Figure 5.4 Stress-deformation relations for multiple-shot loading.

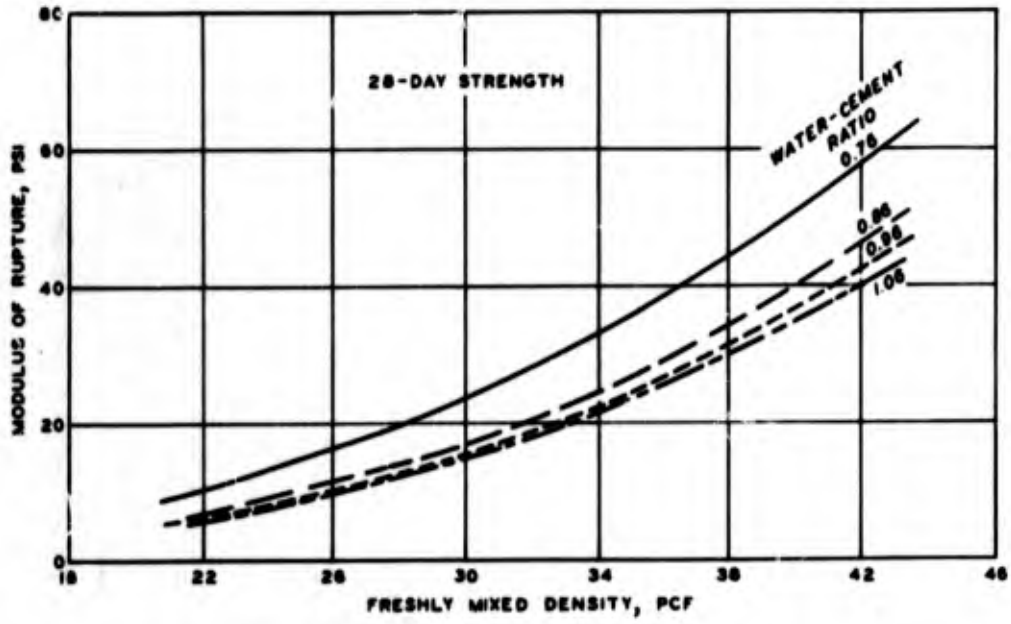

Figure 5.5 Summary of the modulus of rupture versus freshly mixed density relations.

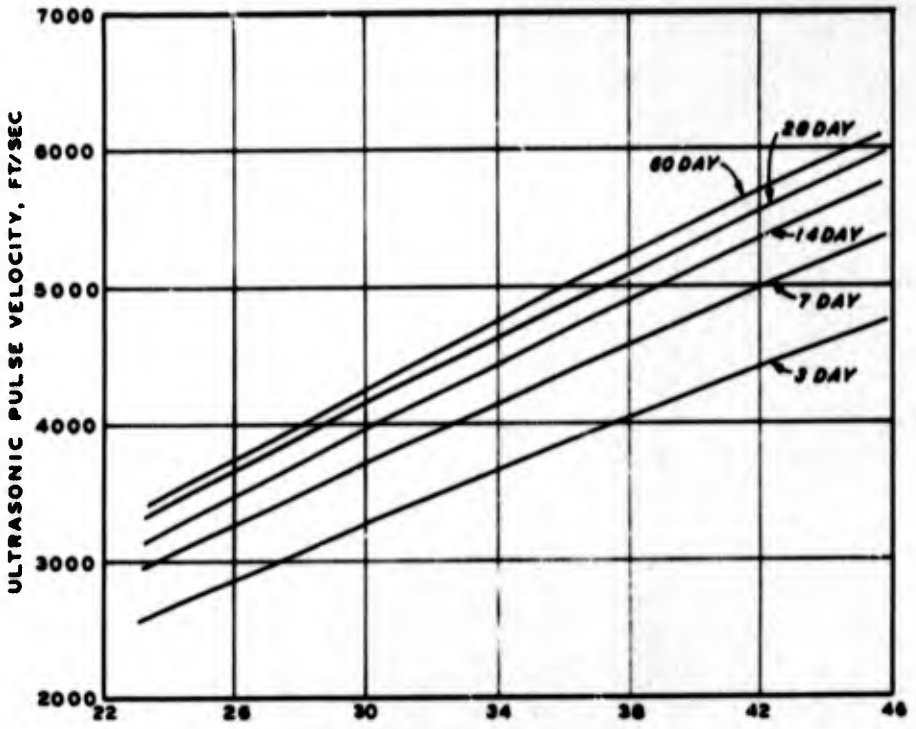

a. WATER-CEMENT RATIO 0.66

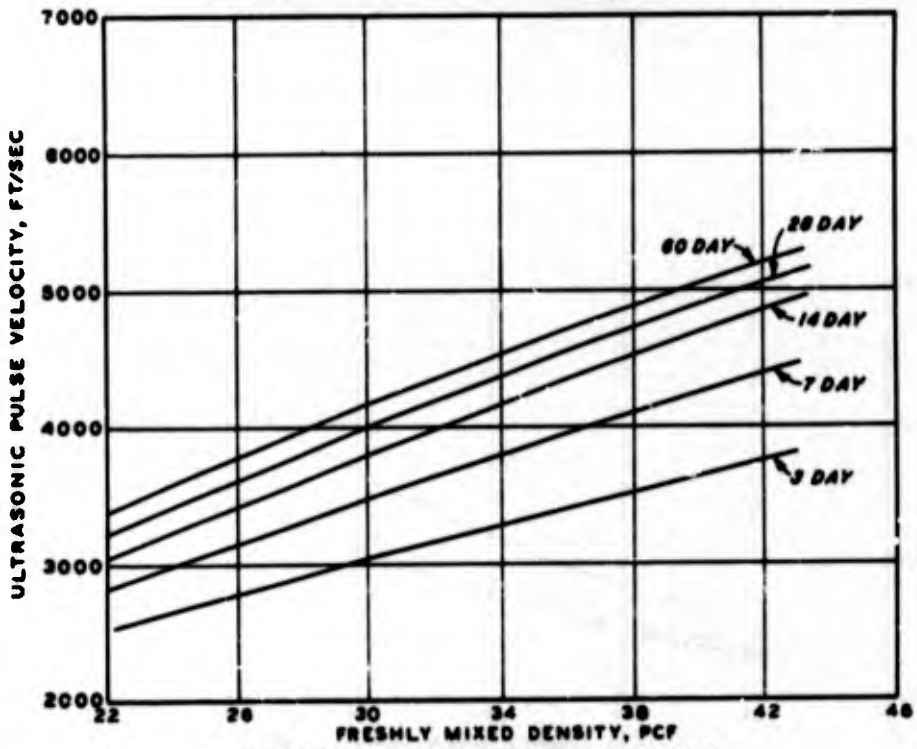

b. WATER-CEMENT RATIO 0.76

Figure 5.6 Summary of ultrasonic pulse velocity versus freshly mixed density relations for water-cement ratios 0.66 and 0.76.

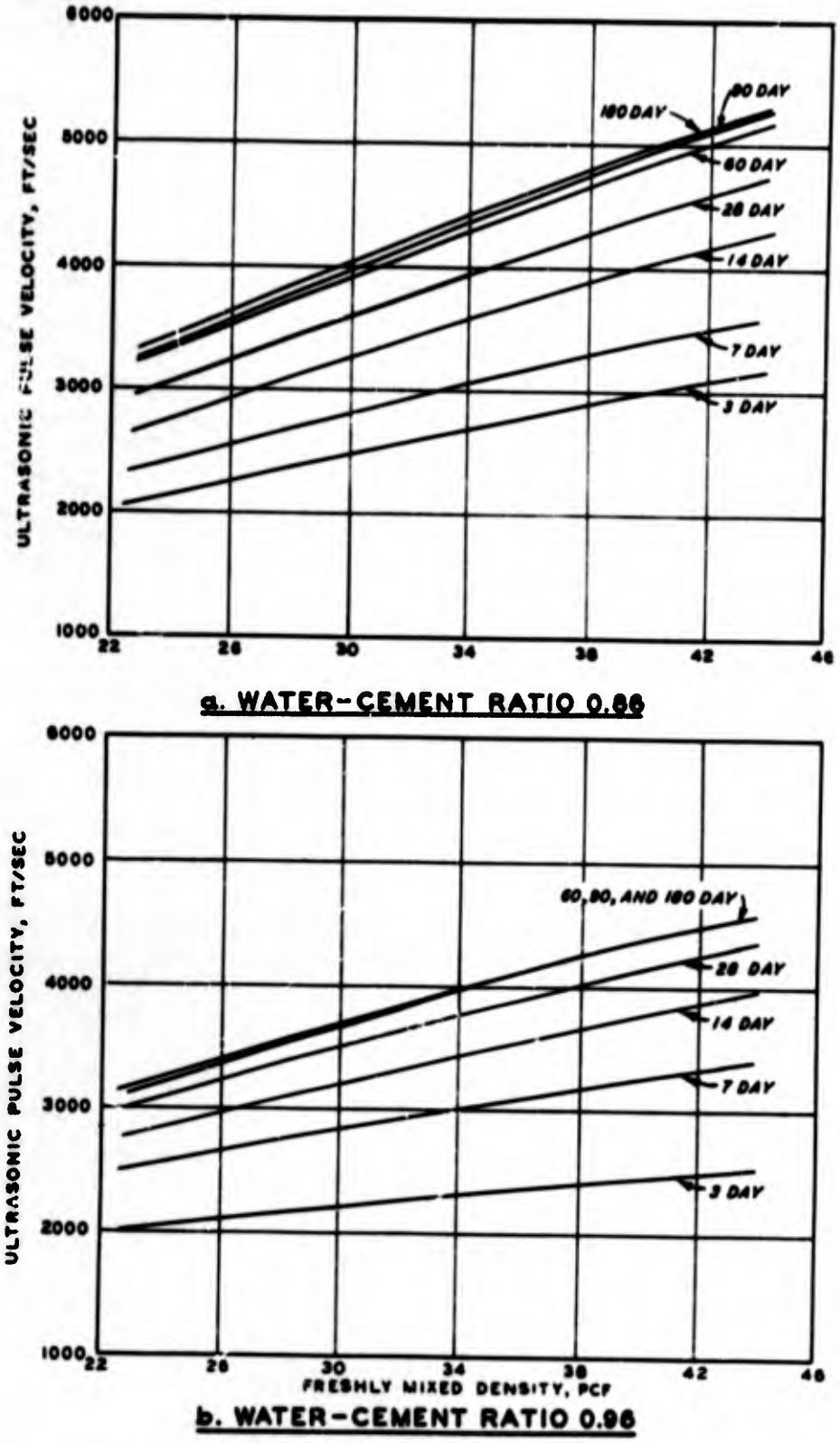

Figure 5.7 Summary of ultrasonic pulse velocity versus freshly mixed density relations for water-cement ratios 0.86 and 0.96.

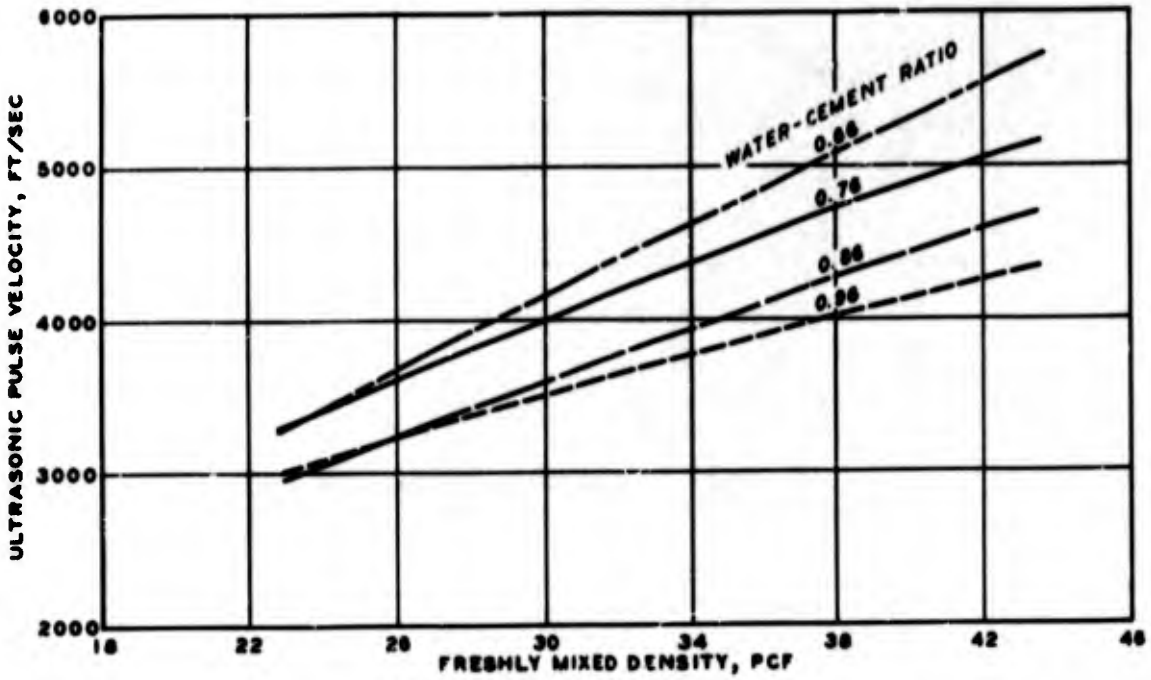

Figure 5.8 Summary of ultrasonic pulse velocity versus freshly mixed density relations showing effect of water-cement ratio, 28 days age.

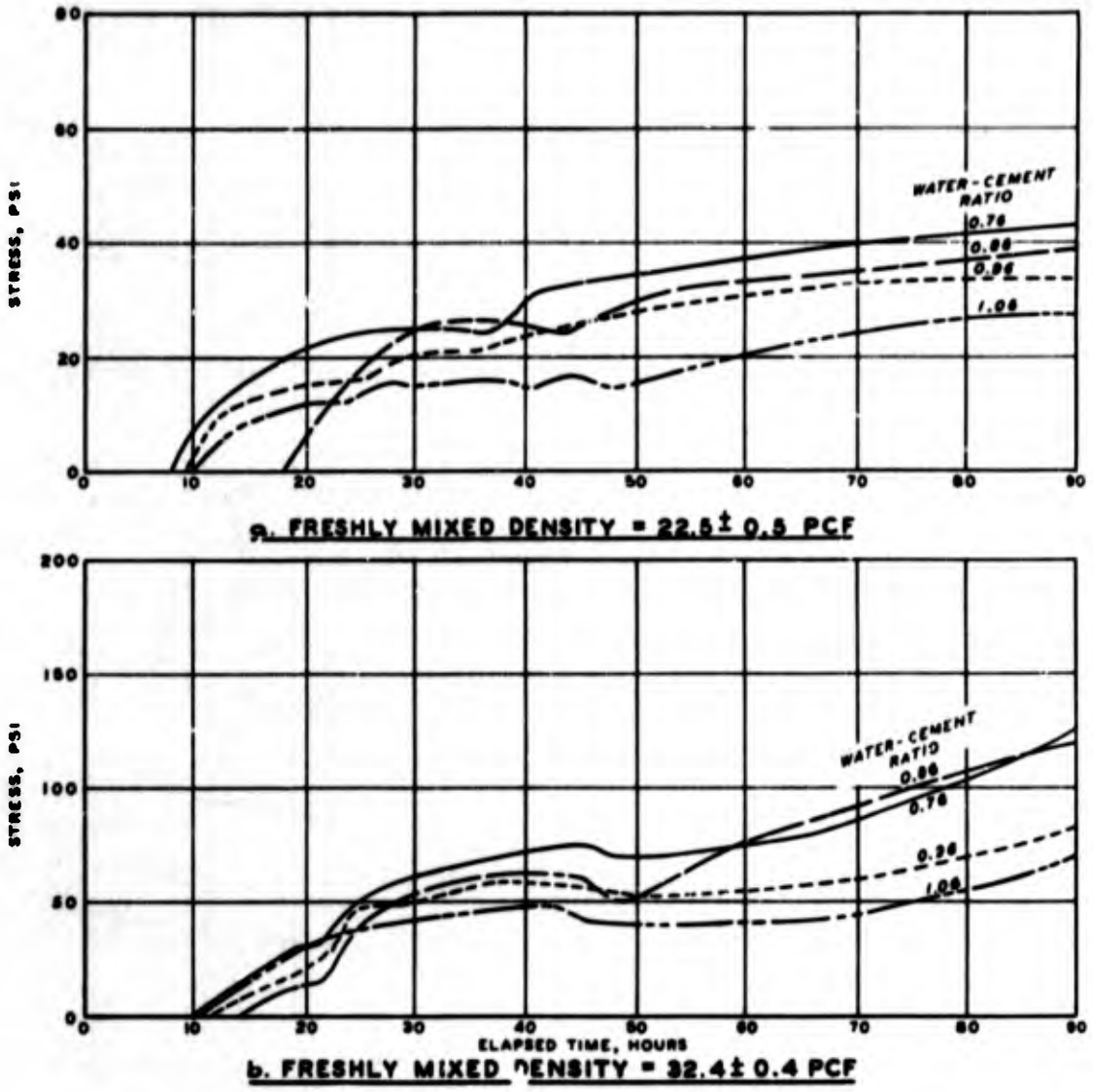

Figure 5.9 Penetration resistance versus time relations for 23- and 32-pcf nominal density concretes.

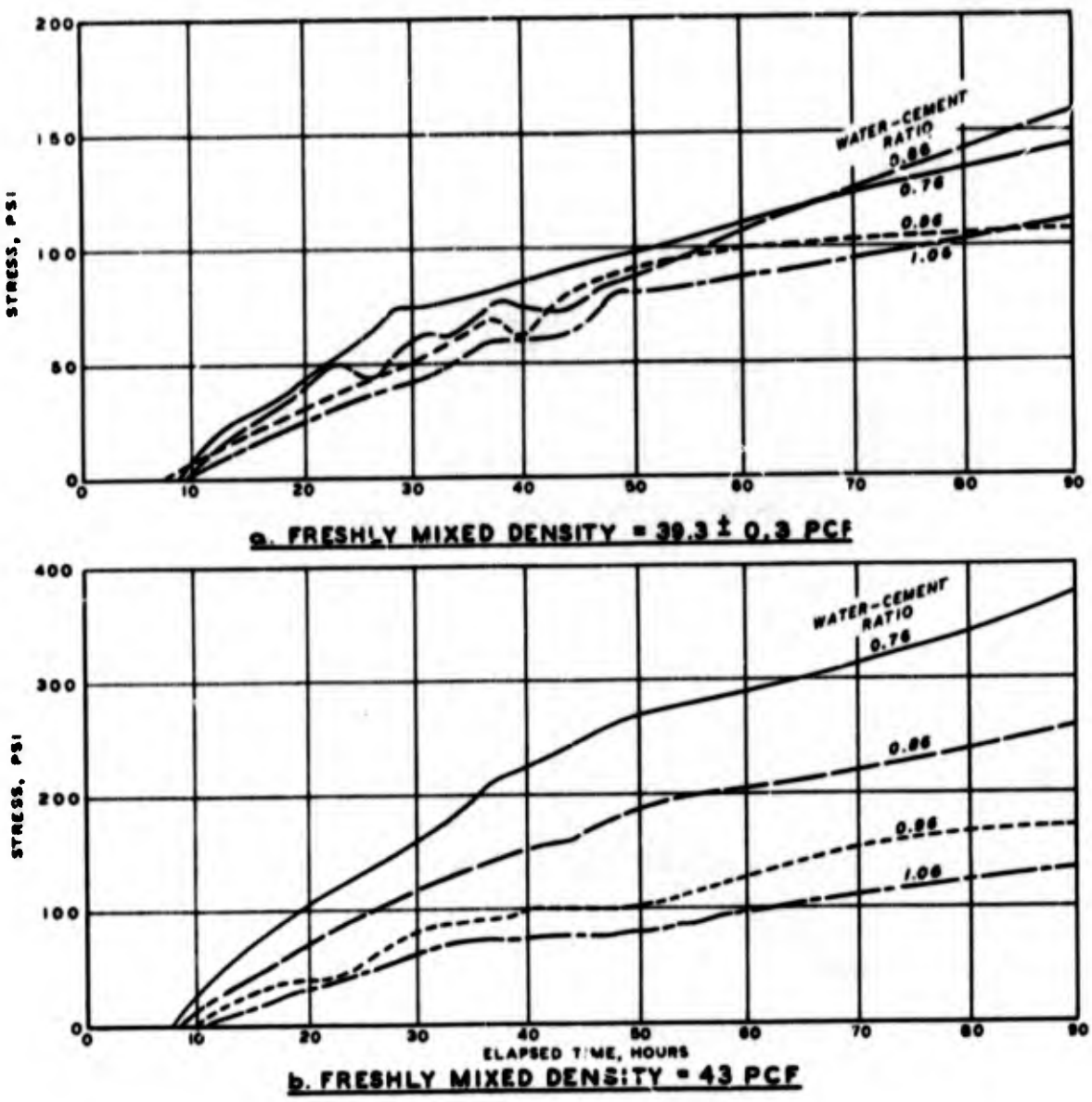

Figure 5.10 Penetration resistance versus time relation for 39- and 43-pcf nominal density concretes.

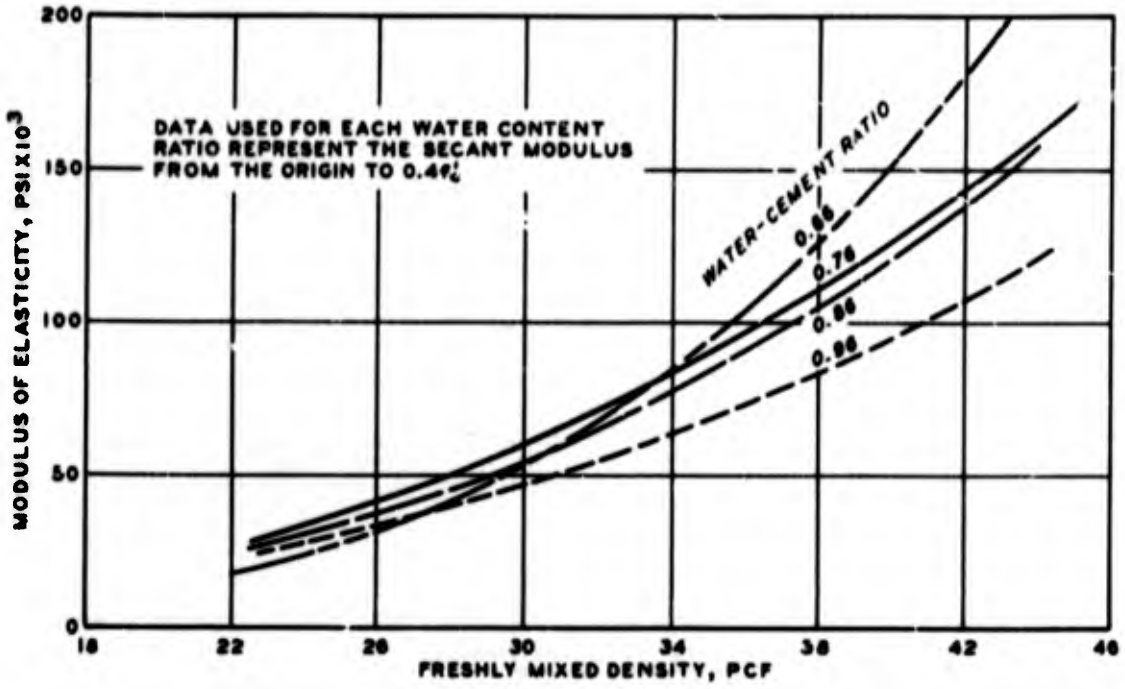

Figure 5.11 Summary of secant modulus of elasticity versus freshly mixed density relations.

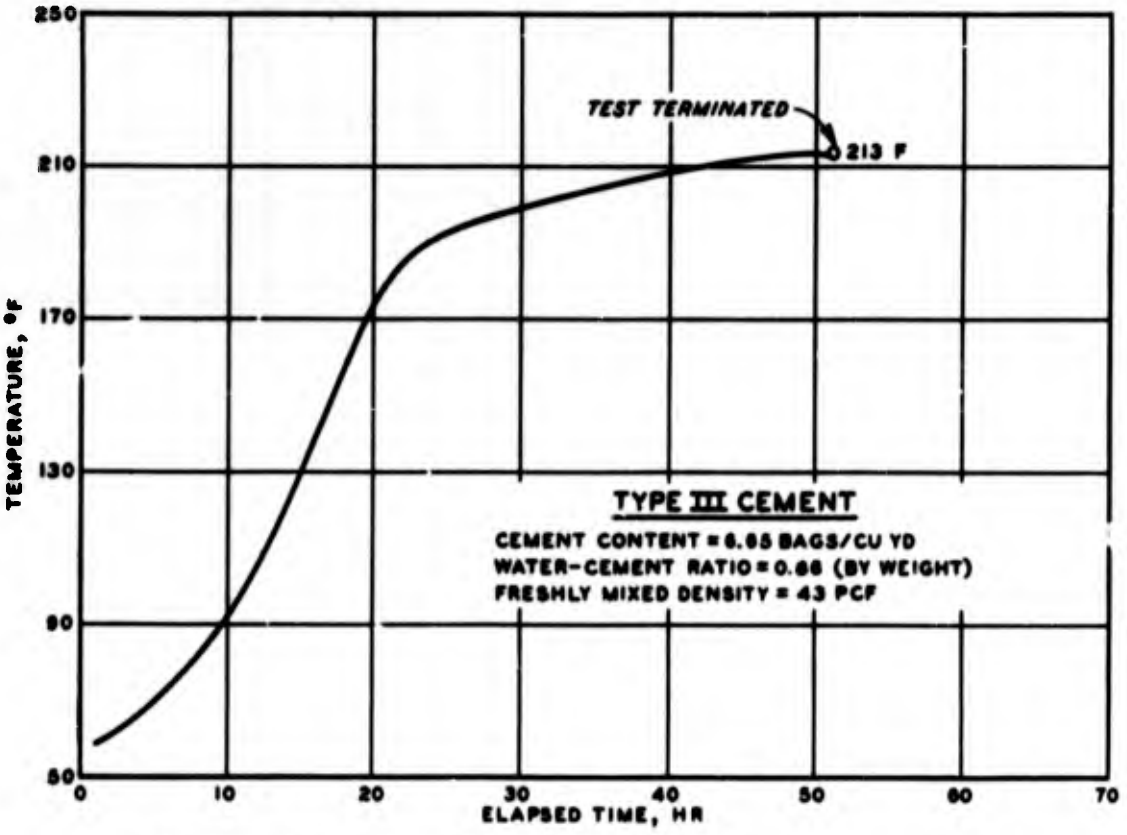

Figure 5.12 Adiabatic temperature development curve.

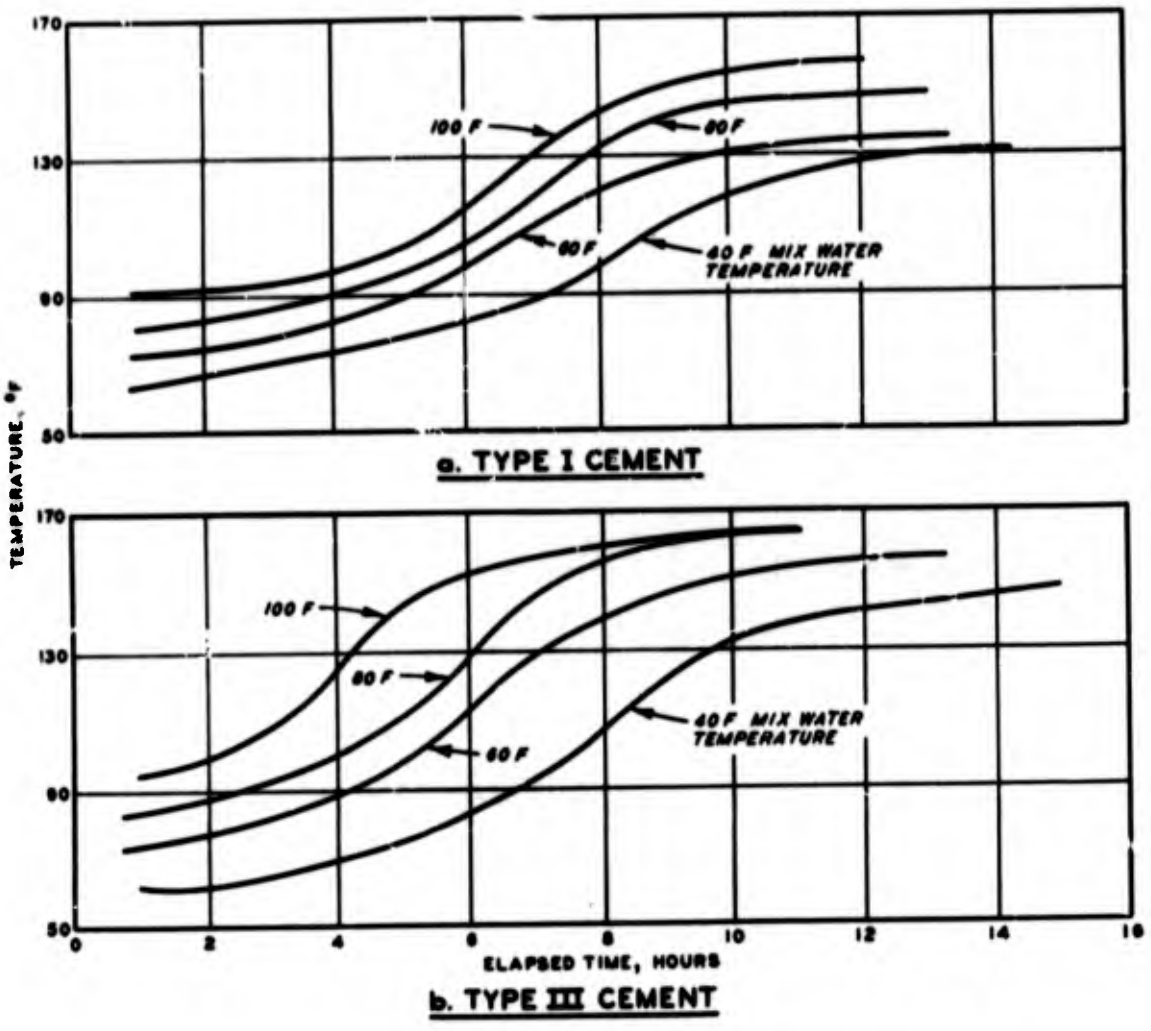

Figure 5.13 Effect of mixture water temperature on early-age heat.

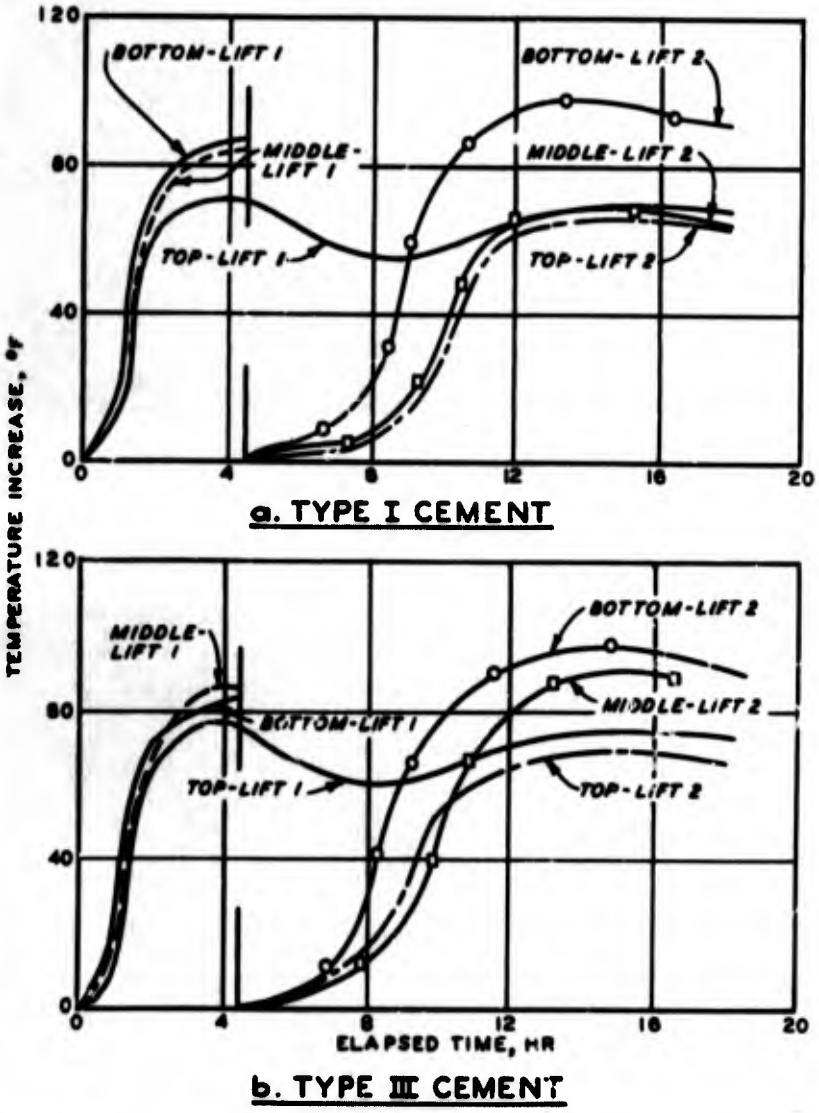

Figure 5.14 Fffect of hydration heat on adjoining lifts of concrete.

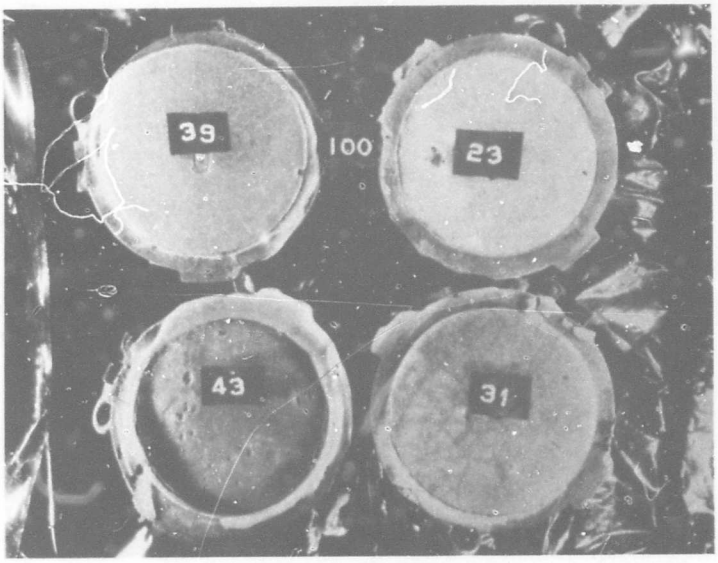

a. Top view.

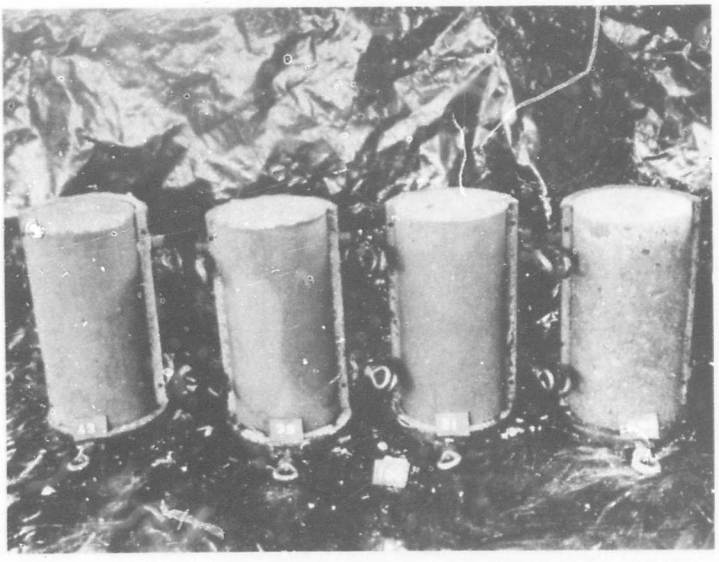

b. Side view.

Figure 5.15 Effect of 100 F air-curing temperature.

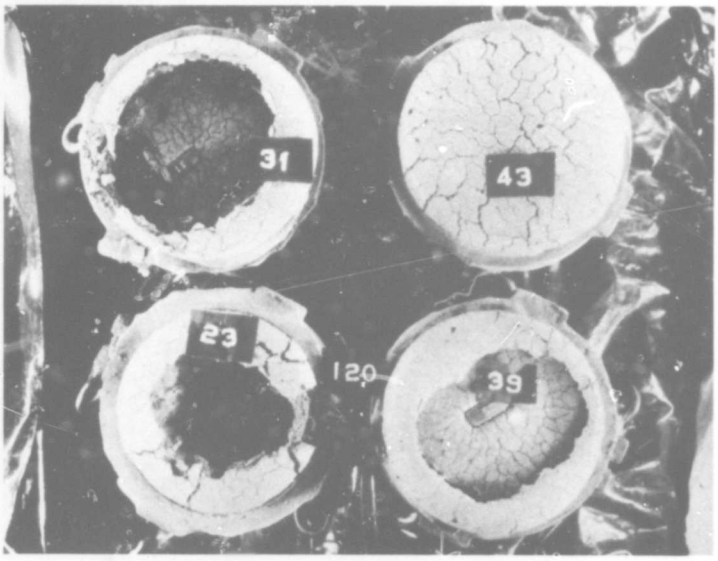

a. Top view.

b. Side view.

Figure 5.16 Effect of 120 F air-curing temperature

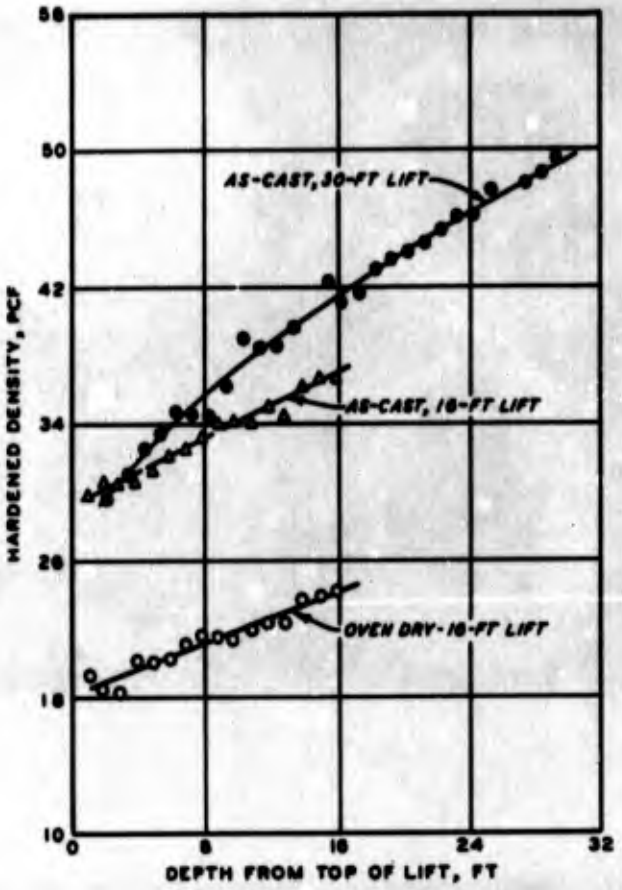

Figure 5.17 Effect of lift height on concrete density.

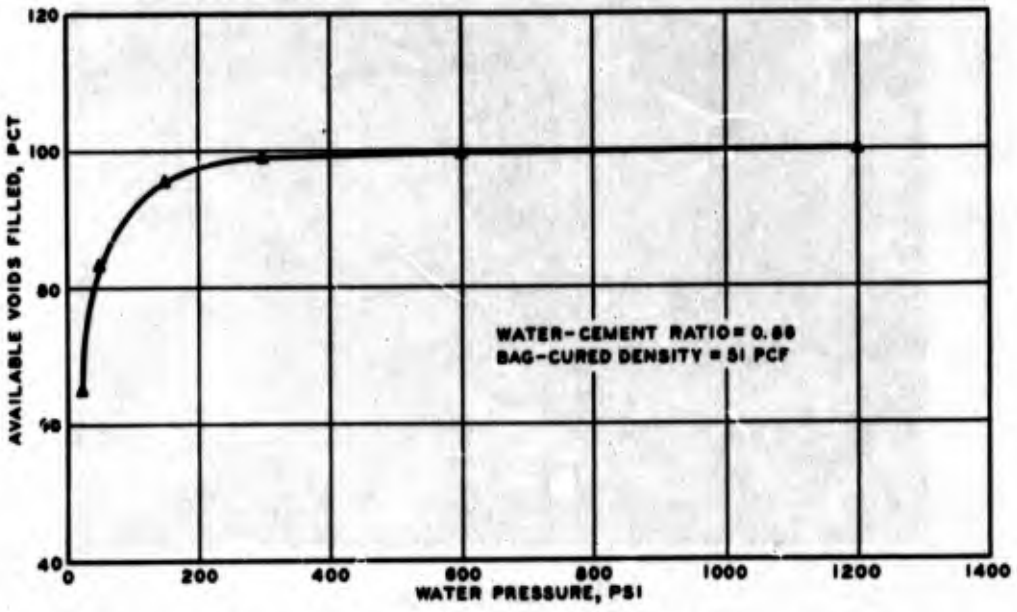

Figure 5.18 Saturation curve for a cellular concrete.

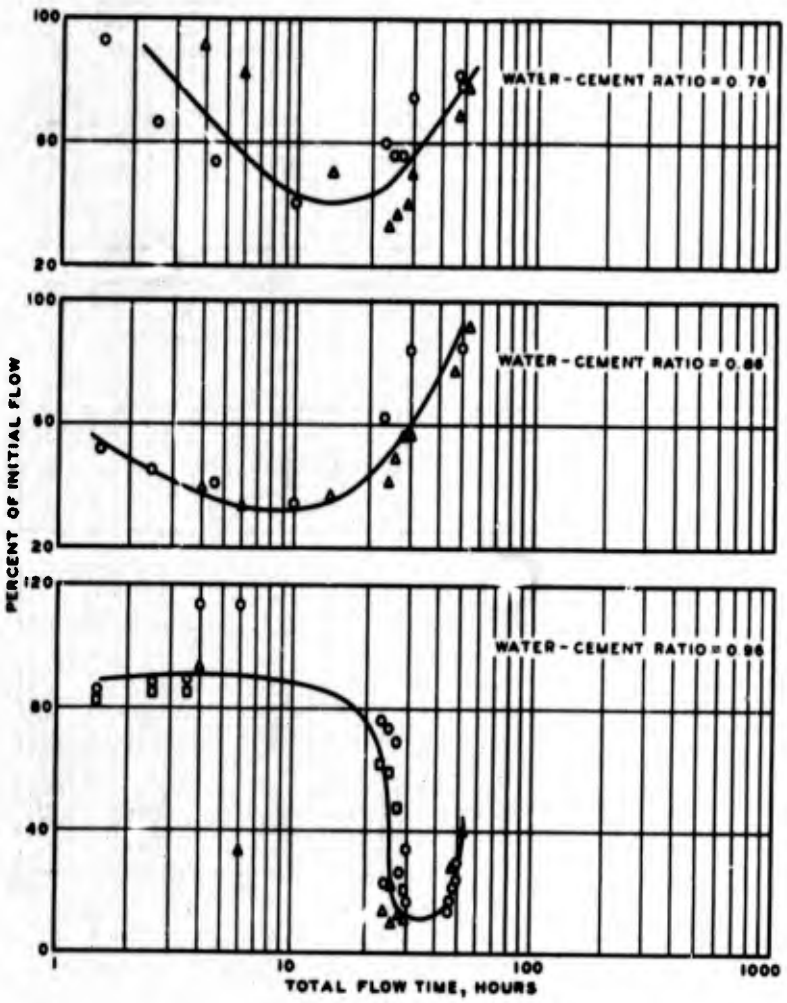

Figure 5.19 Flow data for 23-pcf concrete.

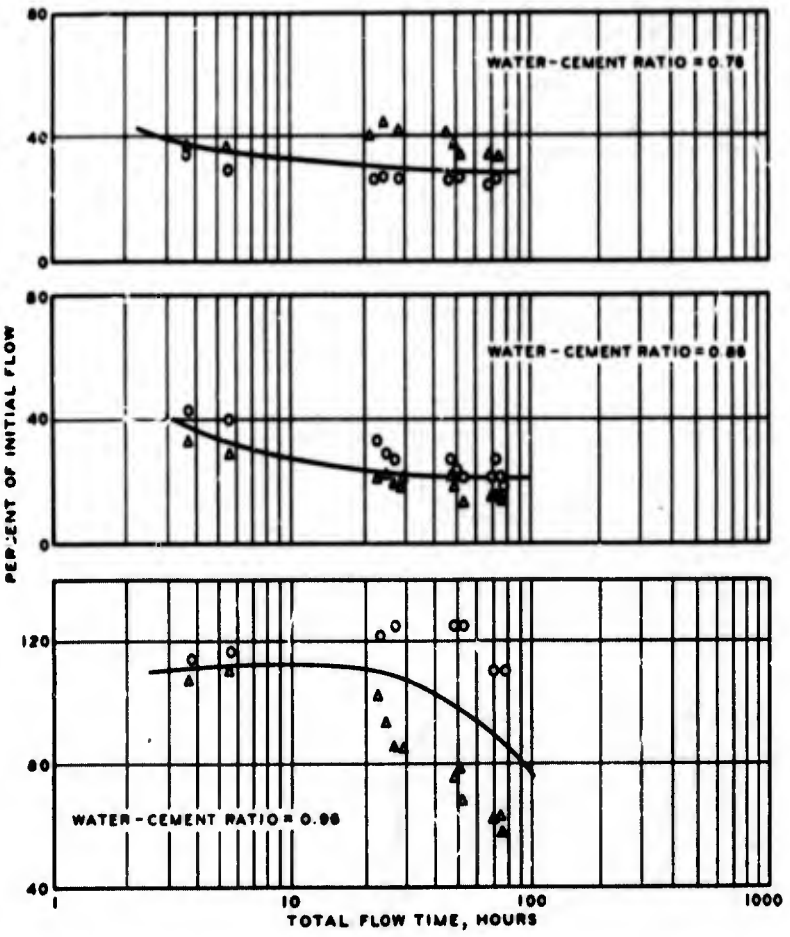

Figure 5.20 Flow data for 32-pcf concrete.

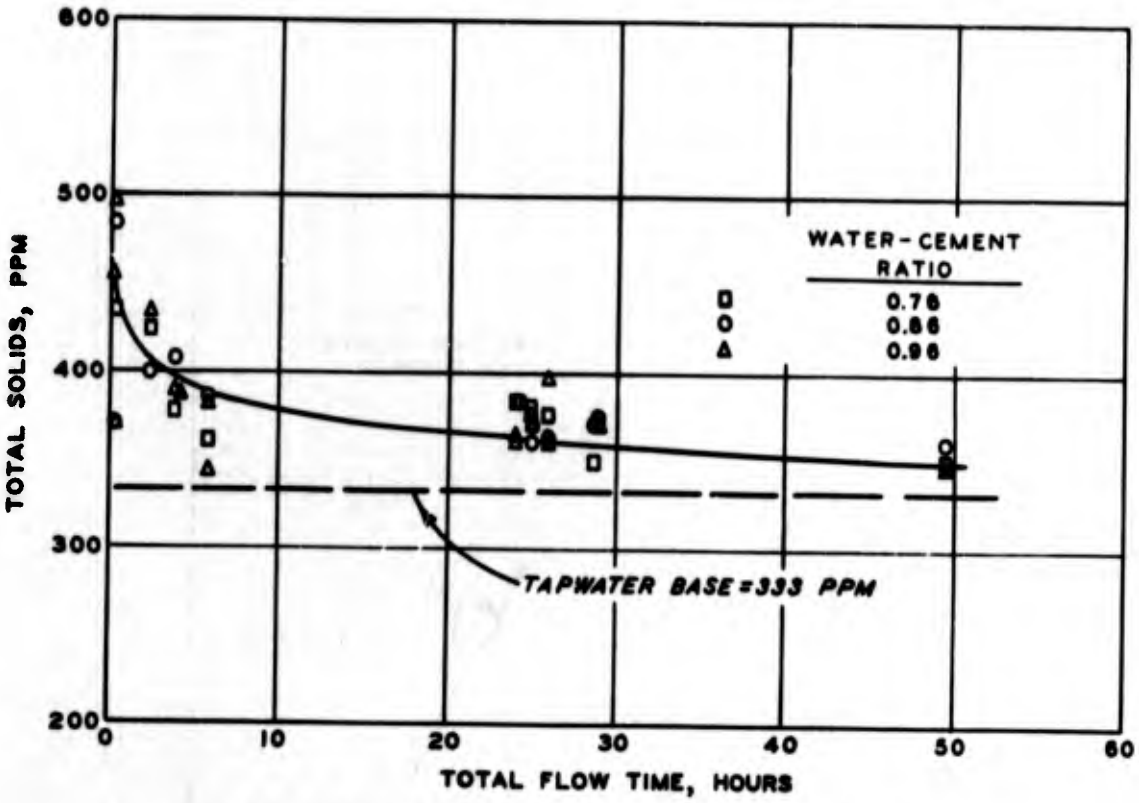

Figure 5.21 Erosion data for 23-pcf concrete.

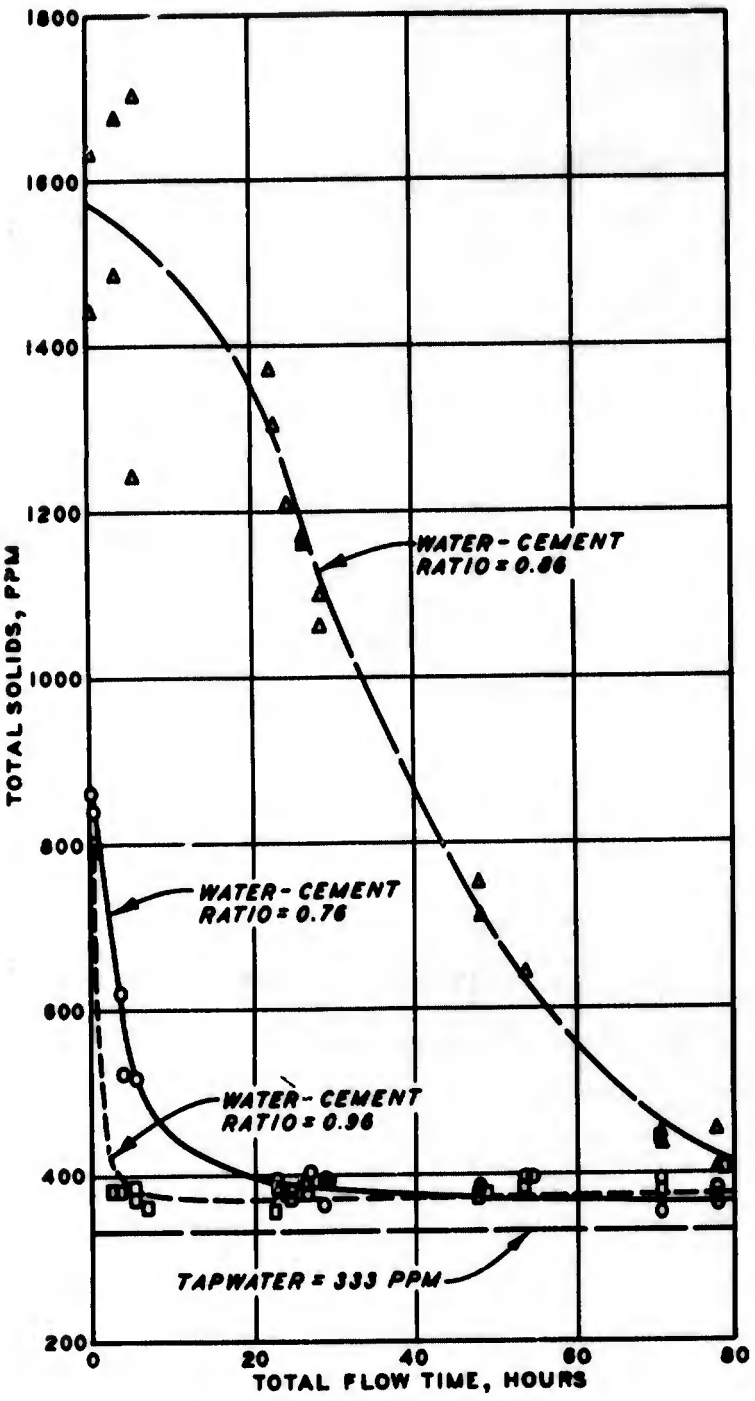

Figure 5.22 Erosion data for 32-pcf concrete.

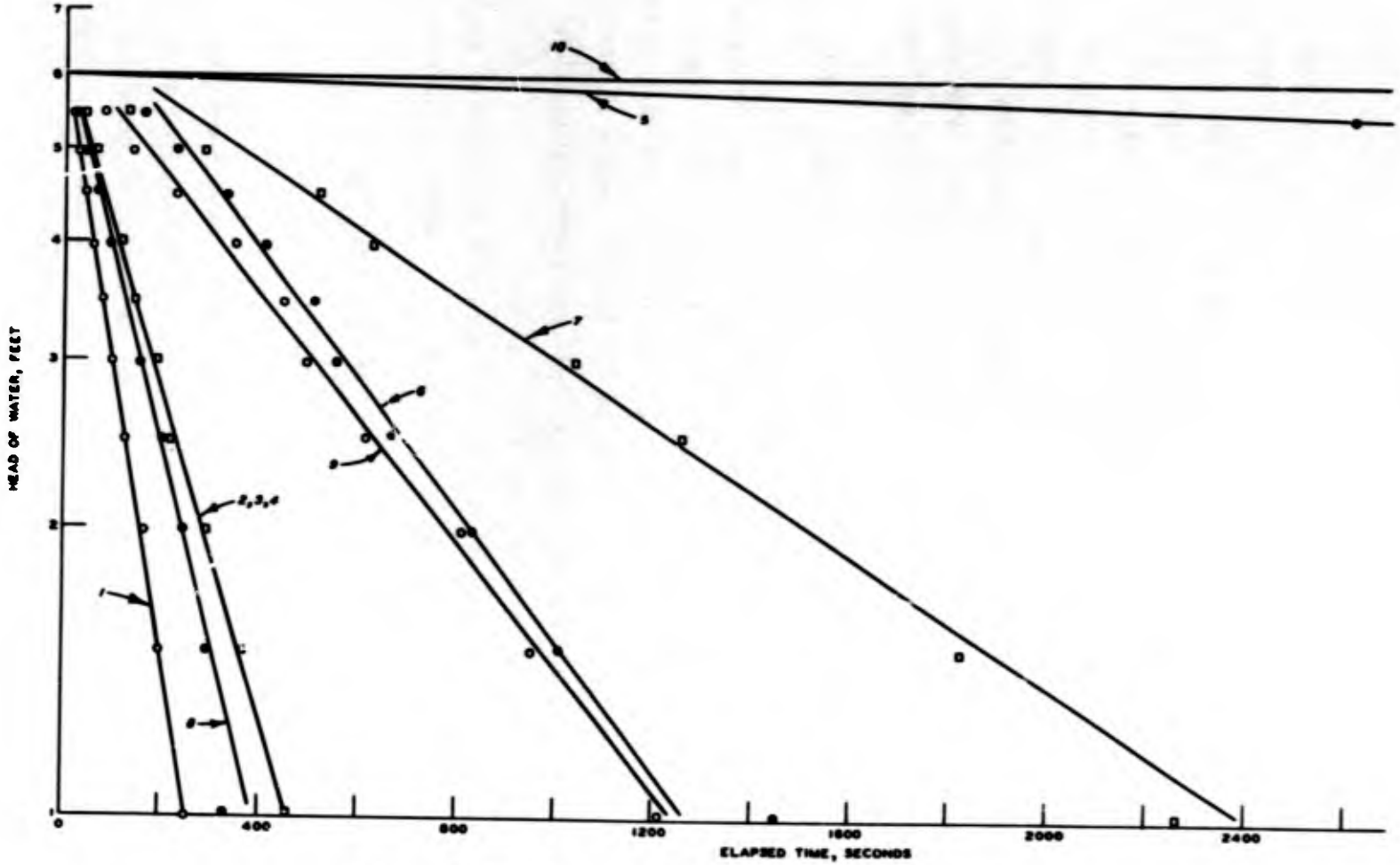

Figure 5.23 Sealer effectiveness test results.

CHAPTER 6

DISCUSSION OF TEST RESULTS

6.1 CONSTRAINED STRENGTH-DEFORMATION CHARACTERISTICS

6.1.1 Slow-Loading Results. As shown in the typical constrained stress versus deformation curves in Figure 5.1, the cellular concretes studied have a curve shape approximating that considered to be better for an efficient backpacking material (Reference 2). In most cases, the slopes of the initial (elastic) portion and the crushing (plastic) portion of the curves increase with increasing densities. Locking of the curves generally did not begin to occur until after 40 percent deformation was reached; but in a few instances involving the higher density, higher strength concretes, the locking regime may have begun between 35 and 40 percent deformation. The start of the locking, in these cases, was not as distinct as that observed for lower densities.

Cellular concrete is limited as far as strength is concerned by the inherent strength of its constituents and by the formulations necessary to produce the desirable characteristics of a backpacking. Neat cellular concrete is basically a hardened cement paste with a large void content. For the purposes of this study, porosity, n , will be defined as the volume of these voids divided by the total volume of the concrete where the voids consist of the pores in the cement paste (both gel pores and capillary pores) plus the entrained and entrapped air voids.

Numerous investigators have related the strength of hardened cement paste to porosity either directly or indirectly. As shown in Reference 6 it was found that:

$$S = 120{,}000 \frac{V_m}{W_o} - 3{,}600 \qquad (6.1)$$

where S is strength of the hardened paste and V_m is the constant in the BET surface area equation. V_m is proportional to the surface area of the cement gel, which in turn is proportional to the amount of cement gel. W_o is the original water content after bleeding. It was later suggested in References 7 and 8 that the strength of the hardened paste could be

empirically related to a volume of gel/space ratio by a power function where:

$$S = S_o(X)^b \tag{6.2}$$

where X = gel/space ratio and could include the effects of entrained and entrapped air (Reference 8) and b varied somewhat but was approximately equal to three.

As shown in Reference 9, it was found from experimental evidence that:

$$S = S_o(1 - V_p)^{2.7} \tag{6.3}$$

where V_p is the porosity. Based on a simple geometric model, it was suggested in Reference 10 that:

$$S = S_o\left(1 - 1.2V_p^{2/3}\right) \tag{6.4}$$

It was suggested in Reference 11 that the data for strength as given in Reference 6 be plotted against $(W_o - W_n) = W_e$, i.e., the original water content less the nonevaporable water content, where W_e is more closely related to porosity than V_m/W_o. As shown in Reference 11, it was then found that:

$$S = (1 - W_e)^6 \tag{6.5}$$

and it was further speculated that the strength of hardened cement paste could be approximated as:

$$S = S_o(1 - V_p)^6 \tag{6.6}$$

In all of the above cases, it is readily obvious that a decrease in porosity will reflect an increase in the strength of the paste.

For backpacking design purposes, a suggested approach is to relate the desired strength to the porosity of the cellular concrete which, in

turn, is a function of the water-cement ratio, concrete density, and specific gravity of the cement. This provides some latitude in the selection of a cellular concrete design for a particular requirement.

Using the notation of Section 2.2, the volume of water in the concrete will be considered as being composed of both evaporable and nonevaporable water (Reference 12), that is:

$$V_w = V_{ew} + V_{nw} \tag{6.7}$$

where

V_{ew} = volume of evaporable water

V_{nw} = volume of nonevaporable water

The space left in the concrete after the evaporable water leaves is considered as void space. The theoretical porosity, n , for a neat cellular concrete, as defined above, is then:

$$n = \frac{V_v}{V_t} \tag{6.8a}$$

$$= \frac{V_a + V_{ew}}{V_c + V_w + V_a} \tag{6.8b}$$

$$= \frac{V_v}{V_c + V_{nw} + V_v} \tag{6.8c}$$

The density expression:

$$d_c = \frac{W_t}{V_t} = \frac{W_c + W_w}{V_c + V_w + V_a} \tag{6.9}$$

can be rewritten in terms of water-cement ratio and specific gravities to be:

$$d_c = \frac{(1 + k)W_c}{V_c + V_{nw} + V_v} \tag{6.10a}$$

$$= \frac{(1 + k)V_c \rho_c \gamma_w}{V_c + V_{nw} + V_v} \qquad (6.10b)$$

where

ρ_c = specific gravity of the cement

γ_w = unit weight of water

The volume of voids is then expressed as:

$$V_v = \frac{1}{d_c}\left[(1 + k)V_c \rho_c \gamma_w - d_c(V_c + V_{nw})\right] \qquad (6.11)$$

Using an average value of 0.20 for the ratio of hydration water to cement by weight (Reference 12)

$$\frac{W_{nw}}{W_c} = 0.20 = \frac{(\gamma_w)V_{nw}}{\rho_c \gamma_w V_c} \qquad (6.12)$$

or

$$V_{nw} = 0.20\ \rho_c V_c \qquad (6.13)$$

Equation 6.11 can then be written as

$$V_v = \frac{1}{d_c}\left[(1 + k)V_c \rho_c \gamma_w - d_c(V_c + 0.20\ \rho_c V_c)\right]$$

$$= \frac{V_c}{d_c}\left[(1 + k)\rho_c \gamma_w - d_c(1 + 0.20\rho_c)\right] \qquad (6.14)$$

Substituting in Equation 6.8a,

$$n = \frac{V_c}{d_c} \frac{\left[(1 + k)\rho_c \gamma_w - d_c(1 + 0.20\rho_c)\right]}{(W_t/d_c)}$$

$$= V_c \frac{\left[(1 + k)\rho_c \gamma_w - d_c(1 + 0.20\rho_c)\right]}{(1 + k)W_c}$$

$$= V_c \frac{\left[(1 + k)\rho_c \gamma_w - d_c(1 + 0.20\rho_c)\right]}{V_c(1 + k)\rho_c \gamma_w}$$

$$n = 1 - \frac{d_c(1 + 0.20\rho_c)}{(1 + k)\rho_c\gamma_w} \tag{6.15}$$

Equation 6.15 is the expression for the theoretical porosity of the cellular concrete in terms of density, water-cement ratio of the freshly mixed concrete, specific gravity of the cement, and the unit weight of water. It has been assumed in this development that the specific gravity of water is unity.

Using the values of specific gravity for the Type III cement of this study and a unit weight of water of 62.3 pcf, Equation 6.15 can be expressed as

$$(1 - n) = \frac{0.00834d_c}{1 + k} \tag{6.16}$$

In relating the constrained strength of the cellular concrete, as measured in this study, to porosity, only the yield stress should be considered as it is basically a compressive stress whereas past the yield point the stresses are more complex, being functions of both compressive action and punching shear. These complex stresses may not relate directly to porosity. Backpackings are usually designed for an average crushing stress, that is, the average stress value of the crushing plateau of the stress-deformation curve. To relate porosity to this design value, the relation between σ_y and $\bar{\sigma}_{0.40}$ must be known. The stress-density relations of Table 5.1 suggest that for a common density, the two stress values are related in a power function form of

$$\bar{\sigma}_{0.40} \propto (\sigma_y)^B \tag{6.17}$$

where $B = \bar{b}_{0.40}/b_y$. In analyzing the relation between σ_y and $\bar{\sigma}_{0.40}$ in the form $\bar{\sigma}_{0.40} = a(\sigma_y)^b$ for each water-cement ratio, correlation coefficients between 0.96 and 0.99 were obtained. Comparing the regressions obtained in each instance, it was found that statistically they were not significantly different, thus indicating an independence from the influence of water-cement ratio. By being independent, all the data were then

combined and analyzed with the resulting relation of

$$\bar{\sigma}_{0.40} = 1.109(\sigma_y)^{1.008} \pm 76 \text{ psi} \qquad (6.18)$$

at the 95 percent statistical tolerance limits. The correlation coefficient was 0.971. For the sake of simplicity, Equation 6.18 can be approximated as

$$\bar{\sigma}_{0.40} = 1.175\sigma_y \qquad (6.19)$$

The data for the 525 constrained slow-loading tests are shown in Figure 6.1 in the form of a yield stress versus theoretical porosity plot. A separate least-squares regression analysis of the data for each of the water-cement ratios indicated that the line-of-best-fit in each instance was in the form

$$\sigma_y = \sigma_o(1 - n)^b \qquad (6.20)$$

where the coefficients σ_o and b varied somewhat between each water-cement ratio. Statistically, however, the lines-of-best-fit were not significantly different from each other. Correlation coefficients varied between 0.94 and 0.98. The relation for all the data together can be approximated by the expression

$$\sigma_y = 42{,}000(1 - n)^3 \qquad (6.21)$$

where the 95 percent statistical tolerance limits are at $\pm$81 psi and the correlation coefficient is 0.94.

Combining Equations 6.15 and 6.17, the yield stress can be expressed as a function of the two principal variables, i.e., water-cement ratio and freshly mixed density, plus the specific gravity of the cement, where

$$\sigma_y = \sigma_o \left[\frac{d_c(1 + 0.20\rho_c)}{(1 + k)\rho_c\gamma_w} \right]^b \qquad (6.22)$$

or

$$\sigma_y = \sigma_o \left(\frac{d_c}{1 + k}\right)^b \left(\frac{1 + 0.20\rho_c}{\rho_c \gamma_w}\right)^b \tag{6.23}$$

From Equations 6.16 and 6.18

$$\sigma_y = 0.02436\left(\frac{d_c}{1 + k}\right)^3 \tag{6.24}$$

Equation 6.24 is shown graphically in Figure 6.2. The relations between $d_c/(1 + k)$ and the freshly mixed density, d_c, are shown in Figure 6.3. Using these two figures together, along with Equation 6.19, a starting point in the design of a neat cellular concrete for particular backpacking requirements of density and strength can be obtained.

The curve in Figure 6.1 represents the results from a particular cement. Other cements may produce slightly different results. A possible approach to a more universal design curve for all cements is to put Equation 6.23 in the form

$$\frac{\sigma_y}{\sigma_o} = \left(\frac{d_c}{1 + k}\right)^b \left(\frac{1 + 0.20\rho_c}{\rho_c \gamma_w}\right)^b \tag{6.25}$$

Reasonable limits of specific gravity for portland cements are from 3.1 to 3.2. The last term in Equation 6.25 varies then between $(0.008388)^b$ and $(0.008226)^b$, respectively. Assuming the value of b to be of the same order and magnitude as indicated in Equation 6.24, the specific gravity term can be assumed to be fairly constant for the practical range of specific gravities, and hence

$$\frac{\sigma_y}{\sigma_o} \propto \left(\frac{d_c}{1 + k}\right)^b \tag{6.26}$$

The value of the coefficient b for a wide range of cement brands and types should be determined by test. The data from the Type III cement of this study indicate that the value is approximately three. As a third power function for a range of specific gravities, Equation 6.25 is shown

in Figure 6.4. This curve, together with Figure 6.3, may provide a design technique applicable to most portland cements.

The range of densities and water-cement ratios used in this study i.. not necessarily the limits of design that can be used to satisfy backpacking requirements. From practical considerations, however, the lower limit of density is approximately 18 pcf. It is also doubtful that water-cement ratios below 0.55 could be used without creating fabrication problems. The upper limits of density with respect to backpacking use are not so well defined. Densities of 60 pcf have been used (Reference 3) with very good success. Water-cement ratios above 1.0 (by weight) begin to create fabrication problems because of the excess of free water, which tends to destroy the stability of the preformed foam.

6.1.2 Rapid Loading. The results of a rapid-loading test often provide only qualitative results. Different loading systems, techniques, and rates will provide different test results for the same material. The rapid-loading test does provide twofold information, however. First, it does show if the material is strain and/or load rate sensitive; second, it gives some indication of the magnitude of load resistance that might be expected. This is evident from the results shown in Figure A.8, Table 5.1, and Appendix C. The rapid-loading tests, as described in Section 3.1.2, might produce the response of cellular concrete at some reasonable distance from the origin of the shock wave producing the loading, while the results of Appendix C may pertain to very close-in loadings.

By comparing the two equation forms for slow and rapid loading (Table 5.1) at a common water-cement ratio and density, a relation between the two in the form of

$$\sigma_r = a_r \left(\frac{\sigma_s}{a_s}\right)^{b_r/b_s} \tag{6.27}$$

is produced where a and b are the equation coefficients of Table 5.1, σ is any of the characterization stresses, and subscripts r and s indicate the rapid- and slow-loading cases, respectively. Comparing the average stress value, $\bar{\sigma}_{0.40}$, for the four water-cement ratios for which both slow- and rapid-loading tests were conducted, it was found that for

all practical purposes, the relation between σ_r and σ_s was independent of the water-cement ratio. By combining all of the data an expression in the form

$$\sigma_r = 2.62\sigma_s^{0.9} \tag{6.28}$$

resulted for the average stress characterization, $\bar{\sigma}_{0.40}$. Equation 6.28 is shown in Figure 6.5 and provides results that are within 10 percent of what might be determined for each water-cement ratio individually. It is shown in Equation 6.28 and Figure 6.5 that cellular concrete as tested by the IAHA is rate-sensitive and, as such, should be treated accordingly in the analysis of the response of backpacked structures.

6.1.3 Multiple-Shot Loading Capability. If a backpacked structure survives the effects of its first shock loading and the deformations of the cavity walls are within the elastic strain region of the medium, the backpacking should retain almost all of its original potential. If the deformations of the cavity wall were such that partial closure of the cavity resulted, there would be a corresponding crushing of the backpacking. Assuming the backpacking does not lock under the initial loading and partial closure of the cavity, some of the potential of the backpacking theoretically should be available for additional loading. This is evident in Figure 5.8. For the range of densities studied at a typical water-cement ratio, the cellular concrete appears to have some multiple-shot resistance capacity provided the initial loading does not completely crush the material. The test configuration approximates the situation where a piece of rock that has broken from the cavity wall is driven into the backpacking by the initial shock loading. The majority of the backpacking crushing takes place in a region adjacent to the area of rock-packing contact. With additional loading (second shot), the rock is driven further into the backpacking with additional crushing occurring. The backpacking can then absorb many thrusts of the rock as determined by its remaining crushing capability after each loading. The effects of the crushing of the backpacking due to liner movement should also be considered but is beyond the scope of this work.

It is doubtful that the cellular concrete will be able to rebound and regain any appreciable amount of its original volume as the forces in the cellular concrete would not be great enough to force and compact the walls of the cavity into some semblance of its original form.

The curves in Figure 5.8 show that the cellular concrete achieves the same crushing stress plateau for both shots. The second shot, however, begins from a zero load point. After the initial loading, assuming partial closure of the cavity has occurred, it is unlikely that the backpacking would achieve its original state of stress before loading because of the dead load of rock mass it would now have to support. Given sufficient time, the backpacking would probably attempt to creep out from under any stress concentrations, thus resulting in a somewhat uniform stress throughout the material. The time it would take to accomplish this, if at all, would depend on the properties of the material in question. With an initial stress simulating dead load in the cellular concrete, it is possible that the second shot crushing stress plateaus as shown in Figure 5.8 would have been somewhat higher. The manner in which the IAHA operates, however, did not permit this aspect of the multiple-shot loading to be evaluated.

6.2 FLEXURAL STRENGTH

6.2.1 Modulus of Rupture. Statistically, the modulus of rupture versus density relations shown in Figure 5.9 for the 0.86, 0.96, and 1.06 water-cement ratio concretes are not significantly different from each other. A trend toward higher moduli with decreased water contents for a given density is evident, however. A substantial increase in moduli is experienced when the water-cement ratio is reduced further from 0.86 to 0.76.

Previous information (Reference 13) has concluded that a reasonable range of ratios for flexural strength to compressive strength of cellular concretes is 0.2 to 0.33. Comparing the regression equations of Tables 5.1 and 5.2, a ratio of

$$\frac{R}{\sigma_y} = \frac{a_r}{a_y} (d)^{b_r - b_y} \qquad (6.29)$$

is obtained where the subscripts r and y denote the modulus of rupture and yield stress values, respectively. From Equation 6.29, the following ratios were obtained for a freshly mixed density range of 22 to 43 pcf.

Water-Cement Ratio	$\frac{R}{\sigma_y}$ = Flexural Strength / Yield Strength
0.76	0.16 to 0.33
0.86	0.19 to 0.21
0.96	0.21
1.06	0.19 to 0.24

These values, in general, appear to fall within the range of ratios usually associated with cellular concretes.

6.2.2 Horizontal Joint Tests. One of the more significant results of the horizontal joint tests was the fact that none of the flexural joint beams failed across the joint. All of the beams except one fractured in the concrete of the lower (or first) lift. In general, the concrete densities, cube strengths, and flexural control beam strengths for the bottom lifts were less than the values obtained for similar specimens from the top (or second) lifts. In most instances, the corresponding values from both lifts statistically were not significantly different. Because the strength of the cellular concrete (Sections 6.1.1 and 6.2.1) is influenced by density, among other things, the lower values of compressive and flexural strength corresponding to the lower densities of the bottom lifts are not unusual.

In all but one instance, the flexural strength of the joint beams is less than the flexural strength of the control beams from either lift. Because the joint beams failed in the lower lift concrete, their strengths might be expected to be the same as the strengths of the lower lift control beams. This is not the case, however. Observation of the bleeding characteristics of cellular concrete leads to the speculation that the difference in flexural strength for the same concrete is due, in large part, to the increased moisture content of the concrete near the surface of the lower lift. The excess mixture water in neat cellular concretes bleeds downward into the concrete. Because of the permeable nature of the concrete (Section 6.8), the bleed water from the top lift can pass

completely through the concrete, carrying with it some finer particles of cement. This "erosion" is not of the same magnitude as that discussed in Section 6.8. It occurs during the setting period of the concrete. Upon encountering the hardened joint, some of the cement particles are deposited, thus reinforcing the joint. The bleed water passes into the more mature concrete of the lower lift and is retained in the upper regions of that lift. This increases the moisture content of the top regions of the lower lift and reduces the tensile stresses that develop there as the concrete attempts to reach a moisture equilibrium while bag-curing. This condition lowers the flexural strength in the vicinity of the joint.

The average flexural strengths of the joint beams having an air-cured joint were 12.1 and 12.3 psi for the unprepared and prepared conditions, respectively. The average flexural strengths of the joint beams having moist-cured joints were 14.5 and 14.4 psi for the unprepared and prepared conditions, respectively. For both the moist-cured and air-cured joints, the effects of joint roughness appear to be minimal with either roughness condition being adequate. The moist-curing of the lower surface of the joint seems to provide some benefits by increasing the flexural strength of the concrete in the top of the lower lift. The increase is not significant however. The presence of the joint, in general, reduced the flexural strength of a beam by approximately 6 psi. While this is approximately 30 percent of the strength of the control beams, the magnitude is such that the reduction in strength should not affect the overall performance of a mass of cellular-concrete backpacking that contains horizontal cold joints.

In summary, for cellular concretes that will be used as backpacking, the presence of horizontal cold joints does not appear to be a problem area. The benefits of surface roughness are minimal and the as-cast surface should suffice. The joint appears to be stronger than the concrete in the immediate vicinity of the joint with most flexural failures occurring in the weaker concrete. Curing of the joint surface by covering with plastic shortly after casting as opposed to no special curing will improve the strength of the weaker concrete but not significantly. Addition of free moisture for curing is not desirable as it fills the voids needed

for the deformation capability of the concrete. Curing compounds have not been studied.

6.3 ULTRASONIC PULSE VELOCITIES

The curves in Figures 5.6 and 5.7 indicate that the compressional wave velocity of cellular concrete is continuing to increase with age of the concrete. The curing conditions of the specimens (Section 2.3) were such that no additional moisture was added to the concrete; hence the principal phenomenon occurring in the concrete was the formation of additional cement gel with subsequent decreases in free moisture and porosity. Increases in the freshly mixed density of the concrete as shown in Figures 5.6 to 5.8 (at any given age or water-cement ratio) also produce increases in the compressional wave velocity. Again the changing phenomenon is an increase in cement gel content.

As the cement gel content appears to be influencing the magnitude of the compressional wave velocity, a definite relation between the two can probably be established. Equation 6.15 can be rewritten to represent the amount of cement gel present in a given cellular concrete. In the assumptions made to arrive at the form of Equation 6.15, however, the degree of hydration of the cement at a given age with respect to complete hydration is not considered. Because a number of factors such as cement composition, fineness, and particle size will affect the amount of hydration products at a given age, for design purposes it is simpler to relate the wave velocities to something more definite such as the initial cement content of the concrete. The relations between compressional wave velocity and cement content for bag-cured neat cellular concrete at various ages are shown in Figure 6.6. A summary of the equation coefficients can be found in Table 6.1. The correlation between cement content and compressional wave velocity appears to improve with age. No reasonable correlation could be made for data obtained at 3 days age. This is probably due to the smaller amounts of cement gel and the larger quantities of free moisture present in the concrete at early ages. The higher water-cement ratio concretes provided the most dispersion to the data at 3 days age.

The effect of path length for the compressional waves was not studied.

The void size and distribution may result in longer path lengths as the wave travels around the voids. This may result in other values of wave velocity. The difference may not be significant, however. The effect of moisture content of the concrete also was not studied. The compressional wave velocity of pure water is approximately 4,800 ft/sec. At high moisture contents (after some saturation) and low cement contents, the velocity results may be affected.

6.4 RATE OF HARDENING

Rate-of-hardening information is necessary to determine the accessibility of the top surface of the cellular concrete and also for form removal purposes. It has been suggested (Reference 14) that the concrete possesses a certain "walkability" before it sustains nominal construction foot traffic. Acceptable walkability occurs at such time as the average of five tests by a Proctor penetrometer on the periphery of a 30-inch-diameter circle produces a bearing value in excess of 10 pounds with a 1/4-inch penetration of a 1/20-in^2 needle. Walkability, as such, was not measured for the concretes of this study but may have great utility in the preparation of job specifications with regard to surface accessibility.

The rate-of-hardening curves in Figures 5.9 and 5.10 provide some insight as to the early age strength development of cellular concrete. In general, the concretes with the lowest water-cement ratio, and hence the highest cement content for a given density, begin to stiffen earliest as might be expected. The data indicate that there are exceptions to this observation but these must be weighed against the fact that only small populations are being studied. In no instance was any penetration resistance encountered before 7 hours had elapsed. With one exception, the range of elapsed time for a resistance value of 1 psi at a particular density was less than 4 hours. All of the tests were conducted at 73 F. In a prototype situation, the early stiffening may be accelerated by higher curing temperatures (Section 6.6), thus permitting earlier construction traffic and form removal. At densities greater than 30 pcf, forms have been removed as early as 5 hours after completion of placing when the cellular concrete sections were very thick and the ambient curing

temperatures between 95 and 100 F (Reference 5). The effects of these conditions should be determined by test for each particular job, however.

6.5 MODULUS OF ELASTICITY AND POISSON'S RATIO

Elasticity data on moist-cured low-density cellular concretes appear to be meager. The elastic moduli generally have design significance when the concrete is of a semistructural or structural grade and, hence, are usually not measured for the very low-density concretes. In understanding the performance of and designing backpacked protective structures, however, the elastic modulus of the backpacking is an important parameter.

The data represented by the curves in Figure 5.11 indicate that the elastic modulus increases in a power function form for increasing values of freshly mixed density. The results of other studies (Reference 14) involving freshly mixed density ranges, which begin at approximately the densities at which this study ends, tend to substantiate the curvilinear relation. At densities greater than 50 pcf, the moduli density relations have been represented by parabolic curves of approximately the fourth degree (Reference 15).

It has been shown (Reference 15) that the modulus of elasticity of concrete is a function of unit weight and compressive strength. The formula

$$E_c = W^{1.5} 33 \sqrt{f'_c} \tag{6.30}$$

presented in the ACI Code (Reference 16) defines this relation for values of W between 90 and 155 pcf. For a given compressive strength, the modulus of elasticity of lightweight concrete is usually lower than that of normal weight concrete (Reference 17); however, in some instances, it has been shown to be greater (Reference 18). Using Equation 6.30 with the data obtained from the 75 moduli tests of this study, the relation in Figure 6.7 was developed. The line-of-best-fit for the data points involved a decision to use either a straight-line or a simple-power function. For the range of values on the abscissa, the statistical differences between the two curves are marginal. For a zero value of density or strength,

however, the modulus would also be zero; hence, the selection of the power function was made. Its use may not be warranted beyond the range of these data, however.

The line-of-best-fit in Figure 6.7 is expressed as

$$E_c = (0.0875w^{1.365}(f'_c)^{0.455} \pm 25) \times 10^3 \text{ psi} \qquad (6.31)$$

at the 95 percent statistical tolerance limits. The scatter in the data is such that Equation 6.30 could possibly be considered as a lower bound in lieu of a tolerance limit as shown in Figure 6.7. Additional tests are needed to firmly establish this, however. Depending on the importance of E_c in the structure-backpacking design, the designer should decide whether values determined by Equations 6.30 or 6.31 are adequate or whether additional tests on specific concrete are warranted.

Values for Poisson's ratio of the moist-cured cellular concrete varied between 0.192 and 0.252. These values are not unreasonable or unusual and are similar to those reported by other investigators (Reference 13).

6.6 TEMPERATURE PROBLEMS

Heat buildup and temperature rise associated with the hydration of the cement in the cellular concrete can create serious problems during construction if proper precautions are not taken. The cement contents of the concretes of this study varied from 3 bags/cu yd for the very low-density, high water-cement ratio concrete to approximately 8 bags/cu yd for the high-density, low water-cement ratio concrete. Although at the lower limit of cement content excessive temperatures might not be expected, the heat buildup is aided by the insulating characteristics of the concrete (high air content), which inhibits the dissipation of the heat with time. The problem is further compounded by the fact that, when used as a backpacking, the material is placed in very thick sections in a containing media such as rock which behaves as a very effective heat sink. Cellular concrete thicknesses of 11 to 12 feet around cylindrical tunnels of substantial lengths have been placed (Reference 5).

The problems associated with the concrete temperatures are primarily

related to fresh concrete in its unhardened state. As shown in Figure 5.12, in an adiabatic condition, which is approximated by the conditions at the center of a large mass of cellular concrete, temperatures can become quite excessive and actually create steam pressure in the concrete. Steam has been observed coming from thermal cracks in sections of concrete with thicknesses as small as 2 feet (Reference 19). Once the concrete has hardened, the elevated temperatures are no problem except that the curing conditions of the interior mass will produce concrete strengths which may be different from those obtained from the quality control cylinders representing that mass of concrete. Thermal cracking generally has little effect in the overall performance of a backpacking mass. Problems occur when unhardened concrete is placed in close proximity to the hot, hardened concrete. When this occurs, the elevated temperatures cause the air in the air-bubble system of the concrete to heat up and expand. This is accompanied by a reduction in the surface tension of the liquid film forming the bubble skin. Upon reaching a critical point, the bubble bursts. Many bubbles may join together to form large voids that then collapse. These collapses result in either localized "potholing" or a general subsidence of the surface of the concrete. Subsidence of 4 feet in 12-foot lifts has been observed (Reference 5). This phenomenon can be seen in Figures 5.16 and 5.17. The unhardened concrete was placed in and allowed to cure at elevated air temperatures of 100 and 120 F with 80 F being the control (results not shown). These air temperatures are not uncommon behind bulkheads on tunnels that already have some cellular concrete placed behind the bulkhead. Air temperatures as high as 155 F have been observed. No collapse was observed at 80 F. At 120 F (Figure 5.16), the results are obvious. The only concrete not collapsed is the 43-pcf concrete, which had the lowest air content and highest cement content. The air bubbles in the 43-pcf concrete have expanded, thus producing the cracked dome of material on its top surface. At 140 F (results not shown), even the 43-pcf concrete experienced complete collapse.

The potential collapse problem associated with the elevated temperatures can be experienced at any stage of a cellular concrete placing operation. The problem can exist in situations where a new lift is placed on

an existing hardened lift that is very hot and has not had its surface cooled to a sufficient depth before placing of the next lift. The heat given off by the hardened lift is contained by the fresh concrete; and if it can build up to a harmful temperature before the fresh concrete has set, collapse in the lower regions of the new lift may occur. This is shown in Figure 5.15 for both Type I and Type III cements. The temperatures recorded for the upper region of the first lift in each case are lower than the temperatures at the interior and bottom of the lift, due to the dissipation of the heat through the top of the lift into the air. This transfer of heat causes the air above existing lifts and behind bulkheads to become very hot and this hot air in turn can cause the problems mentioned earlier. After the placement of the second lift in each case, the temperatures in the bottom of the second lift become greater by as much as 30 F than at other locations in the lift (Figure 5.15). This is the effect of the heat of the first lift. If the initial temperature of the fresh concrete of the second lift is sufficiently high, the fresh concrete can become too hot after a very short time with resulting bubble collapse. The problem can also exist in very large volume lifts, such as those experienced when the total time of placement of the lift exceeded the time required for some of the concrete placed during the earlier stages of the same lift to reach its maximum temperature buildup. The concrete between the region that has begun to harden near the bottom of the lift and the concrete that was most recently placed is then affected in the same manner as fresh concrete placed on an existing hot lift. An overall subsidence of the surface of the lift may then be observed, perhaps even while placing is still going on. While placing a large section of cellular concrete (which experienced some subsidence) made with a water-cement ratio of 0.85 and a cement content of 6 bags/cu yd at an ambient air temperature of 95 F, thermocouples in the bottom of a large lift indicated temperatures of 160 F while placing was still in progress (Reference 5). Internal temperatures in this section peaked at 185 F.

To avoid these problems, the initial temperature of the fresh concrete should be kept as low as practical. Figures 5.13 and 5.14 show the effect of mixture water temperature on the early age heat in cellular

concrete for Type I and Type III cements, respectively. As has been shown many times for structural and mass concrete, the cooler the water, the cooler the concrete. The reduced initial temperatures allow the concrete to harden before higher damaging temperatures are reached. The effect of cement fineness is also a factor as the more surface area of cement that is hydrating initially, the more heat that is generating. The Type III cement is more finely ground than the Type I and thus contributes more surface area for early hydration and, hence, more heat. The requirement for fineness of the cement must be balanced with the water requirement for the backpacking design to prevent excessive water in the concrete. The data from the cement analysis (Section 2.1.1) show the fineness for the Type I and Type II cements to be 3,845 and 4,790 cm^2/gm, respectively. This difference is reflected in the temperature curves of Figures 5.13 and 5.14 with the finer cement, i.e. the Type III, producing higher temperatures than the Type I cement at comparable periods of early hydration. The total heat produced by each cement over an extended time period will be approximately the same, however, as the compositions are not significantly different. The use of coarser cements, or depressed concrete temperatures, or both, will produce cement pastes that stiffen at slow rates. The time needed for stiffening to occur must be balanced against the time that the preformed foam will retain its bubble structure. If the paste does not harden sufficiently before the bubbles begin to break down, the cellular concrete will collapse in the same manner as the high temperature collapse.

In summary, elevated temperatures can cause collapse of the air-bubble system of the cellular concrete while it is in the unhardened state. This collapse results in localized "potholing" or general subsidence of the unhardened cellular concrete, which produces density increases and hence changes in physical properties. These elevated temperatures can be present in the air behind sealed bulkheads used as the formwork during placing of the concrete. They can also exist in the lower regions of a lift of unhardened concrete that is either influenced by the heat of a hardened lift of concrete adjacent to it or by the temperatures developed in the new lift itself because of excessive placement times. The problems can be avoided by (1) using cooled mixing water and, if possible, cement, (2) using

minimum handling and placing times, (3) using low-heat, coarser ground cements, (4) restricting total placement times to periods that do not allow internal temperatures to become excessive, and (5) adequately cooling (by air blowing) the surface of adjacent sections of hardened concrete and the ambient air in which the fresh cellular concrete is to be placed.

6.7 LIFT HEIGHT RESULTS

The results of both the 16- and 30-foot lifts indicate that density increases do occur with increasing depth of concrete. The increases may indicate an increase in the amount of water in the concrete because the excess water in the mixture (bleed water) has a tendency to flow down into the concrete. The lower sections might then contain the excess water in the air void system. The comparison between the as-cast and the oven-dried cubes from the 16-foot lift tends to discount this as the amount of evaporable water in the concrete appeared to be the same from top to bottom. The density changes then are only a function of the amount of cement paste in a given volume. For a density increase, either the number of air voids per unit volume is decreased, or the existing air voids are compressed, due to the superincumbent load, while the concrete is still in the unhardened state. Upon hardening, the number of air cells would then still be the same but their size would be smaller with the difference in the original and final volumes being replaced by additional paste.

Figure 5.2 shows that changes in density result in changes in strength. The change in density of 7 pcf in the 16-foot lift can produce a change in the crushing level stress ($\bar{\sigma}_{0.40}$) from approximately 100 to 190 psi (Figure 5.2a) for the concrete design used in that section. Changes of this magnitude are not desirable because if the stress transmitted through the backpacking to a structural liner is not fairly uniform, ovaling or distortion of the liner may result and thus destroy the effectiveness of the liner's original design.

It is desirable to restrict the lift height of the cellular concrete to some value that is consistent with the allowable stress differences the liner in question can stand and the quality control that can be achieved for the cellular concrete placement. For example, if variation in density

due to lift height of ±3 pcf from a design density, d_c , is acceptable from a strength standpoint, but the quality control during placement can be expected to be no better than ±2 pcf, then the actual lift height that can be placed should be restricted to that height which yields d_c ±1 pcf.

6.8 SATURATION PROBLEMS

After placement of backpacking around tunnel liners or silos is complete, the problem of groundwater infiltration into the backpacking arises.

All of the materials currently under investigation for use as backpacking are very porous, with void contents to 80 percent being commonplace. Cellular concrete is no exception. This high void content is necessary to meet the structural behavior requirements of the material, i.e., to deform in excess of 40 percent of the initial thickness of the material with no appreciable increase in the stress level necessary for yielding to occur. This deformation is essential in absorbing the movements of the surrounding medium and in changing the input loading pulse accompanying a nuclear explosion into an input pulse less detrimental to the buried structure and its contents. Once the desired stress-strain relation for the materials is developed, the question then asked about the backpacking is what will happen if water, from a ground source or introduced by other means, infiltrates the backpacking material to such a degree that all the available permeable void space in the material becomes filled with water. Will the material still be able to absorb the ground movements and change the dynamic loading pulse into a less detrimental form?

Cellular concrete possesses both interconnecting voids and noninterconnecting voids. For the purposes of water saturation, the first of these void conditions is the less desirable. In this condition, water can quickly fill all the voids in a given specimen with little difficulty. The second void condition is perhaps the more desirable condition as each void would be a separate cell filled with a gas. A rupturing of each cell wall would be necessary for water to migrate into the cells.

The void space in any given specimen is composed of the space filled with gas (air and others), both entrained and entrapped, plus the space filled with free water. This void space is composed of permeable pores

available for saturation, permeable pores unavailable for saturation, and impermeable pores. The short-term saturation tests run on all the concretes fill only the permeable pores available for saturation and those are not filled completely because of the gas in the pores being compressed and having no place to go. When referring to a material being completely saturated in this study, what in effect is meant is that no more fluid can be forced into the available permeable pore spaces without further large increases in water pressure being applied.

The degree to which saturation of the material will occur will depend not only on the type of void structure but on the strength of the matrix, and the method by which the water is introduced or applied to the material. The crushing stresses of the cellular concretes vary from 20 to 900 psi, depending on their particular design. In a closed cell situation, the walls of the cell will rupture, when subjected to increasing pressures, at pressure levels governed by the strength of the matrix. A low-strength matrix will fracture and allow the closed cells to fill at much lower water pressures than a high-strength matrix. When we say the cell walls rupture or fracture, it is not in the catastrophic sense of the word but in the formation of microcracks, perhaps only one or so per cell, that would allow the water to migrate into the cell and equalize the pressure in that cell to that of the cells or other areas supplying the pressurized water. The stability of the material in mass is not destroyed by this type of saturation, but the strength is somewhat reduced due to the moisture and the cracking.

Assuming that the above situation is occurring, the question now arises as to what happens to the gas that originally filled the cells. This problem relates itself to the manner in which the water is introduced or applied to the material. Under almost all field conditions, the groundwater will be transient with respect to location of the material. The gas in the voids will become compressed as the water pressure increases and with the migration of the water into the material, the gas will be forced ahead under pressure with a portion of it probably being moved out with the transient water. Some of the gas will undoubtedly remain behind in a compressed state in the material. If the material were subjected to a stationary hydrostatic pressure, which is highly improbable but could happen, all

the gas would remain in the compressed state and it would be virtually impossible to fill every void space.

The data shown in Figure 5.18 indicate that water pressures in excess of 300 psi for a short-time test are necessary to saturate most of the available permeable void spaces in a very dense (with respect to cellular concrete backpacking densities) concrete made at an average water-cement ratio. Under long-term conditions this same degree of saturation could possibly result at lower water pressures. This saturation results from a stationary constant pressure situation where the gas remains compressed in the material. Specimens statically loaded in this condition show a negligible amount of deformation if the volume of water in and around the specimen is not allowed to change as loading progresses. If free water is allowed to escape from the system as the static loading progresses, the usual stress-strain relation for an unsaturated material will result but at a higher crushing strength level due to the increased water pressure necessary to keep the water in the voids. However, under the dynamic loading that would result from the shock wave accompanying an explosion, the free water in the system would not have time to migrate; the shock wave would then pass through the originally porous material as if it were rigid. Very little, if any, deformation would result; and in all probability, severe damage would result to the structure being protected.

The curve in Figure 5.18 indicates that very low water pressures are all that is required to fill at least half of available voids in cellular concrete. The results of the low-head permeability testing are shown in Figures 5.19 and 5.20 and tend to indirectly substantiate this. At average water heads of approximately 6 feet, water readily passes through the lower density concretes and tends to fill some of the voids with water. Regardless of the water-cement ratio, all of the 23-pcf concretes exhibited the same general pattern. Initially, the concrete appeared to be experiencing a flow-rate reduction with time of test run; however, the amount of reduction reached a maximum within the first 24 hours. A flow-rate increase then began with most of the maximum reduction in flow rate being regained within the next 24 to 30 hours. The amount of total solids measured in the discharge water (Figure 5.21) after the initial total solids was established

leveled off at approximately 30 ppm more than the total solids of the tap water before it passed through the concrete. This leveling off occurred about the same time as the maximum flow reduction occurred. All the test specimens were badly eroded and damaged after testing.

Regardless of the water-cement ratio of the 32-pcf concrete, all specimens exhibited the same general behavior pattern (Figure 5.20). The flow rate through the specimens appeared to decrease with time of the test run. Within the 80-hour test period, the total solids of the discharge water decreased (Figure 5.21) to approximately 30 ppm more than that of the original tap water before it passed through the specimens. These specimens did not appear to be eroded at the top surface as were the 23-pcf specimens.

No appreciable flow could be determined through the 43-pcf concrete with a water-cement ratio of 0.76; however, some small flows were noted for the 0.86- and 0.96-water-cement ratio material. These flows were not enough to accurately measure. The specimens did not appear to be physically altered by the flow.

The most obvious conclusion drawn from these tests is that the cellular concrete is very permeable at low densities and low hydrostatic pressure. In being very permeable, the concrete allows the water to reach most areas of the concrete mass and fill some of the available voids in those areas. The higher density concretes seem to indicate that, with sufficient strength development and subsequent reduction in void content, the permeability at low heads is greatly reduced for short-term flow conditions. Whether or not the concrete will maintain its reduced permeability for extended periods of time under low heads or for shorter periods of time under greater heads is not known. Tests of specimens fabricated by two major manufacturers of foaming agents for cellular concrete were conducted by an independent testing laboratory. The results of those tests[1] showed that at water pressures of 80 psi, maintained for 24 hours, no water could be

---

[1] Private communications; letter dated 26 Jan 1965 from Chemical Concentrates, Redondo Beach, Calif.; and letter dated 3 Feb 1965 from Mearl Corporation, Roselle Park, N. J.

forced through cellular concrete, provided the density of the concrete was greater than approximately 70 pcf. At lower densities, the water flowed through the specimens at rates that were related to the concrete density.

The total solids measurements made from the discharge water indicate that the water is picking up some additional total solids as it passes through the specimen, thus eroding the specimen. The very high values of total solids that occurred early during the test indicated the severest period of erosion. Some of the particles eroded evidently plugged the channels through which flow was occurring and gave the appearance that the rate of flow through the concrete was decreasing (Figures 5.19 and 5.30). For the 23-pcf concrete, these plugs were also eroded with time, and the flow rate picked up. The flow channels then became fairly uniform with a somewhat constant rate of erosion occurring as is indicated in Figures 5.21 and 5.22. Evidence of the flow channel plugging was also observed for other backpacking materials tested in a similar manner (Reference 3).

If the material is very permeable, it will probably not be very practical as a backpacking material if it is used by itself with no other systems that could divert or resist the intrusion of groundwater. Even if the cellular concrete can be designed to be almost impermeable by itself, there is no guarantee that under sustained associations with groundwater on the surface of the backpacking that either complete or partial saturation of the concrete will be eliminated. If the material does become saturated, either partially or completely, the pore-water pressures that may develop in the concrete may, under certain conditions, apply destructive pressures to the walls of the pores in the concrete, thus reducing the effectiveness of the material as backpacking.

The obvious solution to the problem is to build the structures requiring protection in media where there is no water. This is, of course, an almost impossible task but areas where the groundwater or other water would present a problem can be treated and maintained in ways that would prevent water from reaching the cellular concrete backpacking. Grout curtains in rock, wellpoint systems in soil, drains around the structures, sandwich-type structures, and many other methods could be applied to eliminate this threat of saturation.

The possibility of waterproofing the surface of the cellular concrete also exists. However, complete waterproofing would not be the answer for elevated pressures. An ideal backpacking can have a crushing stress level that is very low (25-150 psi) and will deform at that crushing stress for strains in excess of 40 percent. If the possibility of invasion by free water from an outside source into this material is eliminated for elevated pressures, what then would happen to the material when the outside water pressure goes above the crushing stress level of the material? The gas that fills the voids in the material would begin to compress, the material would begin to yield, and as the outside pressure increases the material would deform more and more, thus failing the material and destroying its usefulness before it could be loaded by a shock-wave input. Waterproofing is not the complete answer but would improve the effectiveness of the materials at lower water pressures.

As shown in Figure 5.23, there are considerable differences in the effectiveness of the sealers studied. The two most promising appeared to be liquid latex and neat cement slurry. The neat cement slurry, upon hardening, allowed no water into the sample. The liquid latex allowed just small quantities but is probably more effective than the results indicate. The same material has been used on laboratory specimens of many different materials to prevent moisture from entering the material and has been 100 percent effective. Both the neat cement slurry and the latex can be easily applied to the surface of the walls of a tunnel in rock in order to seal it before the backpacking is placed against it.

There are many commercially available products that can be used as surface sealers. Those evaluated in this study were used only because they were readily available in the area in which the investigation was conducted. A proper evaluation should be made of each sealer considered for use in backpacking operations.

TABLE 6.1 SUMMARY OF ULTRASONIC PULSE VELOCITY (V) VERSUS CEMENT CONTENT (C) RELATIONS, $V = aC^b \pm 2 S_{est,y}$, ft/sec

Age	No. of Observations	Equation Coefficients		Correlation Coefficient	Stardard Error of Estimate
		a	b		$S_{est,y}$
days					ft/sec
7	156	593	0.778	0.879	390
14	172	671	0.770	0.929	315
28	172	772	0.741	0.953	256
60	172	844	0.724	0.960	234

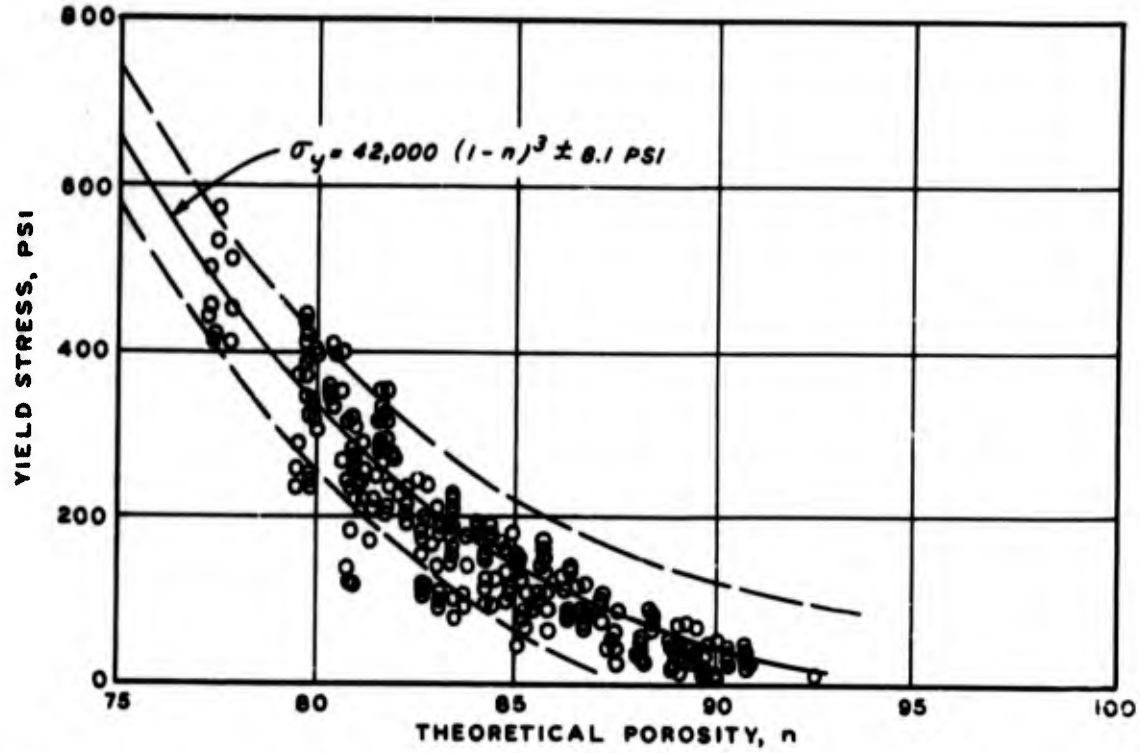

Figure 6.1 Yield stress versus theoretical porosity relation for a neat cellular concrete.

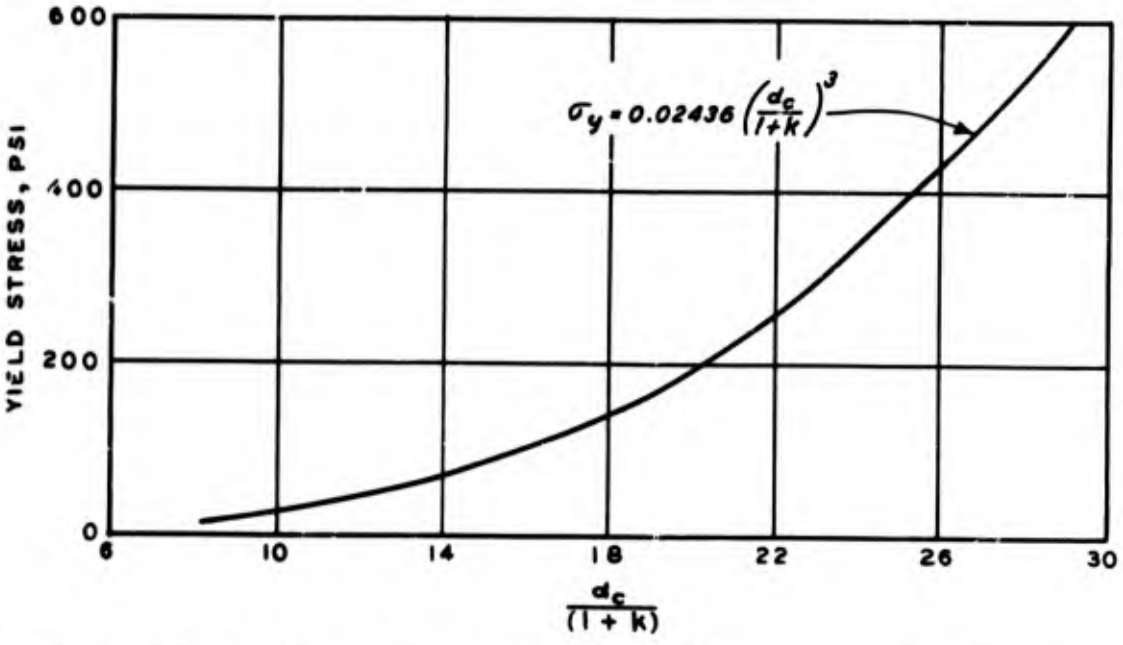

Figure 6.2 Relation between yield stress and the design parameter, $d_c/(1 + k)$.

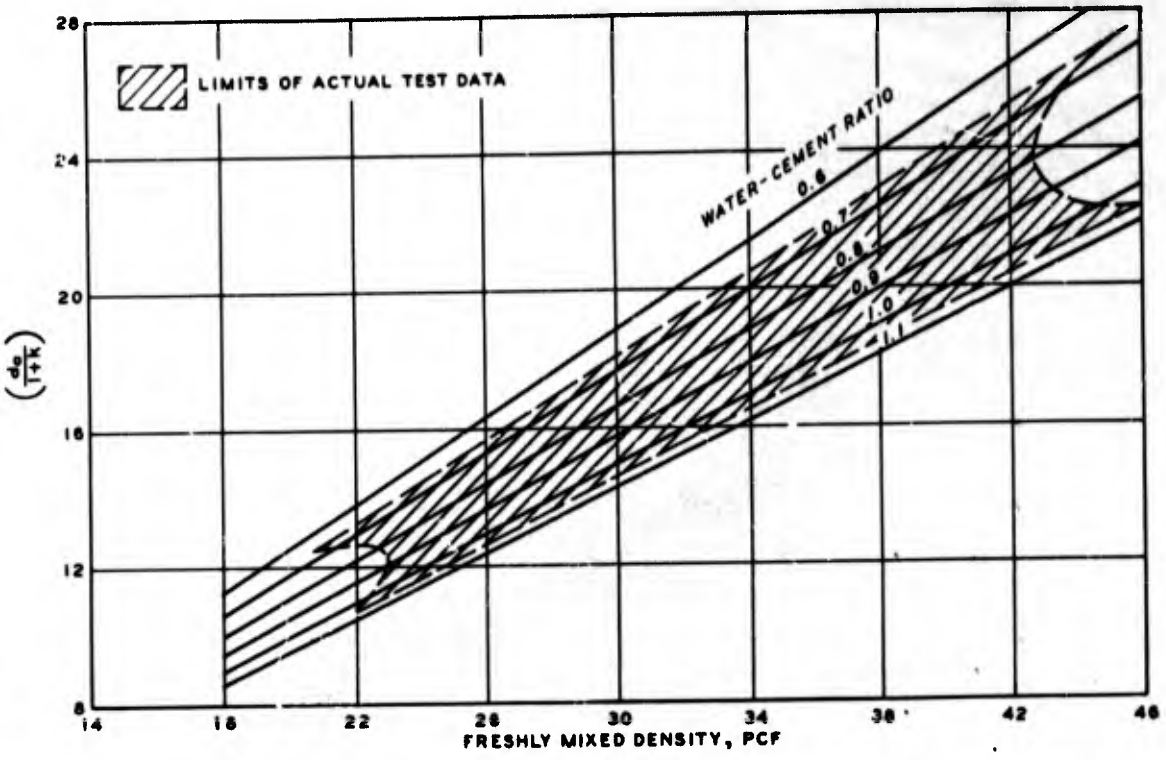

Figure 6.3 Relations between design parameter, $d_c/(1 + k)$, and freshly mixed density for various water-cement ratios.

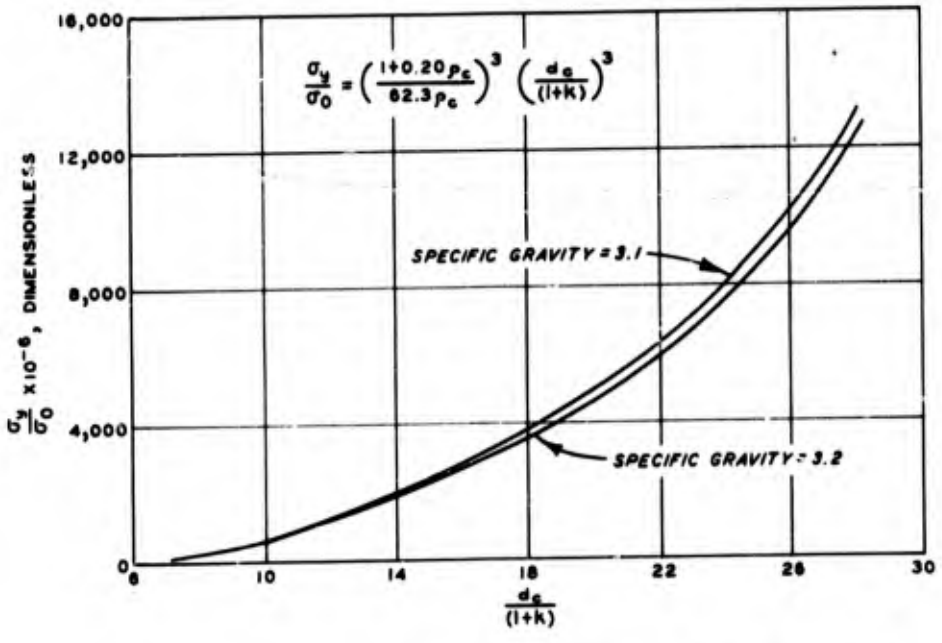

Figure 6.4 Proposed relation between stress ratio and design parameter, $d_c/(1 + k)$, for cellular concrete.

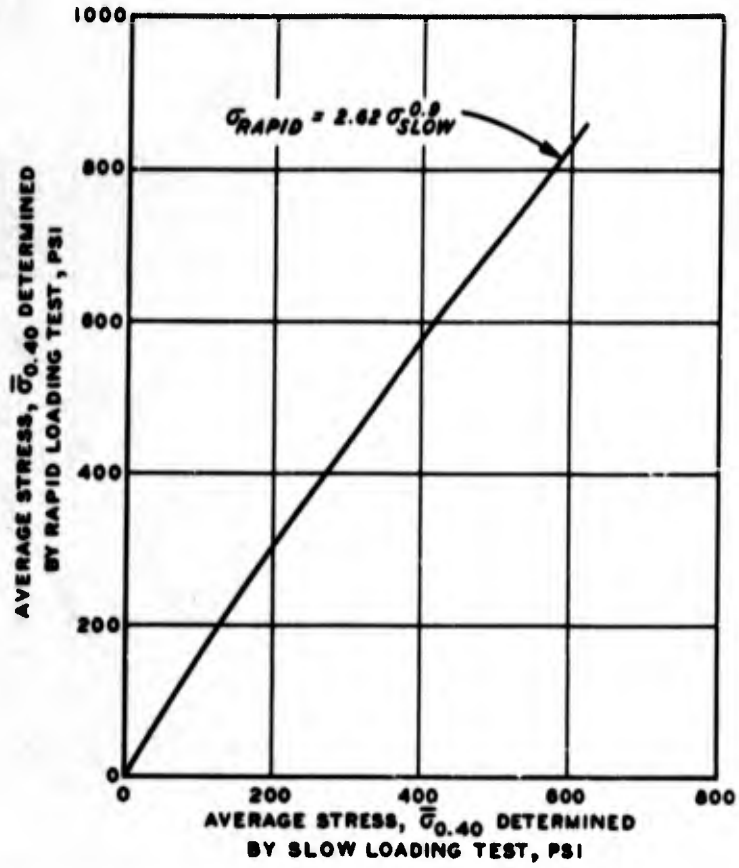

Figure 6.5 Rapid loading versus slow loading relation for the average stress to 40 [illegible]cent deformation chara[illegible]tion, $\bar{\sigma}_{0.40}$.

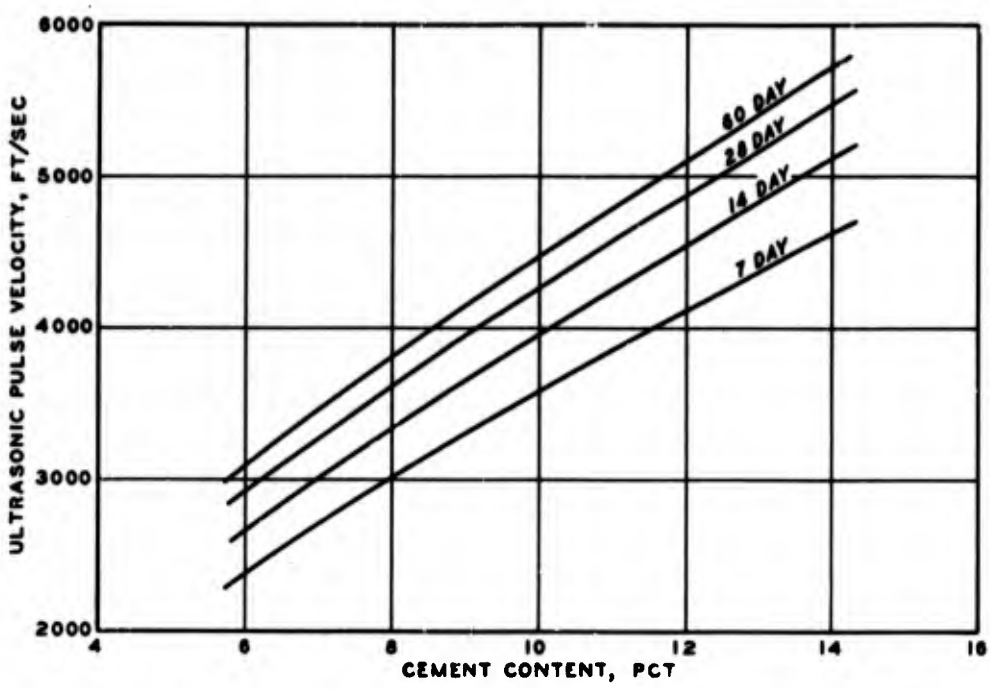

Figure 6.6 Ultrasonic pulse velocity versus cement content relations for neat cellular concrete.

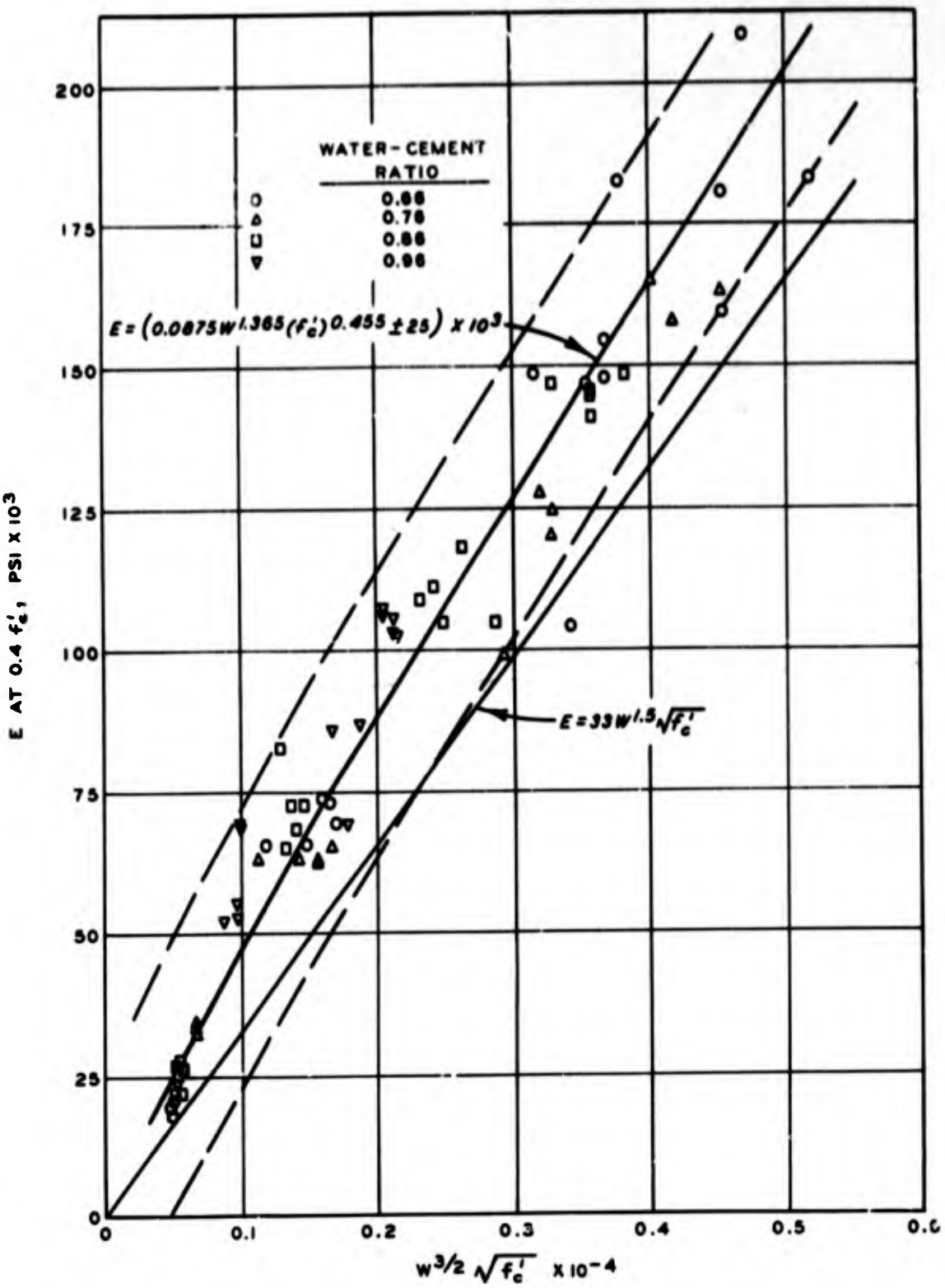

Figure 6.7 Secant modulus of elasticity versus modulus parameter relation.

CHAPTER 7

CONCLUSIONS AND RECOMMENDATIONS

7.1 CONCLUSIONS

Based on the results of the testing of this investigation and the information obtained from published reports and papers reviewed during the investigation, the following specific conclusions appear warranted:

1. The strength of moist-cured neat cellular concrete is principally a function of the concrete density and water-cement ratio, and the specific gravity of the cement. From the data of this study, the yield stress was determined to be

$$\sigma_y = 0.2436 \left(\frac{d_c}{1 + k} \right)^3 \tag{7.1}$$

A more universal design approach was suggested such that

$$\frac{\sigma_y}{\sigma_o} \propto \left(\frac{d_c}{1 + k} \right)^b \tag{7.2}$$

for all cements.

Neat cellular concretes made at densities from approximately 18 to 50 pcf and water-cement ratios from approximately 0.6 to 1.1 (by weight) possess the strength-deformation characteristics required for a suitable backpacking material regardless of the loading rate applied to the concrete. Average crushing stress levels from 20 to 1,000 psi at 28 days for slow-loading rates can be readily obtained depending on the mixture proportions. Strengths in excess of 1,000 psi, with deformations to 40 percent before locking, also appear to be feasible.

2. Cellular concrete is load and/or strain rate sensitive. For the rapid-loading system and techniques used in this study, crushing stress level increases from 95 to 30 percent were observed for the low-strength (20 psi) and high-strength (1,000 psi) concretes, respectively. The shape of the stress-deformation curve for cellular concrete does not appear to change with increased rates of loading.

3. Cellular concrete appears to possess a multiple-shot load-resistance capability provided the initial loadings do not completely crush the material. Each concrete design has a certain deformation capability. The portion of that capability not used to accommodate medium movements associated with earlier shock loadings is available to accommodate additional loadings.

4. The modulus of rupture of cellular concrete is dependent on the mixture proportions with higher cement contents and lower water contents producing higher flexural strengths. The ratio of flexural strength to compressive yield strength varied from 0.16 to 0.33, which is not unreasonable for low-density cellular concretes.

5. The compressional wave velocity (as measured by ultrasonic pulse techniques) of neat cellular concrete appears to be directly influenced by the cement gel content of the concrete. Increased gel contents due to the continuing hydration of the cement result in increased velocities. Increased gel contents, due to increased density (obtained by adding more cement per unit volume and decreasing the air content) also produce increased velocities. Free moisture in the concrete also appears to influence the wave velocity, but only at early ages of the concrete. At later ages ($\geq$ 28 days) the moisture effects are not readily apparent. Twenty-eight-day age concrete produced wave velocities from approximately 3,000 to 6,000 ft/sec depending on the concrete proportions.

6. The modulus of elasticity of moist-cured cellular concrete can be approximated by the relation $E = W^{1.5} 33 \sqrt{f'_c}$ in lieu of actual test measurements. This function appears to be a lower bound for the data of this study. Moduli from 20,000 to 220,000 psi were measured for the concretes studied. Poisson's ratio for the moist-cured cellular concretes varied between 0.19 and 0.25.

7. Cellular concretes with higher cement contents than other cellular concretes at comparable densities begin to stiffen earlier. Based on Proctor penetration tests, no measurable resistance to load was encountered before 7 hours age of the concrete regardless of its proportions. This stiffening may be accelerated in prototype situations due to higher ambient temperature curing. A measure of "walkability," as defined herein, may be

useful in the preparation of specifications for concrete surface accessibility and form removal.

8. The presence of horizontal cold joints in cellular concrete used as backpacking does not appear to be a problem. The benefits of surface roughness and special curing during joint preparation are minimal. The as-cast roughness with air curing should be adequate. Additional free moisture for curing a joint is not recommended.

9. Density increases, which result in strength increases, do occur with increasing lift height. This is due primarily to the change in air content brought about by the compressive action of the superincumbent load while the concrete is still in the unhardened state. Lift heights should be restricted to some value that is consistent with the allowable stress differences (brought on by the density changes) that the backpacked liner in question can accommodate and the quality control that can be achieved for the cellular concrete placement.

10. Elevated temperatures can cause collapse of the air-bubble system of the cellular concrete while it is in the unhardened state. This collapse results in localized "potholing" or general subsidence of the unhardened cellular concrete, which produces density increases and hence changes in physical properties. These elevated temperatures can be present in the air behind sealed bulkheads used as the formwork during placing of the concrete. They can also exist in the lower regions of a lift of unhardened concrete that is either influenced by the heat of a hardened lift of concrete adjacent to it or by the temperatures developed in the new lift itself because of excessive placement times. The problems can be avoided by using (a) cooled mixing water and, if possible, cement, (b) minimum handling and placing times, (c) low heat, coarser ground cements, (d) restricted total placement times to periods that do not allow internal temperatures to become excessive, and (e) adequately cooled (by air blowing) surface of adjacent sections of hardened concrete and the ambient air in which the fresh cellular concrete is to be placed. Care must be exercised when using approaches (a) and (c) so that the stiffening behavior of the cement paste is not delayed beyond the time when the bubble structure of the preformed foam begins its normal breakdown.

11. Cellular concretes at densities less than 35 pcf are extremely vulnerable to water infiltration at very low pressures. At densities from 35 to 70 pcf, the concretes are still quite permeable, the permeability decreasing with increasing density. Saturated backpacking loses its deformation capability. The flow of water into cellular concrete also tends to erode the same, thus damaging its structural integrity. Waterproofing the concrete improves its effectiveness at lower water pressures, but by itself is not a solution to the saturation problem. Structures backpacked with cellular concrete should be built in media where there is no water available for saturation of the concrete. In a water-bearing medium, water can be prevented from reaching the cellular concrete by using conventional construction techniques.

7.2 RECOMMENDATIONS

Additional information on the physical properties of cellular concretes made with different cements should be developed. Emphasis should be placed on cements that are coarsely ground and whose constituents will produce low-early heat.

The effects of concrete and curing temperature on all aspects of construction to include rate-of-hardening and physical characteristics should be studied in depth. Criteria for cellular concrete backpacking specifications should be developed.

The effects of rate sensitivity on the performance of cellular concrete should be explored for the entire range of rise times, amplitudes, and durations that might be expected in a prototype situation.

APPENDIX A

DEVELOPMENT OF A LABORATORY TEST METHOD FOR LOW-DENSITY CONCRETE BACKPACKING

The following observations, reasoning, and experimental results are presented as an insight to the development of the test method and procedures used in the study of cellular concrete when used as a backpacking. These results and suggestions can be readily extended to the testing of other types of backpacking materials.

A.1 CONSTRAINMENT

The behavior of backpacking when subjected to shock-wave loading is complicated and has not yet been precisely defined. The following observations as to expected backpacking behavior are somewhat simplified but can be considered adequate as a first approximation.

Consider the backpacking as completely filling the void between a buried structure and a rock opening (Figure A.1). The backpacking will be constrained at the outer surface by the rigid rock mass and at the inner surface by a structure that may vary in stiffness from flexible to very rigid. The traveling compressive shock wave in the rock, impinging on the rock-backpacking interface, is partially reflected, thus establishing tensile stresses in the rock that will cause the rock to fracture. The fractured rock is imparted some kinetic energy by the shock wave. It then leaves the interface and moves into the backpacking until its energy is dissipated. Some translation of the structure may also occur. In both cases, crushing of the backpacking will occur at the interface of the moving element and the backpacking. More severe rock fracturing and backpacking crushing would be expected at the interface of first contact by the shock wave than at the opposite side of the section.

Because of the speed of the shock wave, the entire backpacked opening will become loaded in compression in a very short time interval. The uniformity of the loading across the opening is dependent on the decay history of the loading wave. A reasonable assumption is that the entire section will be loaded in somewhat uniform compression shortly after initial

loading and at a time when the fractured rock elements will still be driving into the backpacking mass.

Neglecting translatory motions of the structure and the fracturing of the rock for the moment, consider the backpacking to be a thick-walled cylinder of semi-infinite length behaving elastically under both internal and external compressive loading. From Lame's equations for thick-walled cylinder stresses (Figure A.2), the general case for tangential stresses can be expressed as:

$$\sigma_t = \frac{p_i r_i^2 - p_o r_o^2}{r_o^2 - r_i^2} + \frac{(p_i - p_o) r_o^2 r_i^2}{r_o^2 - r_i^2} \left(\frac{1}{r^2}\right) \tag{A.1}$$

where

p_i = internal pressure

p_o = external pressure

r_i = internal radius

r_o = external radius ($r_o > r_i$)

r = radius to point of interest ($r_o > r > r_i$)

Rewriting, where $p_i = p_o \pm \Delta p$

$$\sigma_t = -p_o \pm \frac{\Delta p r_i^2}{r_o^2 - r_i^2}\left(1 + \frac{r_o^2}{r^2}\right) \tag{A.2}$$

$$= -p_o \pm K(\Delta p)$$

where

$$K = \frac{r_i^2}{r_o^2 - r_i^2}\left(1 + \frac{r_o^2}{r^2}\right) \tag{A.3}$$

K = a positive constant depending on cylinder geometry and point of interest

The sign convention is that a positive sign indicates tension while a negative sign indicates compression.

When $p_i < p_o$, σ_t is always a compressive stress. When $p_i > p_o$, Δp is a positive value and σ_t may represent either a tensile or compressive stress, depending on the relative values of p_o and p_i for a given geometry. It is expected that the resistance offered by the prototype structure (and represented by p_i) will be something less than the shock-wave overpressure (represented by p_o), hence the first case will prevail. An element of backpacking at any distance r will then be subjected to compressive tangential stresses.

The use of Lame's equations infers that the internal and external pressures are statically applied and of known constant magnitudes, where, in fact, the inferred situation exists only when any instant of time is isolated and the pressures existing at that time are determined. For a finite time interval, both p_o and p_i will be continually changing and, hence, so will σ_t. The sense of the tangential stress will remain compressive, however, regardless of its magnitude.

The compressive tangential stresses have the effect of providing some lateral constraint to a backpacking element that is being additionally loaded by the driving pieces of fractured rock. To reproduce realistic compressive constraining stresses or forces in a backpacking evaluation test would be difficult in view of the many variables and unknowns associated with each prototype. A simple solution, and the one pursued for this study, is to use cylindrical backpacking samples and enclose the sample in a steel pipe. The steel pipe, being much more rigid than the backpacking, resists the lateral expansion of the cylinder once loading has begun and thus provides some degree of constraint to the material while it is being tested.

The actual relation between the prototype compressive constraining forces and the constrainment provided by the steel pipe cannot be defined due to the lack of information on prototype behavior. However, it is believed that the overall effects of constrainment by the pipe contribute to the performance of the backpacking in such a manner that the results obtained from this type of evaluation test more closely approach that of the actual behavior of the prototype backpacking than if no constrainment were provided at all.

A.2 SPECIMEN AND TEST PREPARATIONS

The cylindrical specimen of backpacking that is placed in the constraining pipe should be of a size that is conveniently available to almost anyone. For low-density concretes, the 6- by 12-inch cylinder is an ideal size. Standard cylinder casting procedures can be followed for these concretes with the exception that the concrete should not be vibrated or excessively consolidated.

The curing of the low-density concrete cylinders should not be done in an environment where free moisture can come in contact with the concrete. This includes moist-curing rooms. Because of the porous and absorptive nature of these concretes, free moisture readily penetrates into the concrete and fills the voids necessary for satisfactory performance as a backpacking. The concrete should, instead, be cured in sealed plastic bags. Shortly after sealing, the humidity in the bag approaches 100 percent and the specimen still cures adequately with no additional free moisture being added to the system.

In preparing the cylinder for testing, the top and bottom 3 inches of each cylinder should be sawed off and discarded, thus avoiding surface irregularities due to casting, bleeding, and handling. In most instances, the sawing can be done with a handsaw. Care must be taken to ensure that the ends of the cylinder remain perpendicular to the sides.

The confining pipe should be of split-wall construction (Figure A.3) so that the specimen can be easily enclosed in or removed from the pipe. The pipe requires a nominal 6-inch inside diameter and should have walls no thinner than 1/4 inch. Closure of the pipe around the specimen can be effected by two closure bolts set 180 degrees apart at the midpoint of the pipe height. Other arrangements are also possible. Reproducibility in testing can be achieved by torquing each of the closure bolts on the pipe to the same value just prior to testing. For two-bolt closure (Figure A.3), experimentation has indicated that a closure torque of 5 ft-lb was adequate to obtain reproducible results with a minimum of additional triaxial compressive forces due to the torquing. If desired, the constraining pipe can also be bolted to a fixed baseplate.

After closure of the pipe is complete, the specimen is ready to be tested. This is done by forcing an appropriate piston into the concrete at a desired rate of specimen deformation.

A.3 PISTON SIZE

To represent the rock fragments that will be driven into the backpacking, a loading piston with a flat, circular end area was determined, from practical considerations, to be most desirable. Three different size pistons were studied: 3-, 4-, and a nominal 6-inch diameter (Figure A.4). The 3-inch-diameter piston was also studied for two-side taper configurations.

By forcing any of the pistons into a low-density concrete sample at a constant rate, a stress-deformation test record similar to that shown in Figure A.5 will be obtained. Stress is determined as the load acting on the area of the piston face; and deformations are determined as the displacement of the contact face of the loading piston into the specimen with respect to the original height of the specimen and are usually expressed as percentages. This constrained stress-deformation curve (Figure A.5) is characterized by four values of the curve: (1) yield stress, σ_y ; (2) deformation at yield, ϵ_y , percent; (3) average stress $\bar{\sigma}_{0.40}$ between ϵ_y and 40 percent deformation $\epsilon_{0.40}$; and (4) stress $\sigma_{0.40}$ at 40 percent deformation. The values of items (1), (2), and (4) can be read directly from the test record. Item (3), the average stress, is determined as:

$$\bar{\sigma}_{0.40} = \frac{(\text{area under curve between } \epsilon_y \text{ and } \epsilon_{0.40})}{100(\epsilon_{0.40} - \epsilon_y)}$$

One mixture design of cellular concrete was selected for the piston study. Three rounds of concrete were cast with samples from each round being evaluated for each of the piston configurations. The results are shown in Figure A.6 The deformation rate was 0.3 in/min.

The results indicate that higher stress values are achieved with smaller sized pistons. The test records also reveal that the 6-inch piston tests "bottom" at smaller deformations than the other piston tests. Figure A.7 shows a typical set of test records for the three sizes of

pistons. The taper effect on the 3-inch piston did not significantly affect the test results.

If the mode of resistance of a test specimen is only normal compression, the magnitude of the observed stresses should be the same regardless of the area of the sample loaded. In the case of the 6-inch piston on the constrained 6-inch cylinder, normal compression was the predominant resistance mode. When the smaller diameter pistons were used, the test became a punching test and the resistance mode became a combination of normal compression and shear accompanied by horizontal compressive components due to the constrainment. It is this combination of compression and shear that resulted in the higher observed stress values for smaller sized pistons. A penetrating rock projectile will be resisted by both shear and compressive forces and, hence, would be best represented by a punch-type test.

The bottoming of the stress-deformation record occurs when the slope of the crushing plateau begins to increase rapidly. Ideally, this should begin to occur when most of the voids under the loaded area have been crushed and the remaining solid material begins to resist compression with little additional deformation. Some increase in the shear resistance may also develop and, in the case of the 6-inch piston, may be the predominant mode of resistance. The frictional sidewall resistance that develops when the 6-inch piston is used becomes so great that the lower portion of the specimen is never deformed. This does not produce a desirable test result. The sidewall friction effect will probably persist even when the piston edge is moved slightly away from the constraining pipe. For this reason, 5-inch pistons were not considered.

Based on the above observations, it was believed that a piston that loaded the most area so as to obtain the greatest compressive resistance and yet minimized the sidewall friction effects so that a more realistic bottoming point could be discerned should be used for the test method. As the 4-inch piston as shown in Figure A.4 appeared to satisfy these requirements, its use was adopted.

A.4 DEFORMATION RATES

The rate-of-deformation studies were conducted using a 30,000-pound

universal testing machine operated at controlled rates of loading head travel. A 4-inch piston was affixed to the loading head through a ball and socket arrangement that allowed easy alignment of the piston. The same cellular concrete mixture used in the piston size study was used in this evaluation. Three rounds of 12 cylinders each were tested. From each round, three 6- by 6-inch cylinders were tested at a base rate of piston travel of 0.18 in/min and in accordance with procedures discussed above. The remaining nine cylinders were tested in groups of three at three different but faster rates of piston movement. Figure A.8 shows the test results. The strength ratio is the value of the average stress to 40 percent deformation, $\bar{\sigma}_{0.40}$, for the faster rate of deformation for a given round divided by the corresponding value for the base rate of that round.

Only at rates of 10 in/min or greater did the mean strength values at faster rates of deformation become significantly different from the corresponding base rate values. The data in Figure A.8 indicate that a strength increase with increasing deformation trend is developing as was expected. For testing purposes, it is suggested that deformation rates be kept to less than 1 in/min to minimize the deformation rate sensitivity effects in the concrete.

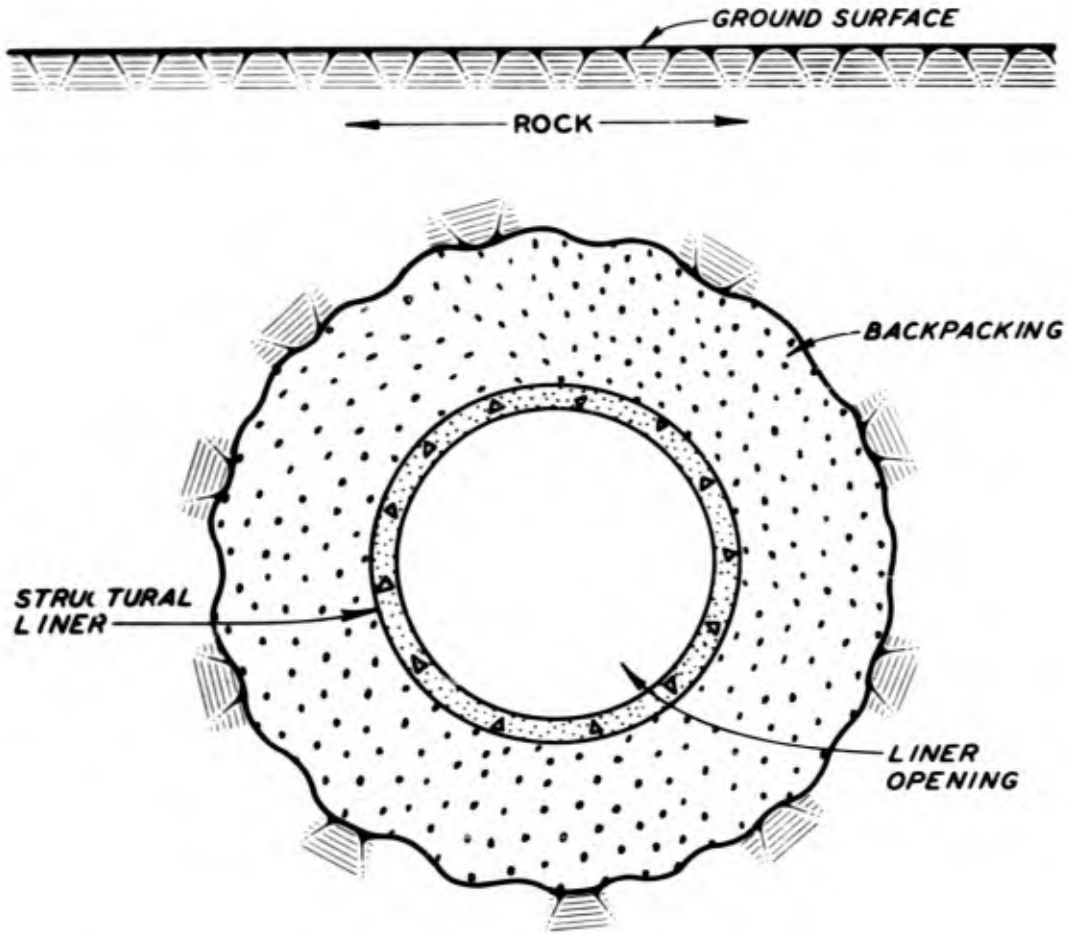

Figure A.1 Rock-backpacking-structure configuration.

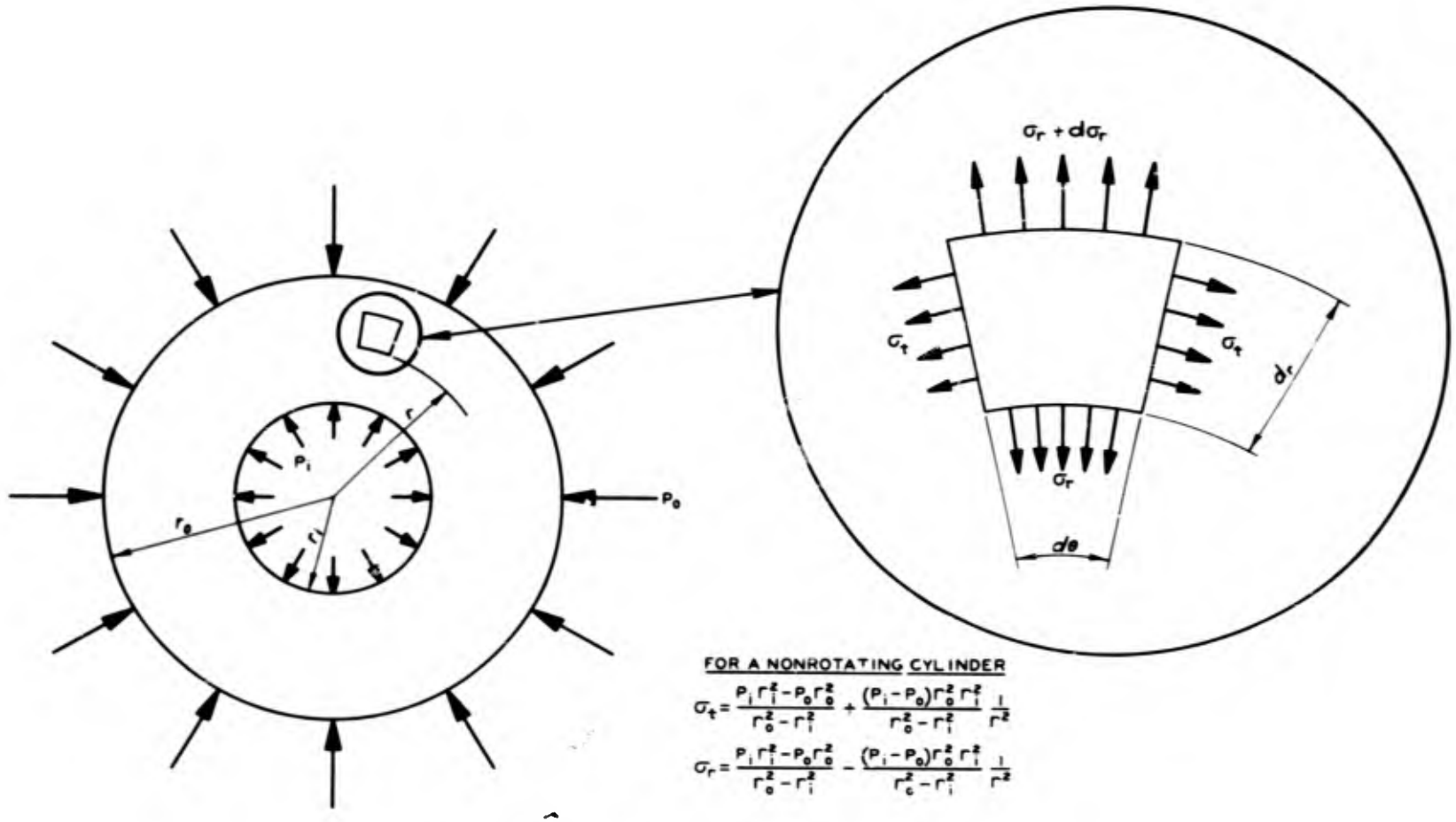

Figure A.2 Thick-walled cylinder stresses.

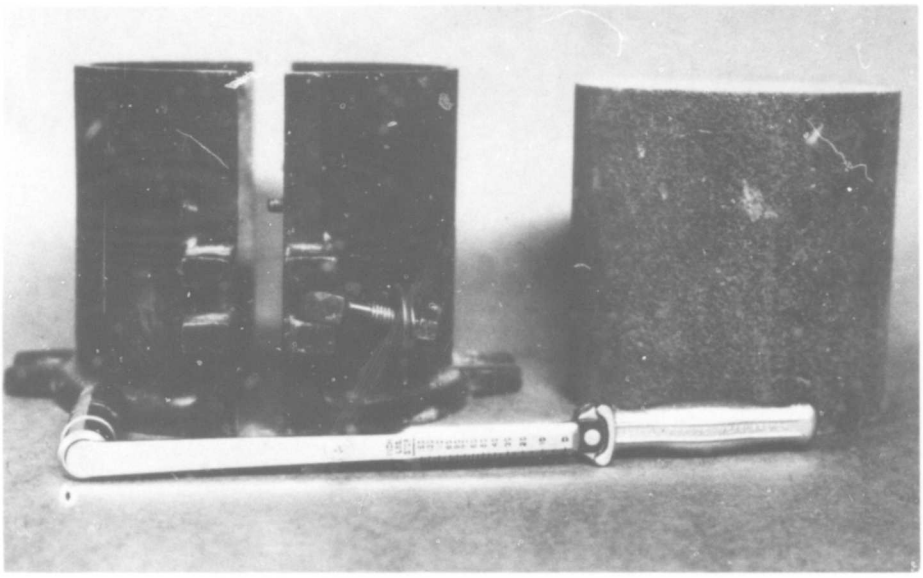

Figure A.3 Split-wall confining pipe.

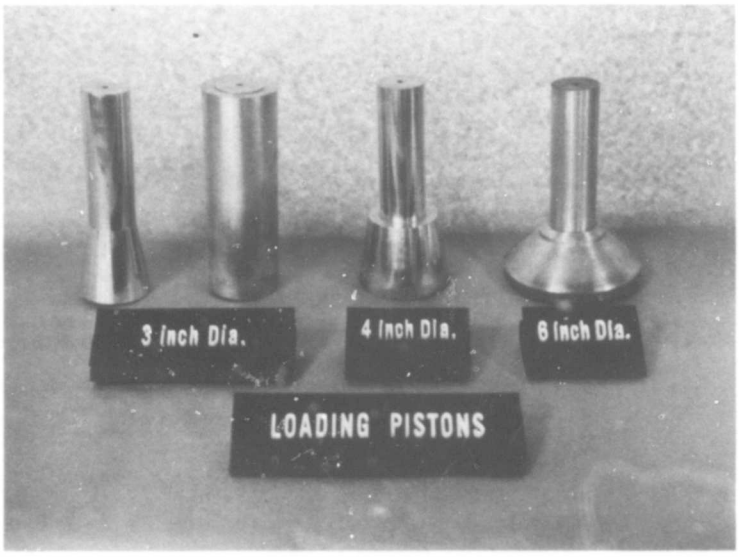

Figure A.4 Loading pistons.

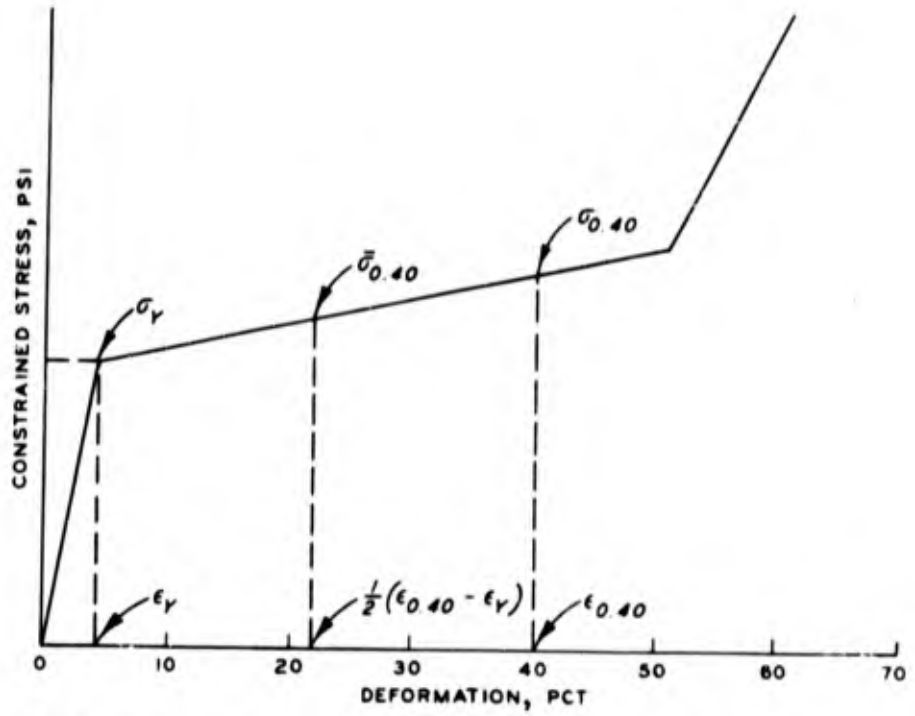

Figure A.5 Typical constrained stress versus deformation relation.

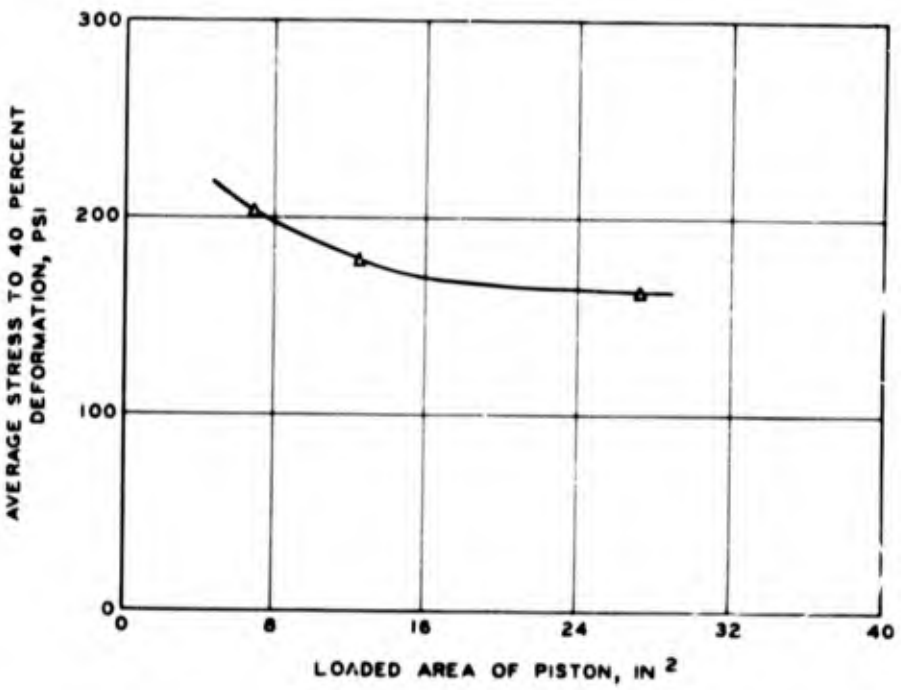

Figure A.6 Effect of piston diameter on stress.

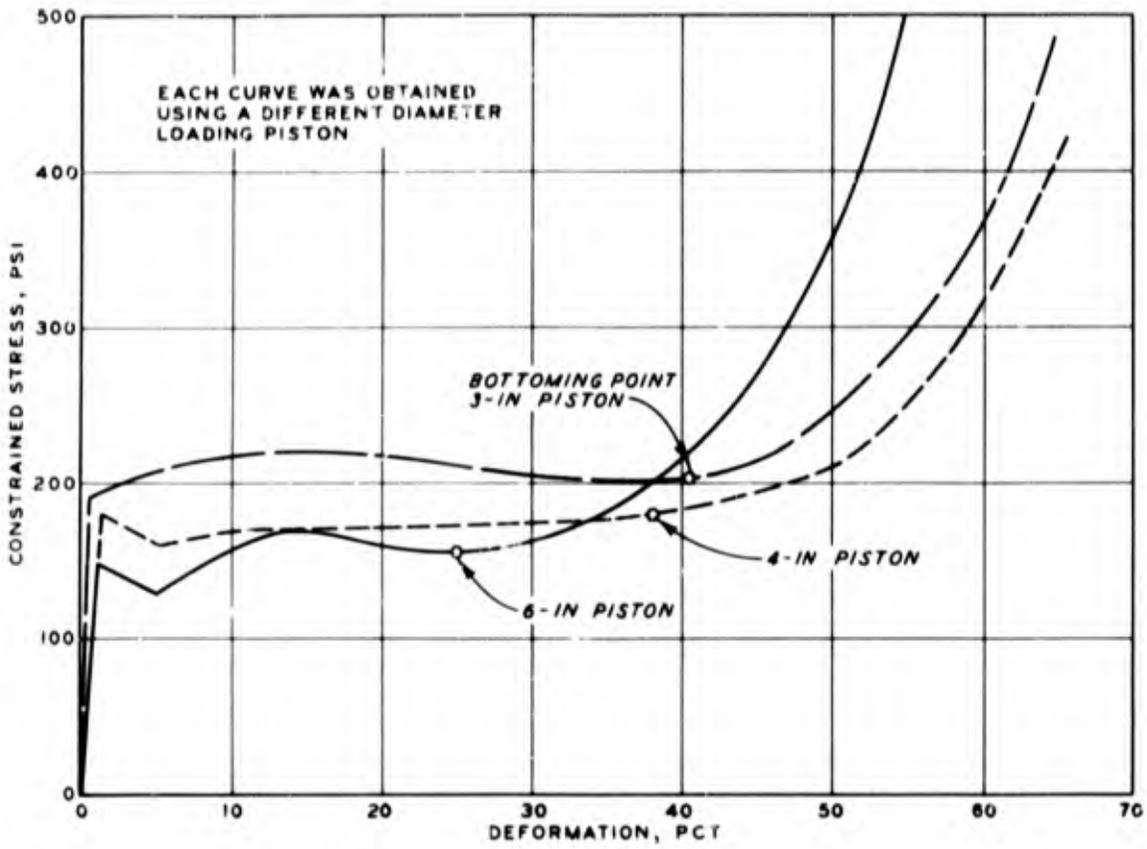

Figure A.7 Effect of piston size on bottoming point.

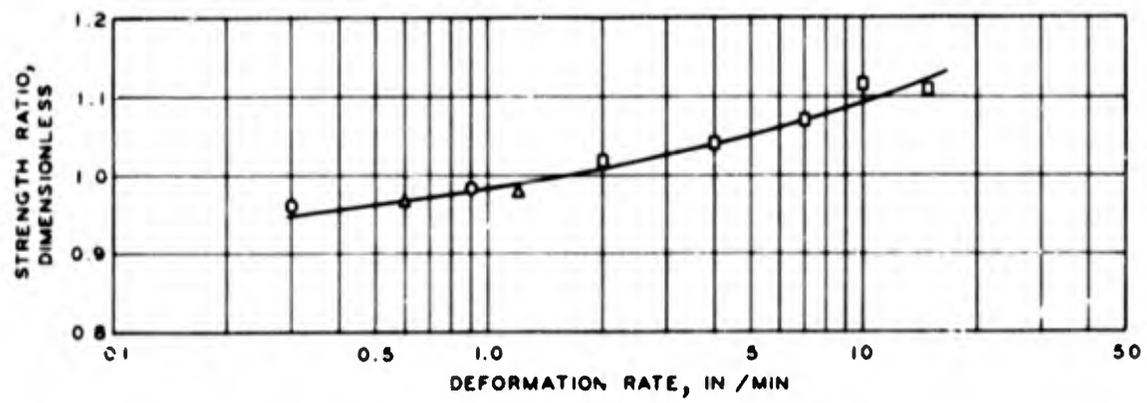

Figure A.8 Rate of deformation effects.

APPENDIX B

TEST DATA

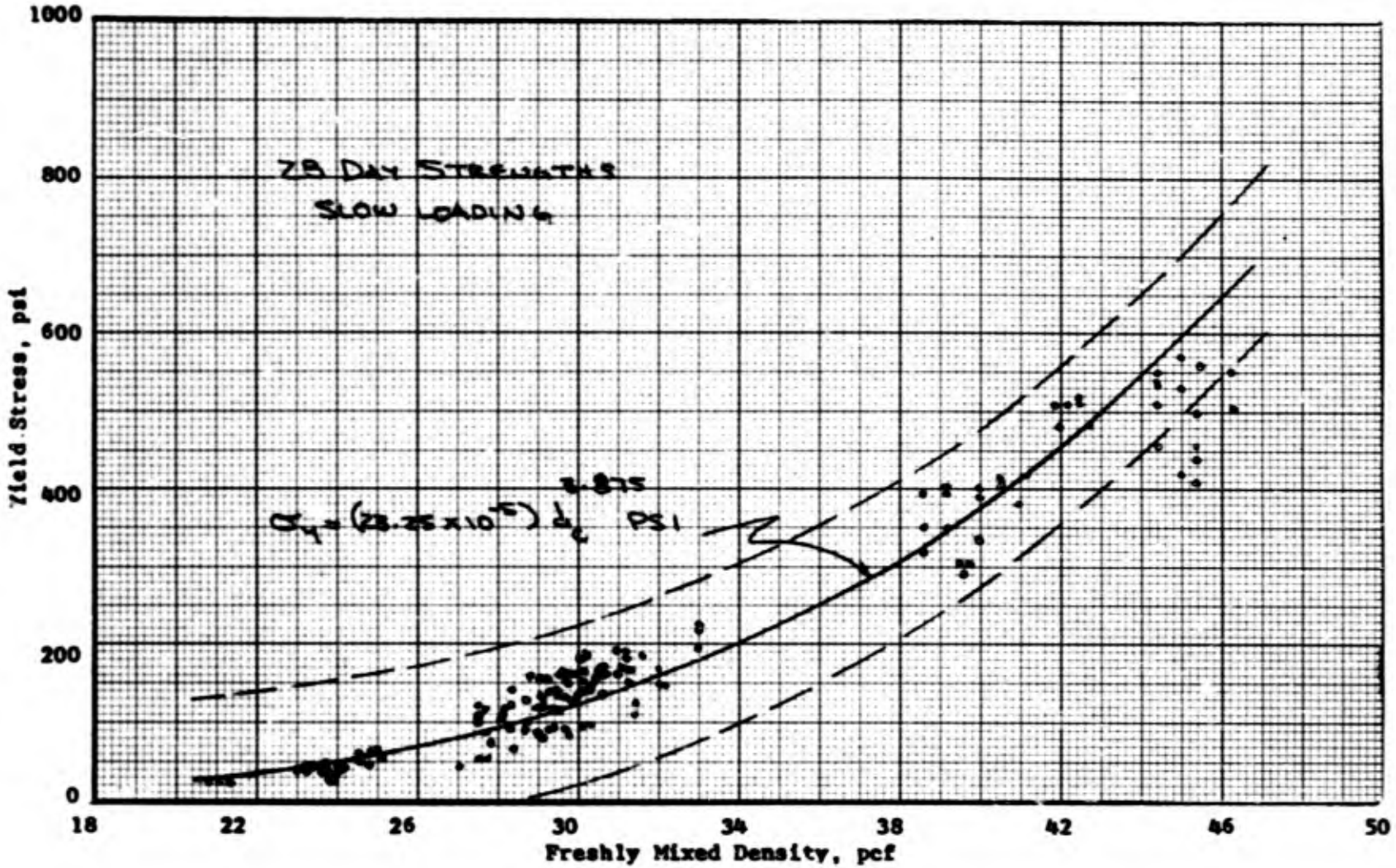

Figure B.1 Yield stress versus freshly mixed density relation for cellular concrete with an 0.66 water-cement ratio.

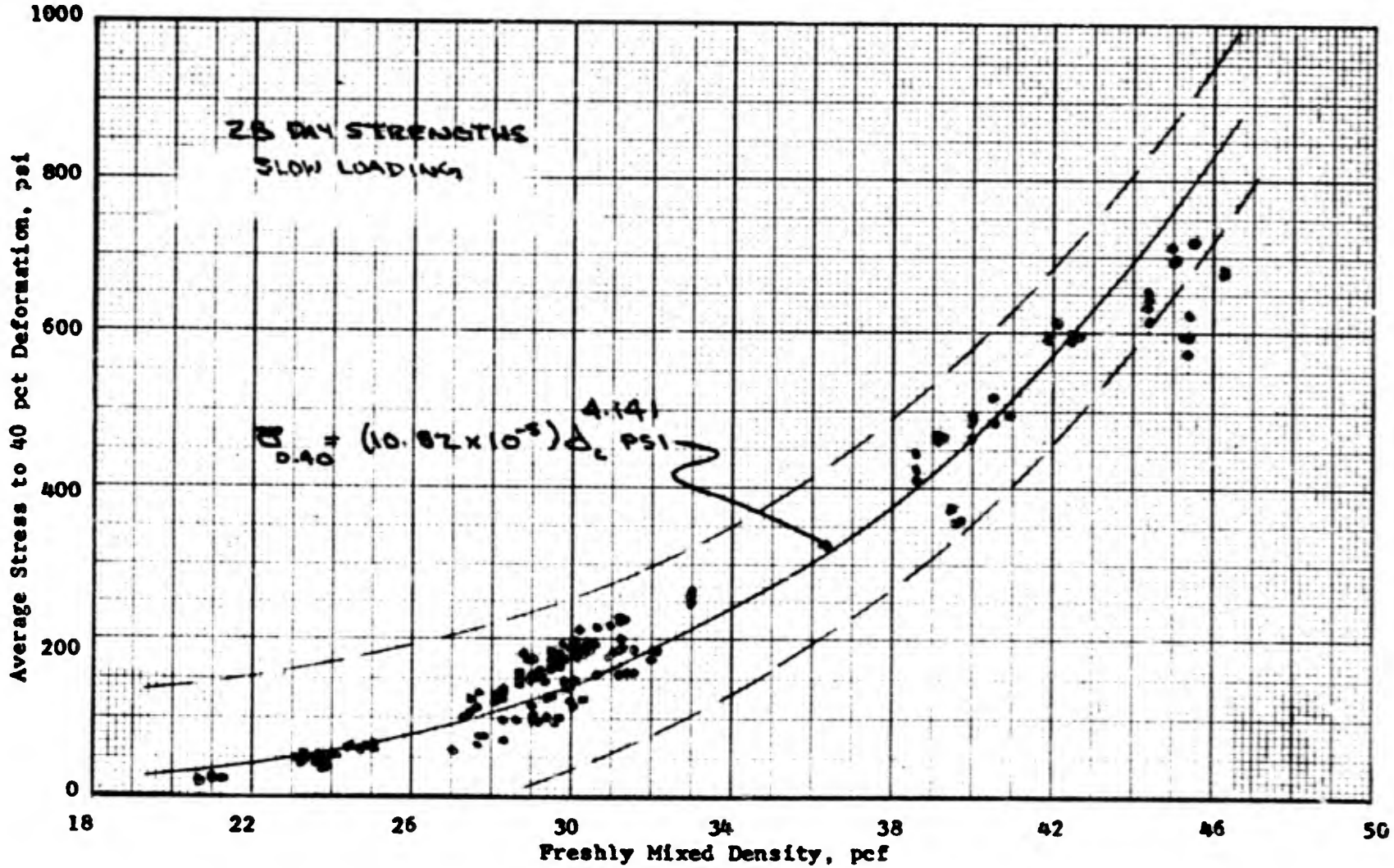

Figure B.2 Average stress versus freshly mixed density relation for cellular concrete with an 0.66 water-cement ratio.

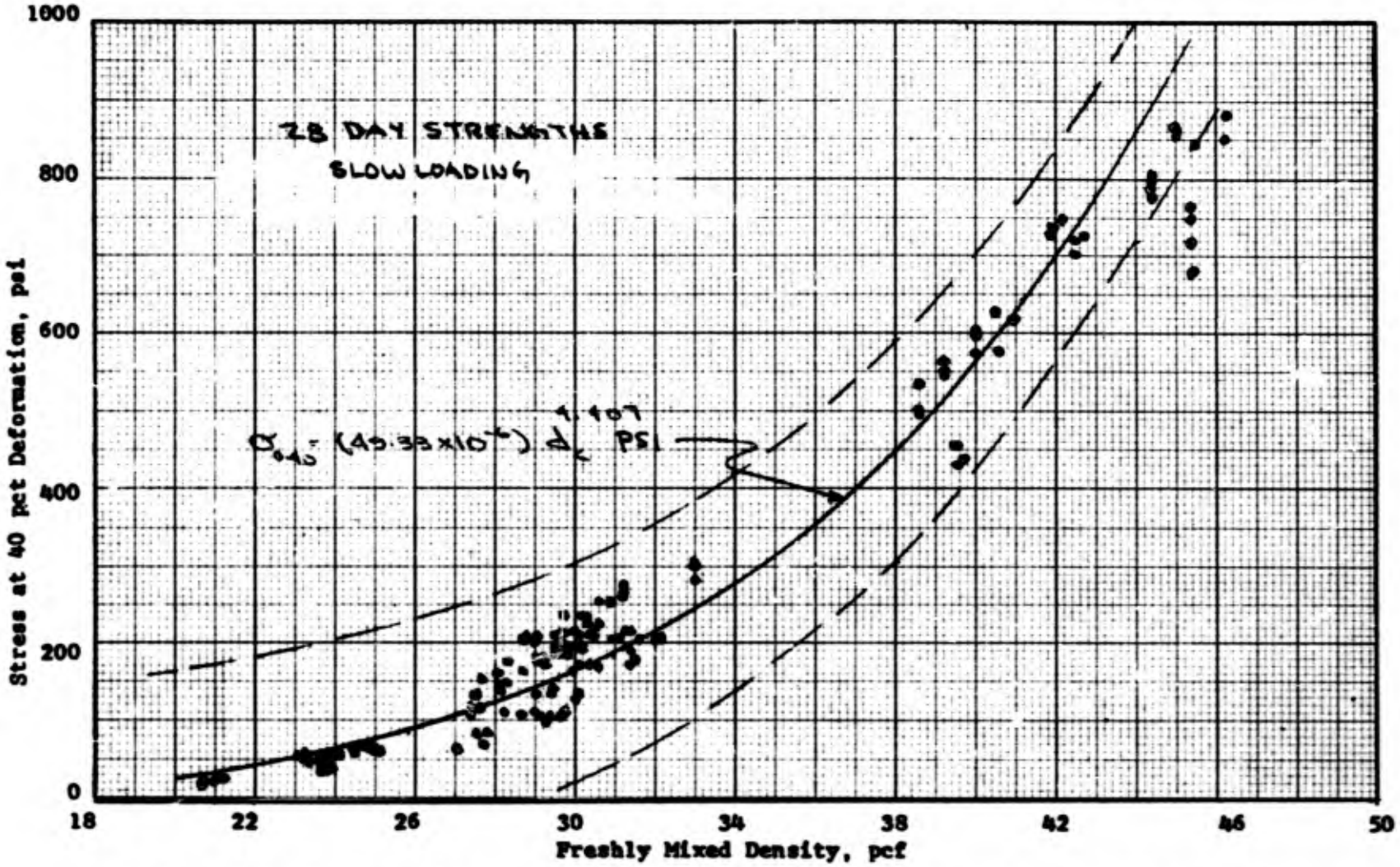

Figure B.3 Stress at 40 percent deformation versus freshly mixed density relation for cellular concrete with an 0.66 water-cement ratio.

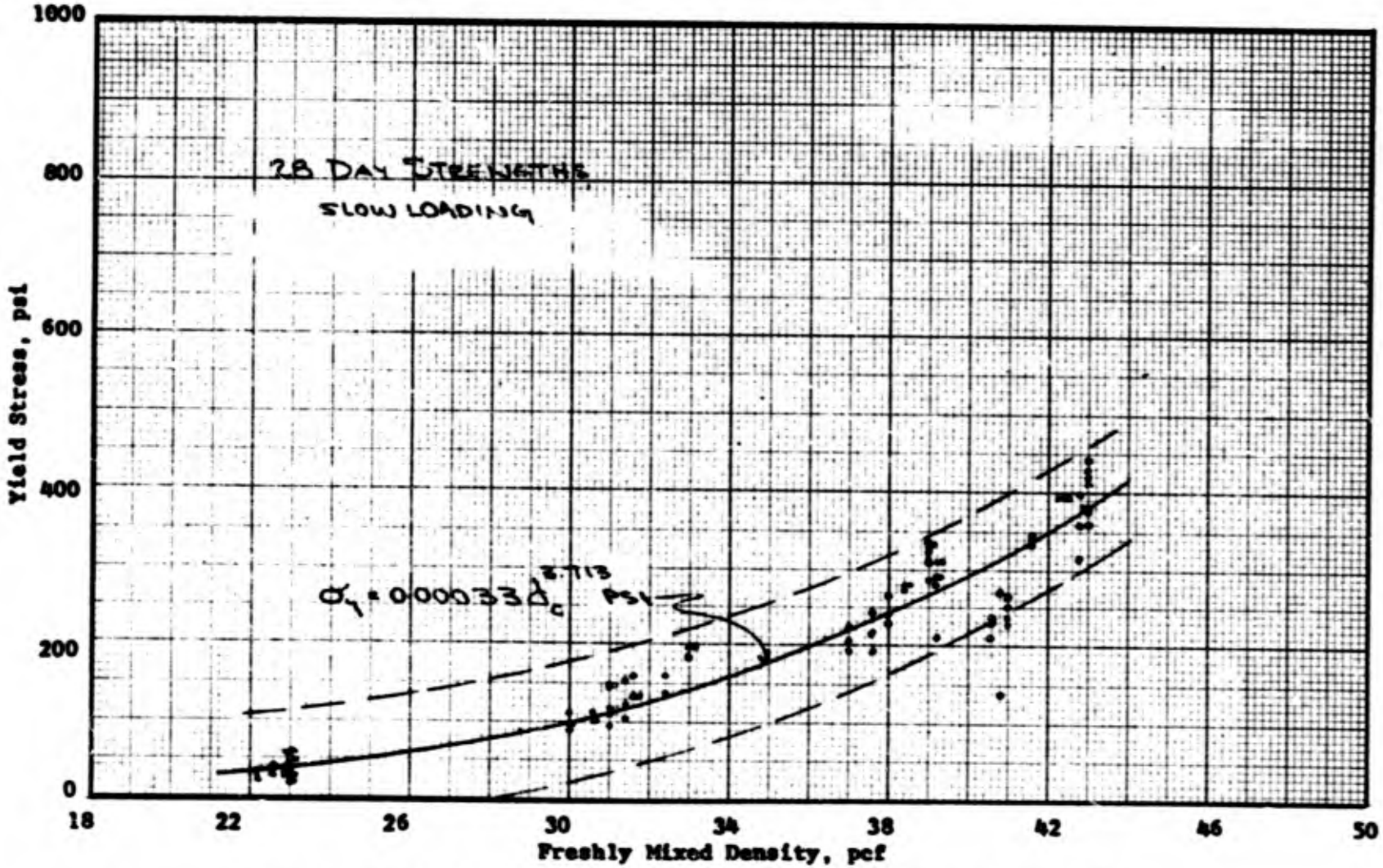

Figure B.4 Yield stress versus freshly mixed density relation for cellular concrete with an 0.76 water-cement ratio.

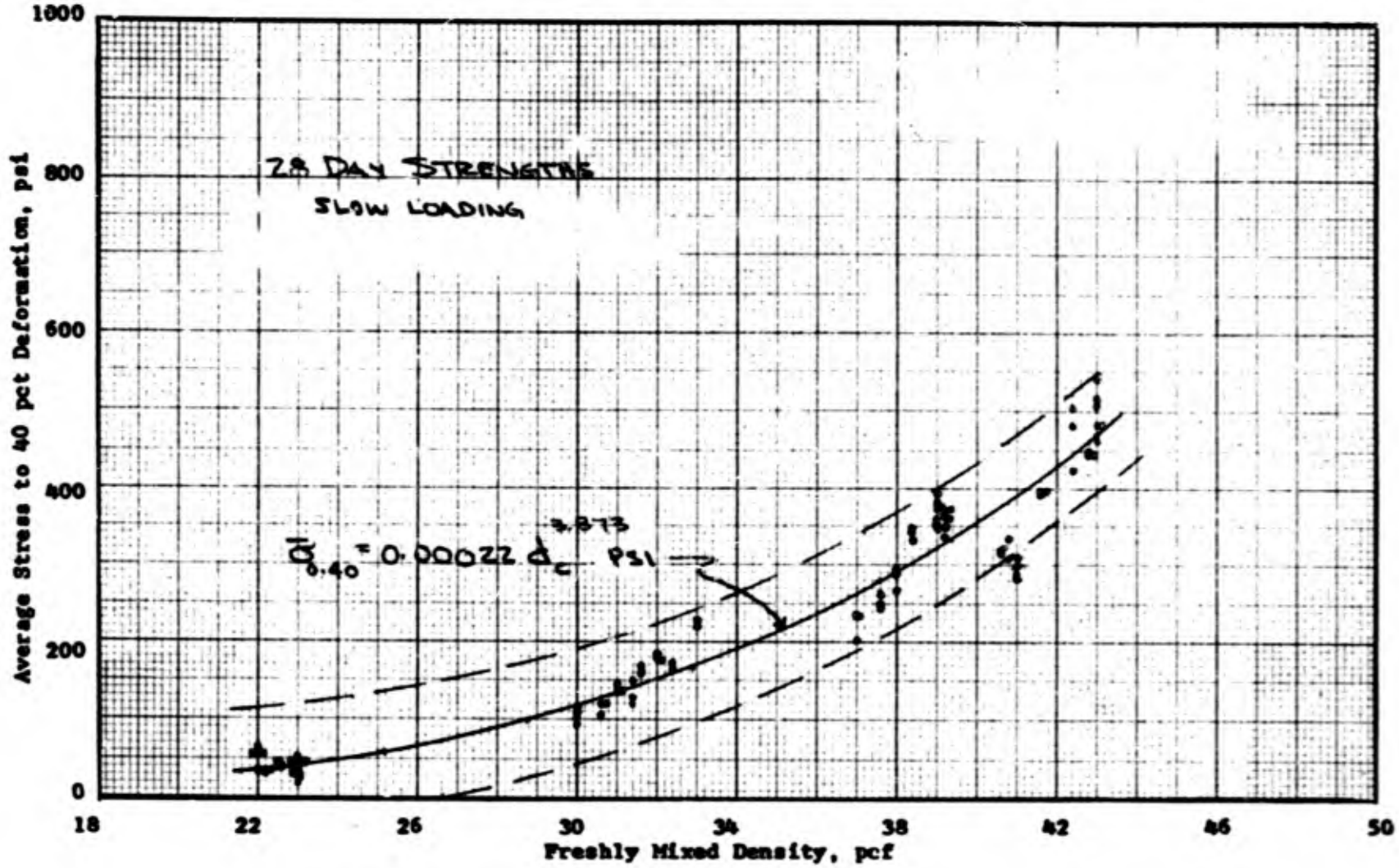

Figure B.5 Average stress versus freshly mixed density relation for cellular concrete with an 0.76 water-cement ratio.

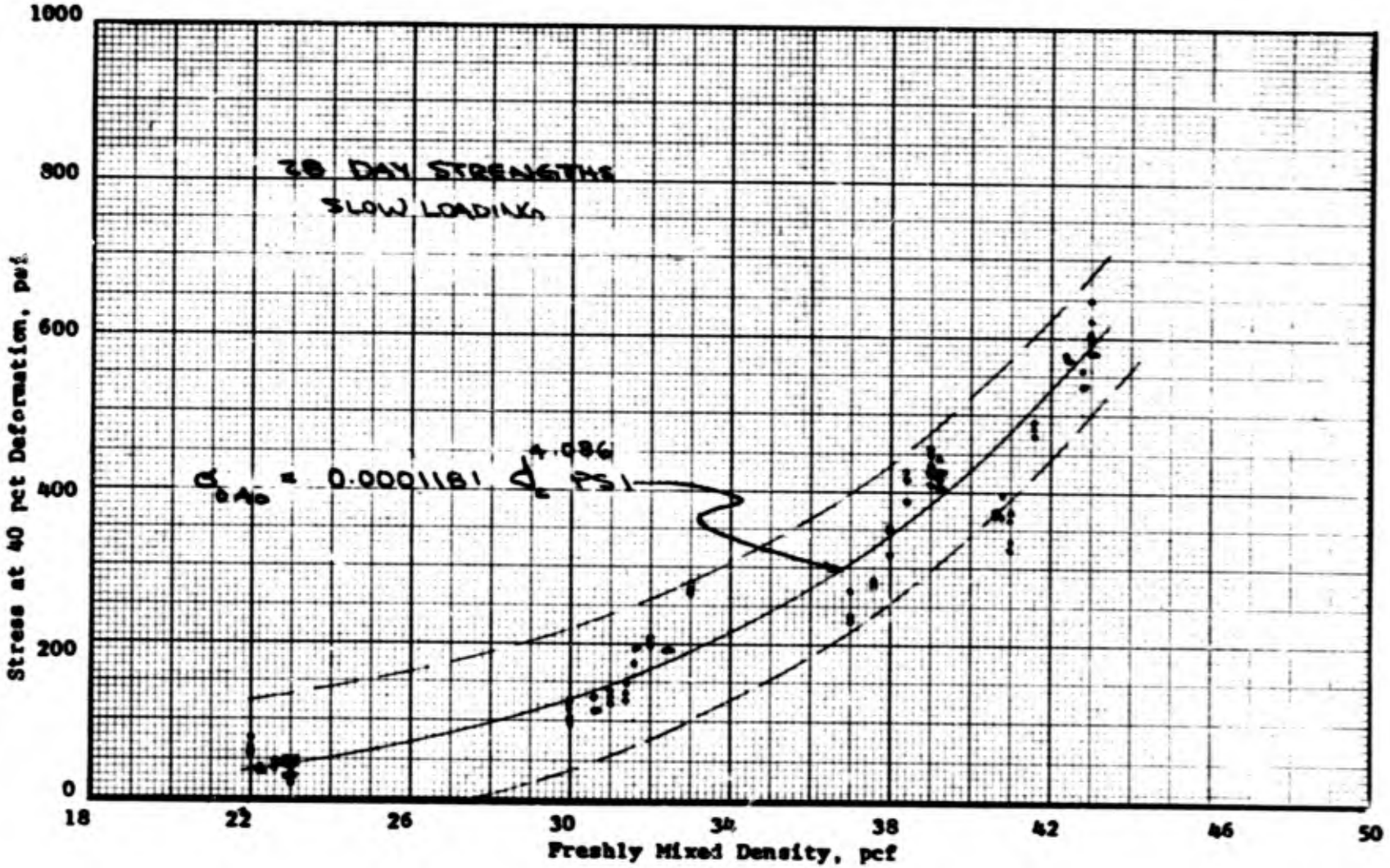

Figure B.6 Stress at 40 percent deformation versus freshly mixed density relation for cellular concrete with an 0.76 water-cement ratio.

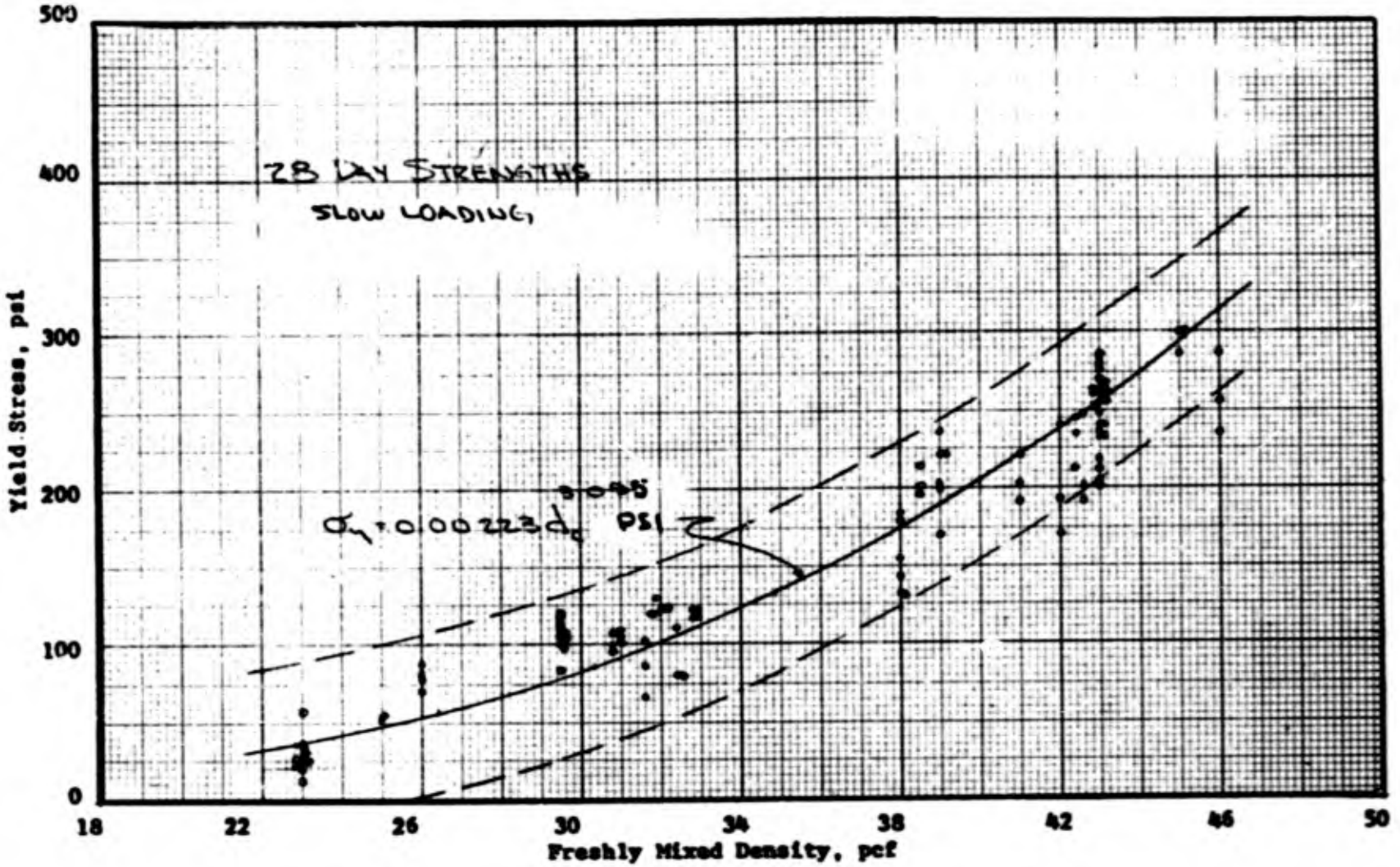

Figure B.7 Yield stress versus freshly mixed density relation for cellular concrete with an 0.86 water-cement ratio.

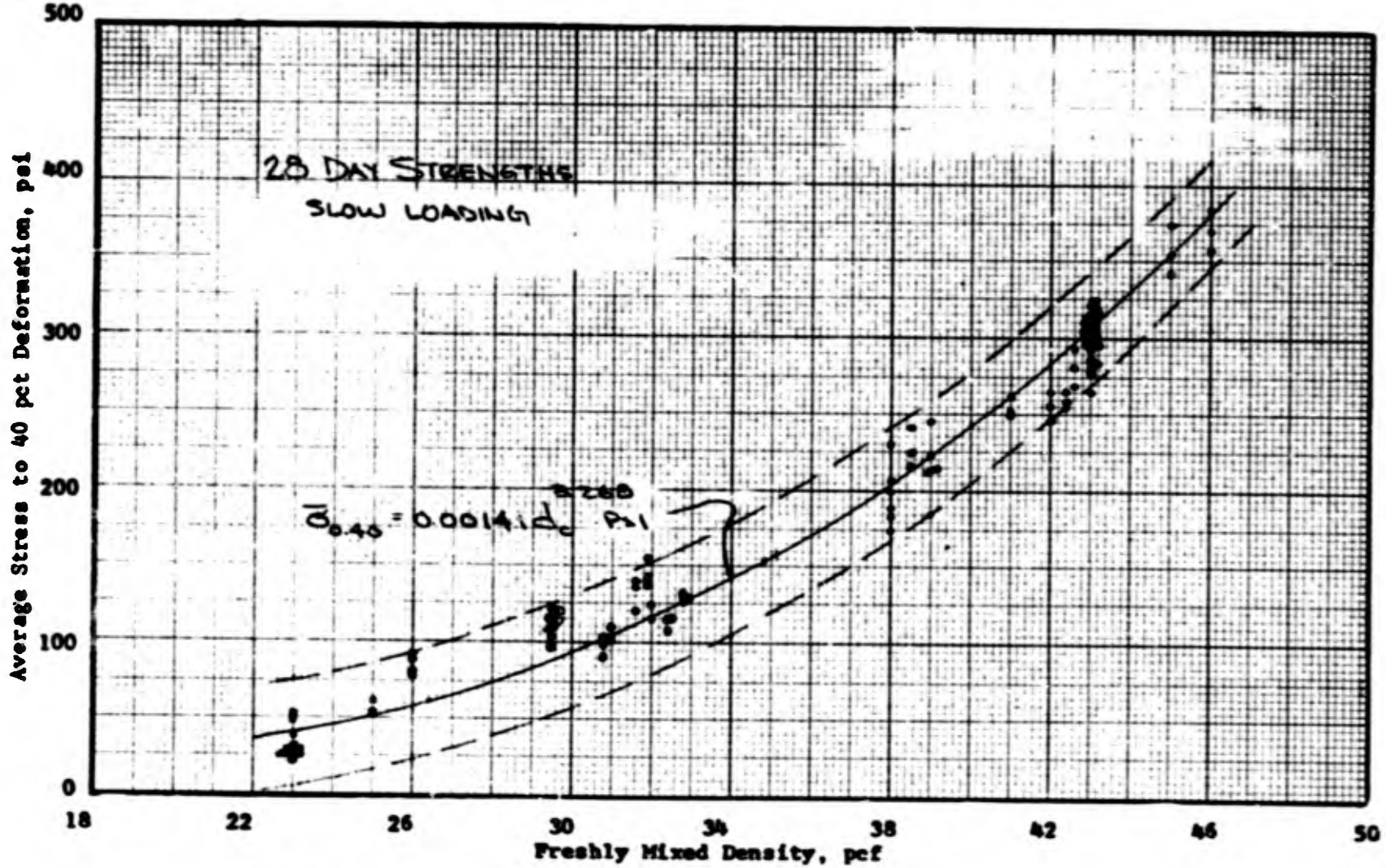

Figure B.8 Average stress versus freshly mixed density relation for cellular concrete with an 0.86 water-cement ratio.

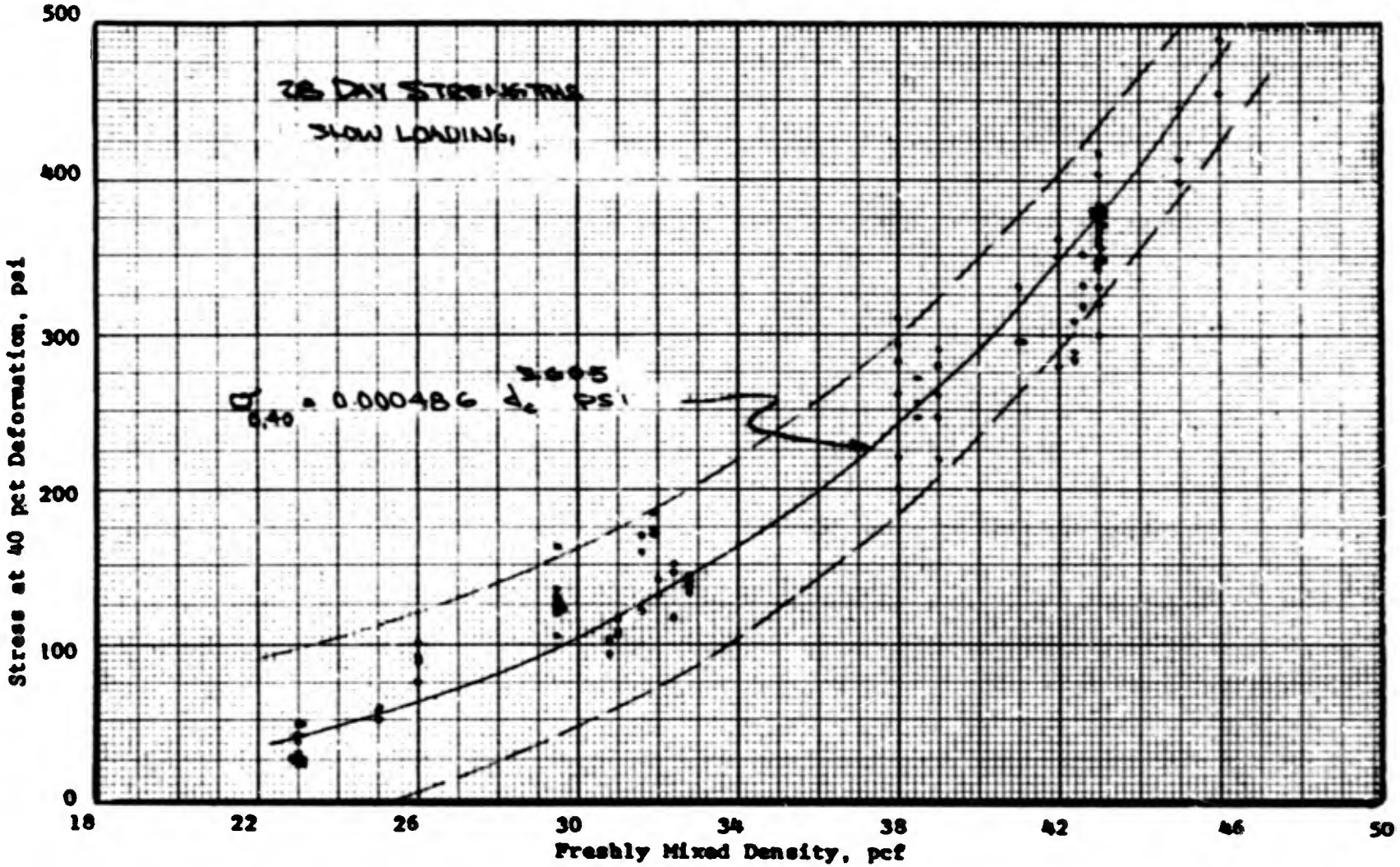

Figure B.9 Stress at 40 percent deformation versus freshly mixed density relation for cellular concrete with an 0.86 water-cement ratio.

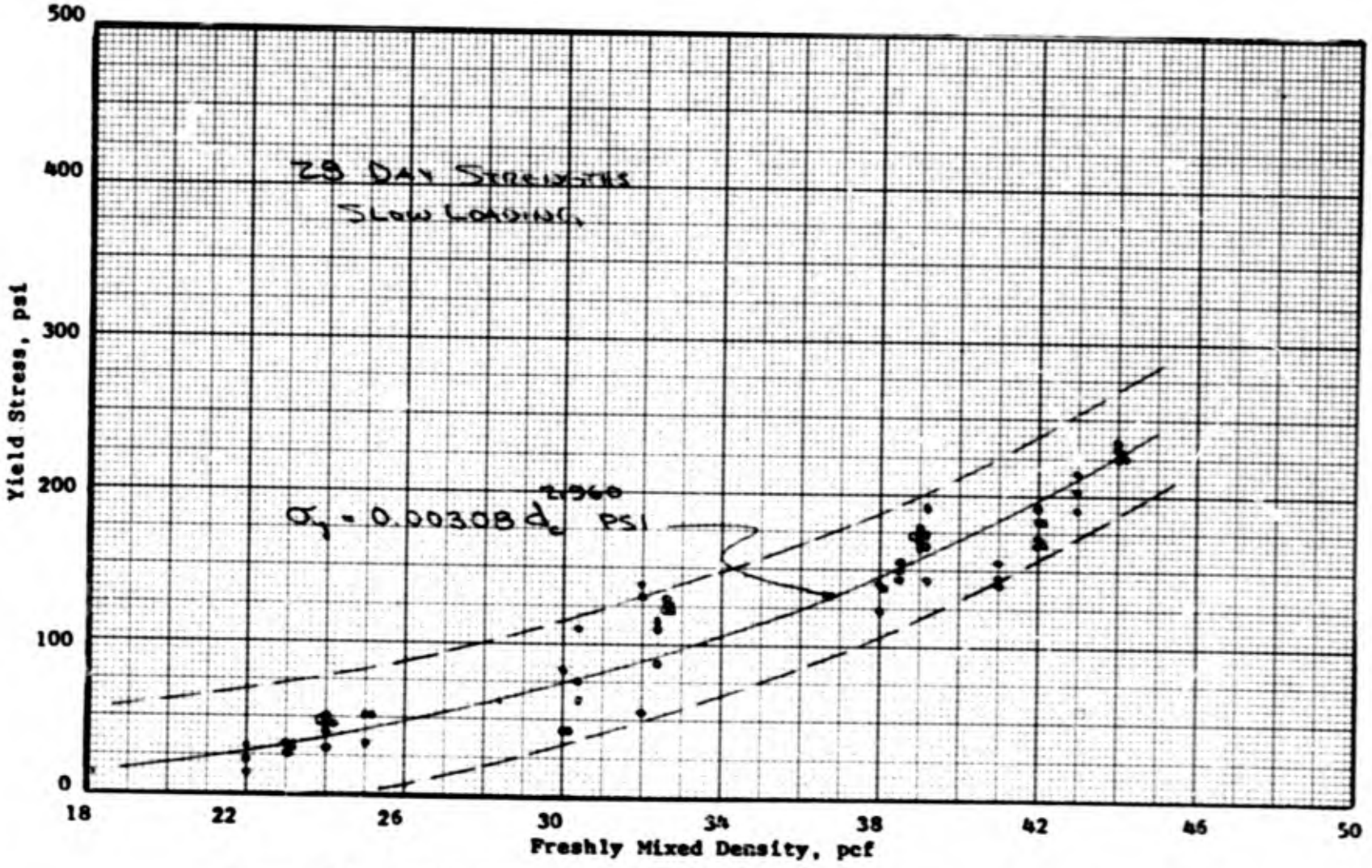

Figure B.10 Yield stress versus fresnly mixed density relation for cellular concrete with an 0.96 water-cement ratio.

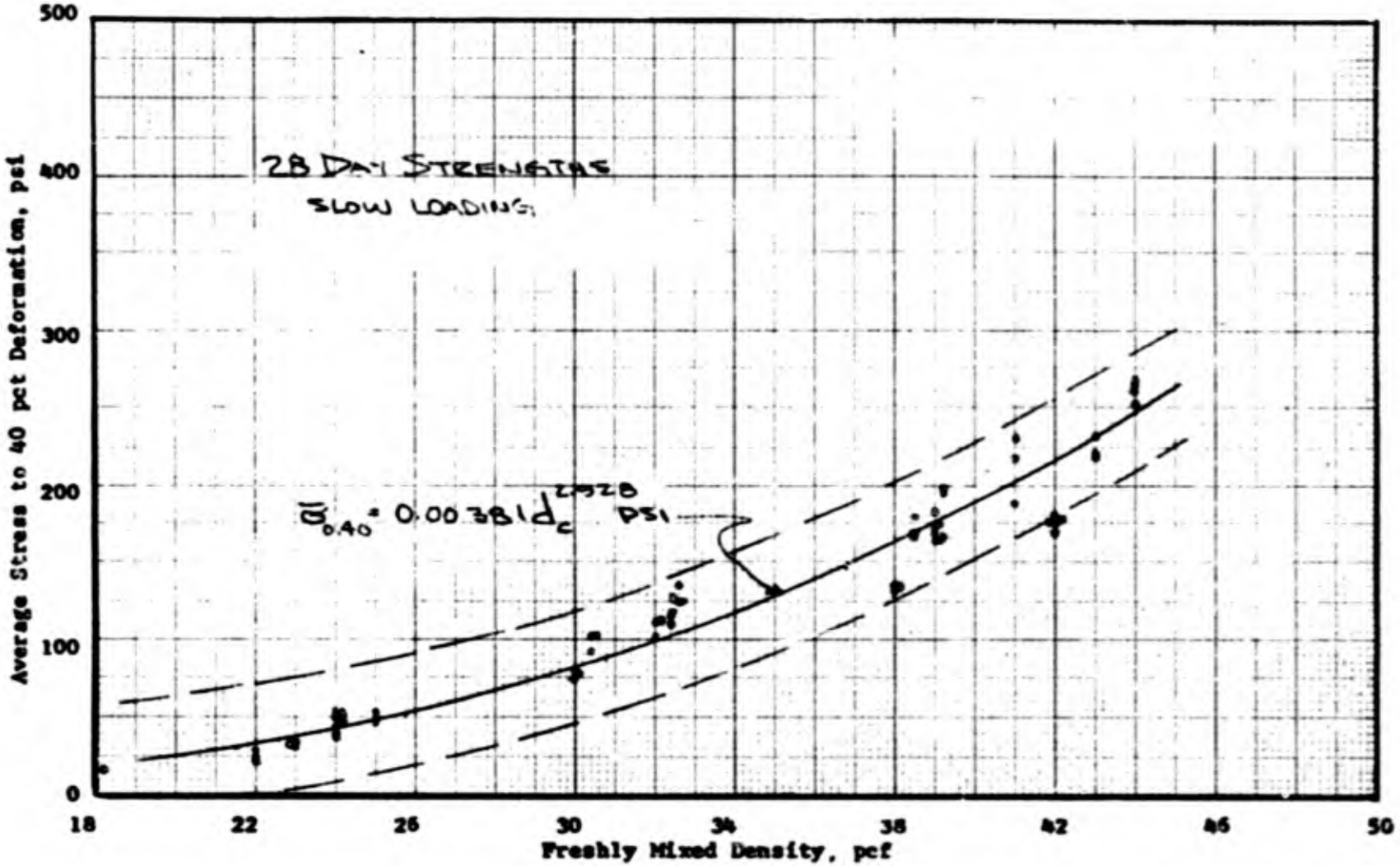

Figure 3.11 Average stress versus freshly mixed density relation for cellular concrete with an 0.96 water-cement ratio.

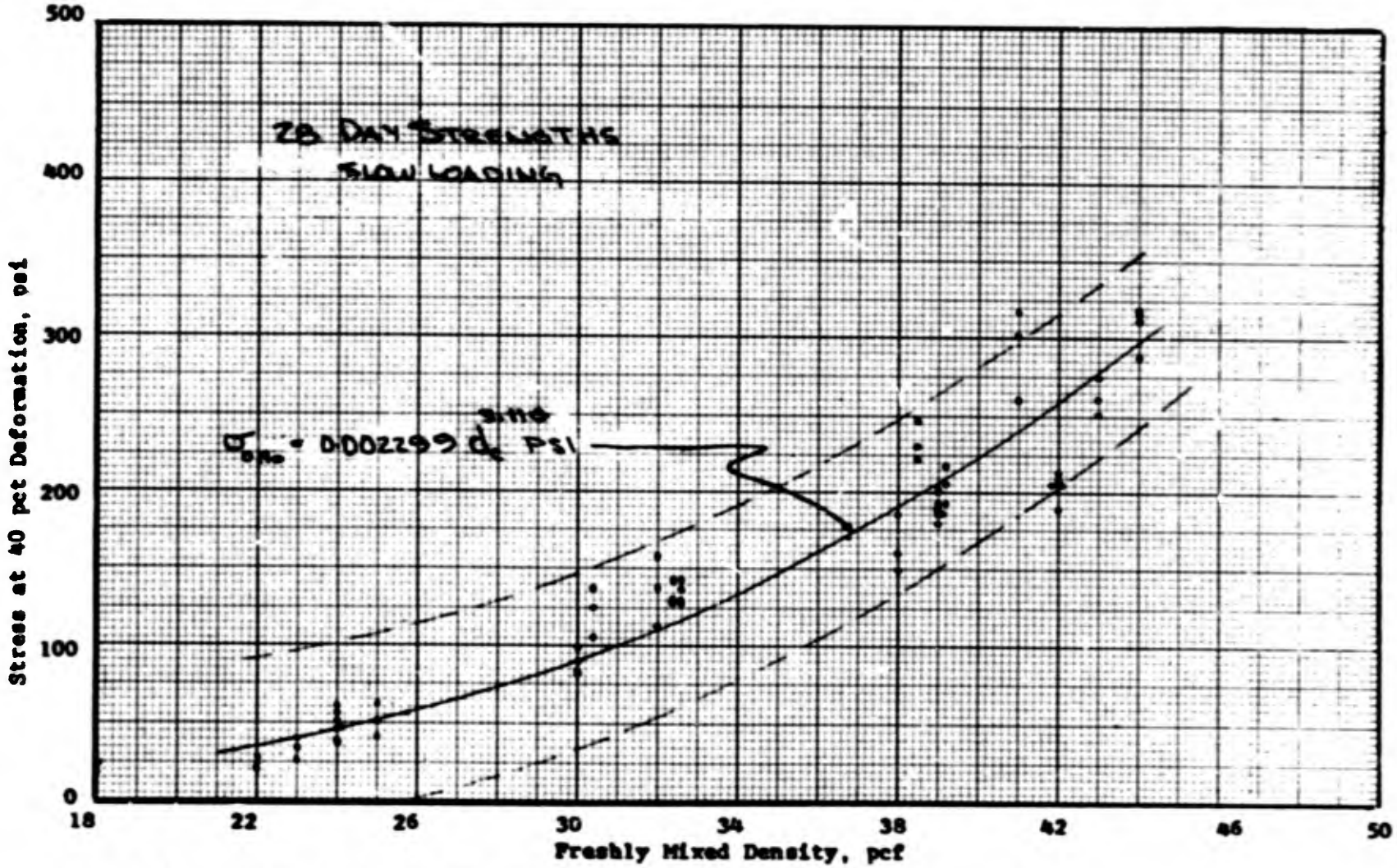

Figure B.12 Stress at 40 percent deformation versus freshly mixed density relation for cellular concrete with an 0.96 water-cement ratio.

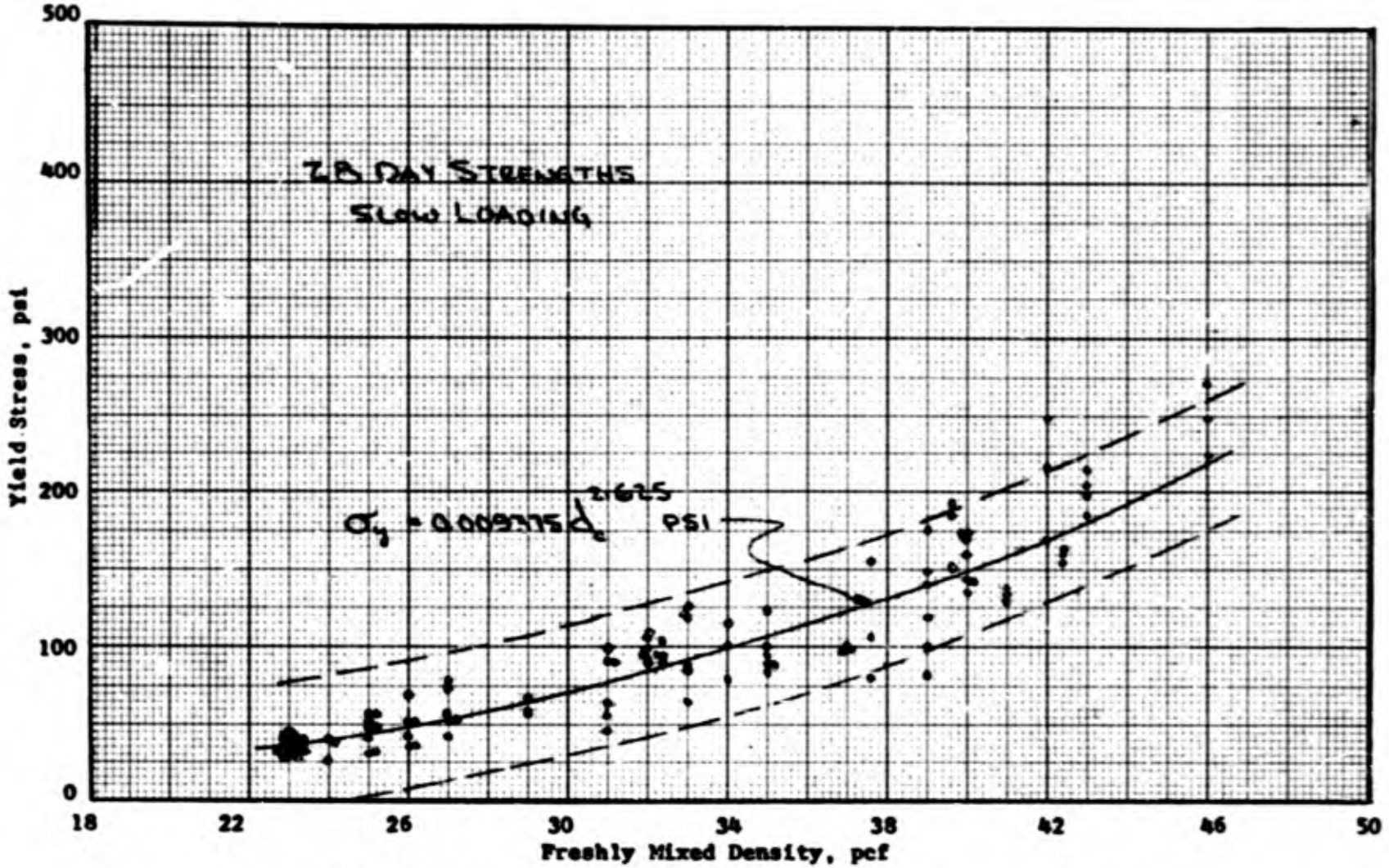

Figure B.13 Yield stress versus freshly mixed density relation for cellular concrete with a 1.06 water-cement ratio.

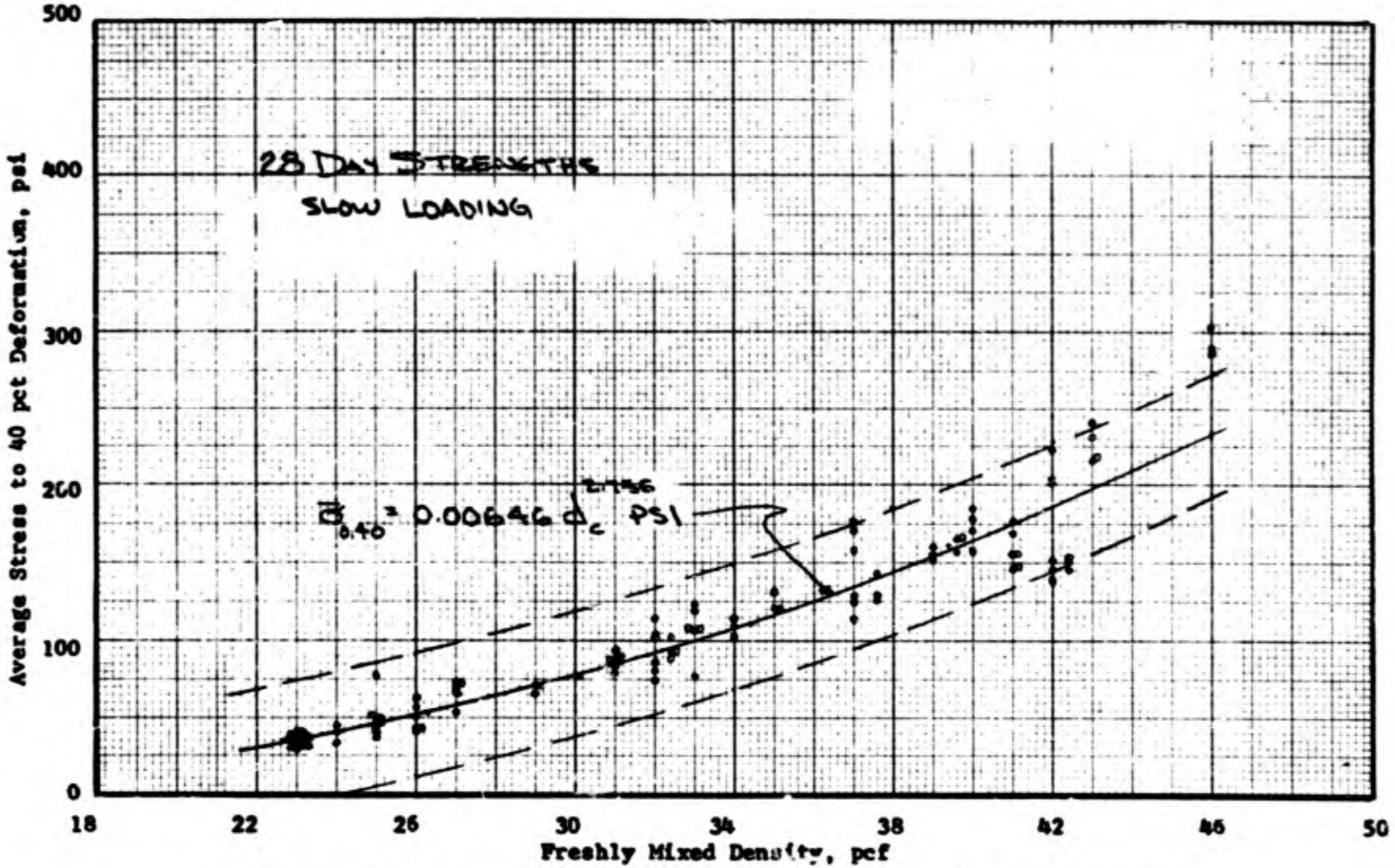

Figure B.14 Average stress versus freshly mixed density relation for cellular concrete with a 1.06 water-cement ratio.

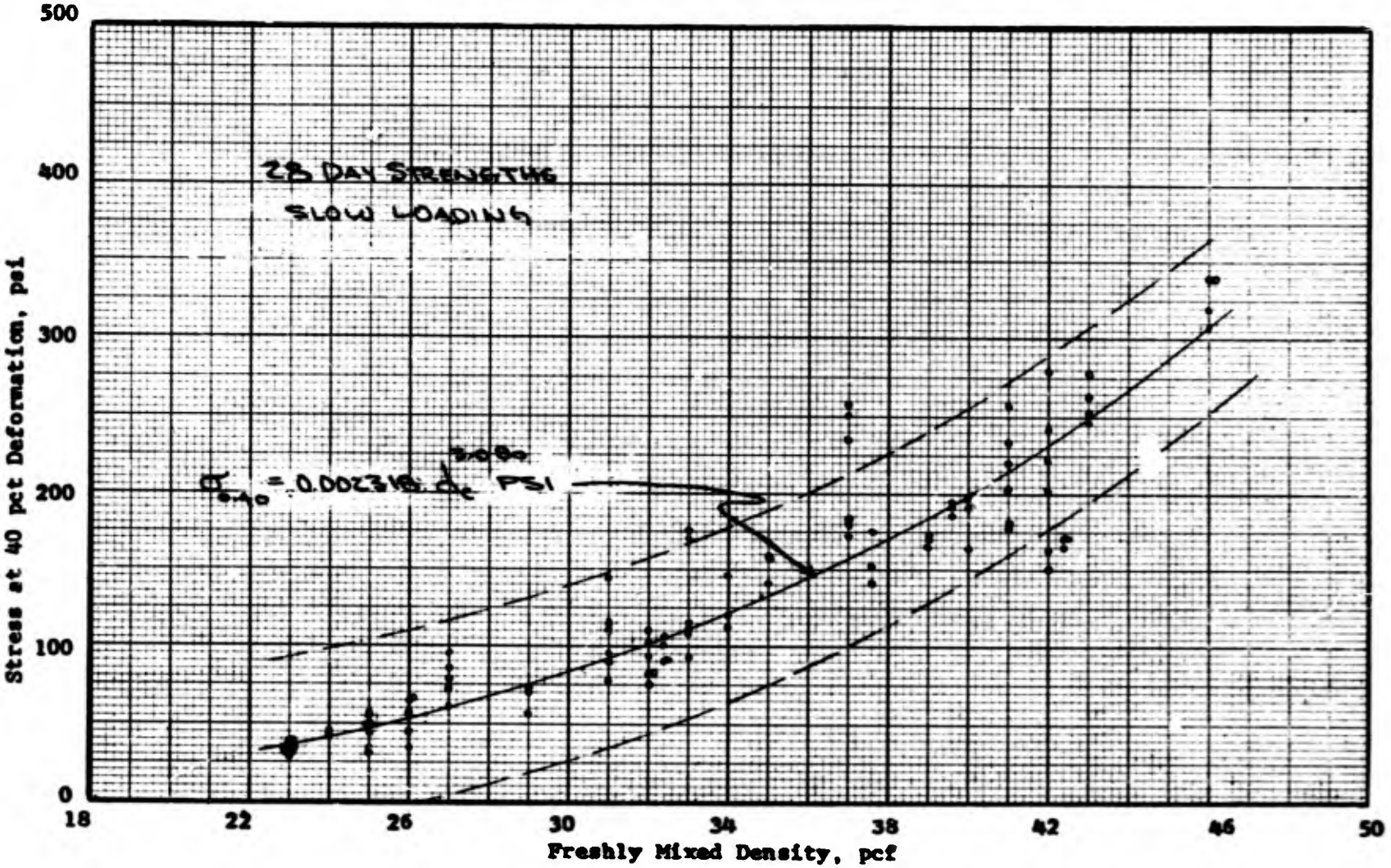

Figure B.15 Stress at 40 percent deformation versus freshly mixed density relation for cellular concrete with a 1.06 water-cement ratio.

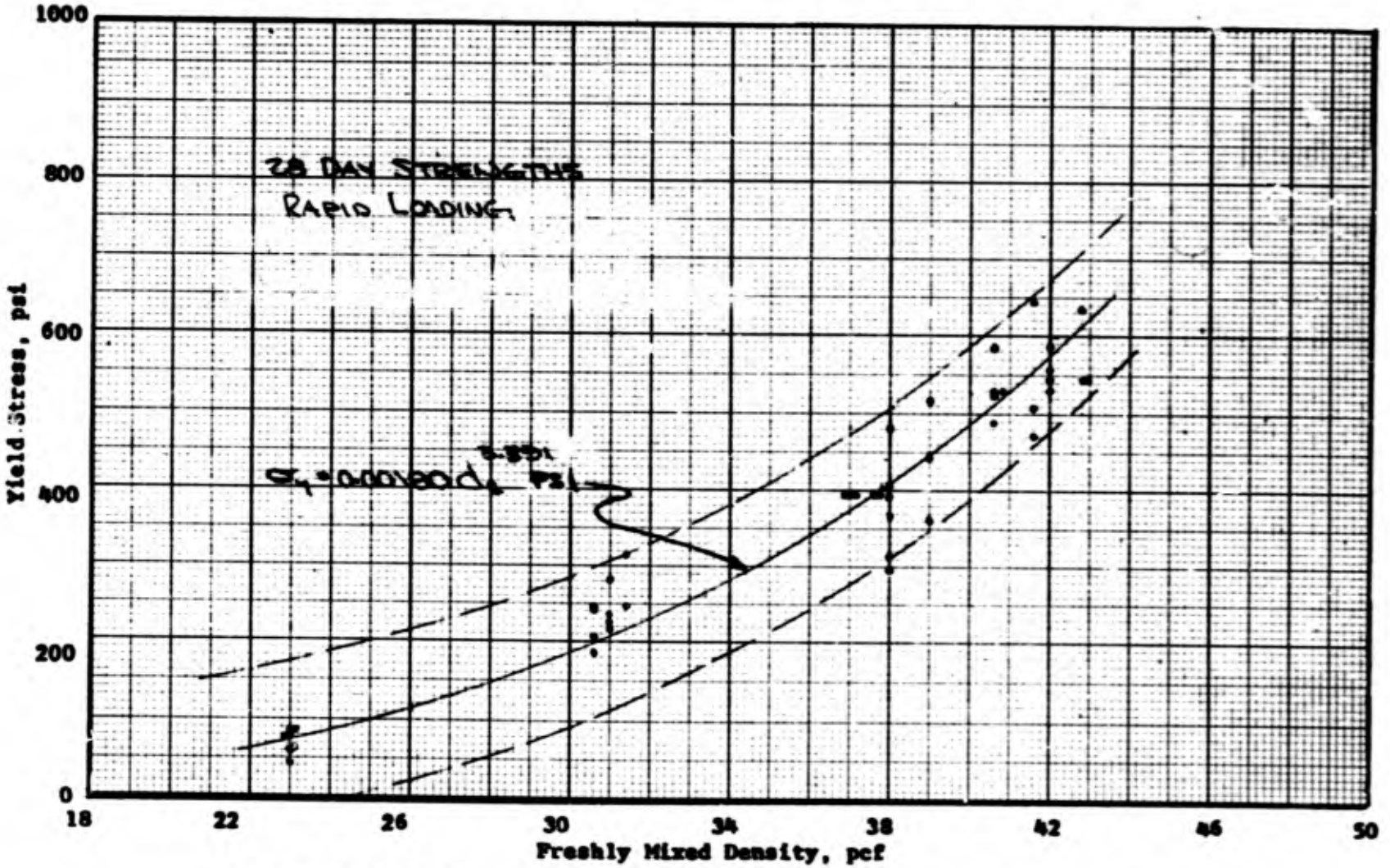

Figure B.16 Yield stress versus freshly mixed density relation for rapidly loaded cellular concrete with an 0.76 water-cement ratio.

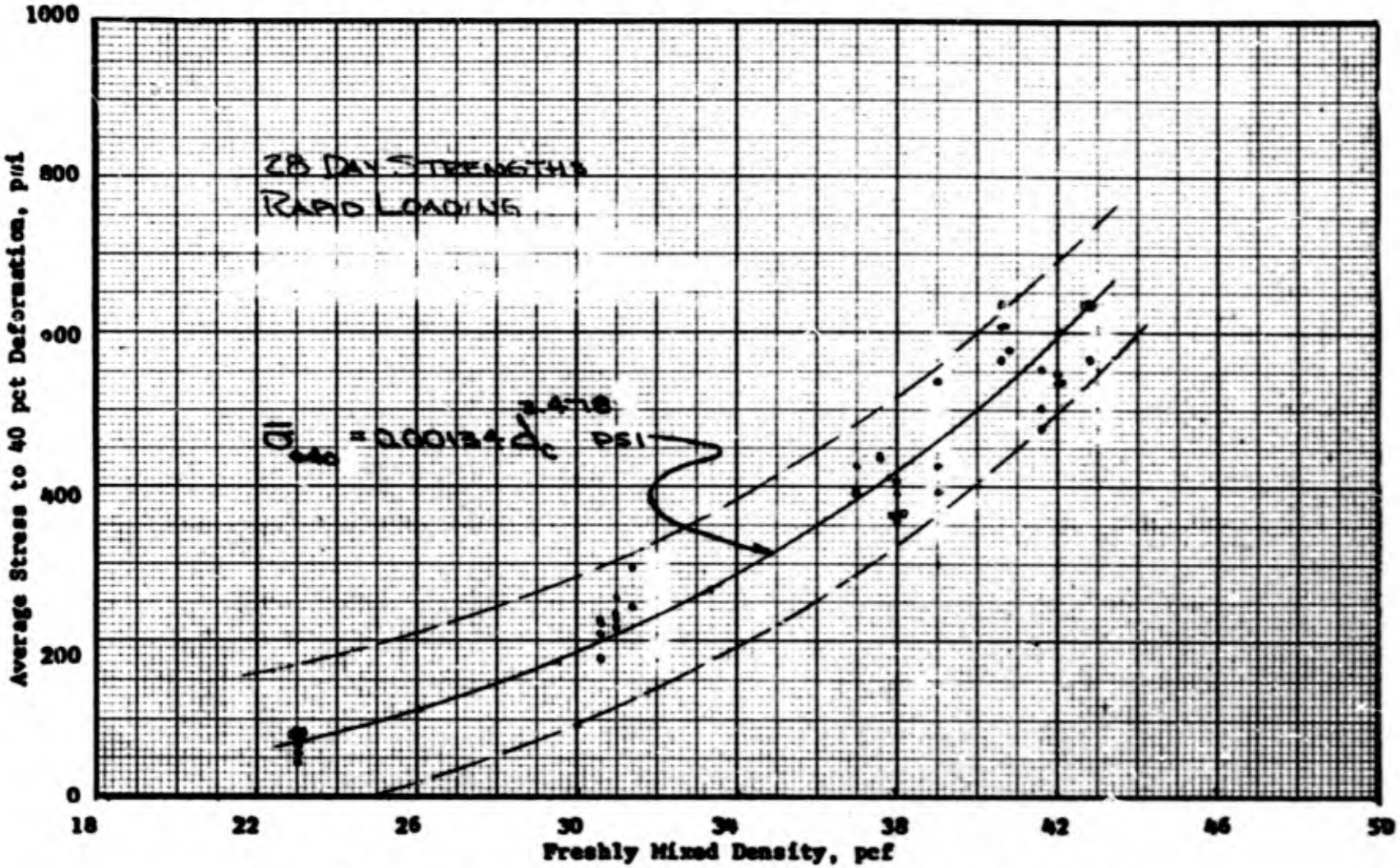

Figure B.17 Average stress versus freshly mixed density relation for rapidly loaded cellular concrete with an 0.76 water-cement ratio.

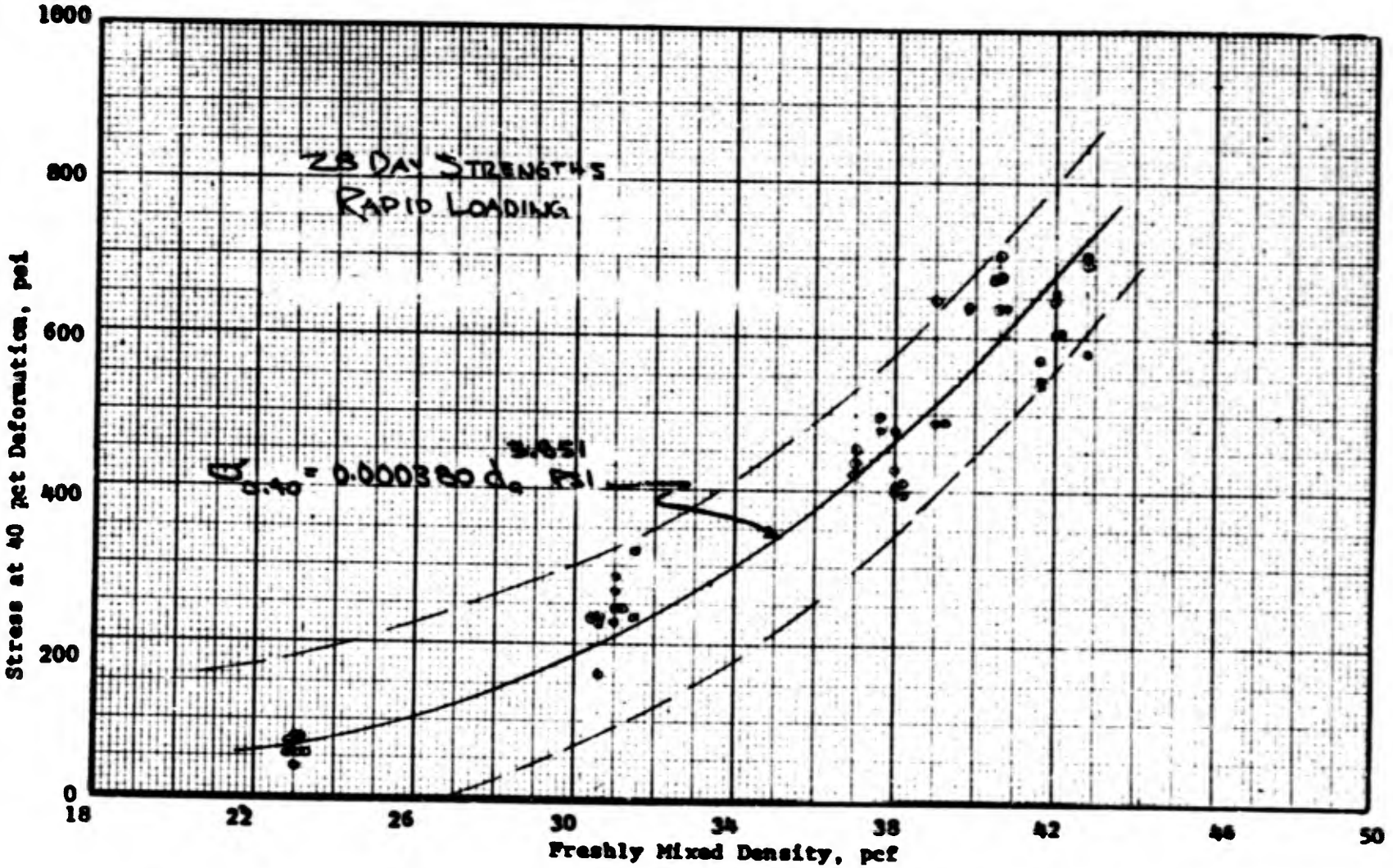

Figure B.18 Stress at 40 percent deformation versus freshly mixed density relation for rapidly loaded cellular concrete with an 0.76 water-cement ratio.

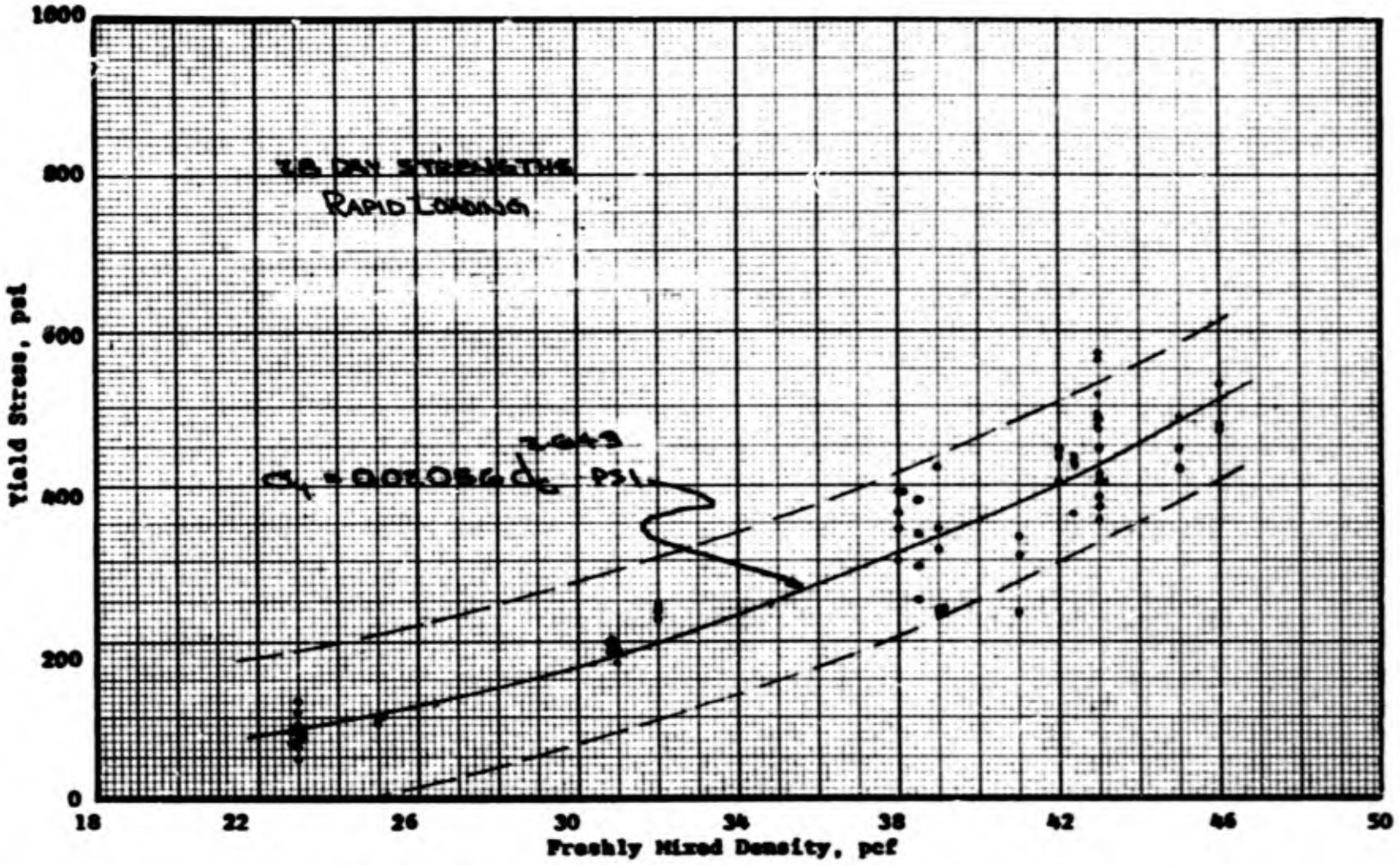

Figure B.19 Yield stress versus freshly mixed density relation for rapidly loaded cellular concrete with an 0.86 water-cement ratio.

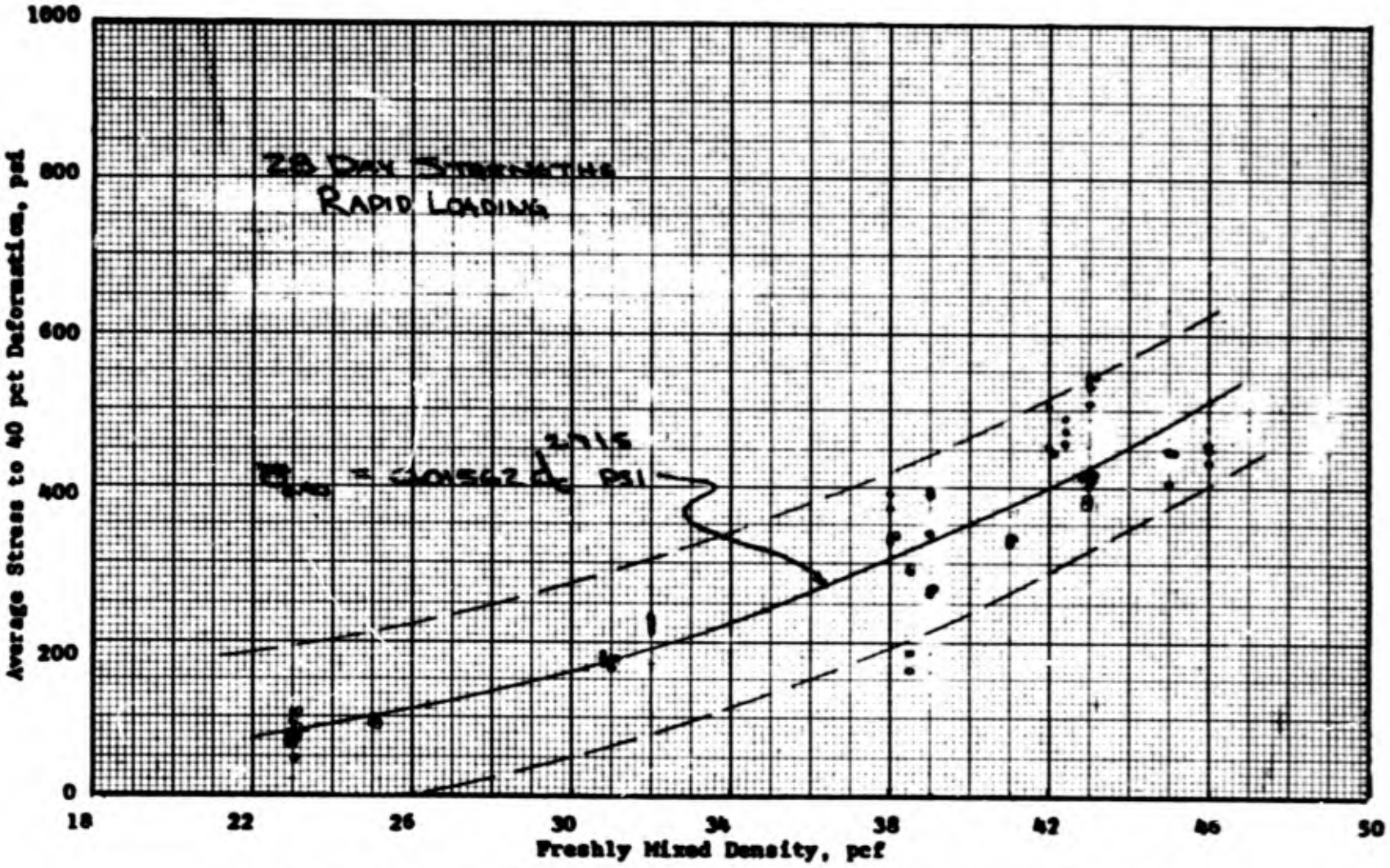

Figure B.20 Average stress versus freshly mixed density relation for rapidly loaded cellular concrete with ar 0.86 water-cement ratio.

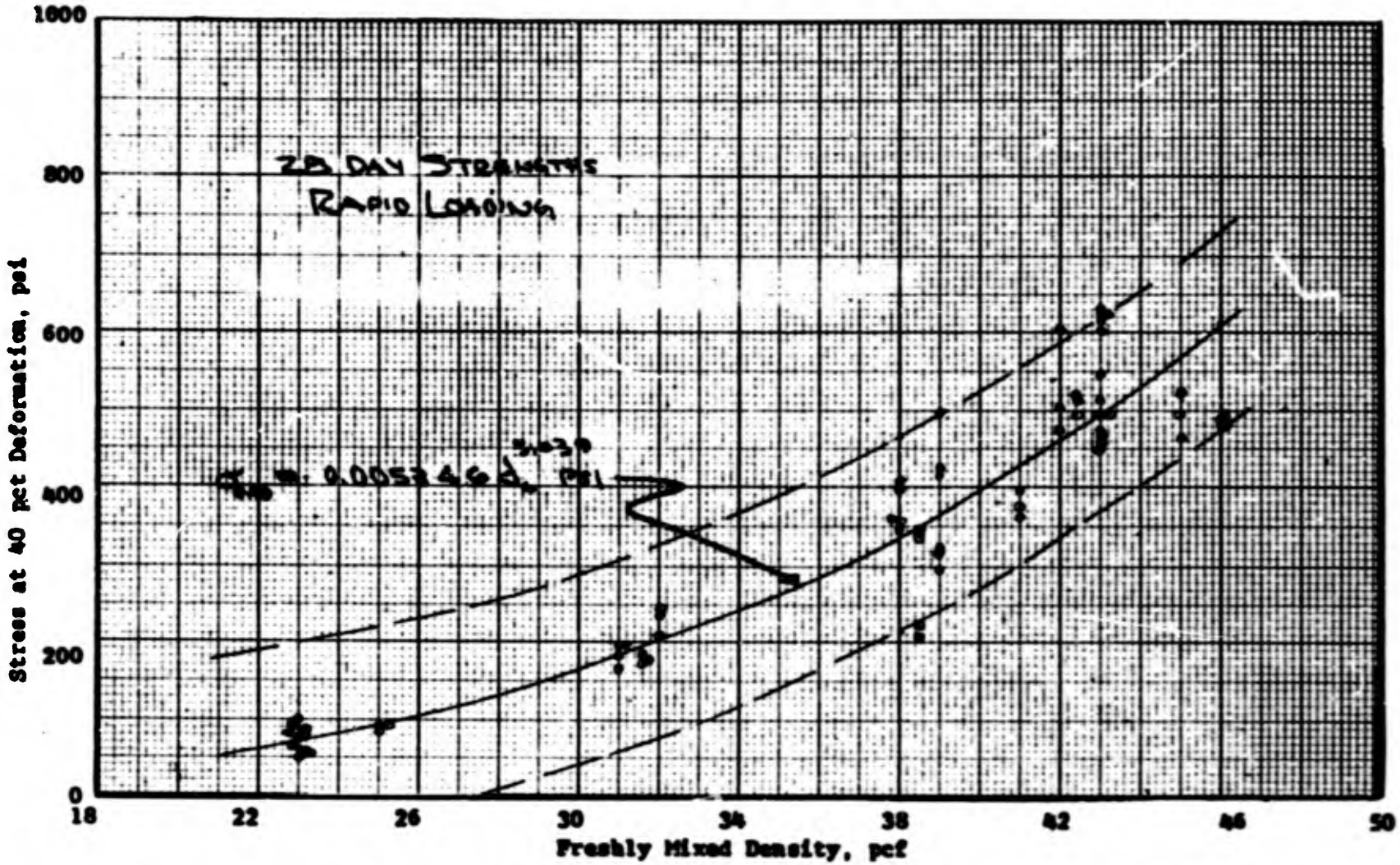

Figure B.21 Stress at 40 percent deformation versus freshly mixed density relation for rapidly loaded cellular concrete with an 0.86 water-cement ratio.

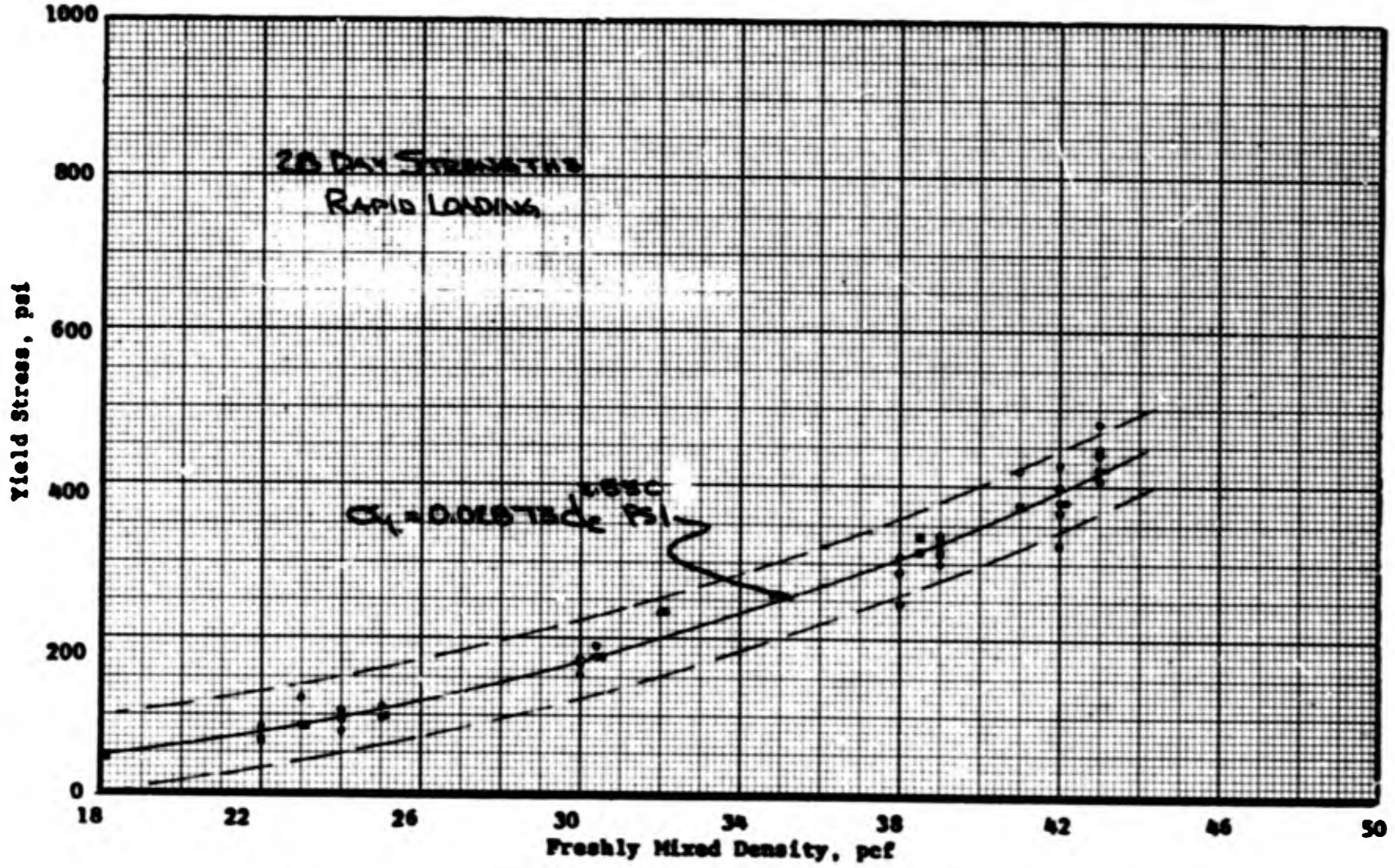

Figure B.22 Yield stress versus freshly mixed density relation for rapidly loaded cellular concrete with an 0.96 water-cement ratio.

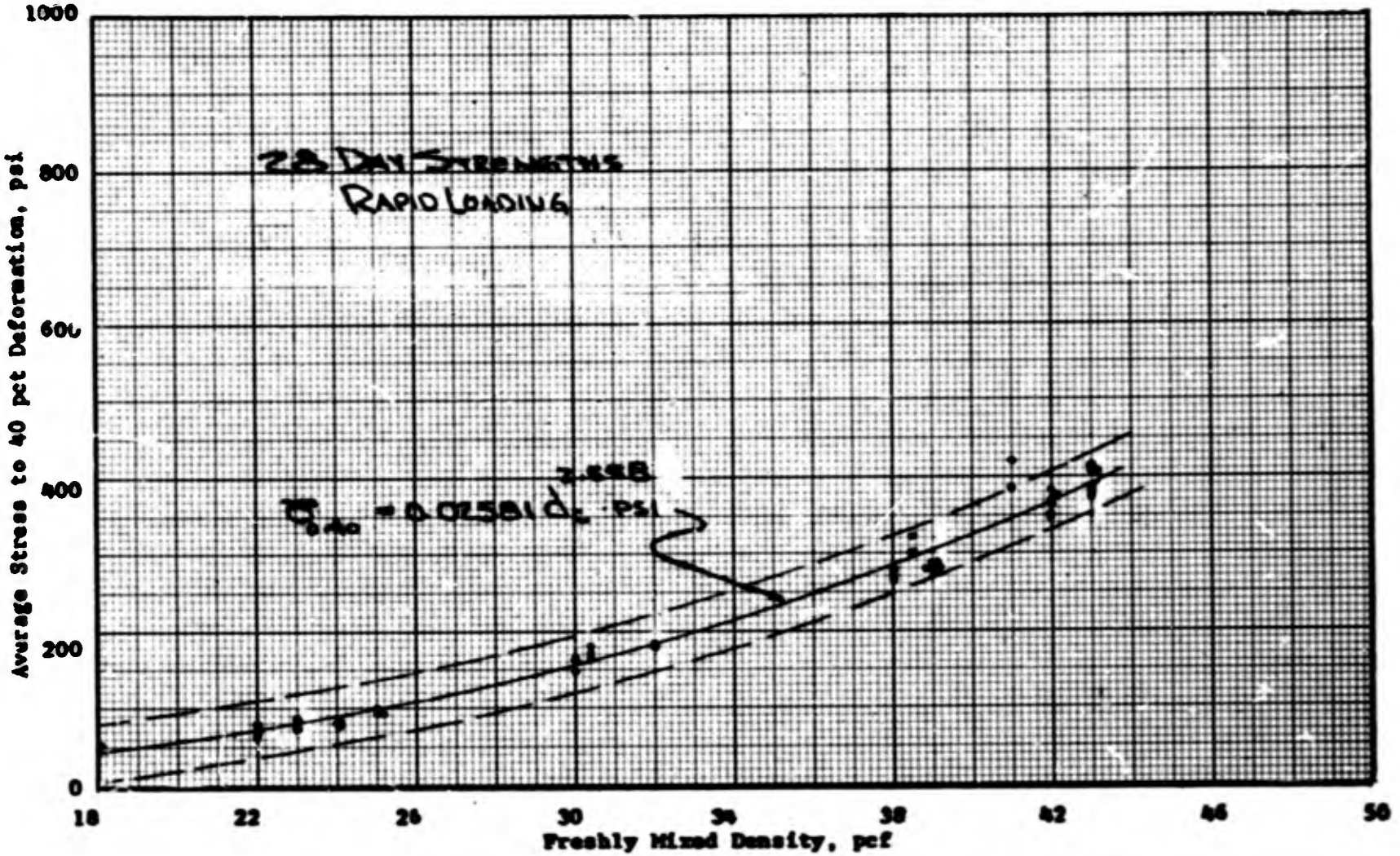

Figure B.23 Average stress versus freshly mixed density relation for rapidly loaded cellular concrete with an 0.96 water-cement ratio.

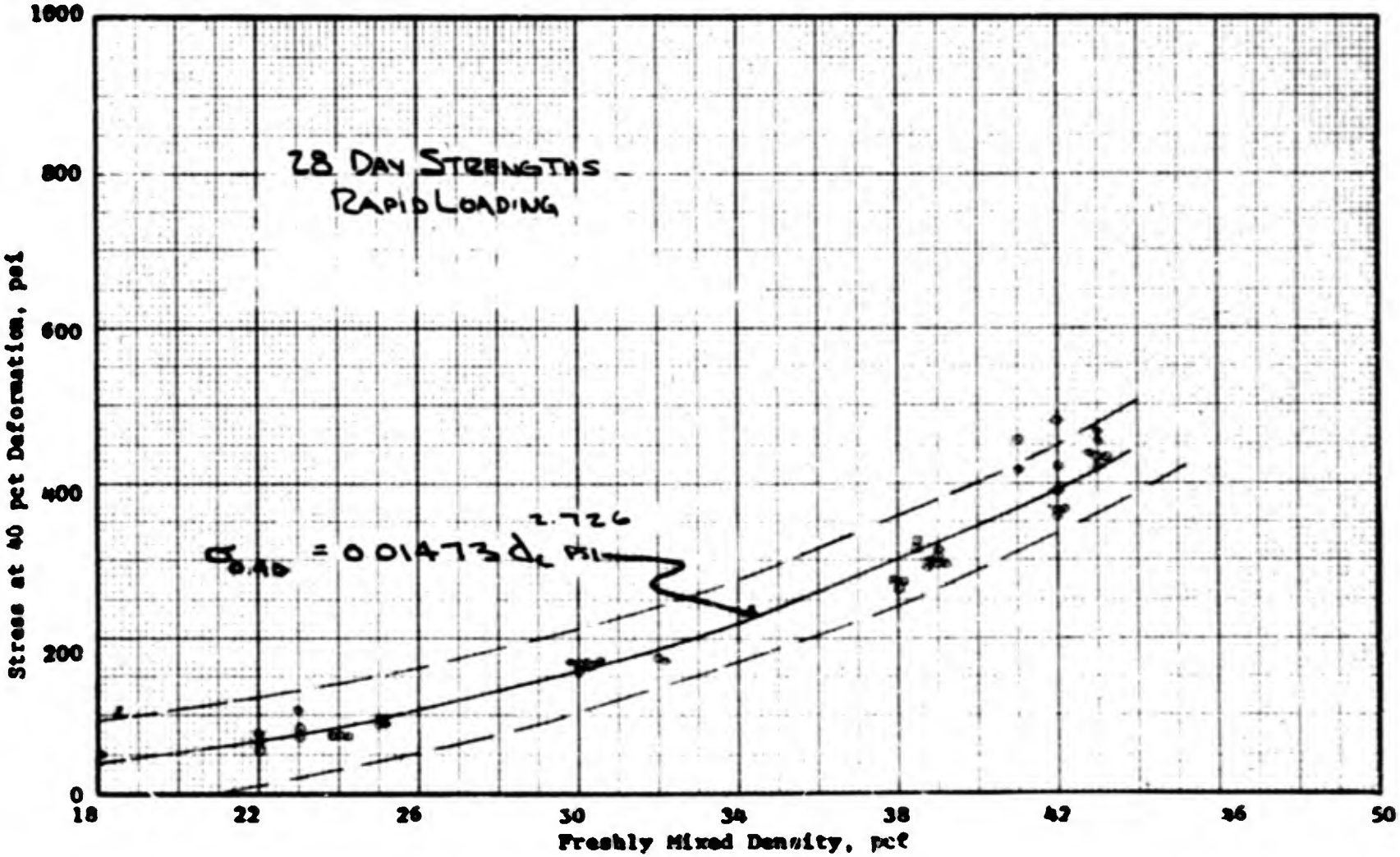

Figure B.24 Stress at 40 percent deformation versus freshly mixed density relation for rapidly loaded cellular concrete with an 0.96 water-cement ratio.

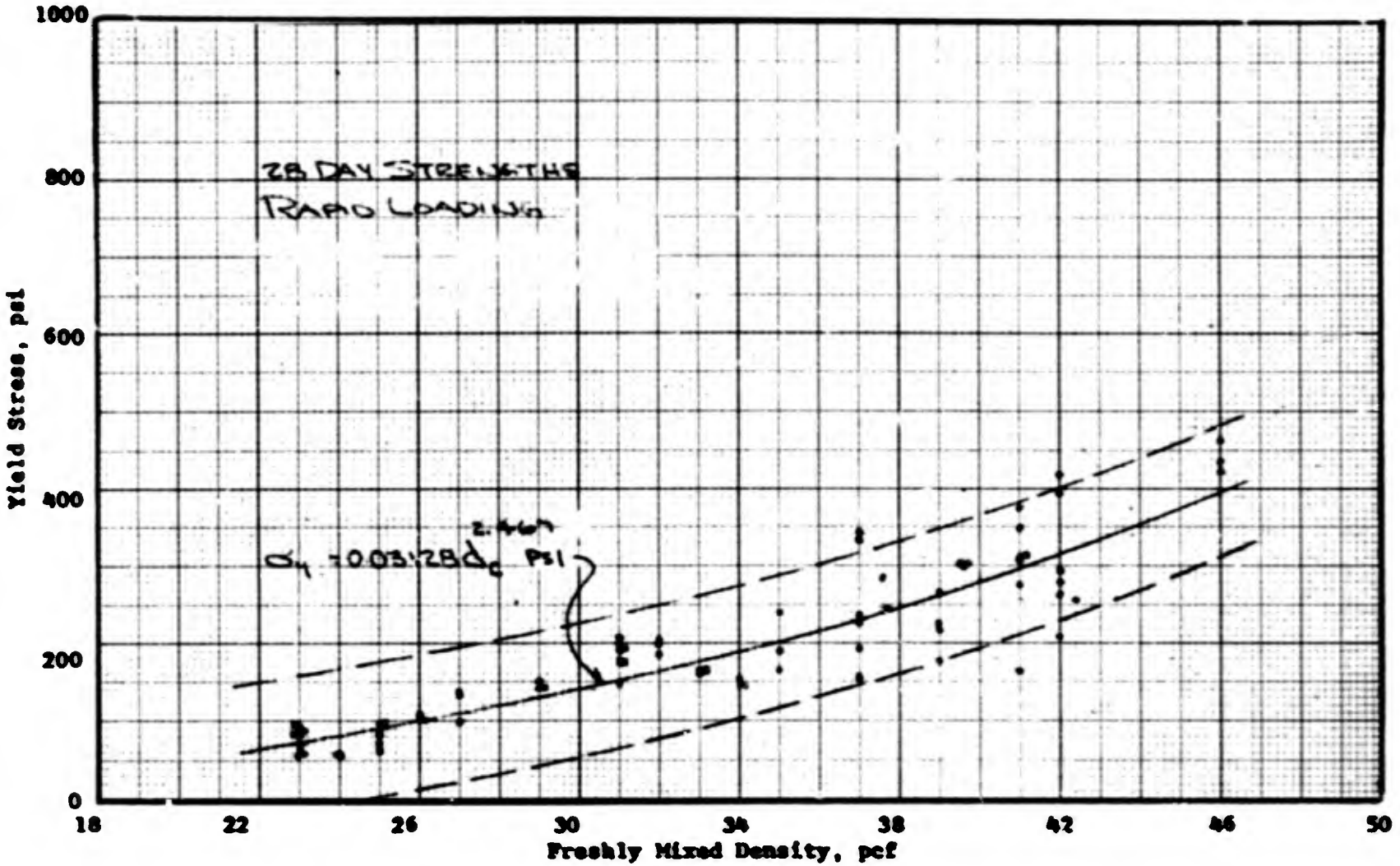

Figure B.25 Yield stress versus freshly mixed density relation for rapidly loaded cellular concrete with a 1.06 water-cement ratio.

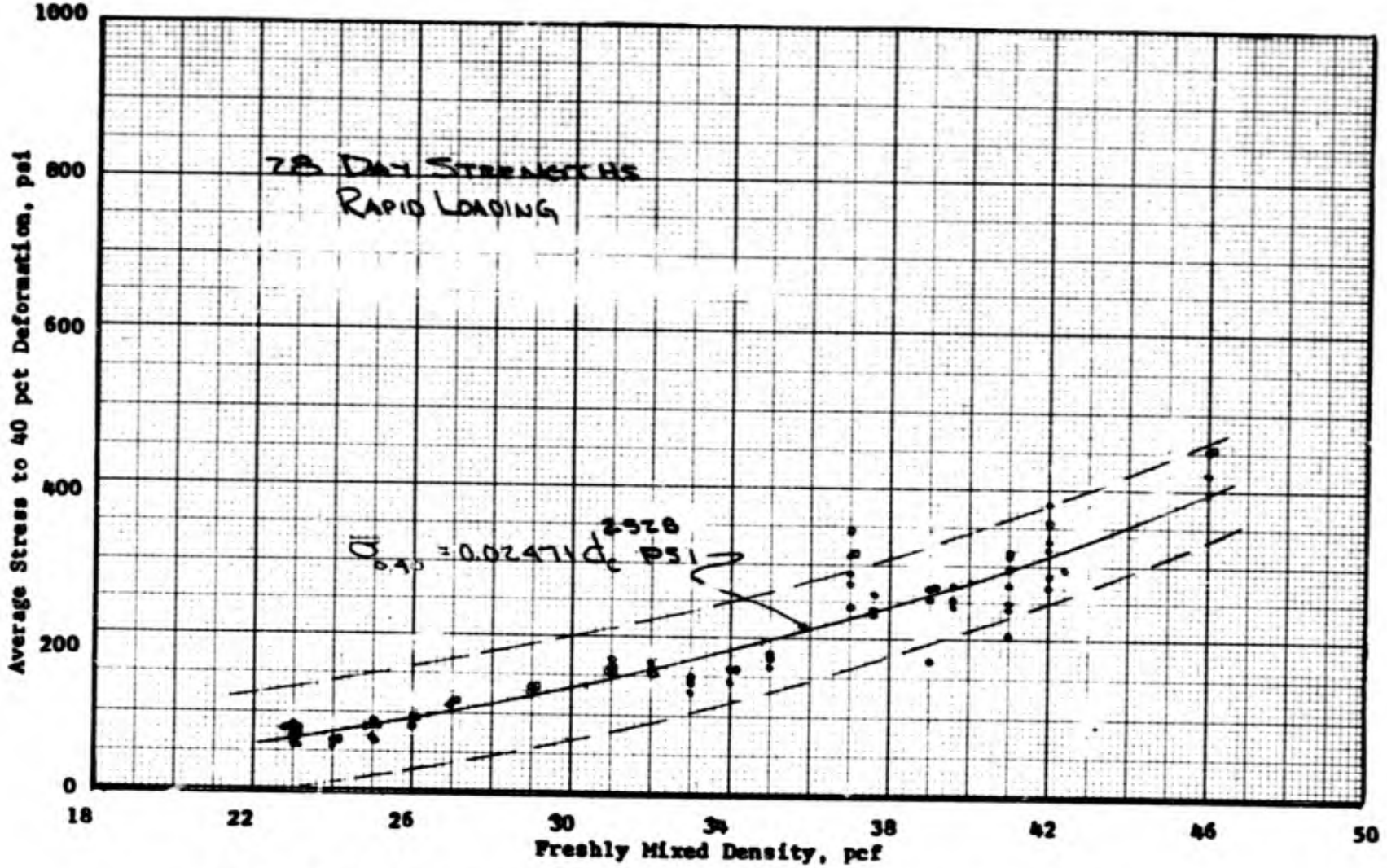

Figure B.26 Average stress versus freshly mixed density relation for rapidly loaded cellular concrete with a 1.06 water-cement ratio.

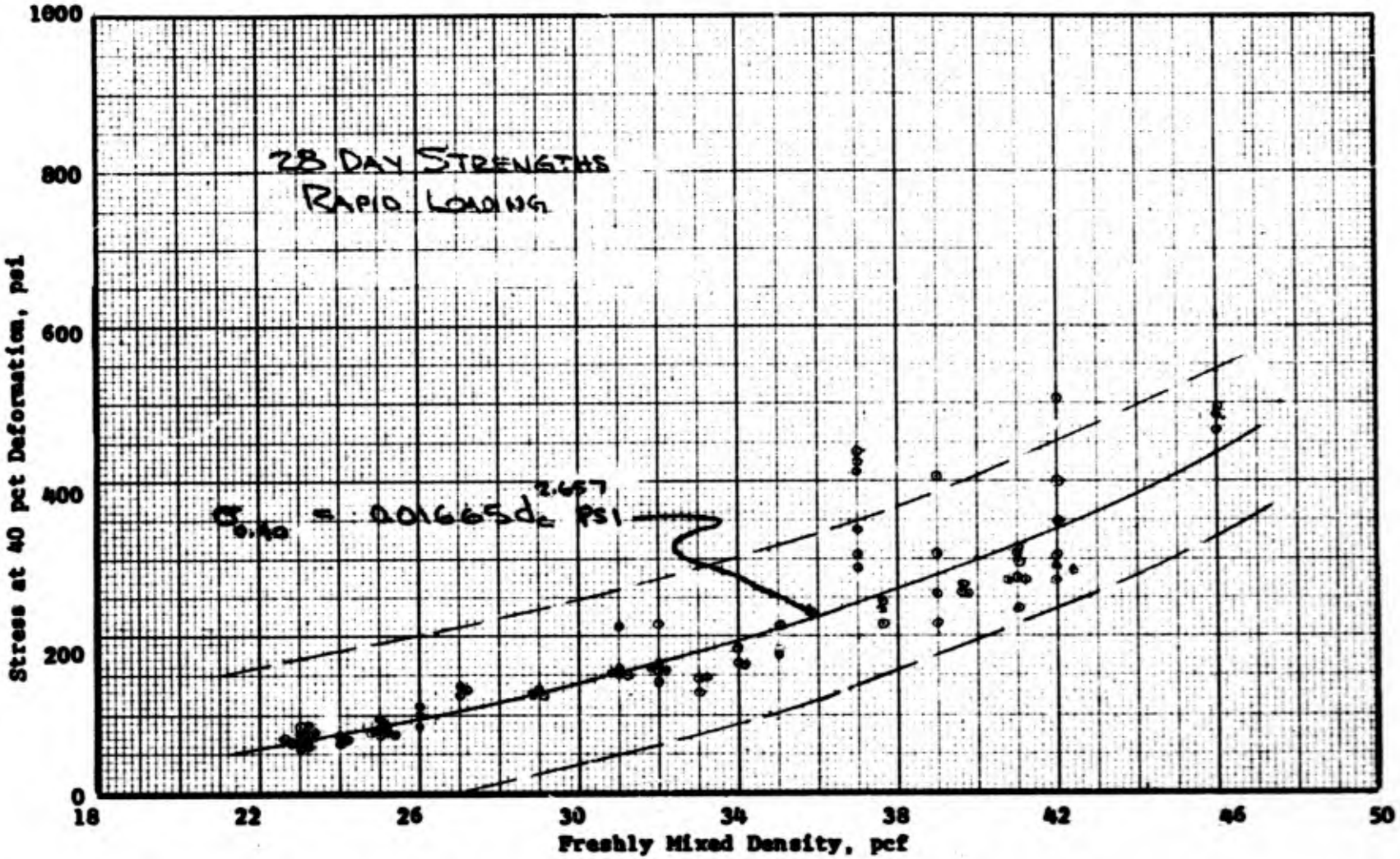

Figure B.27 Stress at 40 percent deformation versus freshly mixed density relation for rapidly loaded cellular concrete with a 1.06 water-cement ratio.

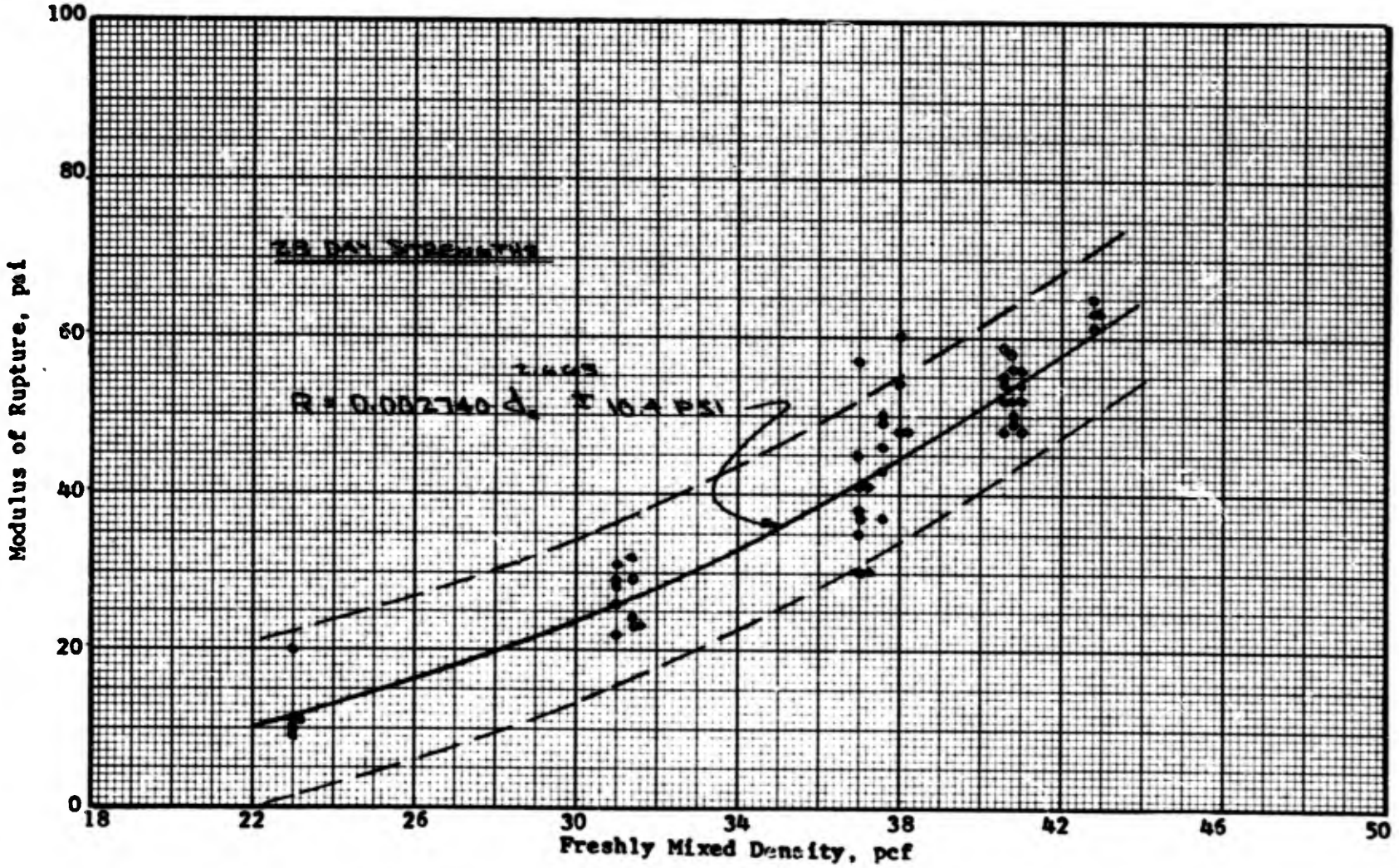

Figure B.28 Modulus of rupture versus freshly mixed density relation for cellular concrete with an 0.76 water-cement ratio.

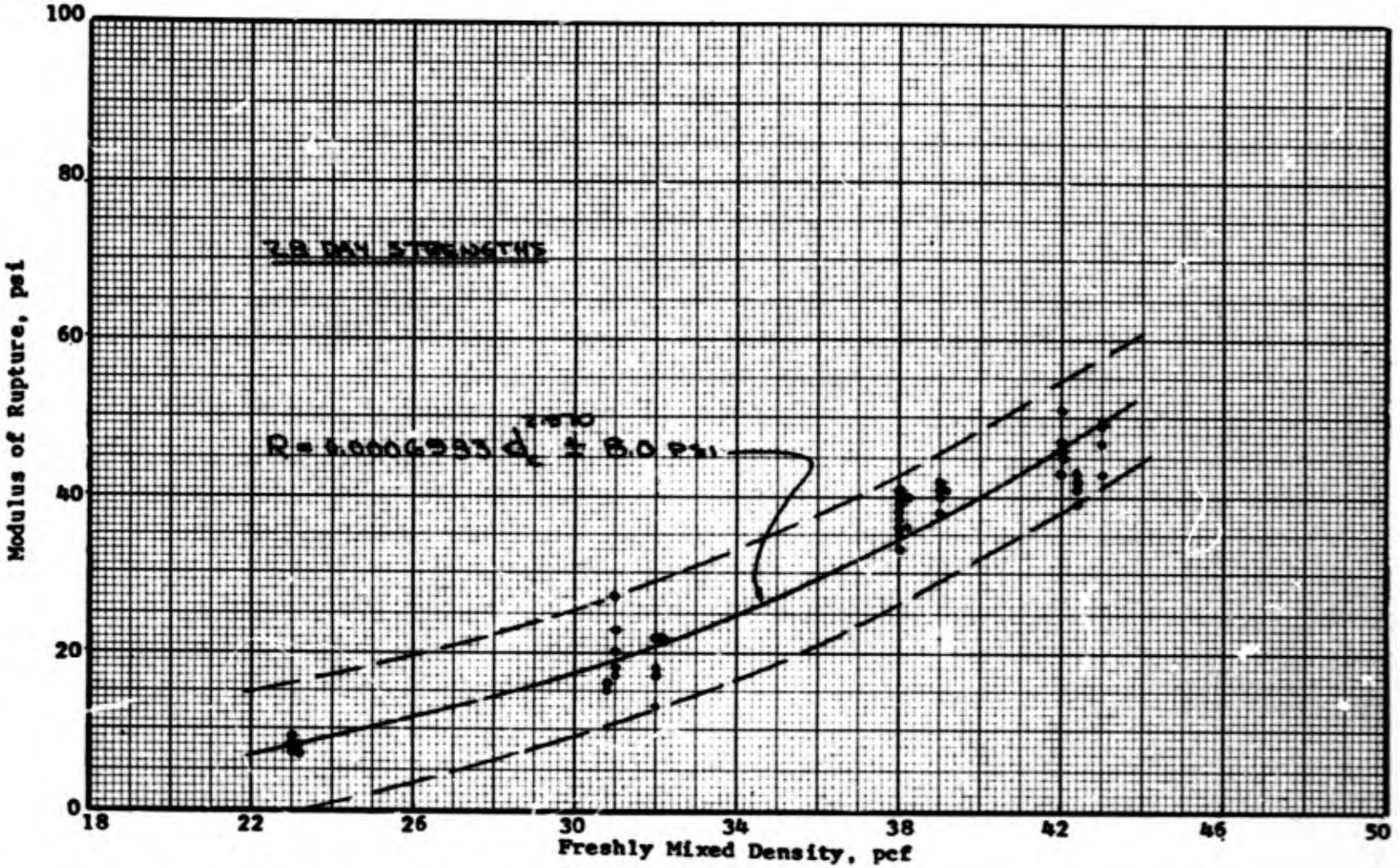

Figure B.29 Modulus of rupture versus freshly mixed density relation for cellular concrete with an 0.86 water-cement ratio.

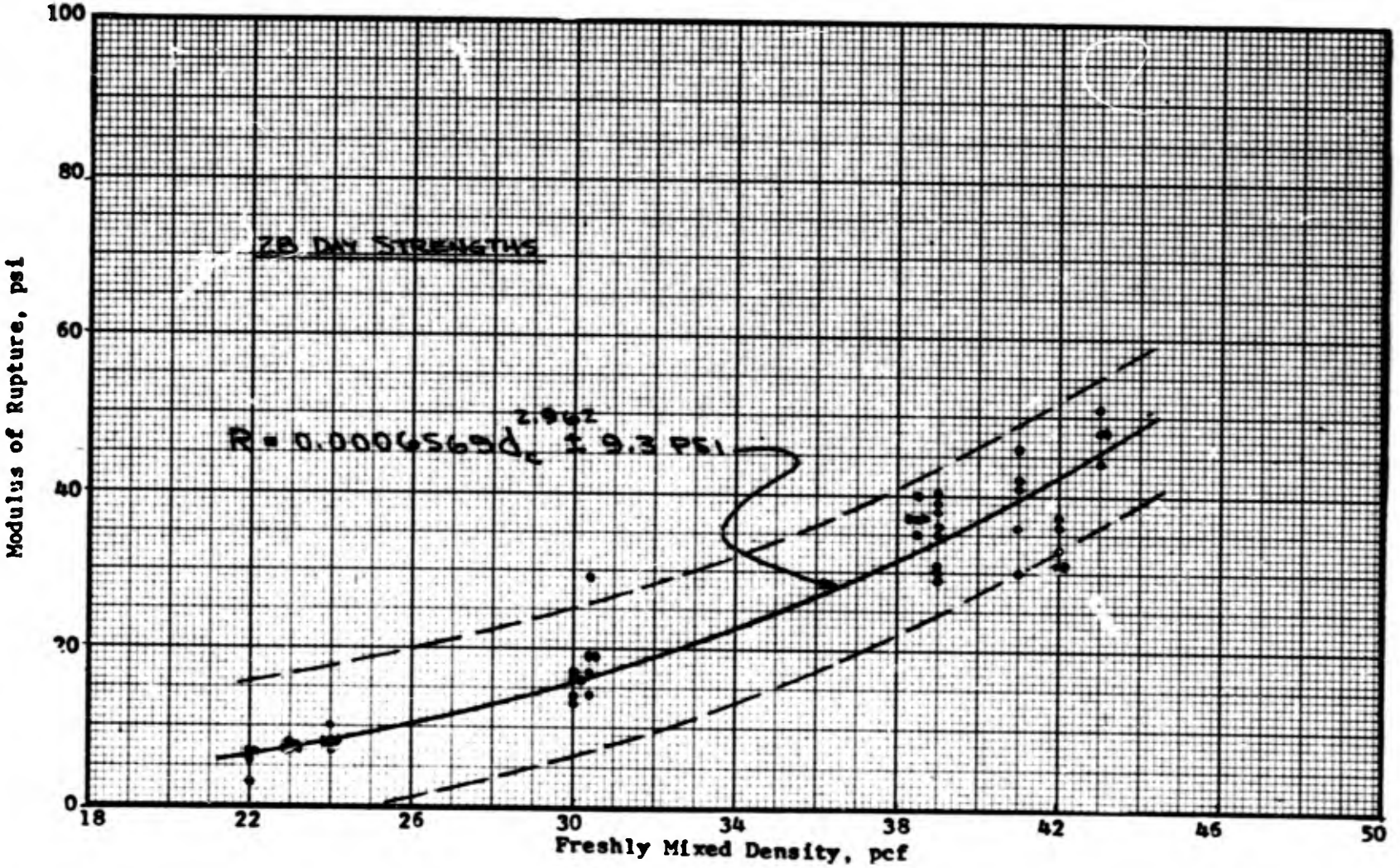

Figure B.30 Modulus of rupture versus freshly mixed density relation for cellular concrete with an 0.96 water-cement ratio.

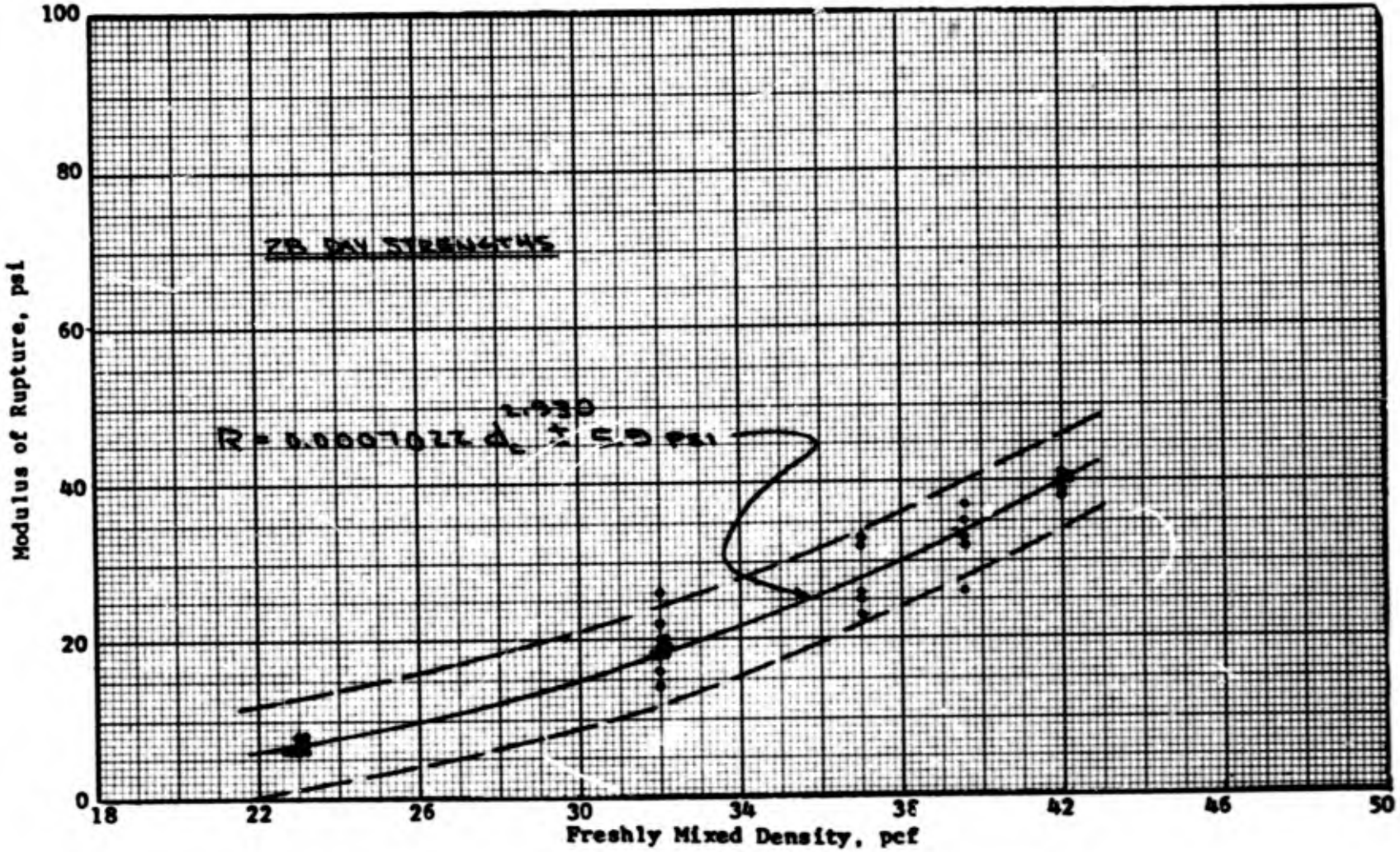

Figure B.31 Modulus of rupture versus freshly mixed density relation for cellular concrete with a 1.06 water-cement ratio.

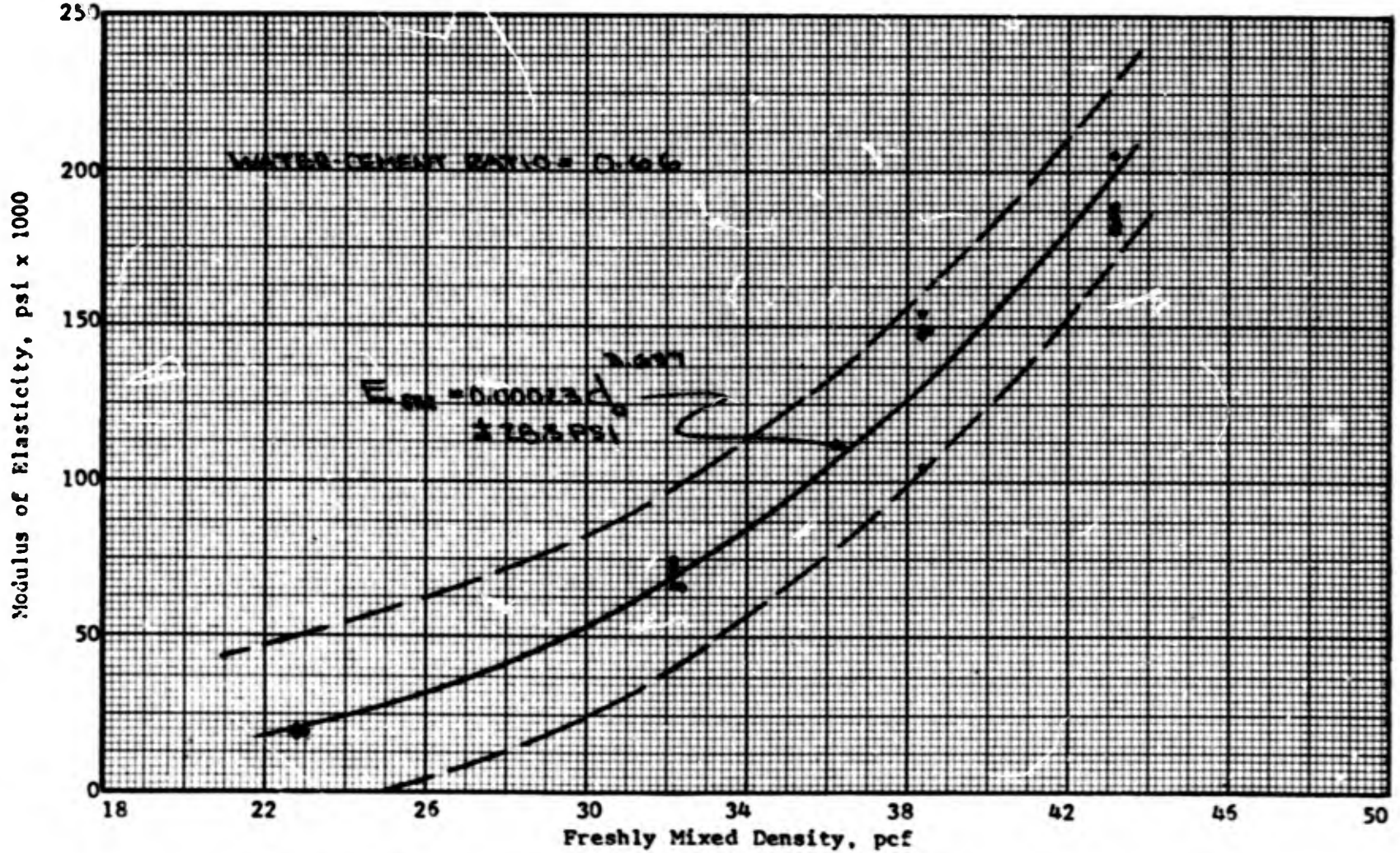

Figure B.32 Modulus of elasticity versus freshly mixed density relation for cellular concrete with an 0.66 water-cement ratio.

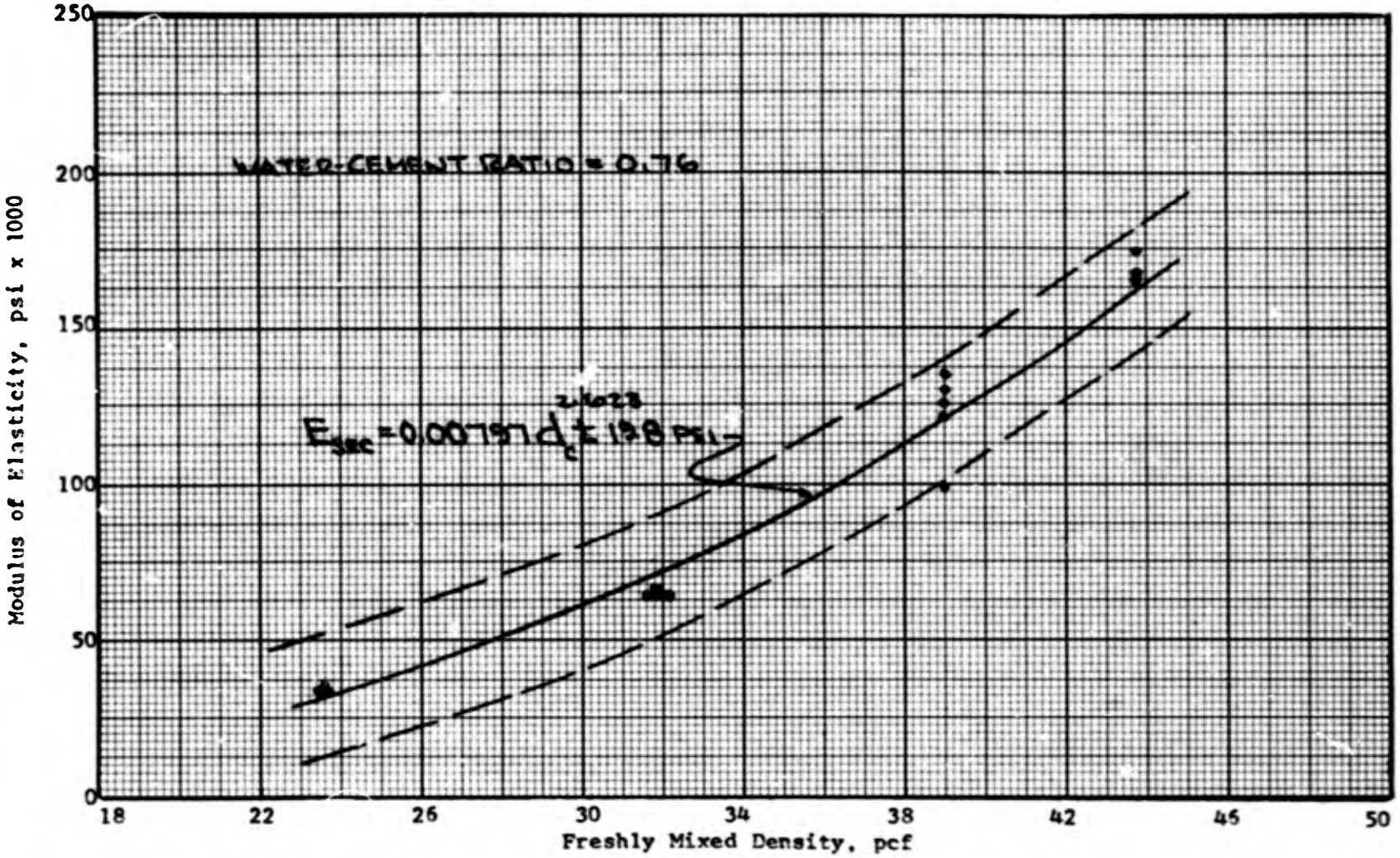

Figure B.33 Modulus of elasticity versus freshly mixed density relation for cellular concrete with an 0.76 water-cement ratio.

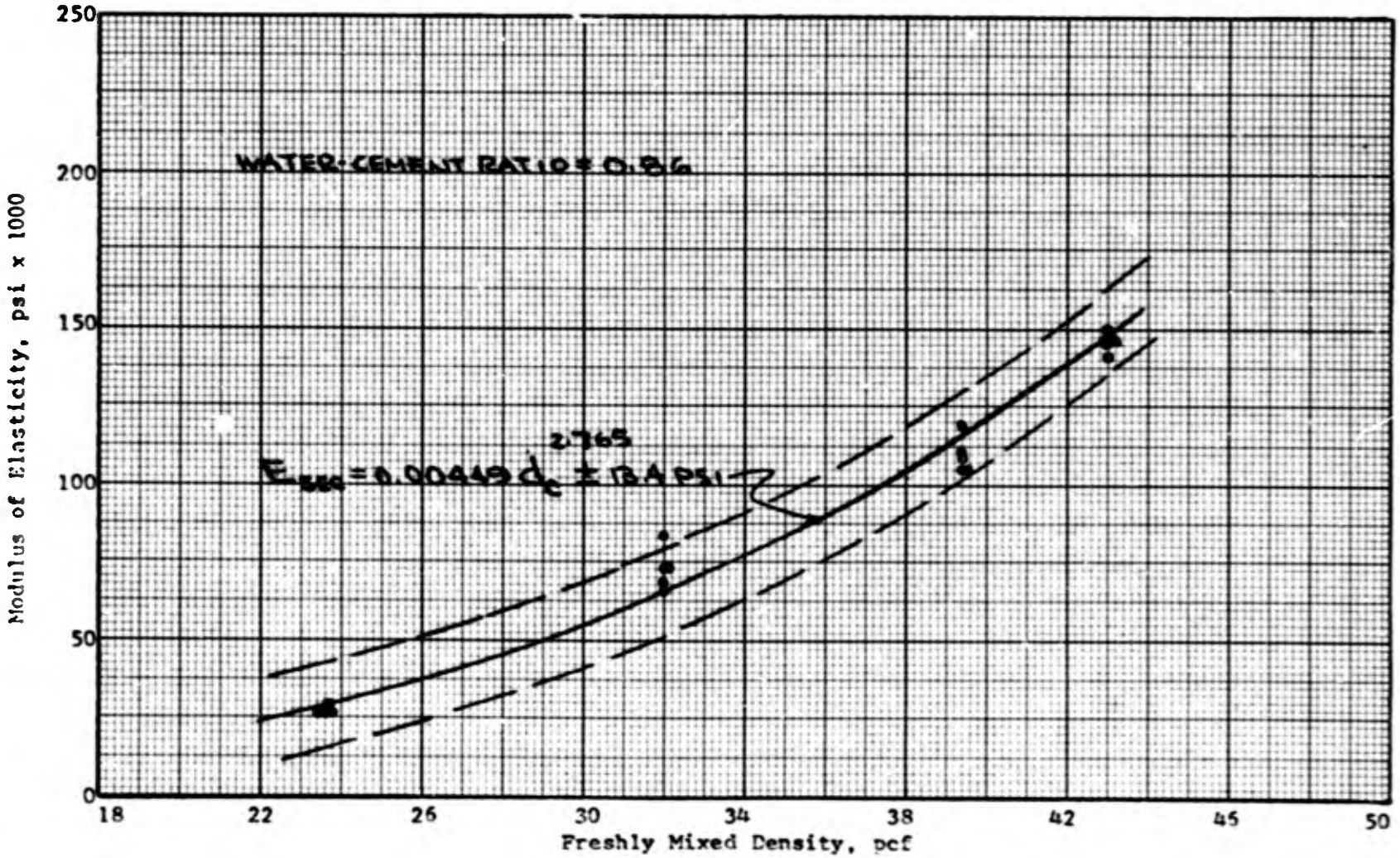

Figure B.34 Modulus of elasticity versus freshly mixed density relation for cellular concrete with an 0.86 water-cement ratio.

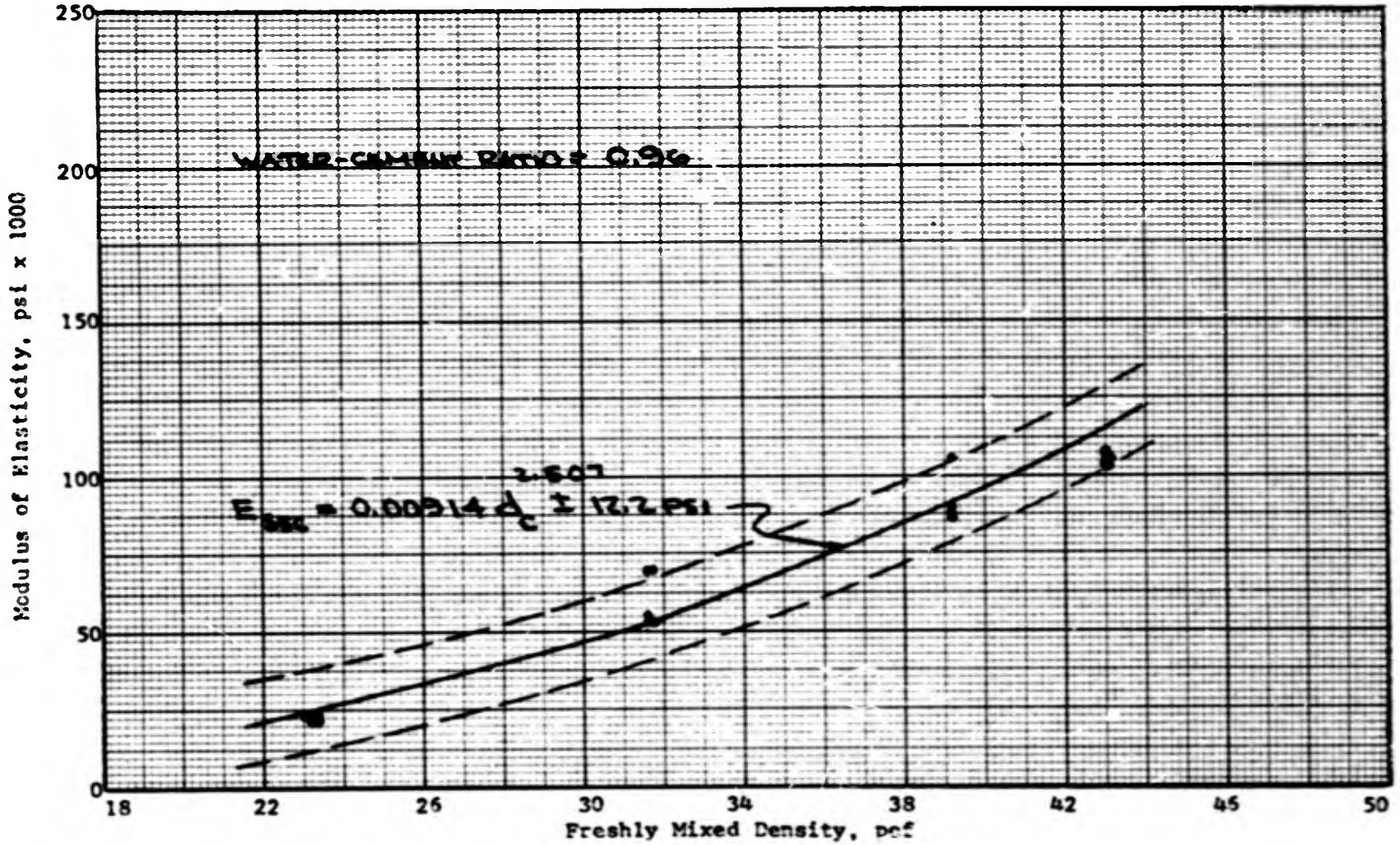

Figure B.35 Modulus of elasticity versus freshly mixed density relation for cellular concrete with an 0.96 water-cement ratio.

APPENDIX C

OBSERVATIONS ON THE EQUATION OF STATE OF CELLULAR CONCRETE

The mechanism of attenuation of pressure waves in cellular concrete has been studied previously from the rigid mechanical point of view that is applicable for the lower rates of loading as contained in this report. For loading rates sufficiently rapid that wave mechanics influence the behavior of the material, the mechanism of attenuation may be appreciably altered. Wave propagation experiments with cellular concrete have indicated the shock structure of cellular concrete to consist of an elastic precursor followed by a slower crushing wave (Reference 20). The pressure associated with the elastic precursor is a function of the input pressure of the incident wave and is observed to exceed the static yield strength of the cellular concrete for higher impact velocities. This indicates that this material, prior to locking, may transmit stresses to a structure in excess of the elastic yield stress. From a few tests conducted on cellular concrete, data were produced relating to wave propagation velocities, width of the transition zone for a step pressure input, and rate of decay of stress waves in cellular concrete.

C.1 THEORETICAL CONSIDERATIONS

The description of elastic-plastic wave propagation in a material is predicated on a constitutive relation of the material behavior and the equations of motion. In the simplest cases, a strain rate independent behavior leads to many important simplifications that allow computation of stress and strain relations in a fairly straightforward manner. In this instance, the Hugoniot jump conditions for one dimension involving stress (σ) and strain (ϵ) are given as

$$\sigma = \rho U u \tag{C.1}$$

$$\epsilon = \frac{u}{U} \tag{C.2}$$

where

ρ = density ahead of the wave

U = velocity of propagation of the wave

u = particle velocity behind the wave front

This description of materials behavior is essentially hydrodynamic; and for very soft materials where shear stresses and strain rate dependence are negligible, these equations should be a fair approximation.

In the elastic range, the relations are essentially the same but are derived from considerations of elastic behavior, where $U = C$, the velocity of propagation of elastic waves.

In the case of an elastic-plastic wave reflecting from a liner, the stresses delivered to the liner can be derived by making the assumption of purely elastic behavior of the liner. Under these simplifying conditions, reflected stresses at the liner can be determined from the behavior of the shock-absorbing concrete under shock loading.

C.2 EXPERIMENTAL METHOD

The shock behavior of cellular concrete was studied from the wave propagatic . point of view using impact experiments conforming to one-dimensional strain conditions. Continuous measurements of propagation and particle velocities were made using an induction wire transducer. Plane impacts were produced using a gas-operated gun to launch a flat plate onto the specimen. The gas gun has a 2-inch bore, 10-foot launch tube, and a pressure chamber designed for 12,000 psi (Reference 21). Both the weight of the projectile and breech pressure can be varied to attain different impact velocities.

Test specimens were prepared with induction wires placed at varying depths from the impact surface along the centerline of the axis of loading as shown in Figure C.1. The specimen was then placed in a dc magnetic field such that any axial motion caused the effective length of the wire to cut lines of magnetic flux thus producing an emf or voltage proportional to the velocity of motion. The output voltage from each wire, therefore, was recorded as a function of time. The amplitude of the signal was calibrated in units of particle velocity and the time displacement between each wire was a measure of the propagation velocity.

C.3 EXPERIMENTAL RESULTS

The observed particle velocity records for three signal wires are shown in Figure C.2. The test configuration for shots 1 and 2 was such that the cellular concrete was impacted directly. The first two shots indicate the existence of an elastic forerunner wave preceding a plastic wave. However, this forerunner cannot be distinguished from an air shock effect since the range facility was not evacuated in this case. An effort was made to vent the gun barrel at the sample interface; however, it was difficult to determine if this was sufficient to eliminate all effects of an air cushion. Therefore, a 1/8-inch-thick aluminum plate was affixed to the impact surface of the specimen to permit the range facility or barrel to be evacuated to approximately 10 microns. The records produced using this test configuration are shown in Figure C.3. Signals for two wires that were spaced at 12.7-mm intervals from the impact surface at a faster sweep rate, which was selected to show the elastic portion of the wave structure, are shown. These same signals were displayed at slower sweep rates for observing any plastic wave structure. No plastic wave structure was observed on any of these four tests for a period of observation covering 200 μsec. Propagation velocities correlate closely with the sonic velocity or the velocity predicted from the slope of the elastic portion of a static stress-strain relation for the samples tested.

The observed pressure-time histories shown in Figure C.4 as computed from the measured velocity histories show a decay in pressure of approximately 50 percent over a propagation distance of 12.7 mm. This rate of decay is not expected to be constant with distance from the impact surface. Additional data points as a function of distance from impact surface would be required to determine this. It is possible that this apparent decay is a function of the test conditions; however, a correlation between this and wave reflections for this test geometry has not yet been achieved. One point in question is the velocity of release waves emanating from the outer edges of the projectile input surface that could diminish the region of one-dimensional strain. More experiments are required to establish the contribution due to test geometry.

Under certain conditions, an interposed layer of foamed or distended material may substantially reduce peak pressures transmitted to a structural wall. The initial shock front does not seem to occupy the relatively narrow zone usually imagined to exist in solids. Therefore, it may be more accurate to say the pressure attenuation effect is related to a broadening of the condensing front. Beneficial effects can also be derived from the existence of forerunners similar to elastic precursors in solid materials since these carry off momentum from the crushing wave and deliver it to the structure at a lower pressure.

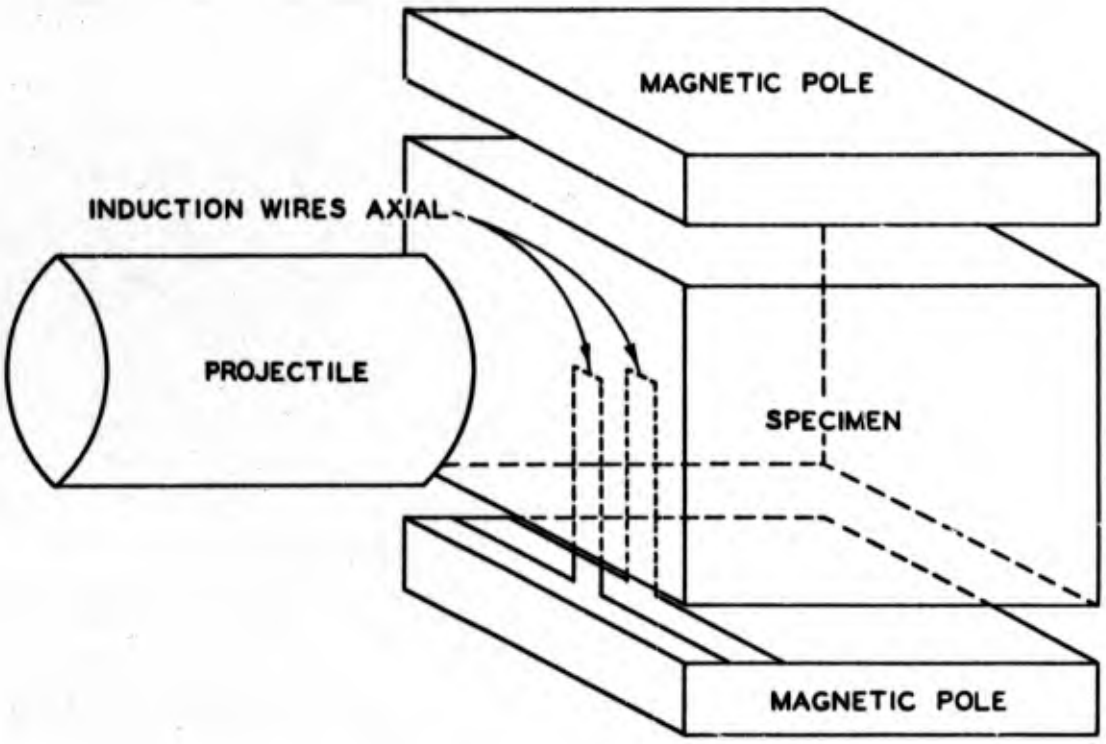

Figure C.1 Schematic of experimental setup.

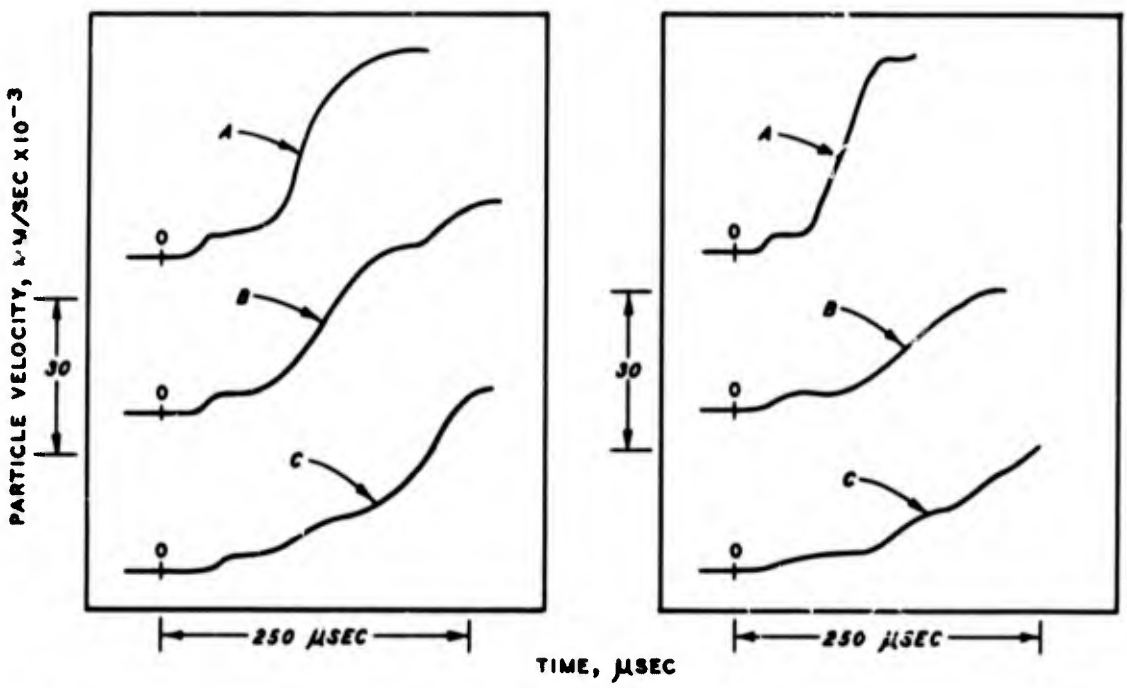

NOTE: LOCATION OF ZERO POINTS IS ARBITRARY. THE STACKING OF CURVES A, B, AND C IS DONE ONLY TO SHOW THE CHANGE IN WAVE PROFILES.

Figure C.2 Particle velocity versus time histories.

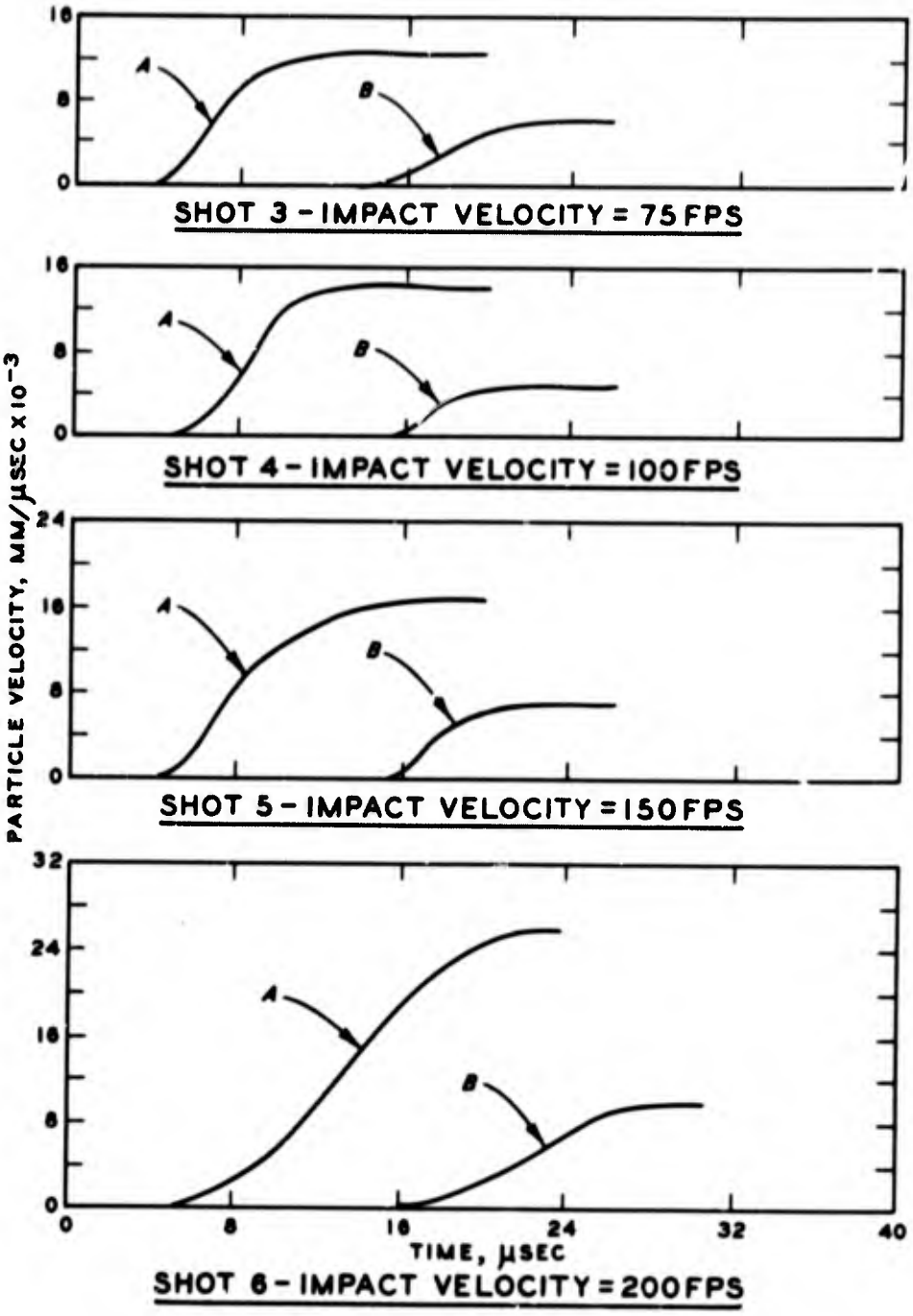

NOTE: ZERO OF CURVE A IS ARBITRARY BUT CURVE B IS IN THE PROPER TIME LOCATION WITH RESPECT TO A.

Figure C.3 Particle velocity versus time histories when impacted with aluminum driver plate.

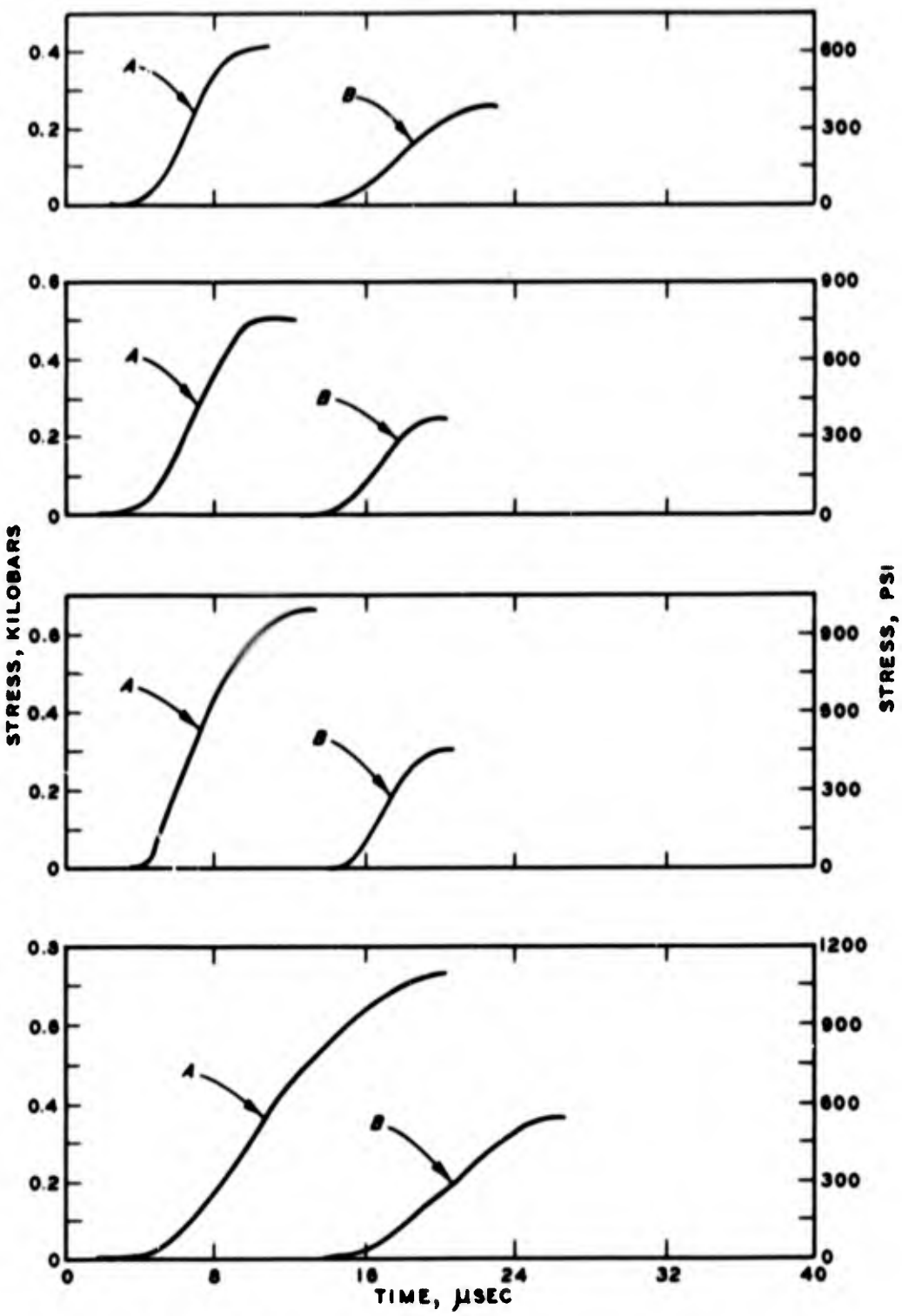

NOTE: ZERO OF CURVE A IS ARBITRARY BUT CURVE B IS IN THE PROPER LOCATION WITH RESPECT TO A.

Figure C.4 Pressure versus time histories.

REFERENCES

1. ACI Committee 523; "Guide for Cast-In-Place Low Density Concrete"; Journal, American Concrete Institute, September 1967, Vol. 64, No. 9, Pages 529-535; Detroit, Mich.; Unclassified.

2. G. C. Hoff; "Shock-Absorbing Materials; Backpacking Materials for Deeply Buried Protective Structures"; Technical Report No. 6-763, Report 1, March 1967; U. S. Army Engineer Waterways Experiment Station, CE, Vicksburg, Miss.; Unclassified.

3. G. C. Hoff, W. F. McCleese, and J. M. Holzer; "Shock-Absorbing Materials; Aging of Backpacking Materials"; Technical Report No. 6-763, Report 4, November 1968; U. S. Army Engineer Waterways Experiment Station, CE, Vicksburg, Miss.; Unclassified.

4. G. C. Hoff; "Shock-Absorbing Materials; Selection of a Suitable Low-Density Concrete for Backpacking for a Proposed Field Test"; Technical Report No. 6-763, Report 3, April 1968; U. S. Army Engineer Waterways Experiment Station, CE, Vicksburg, Miss.; Unclassified.

5. G. C. Hoff; "Operation Flint Lock, Shot Pile Driver; Grouting and Materials Control"; Miscellaneous Paper C-69-7, March 1969; U. S. Army Engineer Waterways Experiment Station, CE, Vicksburg, Miss.; Unclassified.

6. T. C. Powers and T. L. Brownyard; "Studies of the Physical Properties of Hardened Portland Cement Paste"; Journal, American Concrete Institute, 1947, Vol. 43, Pages 101-132, 249-336, 469-504, 549-602, 669-712, 815-880, 933-992; Detroit, Mich.; Unclassified.

7. T. C. Powers; "The Physical Structure and Engineering Properties of Concrete"; Research Department Bulletin 90, July 1958; Research and Development Laboratories of the Portland Cement Association, Chicago, Ill.; Unclassified.

8. T. C. Powers; "The Nonevaporable Water Content of Hardened Portland-Cement Paste--Its Significance for Concrete Research and Its Method of Determination"; ASTM Bulletin No. 158, May 1949, Pages 68-76; American Society for Testing Materials, Philadelphia, Pa.; Unclassified.

9. G. Wischers; "Einfluss einer Temperäturanderung auf die Festigkeit von Zemetstein und Zementmörtel mit Zuschlag-Stoffen Verschiedener Wärmedehnung"; Schriftenreihe der Zementindustrie Verein Deutscher Zementwerke E. V., Düsseldorf, March 1961, Page 50.

10. T. C. Hansen; "Cracking and Fracture of Concrete and Cement Paste"; ACI Publication SP-20, 1968, Pages 43-66; American Concrete Institute, Detroit, Mich.; Unclassified.

11. A. Auskern; "A Model for the Strength of Cement-Polymer and Concrete-Polymer Systems"; BNL 13493R-2, March 1969; Brookhaven National Laboratory, Upton, N. Y.; Unclassified.

12. M. Polivka, J. W. Kelly, and C. H. Best; "A Physical Method for Determining the Composition of Hardened Concrete"; ASTM Special Technical Publication No. 205, 1958, Pages 135-152; American Society for Testing Materials, Philadelphia, Pa.; Unclassified.

13. R. C. Valore, Jr.; "Cellular Concretes; Part 2, Physical Properties"; Journal, American Concrete Institute, Vol. 50, No. 10, June 1954, Pages 817-836; Detroit, Mich.; Unclassified.

14. F. C. McCormick; "A Rational Procedure for Proportioning Preformed Foam Cellular Concrete Mixes"; Ph. D. Dissertation, 1964; University of Michigan, Ann Arbor, Mich.; Unclassified.

15. A. Pauw; "Static Modulus of Elasticity of Concrete as Affected by Density"; Journal, American Concrete Institute, Vol. 57, No. 12, 1960-1961, Pages 679-688; Detroit, Mich.; Unclassified.

16. ACI Committee 318; "Proposed Revision of ACI 318-63, Building Code Requirements for Reinforced Concrete"; Journal, American Concrete Institute, Vol. 67, No. 2, February 1970, Pages 77-186; Detroit, Mich.; Unclassified.

17. ACI Committee 213; "Guide for Structural Lightweight Aggregate Concrete"; Journal, American Concrete Institute, Vol. 64, No. 8, August 1967, Pages 433-469; Unclassified.

18. T. W. Reichard; "Creep and Drying Shrinkage of Lightweight and Normal-Weight Concretes"; NBS Monograph 74, March 1964; U. S. Department of Commerce, National Bureau of Standards, Washington, D. C.; Unclassified.

19. G. C. Hoff, W. F. McCleese, and A. A. Bombich; "Project Big Papa - Phase III, Cellular Concrete Fragmentation Acceptors"; Miscellaneous Paper No. 6-973, February 1968; U. S. Army Engineer Waterways Experiment Station, CE, Vicksburg, Miss.; Unclassified.

20. B. R. Sullivan; "Dynamic Compaction of Porous Concrete"; Miscellaneous Paper C-68-9, November 1968; U. S. Army Engineer Waterways Experiment Station, CE, Vicksburg, Miss.; Unclassified.

21. D. L. Ainsworth and B. R. Sullivan; "Shock Response of Rock at Pressures Below 30 Kilobars"; Technical Report No. 6-802, November 1967; U. S. Army Engineer Waterways Experiment Station, CE, Vicksburg, Miss.; Unclassified.